AFIT/GAE/ENY/92D-13

VIBRATION SUPPRESSION IN LARGE FLEXIBLE SPACE STRUCTURES USING ACTIVE CONTROL TECHNIQUES

THESIS

Chad T. Matheson, LT, USAF

AFIT/GAE/ENY/92D-13

Approved for public release; distribution unlimited

AFIT/GAE/ENY/92D-13

VIBRATION SUPPRESSION IN LARGE FLEXIBLE SPACE STRUCTURES USING ACTIVE CONTROL TECHNIQUES

THESIS

Presented to the Faculty of the School of Engineering

of the Air Force Institute of Technology

Air University

In Partial Fulfillment of the

Requirements for the Degree of

Master of Science in Aeronautical Engineering

Chad T. Matheson, B.S.
LT, USAF

December 1992

Acknowledgements

During the performance of the research and the writing of this thesis, I received a great deal of help from others. I would like to thank Col Ron Bagley, Dr. Brett Ridgely and especially Dr. Bradley Liebst, whose advice and guidance was invaluable during the course of this research. I would also like to express my appreciation to Mr. Jay Anderson who was always available to lend a hand with the many equipment problems encountered during the experimental portion the work. A word of thanks also goes out to the rest of the Laboratory Technicians, as well as Mr. Ron Gordon, whose computer expertise made this report possible.

A very special thank you goes to my wife, Johanna, to whom this report is dedicated. Her sacrifices and support during my stay at AFIT were an essential part of my success.

Chad T. Matheson

Table of Contents

List of Figures

List of Tables

Abstract

This report investigates the use of active vibration control techniques applied to the PACOSS Dynamic Test Article as an experimental structure. In the course of the research, a mathematical model of the lightly damped experimental structure was created based on experimental data. This model was used in the design of two classes of controllers. The first class is pure rate feedback of the structure's measured states such that global stability is insured. The second type of controller investigated was an optimal controller (LQG) that was created using the truncated mathematical model. The rate feedback controller showed significant improvements in the damping of the structures flexible modes. The optimal controller proved to be stable only for negligible gains and did not improve structural damping significantly.

VIBRATION SUPPRESSION IN LARGE FLEXIBLE SPACE STRUCTURES USING ACTIVE CONTROL TECHNIQUES

I. Introduction

The design requirements for future spacecraft will dictate that the structure be relatively large in size. By necessity, they will also have to be lightweight to minimize launch costs. The combination of these characteristics lead to dense modal spectra of the spacecraft flexible body modes, at frequencies which typically overlap the attitude control bandwidth. The mission requirements of these spacecraft may require precise shape control, rapid targeting maneuvers, and stringent line of sight specifications. The excitation of the flexible body dynamics in the space structure are detrimental to these mission requirements, and if left uncontrolled may result in failure to satisfy mission requirements (5:1).

Problem and General Approach

The goal of this thesis is to apply purely active feedback control to attenuate the vibration in a representative space structure. The types of feedback control used are a direct rate feedback controller and a control law formed from the optimization of a linear quadratic performance index (LQG). A secondary goal of the research presented here is to complete a functional check-out of the equipment used in order

to provide a knowledge base for future research. This is necessary since much of the equipment used in this research had not been used since its delivery in March, 1991.

In order to attain these goals, a mathematical model of the structure's flexible body dynamics had to be created. This was done solely through the use of experimental measurements. Once the mathematical model was created the controllers were designed to meet certain damping requirements. The control laws were executed via a Systolic Systems Optima/3 array processor on a large and lightly damped experimental structure named PACOSS.

Background of the PACOSS Program

In 1982, the Flight Dynamics branch of Wright Laboratory contracted the Martin Marietta Astronautics Group to study damping methods for large flexible structures under the Passive and Active Control of Space Structures program (PACOSS). The study was to include a combination of active and passive control designs applied to a realistic structure.

To assure broad applicability of the techniques developed under PACOSS, a representative system article was designed with characteristics that are traceable to future missions, both civilian and military (5:1). The Representative System Article was designed to provide guidance for active and passive control design strategies that would be applied to a full scale laboratory structure.

The Representative System Article consisted of seven substructures: a ring truss; two solar panels; an equipment tripod; an antenna dish; a box truss; and an equipment platform.

The components were all sized to realistically reflect their use in actual space applications. The study of this structure paved the way for the development of the Dynamic Test Article (DTA), a full size laboratory model.

The DTA was designed and constructed to have modal characteristics similar to the representative system article. It consisted of the same seven substructures as the representative system article and included significant amounts of passive damping treatments designed into the structure. Furthermore, it provided a laboratory test bed that captured the challenges of large space structure vibration control implementation and testing. After extensive study, the Martin Marietta team concluded that passive and active damping methods could be combined effectively to attenuate the vibration that occurs in large space structures. They also concluded that better methods of system identification were required to identify the dynamics contained in structures with high modal density.

At the termination of the contract, the DTA and supporting hardware were delivered to the Air Force Institute of Technology (AFIT) for further study. At AFIT the PACOSS experiment is one of several experimental facilities that comprise the Control/Structure Interaction Research Facility (CSIRF) sponsored by the USAF Phillips Laboratories. The research at AFIT will involve the application

of current and future passive and active damping methods as well as model identification techniques.

Since its delivery, the DTA has been modified by removing all of the passive damping treatments as well as the box truss, the antenna, and the equipment platform. New solar arrays were constructed to the same dimensions of the original drawings but without the passive damping treatments.

These modifications were intended to remove all of the passive damping from the structure to approximate an undamped system. After the modifications were made, a modal survey of the structure was completed through the use of finite element analysis and experimental observations to re-characterize the system (see reference 4).

Further research at AFIT will concentrate on improving the current state of the art in system identification methods as well as applying active control techniques to the undamped system.

II. Experimental Equipment

Much of the equipment used in the course of this research was received from Martin Marietta at the termination of the PACOSS contract. A list of this equipment includes the DTA itself, it's suspension system, the motor control units, the Optima/3 array processor and a Sun 3/50 computer. Some of this equipment was created solely for use with the DTA and is one-of-a-kind. The other equipment not obtained from Martin Marietta was procured by the Air Force for use with the continuing research at AFIT.

Figure 1 shows a schematic of the equipment used and its functional relationships. The paragraphs that follow describe the equipment in detail and describe their use in the research effort.

Description of the DTA

The Dynamic Test Article in its present configuration consists of four substructures along with eight structure borne actuators and 151 accelerometers. These substructures include the ring truss, two solar arrays and a tripod. The entire Dynamic Test Article 324" x 116" x 120" inches high. Since its delivery to AFIT, the DTA has undergone several modifications. For a complete description of the nature of these modifications see reference 4. A diagram of the DTA is included in Figure 2.

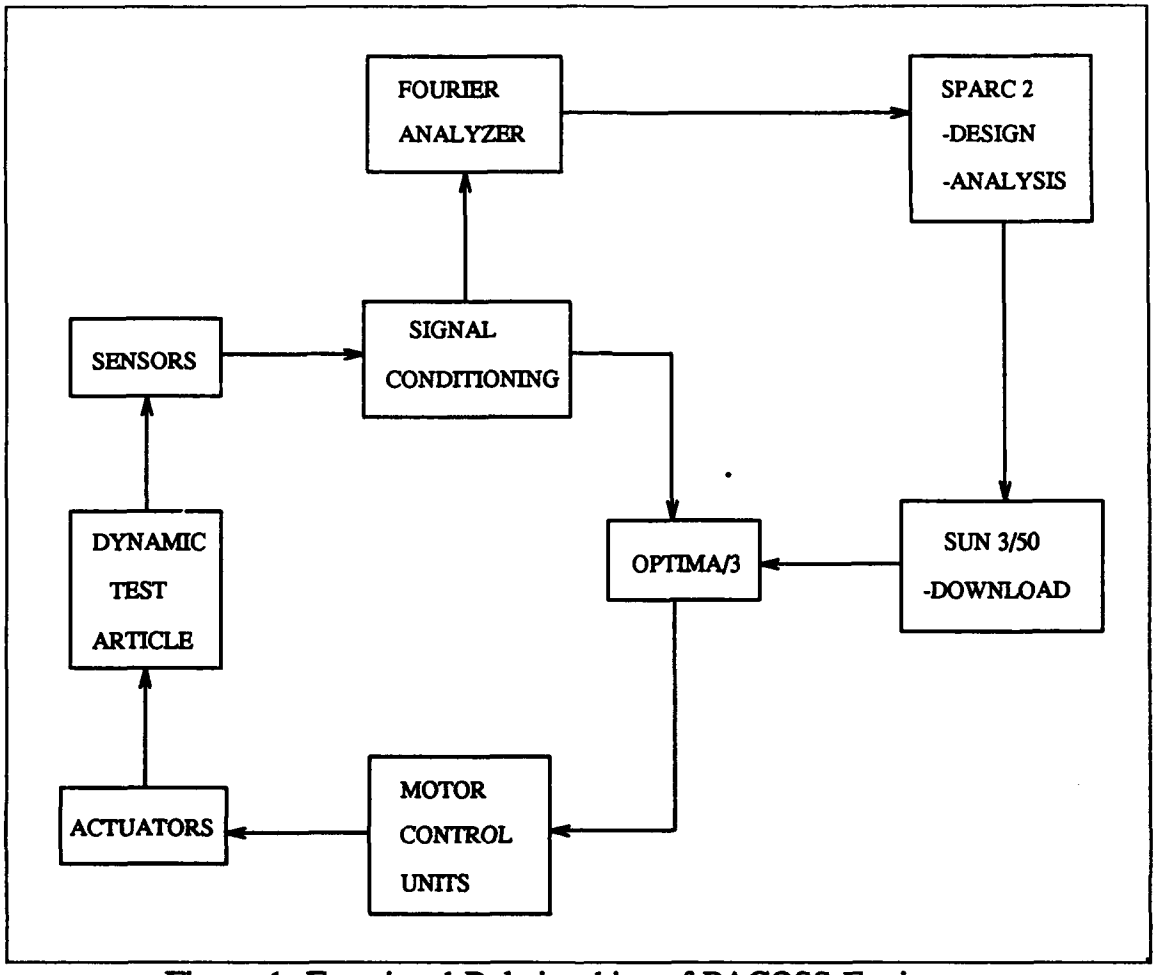

Figure 1: Functional Relationships of PACOSS Equipment

The main structural element of the DTA is the ring truss. The ring truss is a circular truss constructed of 6061-T6 Aluminum tubing bonded between solid aluminum joint blocks. It is approximately 116 inches in diameter. It was designed to support the gravitational load of the entire DTA assembly. The size and shape of the ring was designed to be appropriate for supporting a primary mirror in a Cassegrain optical system (5:42). The suspension system is attached to the ring truss at three locations, such that an axis of symmetry is maintained in

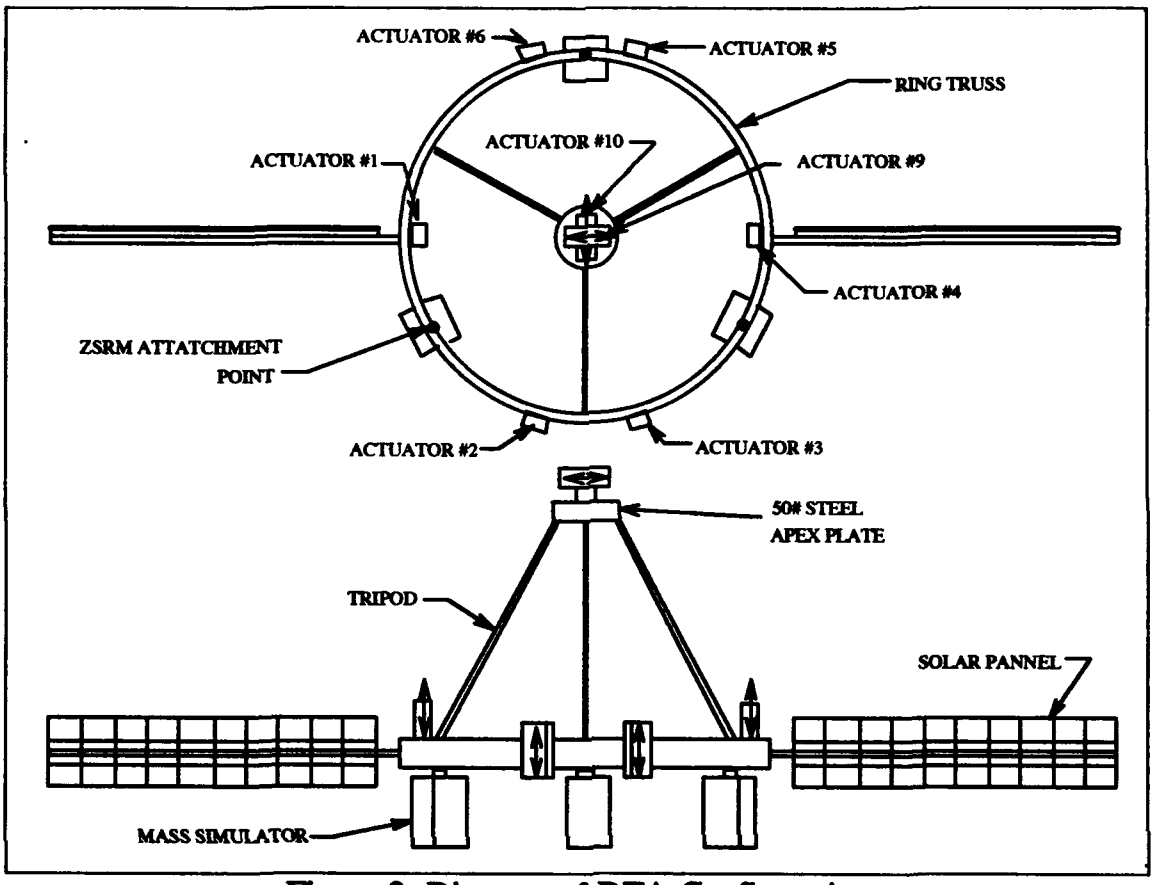

Figure 2: Diagram of DTA Configuration

the structure (See Figure 2). Also attached to the ring truss are six of the eight actuators as well as three mass simulators to simulate the presence of on board control systems and electronics packages. As with the suspension system the actuators and mass simulators are placed to maintain an axis of symmetry in the structure.

The solar arrays were sized to be consistent with the power requirements of future missions and to have typical low frequency resonances displayed by actual solar arrays (5:42). Since delivery to AFIT, the solar arrays have been rebuilt in order to remove the passive damping treatments that were originally applied to

them. The solar arrays are constructed of 1/2" x 1/8" aluminum strips attached to an aluminum mast that is 15 ft long. The strips form a 30 bay flat array to which a solar blanket could be fixed. The solar arrays are attached to the ring truss by a solid aluminum block assembly.

The tripod is composed of three aluminum tubing legs which support a 50lb steel plate at the apex. The steel plate is used to simulate a secondary mirror in an optical system. Mounted on top of the steel plate are the remaining two actuators (see Figure 2). The actuators are aligned with axes perpendicular to one another and their axes are parallel to the ground. The tripod was designed to have low frequency flexible modes. The tripod legs are attached to the ring truss by aluminum mounting plates. Their position on the ring maintains an axis of symmetry.

The entire DTA assembly is suspended via three Zero Spring Rate Mechanisms (ZSRM) developed by CSA Engineering Inc. Cables attach the DTA to ZSRMs which support the entire weight of the structure from above. Figure 3 shows the suspension system and its relationships to the DTA. The ZSRMs operate by applying air pressure to a piston to which the supporting cables are attached. All three ZSRMs are equipped with an air tank to provide air spring volumes for each piston (3:21). Each of the ZSRMs is equipped with an active centering control system that operates with the use of a linear variable differential transformer, a linear motor, and a feedback loop with an adjustable gain. The

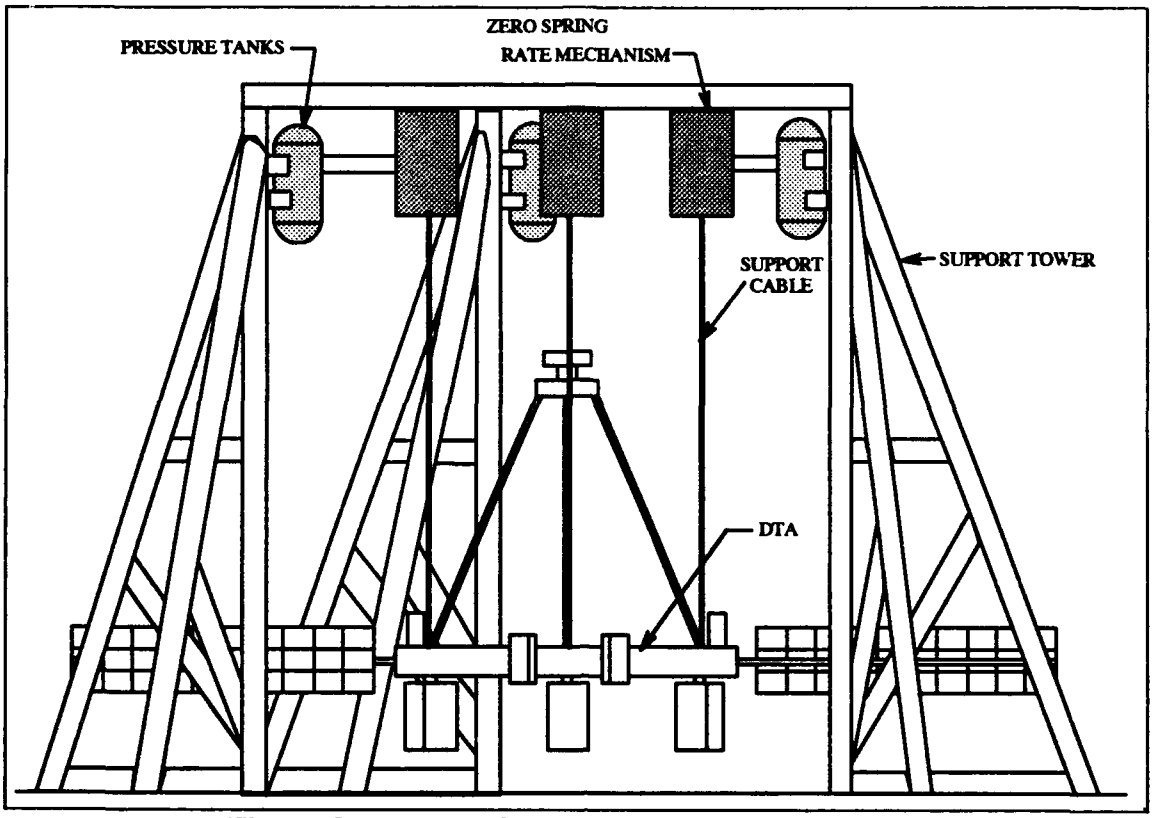

Figure 3: Layout of DTA and Suspension System

pistons float on air bearings which provide almost frictionless support for the structure. The natural frequency of the rigid body modes of the structure when supported are all below 0.6 Hz, which is below the first flexible mode of the DTA (4:30). The reference to rigid body modes here is not accurate in the strictest sense. The term refers to the pendulum modes of the structure while suspended. The term rigid body mode will be used in the sense that none of the flexible body modes are being excited. The low natural frequency of the suspension system and its near frictionless operation effectively isolate the DTA from external disturbances.

The PACOSS Actuators

The actuators used in the active feedback control of the DTA are composed of a solenoid like arrangement with a mass attached to provide an inertial reaction mass. This type of actuator is known as a proof mass actuator or a reaction mass actuator (RMA). A schematic diagram of the actuator assembly is included in Figure 4. The reaction mass is housed in the actuator assembly which includes an accelerometer and a LVDT which measures the relative velocity of the actuator mass with respect to the housing. The accelerometer is attached to the housing and measures the inertial acceleration of the housing itself. A spring is mounted to both the reaction mass and the housing to provide gravity off load for the mass and give the actuator a 1.5 Hz natural frequency relative to the fixed actuator housing (3:38). The location of each of the actuators is depicted in Figure 2. The arrows located on the actuators in Figure 2 show the direction of travel of the reaction masses. The force output of the actuators is along the line of these arrows.

The numbering used to identify the actuators is consistent with the labeling of the structure as it presently exists. Note that numbers 7 and 8 are skipped in this labeling scheme.

One of the actuators was bench tested to confirm the natural frequency using a Hewlett Packard 35660A Dynamic Signal Analyzer. The frequency response function showed that its natural frequency was in fact 1.5 Hz. The actuators have a linear stroke length of approximately ±1 inch. The current drives for the

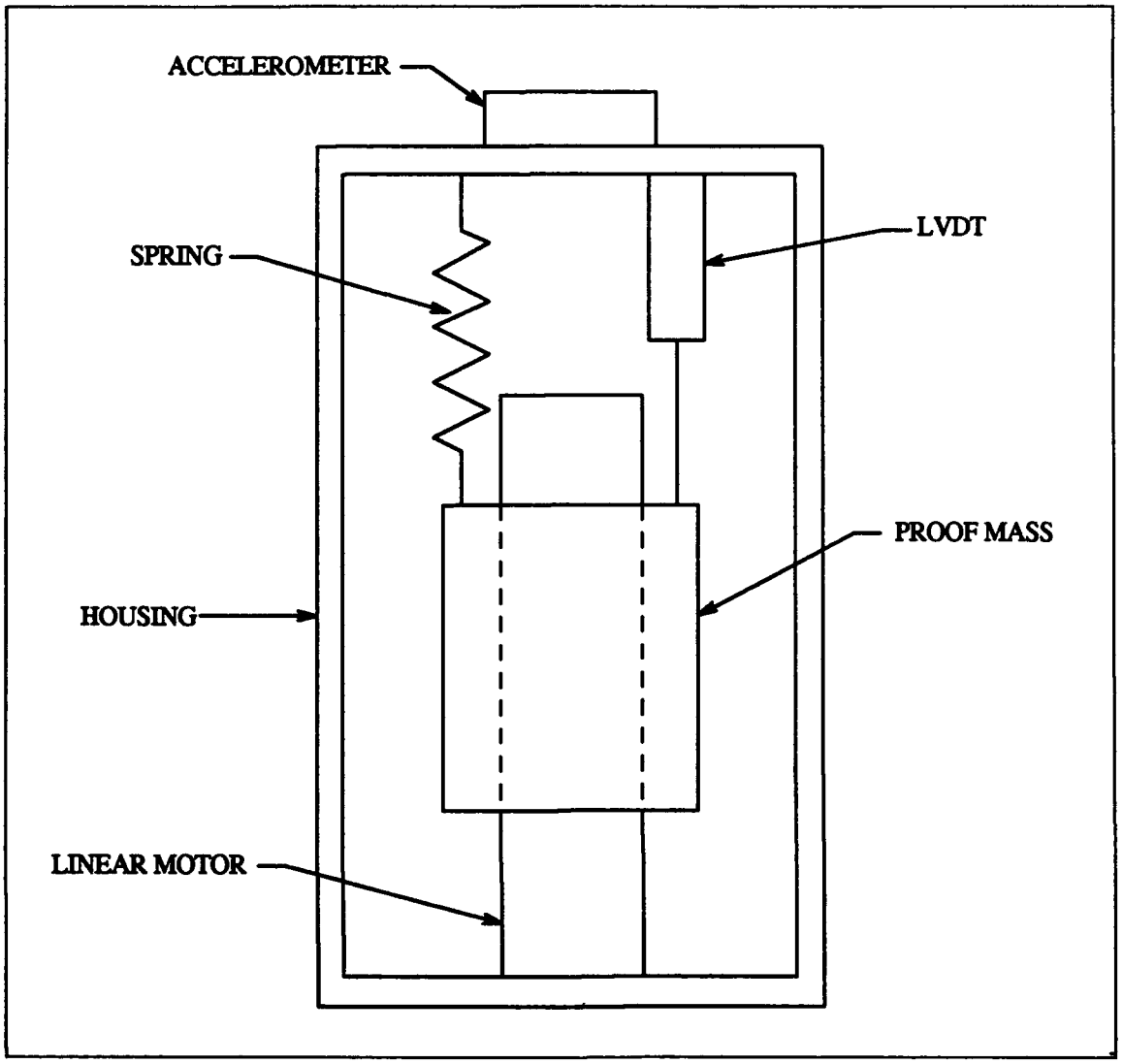

Figure 4: Schematic Diagram of Pacoss Actuator

actuators are located in the PACOSS Motor Control Units.

The accelerometer attached to each actuator housing is a Sunstrand Q-flex Accelerometer model number QA-1400. See Appendix A for serial numbers, certification dates and calibration factors. These accelerometers provide the measurements used in the feedback control of the structural dynamics. The accelerometers are mounted such that the inertial acceleration of the housing and

thus the inertial acceleration of the structure at the attachment point is being measured. Since the accelerometers are virtually collocated with the point of force application, using the measurements at these points does not introduce the problems associated with controlling non-collocated systems, which can be non-minimum phase. As with the actuators, all of the signal processing and power requirements for the accelerometers are supplied by the PACOSS Motor Control Units. The accelerometers are numbered in the same way as the actuators for the purposes here. Thus, the acceleration at actuator location 1 will be referred to as measurement 1, and so on.

The Motor Control Units

As mentioned before, the Motor Control Units provide all of the necessary signal processing and power for the actuator itself and the sensors that are included in the actuator assembly. Figure 5 shows the layout of the motor control units. The control units have been designed with internal analog integrator to yield inertial velocity and relative position from the measured inertial acceleration and the relative position of the masses respectively. They are also capable of performing analog direct rate feedback of the integrated acceleration and the LVDT and integrated LVDT signals (3:34). The gain for the feedback of these signals can be changed by adjustment of the potentiometers located on the front panel of the units.

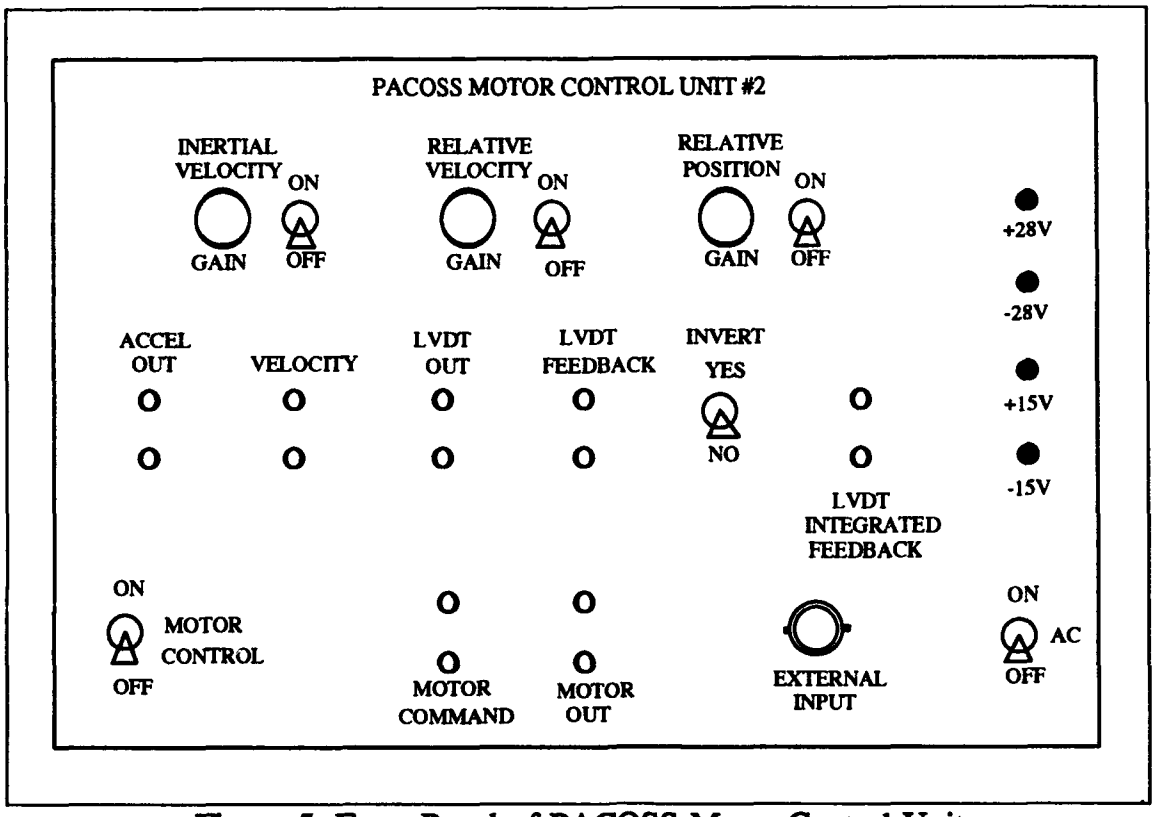

Figure 5: Front Panel of PACOSS Motor Control Unit

In the control systems presented here, the motor control units were only used for integration of the inertial acceleration and as current drives for the actuators. Thus, only these portions of the motor control units will be discussed in depth here. The acceleration output port on the units was connected to a Tektronix Fourier analyzer to generate frequency response data to quantify system performance.

The inertial velocity signal is created from the integration of the inertial acceleration measurement via an analog biquad filter with a 250 DC gain over the inertial acceleration output from the accelerometer. The gain of the integrators was verified through experimental data. The documentation received from Martin Marietta confirms that the gain of the integrators is 250 (3:41). These

measurements were taken with the gain on the potentiometers set to 100 percent. This inertial velocity signal was used in the feedback path for control laws investigated in this report. Although the controller could have been designed to integrate the inertial acceleration, this was not done because it would increase the order of the control law and slow down the digital control system.

The motor control units are equipped with an external motor input port. The control signals were fed into this port to drive the actuators. The model was identified on a voltage in to the external port vs. voltage out from the acceleration port, so the calibration constant for the current drive amplifier is irrelevant to the results. Its calibration constant will be taken into account when the model is identified.

The Systolic Systems Optima/3

The Systolic Systems Optima/3 array processor is very similar to the PC-1000 array processor developed by the same company. However, the Optima has 32 input and output channels and can execute a 64 state linear controller. It is also possible to download programs written in C to allow the processor to execute non-linear control laws. Furthermore, the Optima/3 can be used to acquire data which can be uploaded to the Sun 3/50 host after an experiment. The Optima's maximum sampling rate is limited to 2000 Hz.

In this research, the Optima was used only for linear control law feedback

in conjunction with the Labcom software that provides control over execution times and the downloading of control laws from the host. The analog to digital conversion is provided by 12-bit analog to digital converters with anti-aliasing filters and differential input/output capabilities (1:1). These converters are sampled by the Optima/3 and the signals are processed according to the downloaded control law. Digital to analog converters then output the processed signal.

The host computer for the Optima is a Sun 3/50 computer. The Labcom software is executed on the host which allows controllers to be downloaded into the Optima. The software also allows interactive control of the Optima through the host.

Other Equipment

Several other pieces of equipment and software packages were used to accomplish this research. A Tektronix 2642 Fourier Analyzer was used to collect all of the data and create frequency response functions. The analyzer was supported by a 386 computer and a Tektronix SI5051 Programmable Scanner to expand the available analyzer channels from four to sixteen.

All of the control designs were done using a Sun SPARC Station 2, implementing the control system software MATLAB created by Math Works Inc. This software was also used in all data analysis tasks.

III. Theory

This chapter develops the theoretical basis for the research accomplished in this report. Although most of the terminology used here is standard, some variations do exist in the literature on the subjects discussed.

Model Identification

The method used here for model identification is based on a single premise. That is, if a model can be created which reflects the input to output magnitude and phase information of a system, then that mathematical model is a model of the system in question and no ambiguity exists (8:110).

In light of this, a mathematical model was created to reflect the input to output characteristics of the DTA experimental data. This was done by creating single input to single output (SISO) transfer functions for each of the eight inputs to each of the eight outputs or measurements at the actuator locations. This forms a 64 element multiple input and multiple output (MIMO) transfer function matrix. This transfer function matrix was then assumed to be the MIMO transfer function for the entire system.

In making this assumption, there are several consequences that must be noted. The first it must be assumed that all of the poles that are excited by any input are observed somewhere in the output or measurements (ie. all of the poles

are observable). Also, it is assumed that the interaction between any two inputs does not excite poles that are not excited by either of the inputs taken alone. Furthermore, the resulting model, once placed in state variable form, is not in physical coordinates and cannot be transformed into physical coordinates by any simple similarity transformation.

In developing the SISO transfer functions, the DTA was assumed to be second order in nature. For a one degree of freedom system this yields the transfer function for a damped harmonic oscillator:

$$\frac{Y(s)}{U(s)} = \frac{1}{s^2+2\zeta\omega_n s+\omega_n^2} \tag{1}$$

where Y(s) is the Laplace transform of the output, U(s) is the Laplace transform of the input, ω_n is the natural frequency and ζ is the percent critical viscous damping ratio. A similar representation can be created for a second order damped zero:

$$\frac{Y(s)}{U(s)} = \frac{s^2+2\zeta\omega_n s+\omega_n^2}{1} \tag{2}$$

If the natural frequencies and damping ratios of the poles and zeros can be identified, then finding the SISO transfer function for the system is a simple matter of writing the respective poles and zeros in the form of either equation (1) or (2) and multiplying all of these transfer functions together. In the case where the structure is continuous, as with the DTA, the multiplication of these transfer

functions together represents an infinite series. To obtain a mathematical model of the system the series must be truncated. This leaves a model which is acceptable up to a certain frequency limit. The gain of the system can be adjusted by multiplying the entire SISO transfer function by the appropriate constant.

When the data being fitted is experimental in nature, it becomes necessary to identify the low frequency behavior of the system using means other than the one described above. This is so because generally experimental data below 1 Hz is very poor and unreliable due to the lack of frequency resolution near zero. To overcome this obstacle, a simplified model of a single actuator acting on a structure was created.

Figure 6 shows a simplified model of a structure and actuator pair (7:510). The open loop equations of motion for this system are:

$$\begin{bmatrix} m & 0 \\ 0 & m_a \end{bmatrix} \begin{Bmatrix} \ddot{x} \\ \ddot{x}_a \end{Bmatrix} + \begin{bmatrix} c+c_a & -c_a \\ -c_a & c_a \end{bmatrix} \begin{Bmatrix} \dot{x} \\ \dot{x}_a \end{Bmatrix} + \begin{bmatrix} k+k_a & -k_a \\ -k_a & k_a \end{bmatrix} \begin{Bmatrix} x \\ x_a \end{Bmatrix} = \begin{bmatrix} -f_a \\ f_a \end{bmatrix} \tag{3}$$

where the subscript refers to the actuator and m, c, and k, stand for the mass, viscous damping coefficient and stiffness, respectively. f_a is the force exerted between the two masses by the actuator. The Laplace Transform of this matrix differential equation is:

$$\begin{Bmatrix} X(s) \\ X_a(s) \end{Bmatrix} = \frac{\begin{Bmatrix} m_a s^2 \\ ms^2+cs+k \end{Bmatrix}}{\det[s^2[M]+s[C]+[K]]} F_a(s) \tag{4}$$

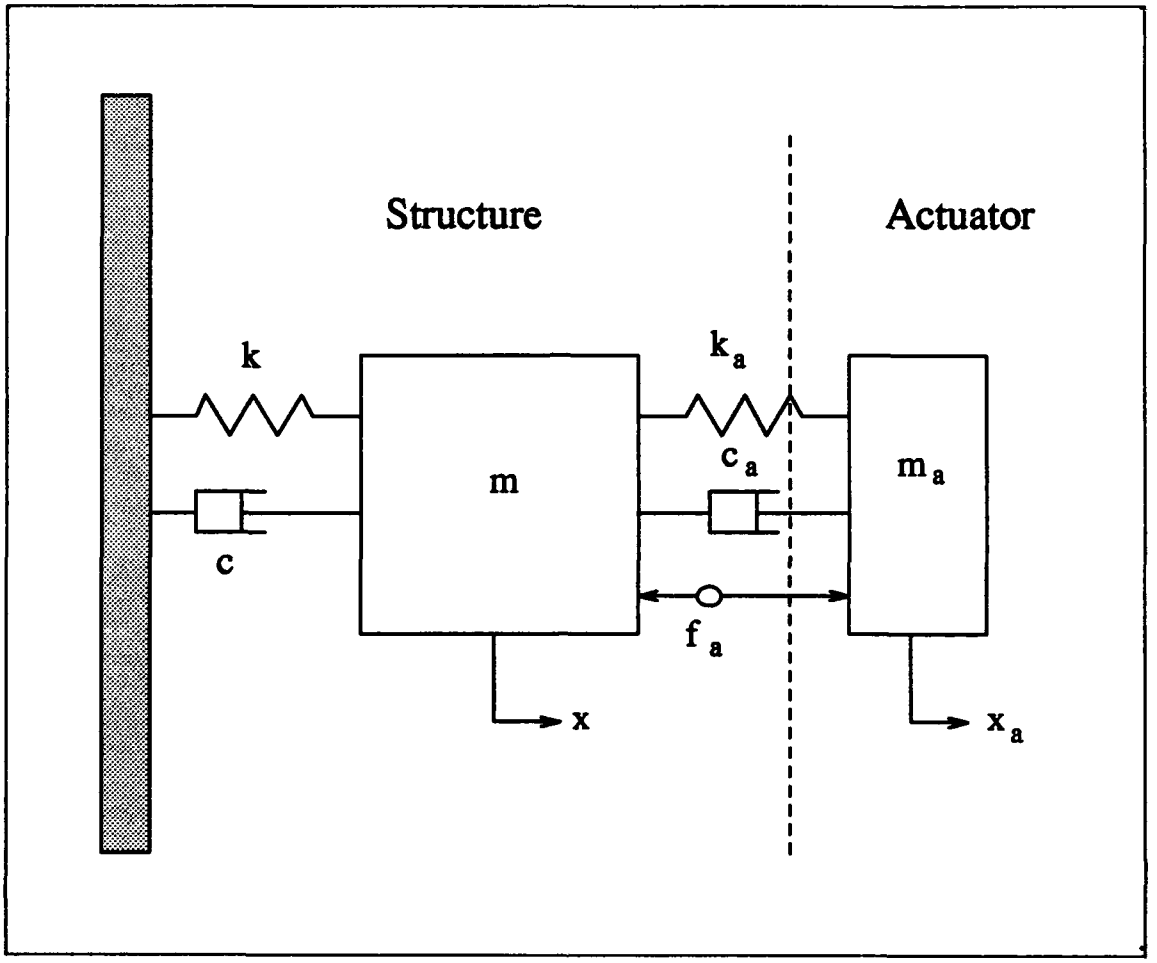

Figure 6: Schematic Diagram of Simplified Structure and Actuator Pair

where [M], [K], and [C] are the mass, damping, and stiffness matrices respectively found in equation (3). Here it is observed that the displacement variable that corresponds to the structure has a double zero at the origin. Thus, it is reasonable to assume that the low frequency behavior of the DTA exhibits the same behavior since this simplified model is in the same configuration.

Now that it is possible to create the transfer function matrix for the system, it becomes necessary to convert the system into a more useable form. In order to use modern control techniques, the system must be represented in state variable

form or state space form. This can be done in any number of ways since there are an infinite number of state space realizations for any given system.

Once a state space realization is found it can be transformed into different but equivalent realizations by applying a similarity transformation to the state variable. The transformation that is of interest is the transformation to the Block Diagonal Form. Take for instance the following state space system:

$$\begin{aligned} \{\dot{x}\} &= A\{x\} + B\{u\} \\ \{y\} &= C\{x\} + D\{u\} \end{aligned} \tag{5}$$

and let [A] have a set of m+1 distinct complex conjugate pair eigenvalues $\lambda_{1,2}=\sigma_1 \pm j\varpi_1$, $\lambda_{3,4}=\sigma_2 \pm j\varpi_2$,..., $\lambda_{m,m+1}=\sigma_m \pm j\varpi_m$, and the remaining eigenvalues real and distinct. Then the real n x n transformation matrix:

$$\begin{aligned} P_b = [&Re\{\xi_1\}, Im\{\xi_1\}, Re\{\xi_3\}, Im\{\xi_3\}, \ldots, \\ &Re\{\xi_m\}, Im\{\xi_m\}, \xi_{m+2}, \ldots, \xi_n] \end{aligned} \tag{6}$$

transforms [A] to the block diagonal form, where Re and Im stand for the real and imaginary parts of the complex eigenvector ξ (8:344). Using this coordinate transformation equation (5) transforms to the new state variables such that:

$$\begin{aligned} \bar{A} &= P_b^{-1} A P_b \\ \bar{B} &= P_b^{-1} B \\ \bar{C} &= C P_b \\ \bar{D} &= D \end{aligned} \tag{7}$$

where [Ã] is now of the special form:

$$\tilde{A}=diag\left\{\begin{bmatrix}\sigma_1 & \omega_1\\ -\omega_1 & \sigma_1\end{bmatrix},\begin{bmatrix}\sigma_3 & \omega_3\\ -\omega_3 & \sigma_3\end{bmatrix},\cdots,\begin{bmatrix}\sigma_m & \omega_m\\ -\omega_m & \sigma_m\end{bmatrix},\lambda_{m+2},\cdots,\lambda_n\right\} \tag{8}$$

This form is very useful in that the states are now decoupled into groups that correspond to the same complex conjugate eigenvalue pair. Once the SISO transfer functions are created, each of them is transformed into state space and then transformed into the block diagonal form using this transformation. Since the states are decoupled according to their complex conjugate pair, it is a simple matter of combining the SISO transfer functions into a MIMO state space system.

Direct Rate Feedback

The simplest form of feedback is proportional feedback of the outputs of a system. If such a feedback scheme can be guaranteed to be stable it is desirable to use this type of control law because it requires very little computational power to execute. Thus it is likely to be more reliable than other more complex controllers, and it is usually very robust.

With this in mind, consider the class of dynamic systems modeled by the equation of motion:

$$M\{\ddot{x}\}+C\{\dot{x}\}+K\{x\}=D\{u\} \tag{9}$$

where {x} is a vector describing the position of the system and {u} is the control input. [M], [C], [K], and [D] are the mass, damping, stiffness, and control influence matrices, respectively. It is assumed that the open loop system is stable. Now let the control input be defined by the proportional feedback of the velocity such that:

$$\{u\} = -GD^T\{\dot{x}\} \tag{10}$$

where [G] is a positive definite symmetric gain matrix and the [D^T] term is included for the case where {x} and {u} are not the same length. This form of the control law is valid for collocated force and sensor locations. The closed loop equation of motion for the system becomes:

$$M\{\ddot{x}\} + [C + DGD^T]\{\dot{x}\} + K\{x\} = \bar{0} \tag{11}$$

For the combination of this type of system and controller, stability is guaranteed. Consider the following positive definite Lyapunov function, which is in this case the system energy:

$$V = \frac{1}{2}\{\dot{x}\}^T M\{\dot{x}\} + \frac{1}{2}\{x\}^T K\{x\} \tag{12}$$

By differentiating Equation (12) with respect to time and substituting equation (11) into this derivative it can be seen that:

$$\dot{V} = -\{\dot{x}\}^T [C + DGD^T]\{\dot{x}\} \tag{13}$$

It is obvious that equation (13) is negative semi-definite and therefore the system

is asymptotically stable (9:390-1).

From the analysis above, it can be seen that for this special situation global stability is guaranteed for any gain [G] as long as [G] is positive definite. As stated before, this alternative for a control law is very attractive because of its simplicity and its guaranteed stability in the face of plant uncertainties. However, this is not a complete picture of the situation presented in this report. This type of analysis neglects the effects of the actuator dynamics.

A more complete picture of the case at hand is illustrated in Figure 6 from the proceeding section. The system is not strictly collocated when a gain is put on the inertial velocity $\{\dot{x}\}$ of the structure and fed back. In fact at some gain this system will become unstable under output feedback. Note, however that the system would be collocated if the relative velocity of the actuator with respect to the housing and the inertial velocity were used in the feedback scheme. The difference of these two values would yield the inertial velocity of the reaction mass and the system would be strictly collocated as well as globally stable. The control law that is generated by this feedback scheme is the same as placing a dashpot between the structure and the reaction mass. Although by itself this type of "dashpot" feedback is rather uninteresting, it has been shown that the combination of rate feedback and "dashpot" feedback can increase the amount of damping introduced by the control system over using rate feedback alone (15:449-58). This type of feedback is not addressed in this thesis.

The closed loop equation for the proportional feedback of the inertial velocity of the structure in Figure 1 is:

$$\begin{bmatrix} m & 0 \\ 0 & m_a \end{bmatrix} \begin{Bmatrix} \ddot{x} \\ \ddot{x}_a \end{Bmatrix} + \begin{bmatrix} c+c_a+g & -c_a \\ -g-c_a & c_a \end{bmatrix} \begin{Bmatrix} \dot{x} \\ \dot{x}_a \end{Bmatrix} + \begin{bmatrix} k+k_a & -k_a \\ -k_a & k_a \end{bmatrix} \begin{Bmatrix} x \\ x_a \end{Bmatrix} = \begin{bmatrix} 0 \\ 0 \end{bmatrix} \tag{14}$$

where g is the scalar gain placed on the inertial velocity (7:511).

Figure 7 shows a root locus plot of this idealized system for increasing

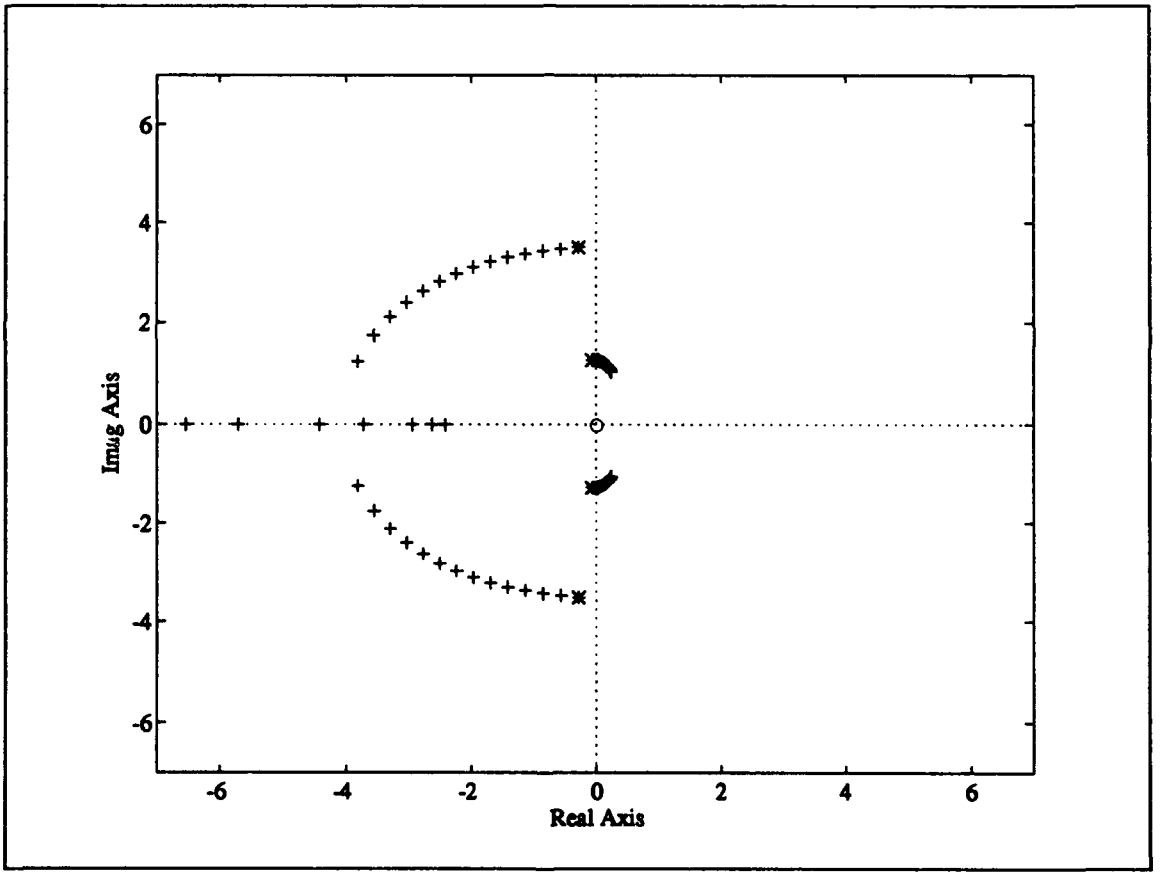

Figure 7: Root Locus Plot of Structure and Actuator Pair Under Direct Rate Feedback

values of gain g. It is observed that one pair of poles heads directly into the right half plane as the gain is increased and becomes unstable. Thus, there is a limit on

the gain if the system is to remain stable. It is expected that the DTA will exhibit this same behavior when subjected to proportional feedback of the inertial velocity. Therefore, there will be a limit on the amount of damping achievable under this type of feedback.

Linear Quadratic Control

Optimal control theory is based upon minimizing a performance index which balances the speed of response of a system with the amount of control energy required. The method is based on the premise that there exists a mathematical model of the system in question and that it is reasonably accurate. If the plant uncertainties are to large, then this method of control can yield unstable solutions. Other methods of optimal control are available which are more able to deal with plant uncertainties such as Loop Transfer Recovery (LQG/LTR), however these methods are not investigated here.

The following development follows that used by Ridgely and Banda (see reference 10). Consider the following state space system:

$$\{\dot{x}\} = A\{x\} + B\{u\} \tag{15}$$

where, for now, there are no assumptions on open loop stability of the plant. The standard steady-state, time-invariant, linear quadratic regulator has the following performance index:

$$J=\int_0^{\infty}[x^T(t)Qx(t)+u^T(t)Ru(t)]dt \tag{16}$$

where [Q] and [R] are positive semi-definite and positive definite symmetric weighting matrices, respectively. These matrices are chosen by the designer to weight the importance of the states and controls. The relative magnitudes of [Q] and [R] with respect to one another increases or decreases the amount of control effort used in the closed loop control. The relative sizes of elements within either [Q] or [R] weight the individual states and controls individually.

If the pair [A],[B] is stabilizable then a full state feedback law of the form:

$$u(t)=-Kx(t) \tag{17}$$

can always be found that makes the closed loop system:

$$\begin{aligned}\dot{x}(t)&=Ax(t)+B[-Kx(t)]\\&=[A-BK]x(t)\end{aligned} \tag{18}$$

asymptotically stable. Here [K] is the full state feedback gain matrix.

The gain matrix [K] can be found via the solution of the following algebraic matrix Riccati equation:

$$0=A^TP+PA-PBR^{-1}B^TP+Q \tag{19}$$

where:

$$K=R^{-1}B^TP \tag{20}$$

In the application of the LQR method here, the weighting matrices will be chosen such that desired closed loop damping ratios will be achieved in the mathematical model. For the most part, this is an iterative process, although starting points for this process can be identified if something is known about the maximum actuator control energy.

Since in general, the full state is not measurable on a system, a method must be used to recreate the full state from knowledge of the plant process and the measurements that do exist. A device that does this is called an observer. A special type of observer called the Linear Quadratic Estimator (LQE) or Kalman Filter will be used here. The use of LQR in conjunction with a Kalman Filter is called Linear Quadratic Gaussian (LQG) control. The development for LQE closely parallels that of LQR.

Consider the stochastic linear system of the form:

$$\begin{aligned} \{\dot{x}\} &= A\{x\} + B\{u\} + G\{w\} \\ \{y\} &= C\{x\} + \{v\} \end{aligned} \tag{21}$$

where {w} and {v} are the process and measurement noise vectors respectively. {w} and {v} are assumed to be zero mean, stationary, uncorrelated white Gaussian noises with autocorrelations:

$$\begin{aligned} E[\{w(t)\}^T\{w(t-\tau)\}] &= Q_0\delta(\tau) \\ E[\{v(t)\}^T\{v(t-\tau)\}] &= R_0\delta(\tau) \end{aligned} \tag{22}$$

where $[Q_0]$ and $[R_0]$ are the intensities of the noises, $\delta(\tau)$ is the delta function and

E[*] denotes expected value. Here, $[Q_0]$ is positive semi-definite and $[R_0]$ is positive definite and both of these matrices are symmetric.

It is possible to find a gain matrix [L] for the estimator that minimizes the mean square value:

$$E[\{e(t)\}^T\{e(t)\}] \tag{23}$$

where {e(t)} is defined as the estimate error by the equation:

$$\{e(t)\}=\{x(t)\}-\{\hat{x}(t)\} \tag{24}$$

and $\{\hat{x}(t)\}$ is defined as the state estimate by:

$$\{\dot{\hat{x}}(t)\}=A\{\hat{x}(t)\}+B\{u(t)\}+L[\{y(t)\}-C\{\hat{x}(t)\}] \tag{25}$$

The solution to this set of equations is found via the solution of another algebraic matrix Riccati equation:

$$0=A\Sigma+\Sigma A^T+GQ_0G^T-\Sigma C^T R_0^{-1} C\Sigma \tag{26}$$

The Kalman filter or estimator gain matrix is given by:

$$L=\Sigma C^T R_0^{-1} \tag{27}$$

The LQG compensator can be derived by substituting u=-K{x} into equation (25). After substitution and some algebraic manipulation this yields:

$$\{\dot{\hat{x}}(t)\}=[A-BK-LC]\{\hat{x}(t)\}+L\{y(t)\} \tag{28}$$

Taking the laplace transform of this equation and rearranging gives:

$$\{\hat{x}(s)\} = -K[sI - A + BK + LC]^{-1}L\{y(s)\} \tag{29}$$

Under the assumption that $\{\hat{x}(t)\}$ is an accurate estimate of $\{x(t)\}$ then equation (17) can be substituted into equation (29) to yield the expression for the LQG compensator:

$$\{u(s)\} = -K[sI - A + BK + LC]^{-1}L\{y(s)\} \tag{30}$$

In generating this type of compensator, it was necessary to define the process and noise intensity matrices Q_0 and R_0. If very little is known about the noise vectors then they can be chosen in a similar manner as Q and R were chosen for LQR. By making the plant disturbance intensity matrix Q_0 large with respect to the measurement noise intensity R_0 the compensator puts more emphasis on the measurement when constructing the state estimate and vice versa. Thus if the plant uncertainties are large due to unmodeled dynamics, Q_0 should be large in order to accurately reconstruct the state vector.

A method is available that can be used to quantify the plant uncertainties of a system. If the frequency response of the true plant is known, which can be obtained through experimental measurements, then a measure of the accuracy of a mathematical model of the system can be found. The measure that will be utilized here is known as additive perturbation and is defined as:

$$\Delta(s) = G_{true}(s) - G_{model}(s) \tag{31}$$

where $\Delta(s)$ is the perturbation or error, $G_{true}(s)$ is the true plant loop transfer matrix and $G_{model}(s)$ is the model loop transfer matrix. The loop transfer matrix is defined as K(s)H(s) where K(s) is the compensator transfer function and H(s) is the transfer function of the plant of true system or the mathematical model. Thus:

$$\begin{aligned} G_{true}(s) &= K(s)H_{true}(s) \\ G_{model}(s) &= K(s)H_{model}(s) \end{aligned} \tag{32}$$

Substitution of equation 32 into equation 31 yields:

$$\Delta(s) = K(s)[H_{true}(s) - H_{model}(s)] \tag{33}$$

The expression in brackets on the right hand side of equation 33 is simply the difference of the frequency responses of the true (or measured) open loop plant and the mathematical model open loop plant (10:3-5). Thus, $\Delta(s)$ is a matrix of the same dimensions as the mathematical transfer function matrix.

The magnitude of $\Delta(s)$ is a metric of the error between the true plant and the mathematical model of the plant. One way to quantify the magnitude of $\Delta(s)$ is by the maximum singular value of $\Delta(s)$. Note that this value will be a function of s or frequency.

The robustness criteria for this type of plant perturbation is:

$$\underline{\sigma}[\Delta(s)] > \bar{\sigma} K[I + G_{model}(s)]^{-1} \tag{34}$$

where σ and $\underline{\sigma}$ denote maximum and minimum singular values, respectively. Thus if the minimum singular value of the error matrix $\Delta(s)$ is greater that the maximum singular value of the sum of the identity matrix mathematical model's loop transfer matrix times K, then the closed loop system is guaranteed to be stable.

It must be noted that this test is conservative and if a system fails this test then it is not necessarily unstable. However, if it passes the test then it is guaranteed to be stable (16:365-357).

IV. Experimental Procedure

The following sections detail the procedures used for model identification, controller design and data analysis. It will be assumed that the operation of standard equipment is well known and will not be reiterated here. However, the settings used on standard equipment will be mentioned. The design and data analysis was accomplished using the control software MATLAB by Math Works Inc. References to the commands used in this software will be italicized to indicate a MATLAB command. For more information on these commands see reference (11).

Identification Procedure

As mentioned in Chapter III the model was identified on an input to output basis based solely on experimental measurements of the open loop system. Figure 8 illustrates the equipment configuration used to gather this data.

The frequency response data that was used in transfer function matching was generated by a Tektronix Fourier analyzer (12). A Hanning windowing type was used with 50% overlap and 2048 samples per frame. Fifteen averages were taken to ensure high quality data. The base bandwidth was set to 20 Hz and the output from the analyzer was set to a 0.6 Vrms random signal with a bandwidth from 0 - 20 Hz. The voltage level of the output was set to keep the actuator from

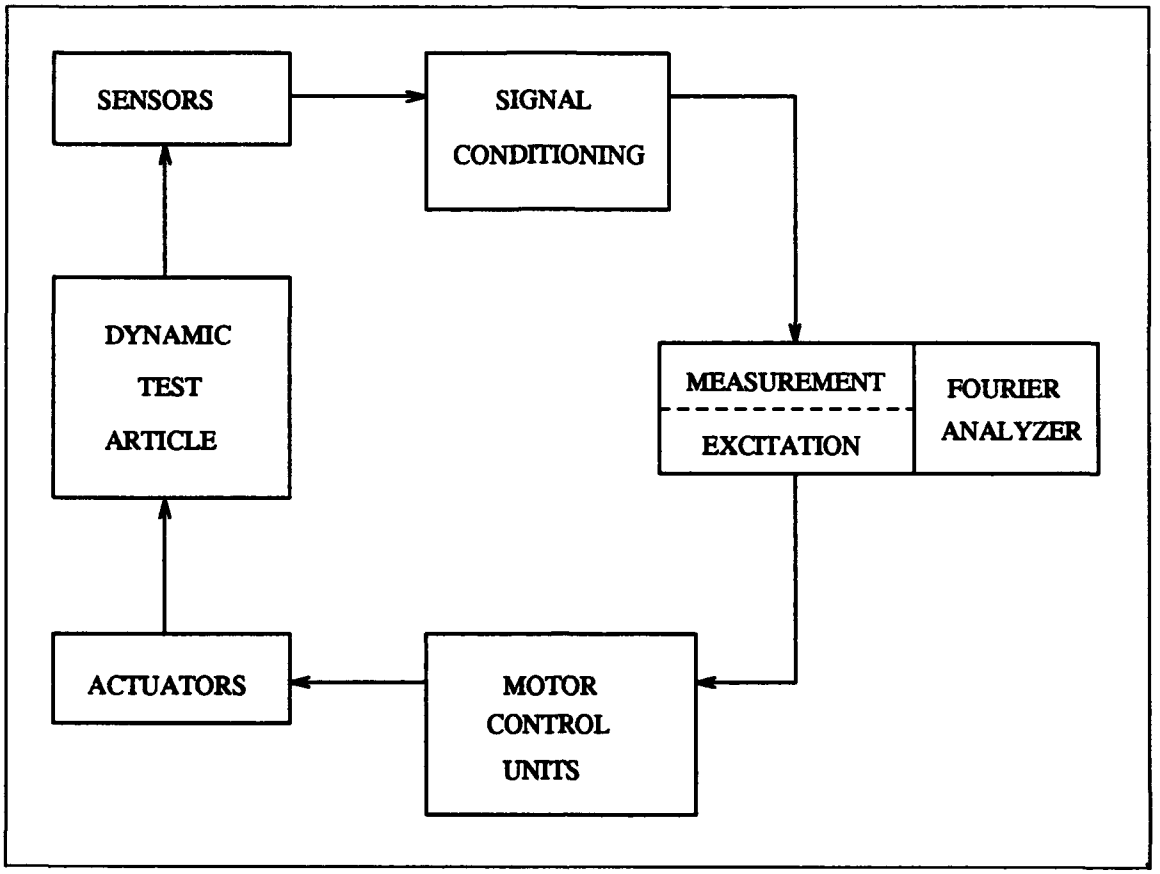

Figure 8: Open Loop Configuration of Equipment

saturating and hitting the stops. These settings give a frequency resolution of .025 Hz. The Martin Marietta Team recommended a frequency resolution of .03125 Hz to accurately measure the structural dynamics of the DTA (13:20).

Measurements were taken for all eight inputs at the actuators to all of the eight outputs at the accelerometers located within the actuator assemblies. This gives a total of 64 frequency response functions, where the units on the magnitude are a voltage proportional to the acceleration per voltage at the input. These frequency response functions were then converted to ASCII format and imported into MATLAB.

The data was matched by picking transfer functions of the form of equations (1) and (2) and multiplying them together using the *CONV* command. The transfer functions were also multiplied by a constant and an s^4 term. The constant adjusted the DC gain of the transfer function and the s^4 term represents a double zero at the origin and two derivatives with respect to time. The derivatives account for the fact that the measurement is proportional to the acceleration. An *M-File* was created that multiplied the individual transfer functions together and displayed their frequency response magnitude and phase information on a plot together with the measured data. The natural frequencies and damping ratios were varied until the plots coincided as closely as possible. Both the magnitude and phase information was used to determine these two parameters.

After all 64 transfer functions were identified, it was assumed that the poles in the different transfer functions that were at the same frequency were in fact the same flexible body mode. For this to occur, the damping ratios of each complex conjugate pair of poles has to be the same. After all 64 transfer functions were found, an average of the damping ratios at each frequency was taken to determine the damping ratio that would be applied to all of the poles at that frequency.

The two plots in Figure 9 show this to be a good assumption. These plots show the experimental response at the accelerometers located at actuator numbers 1 and 2 when a random signal is exciting actuator number 1. These plots are of the final model in which the averaging of the damping ratios has been

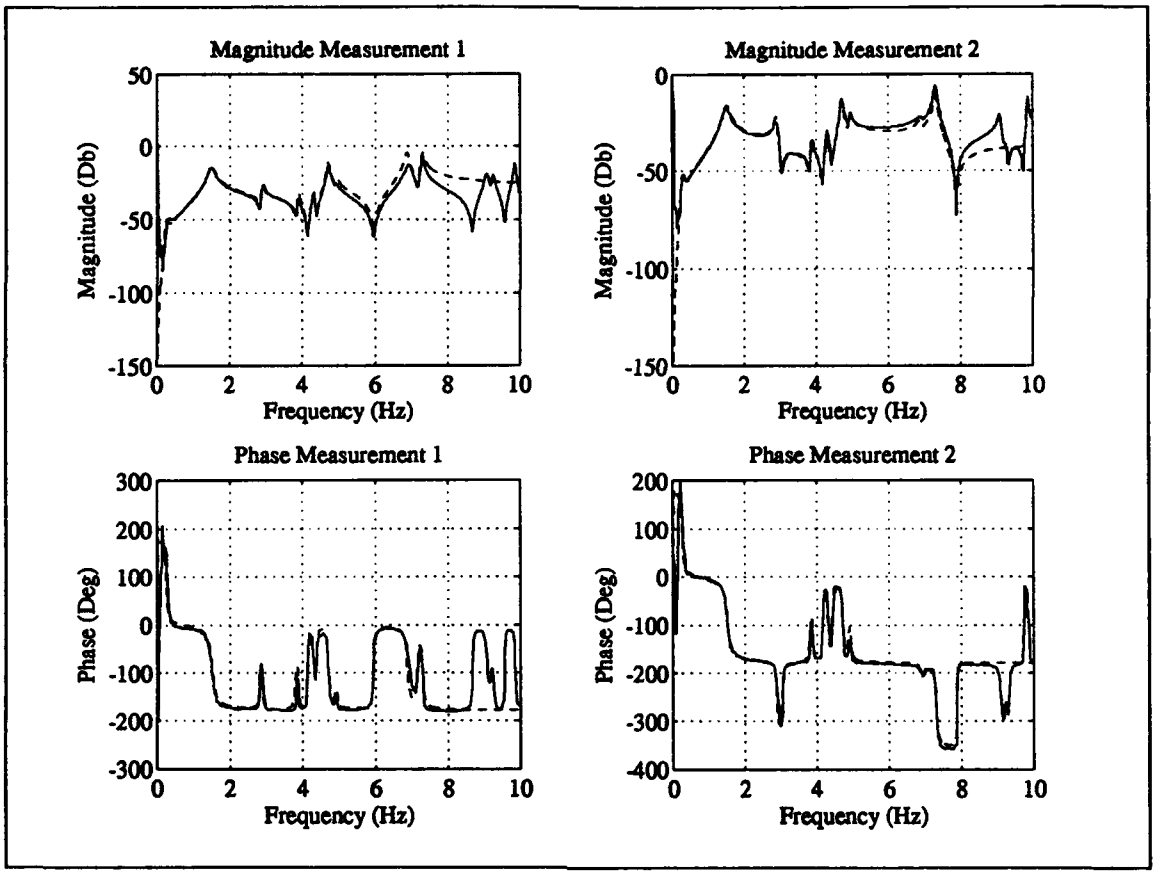

Figure 9: Frequency Response Functions of Excitation of Actuator #1 and Measurement at #1 and #2 (Analytical vs. Experimental)

accomplished. The measured signal is shown in solid lines while the theoretical model is shown in dashed lines. Note that the model was only matched for modes under 8 Hz.

The plots for all 64 transfer functions vs. their respective experimental frequency response functions are included in Appendix B.

The final step in finding the mathematical model for the system is converting the transfer functions into state space form. For SISO systems a state space realization can always be found such that the order of that state space model

is the same as the order of the denominator of the SISO transfer function. However, for MIMO systems, this is not always the case. In general, the order of a minimal realization of a MIMO transfer function is greater than the order of the least common denominator of the transfer function matrix (14:348). That is, for a MIMO transfer function, where the order of the least common denominator is n, the order of the state space realization of that system is in general greater than n. This becomes a serious problem in that the Optima/3 Array Processor can only deal with a limited number of states in the controller. Since an LQG controller is of the same order as the plant model, a large plant may exceed the limitations of the equipment being used.

Other difficulties are encountered in converting large order system transfer functions to state space form. In attempting to convert the entire 64 element transfer function matrix to state space, it was found that the operation is numerically unstable using MATLAB routines. This is due to the fact that the mathematical model has a least common denominator that is 34^{th} order. When this polynomial is multiplied out, its coefficients approach the numerical precision of the computer being used.

To circumvent these problems only the collocated transfer functions were placed into the state realization. That is, the diagonal of the transfer function matrix was used to create the entire state space model. This was accomplished by converting the individual collocated transfer functions into state space individually

using a numerically stable algorithm in MATLAB called *ZP2SS*. This function takes a SISO system described by its pole and zero locations and converts it to state space in lower triangular form. It is numerically stable because it relies on the pole and zero locations instead of the numerator and denominator polynomials which are numerically ill-conditioned in the case at hand.

Once the eight diagonal transfer functions were converted into eight separate SISO state space models they were each transformed to block diagonal state space form using the similarity transformation described in Chapter III. As mentioned before, when the state space model is described in this form the second order modes of the system are decoupled. Furthermore, the eight state space models all have the same flexible body poles. Thus some of the blocks along the diagonal of the [A] matrix are the same in all eight SISO models. This fact allows the eight SISO state space models to be augmented together to form an eight input - eight output MIMO state space system.

Obviously, the use of only the diagonal of the transfer function matrix introduces errors in the state space model. However, they are minimized because the transfer functions that were used to make the state space model were the transfer functions for the collocated sensor and actuator pairs. Since it is likely that the motion of the actuator at the collocated position is apt to affect the output of its collocated sensor more than any other actuator the assumption is reasonable. Furthermore, upon comparison of the non-collocated sensor and actuator frequency

response functions, for the state space model and the experimental data, it is seen that the main effect of these procedures was to move the location of the zeros. The pole locations were not affected by these assumptions.

These procedures yield a state space model for the DTA that has 34 states. The frequency response functions of the state space model vs. their respective experimental measurements are included in Appendix C.

Controller Design

From the development in Chapter III, it is known that a direct rate feedback controller will eventually become unstable as the gain is increased. However, the gain at which this occurs is not predictable from the mathematical model. The modes that are destabilized are the rigid body motions of the suspended structure which are all below 0.4 Hz. Since the data in this region is poor, the frequencies and damping values are not well defined. Therefore, iteration was used to find the direct rate feedback gains that keep the system stable under this type of feedback.

Figure 10 shows a diagram of the closed loop configuration of the equipment. A disturbance was introduced into the system by summing the feedback signal of actuator #1 with the same random signal used in the identification process described above. Actuator #1 was chosen for the disturbance because it excites all of the poles that were included in the mathematical model. There are other actuator locations with this property and they would be suitable for

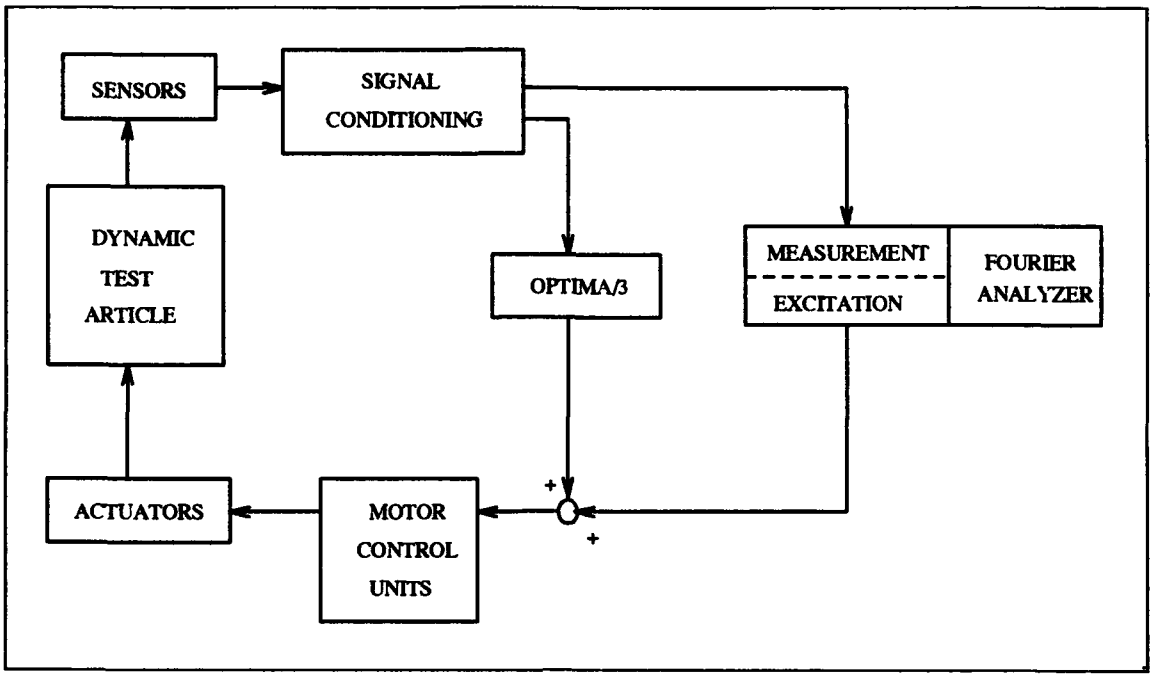

Figure 10: Closed Loop Configuration of Equipment

the disturbance as well. The setup of the Fourier analyzer was the same as that described above for model identification.

For this simple feedback scheme, the Optima/3 is capable of running at a sample rate of 1000 Hz. Since the frequencies of interest are well below this, the system appears to be continuous. Therefore, discrete effects were not considered.

Measurements of the response while the loop was closed were only taken at the accelerometer corresponding to actuators 1 and 2. The measurements at these two points contain all of the poles of the system and adequately reflect closed loop system performance.

The second type of controller used was LQG. This controller was designed using the commands *LQR* and *LQE* in MATLAB. These functions execute the same routines that were described in Chapter III. The weighting matrices were

found by iteration until the theoretical closed loop system had the desired closed loop performance. In this case, the goal was to exceed the damping achieved by the direct rate feedback controller. The controller was then discretized using the *C2D* command. Again because of the uncertainties associated with the rigid body motion of the structure, the weighting of these states was very small to ensure that the LQG routine does not place a large gain on these poles.

The Optima/3 was capable of running this 34 state controller at a sampling rate of 500 Hz. This is still much greater than the frequencies of interest; thus, the controller was designed using continuous time techniques. Once again the measurements were taken only at actuator locations 1 and 2 to evaluate system performance.

Singular value plots of both the transfer function model and the state space model errors were created to show the amount of error that was generated from creating the state space model in this manner. Further more, the stability robustness test was applied to the LQG compensator to see if it had a chance of being stable .

V. Results

The results of the above procedures are described in the paragraphs that follow. The theoretical and experimental values for damping are compared and the respective frequency plots are shown. The values for the closed loop damping ratio are found using the same method as that used in the model identification portion of the research.

Table 1: Experimental and Theoretical Damping Ratios for Closed Loop System

Flexible Mode #	Open Loop	Closed Loop Experimental with Direct Rate Feedback		Theoretical Prediction
		Measurement #1	Measurement #2	
1	0.0500	0.2000	0.2000	0.2012
2	0.0100	0.0310	0.0400	0.1158
3	0.0080	0.0250	0.0150	0.0185
4	0.0120	0.0240	0.0150	0.0277
5	0.0070	0.0250	0.0310	0.0292
6	0.0075	0.0250	------	0.0542
7	0.0068	0.0250	0.0100	0.0491
8	0.0050	0.0300	0.0180	0.0641

Table 1 shows the damping values for the flexible modes of the system for both the Experimental and theoretical cases. Although the experimental damping factors are not as high as those expected from the theory, they still show a significant improvement in the damping characteristics of the structure.

Table 2: Gain Matrix for Direct Rate Feedback

$$[K]= \begin{bmatrix} .32 & 0 & 0 & 0 & 0 & 0 & 0 & 0 \\ 0 & .72 & 0 & 0 & 0 & 0 & 0 & 0 \\ 0 & 0 & .72 & 0 & 0 & 0 & 0 & 0 \\ 0 & 0 & 0 & .72 & 0 & 0 & 0 & 0 \\ 0 & 0 & 0 & 0 & .72 & 0 & 0 & 0 \\ 0 & 0 & 0 & 0 & 0 & .72 & 0 & 0 \\ 0 & 0 & 0 & 0 & 0 & 0 & .16 & 0 \\ 0 & 0 & 0 & 0 & 0 & 0 & 0 & .16 \end{bmatrix}$$

Table 2 shows the gain matrix used in the direct rate feedback scheme. Note that the gain for actuator #1 (.32) is smaller than the gain for the rest of the actuators located on the ring truss. This was necessary to keep actuator #1 from saturating due to the added input disturbance signal. The gain for actuators #9 and #10 which are located on top of the apex plate (.16), is much smaller than the gain for the actuators located on the ring truss. This occurs because the pendulum modes of the system are more controllable from the apex plate due to the added moment of their location.

The data for the damping values obtained from the application of LQG is not available because for any appreciable gain, the closed loop system was unstable. Once the system begins to be unstable, the structure vibrates violently

and the actuators begin to saturate. Whenever this started to occur, the experiment was stopped which precludes the gathering of data. When the gain is very low, using LQG, the system is stable; however, the frequency response data is virtually

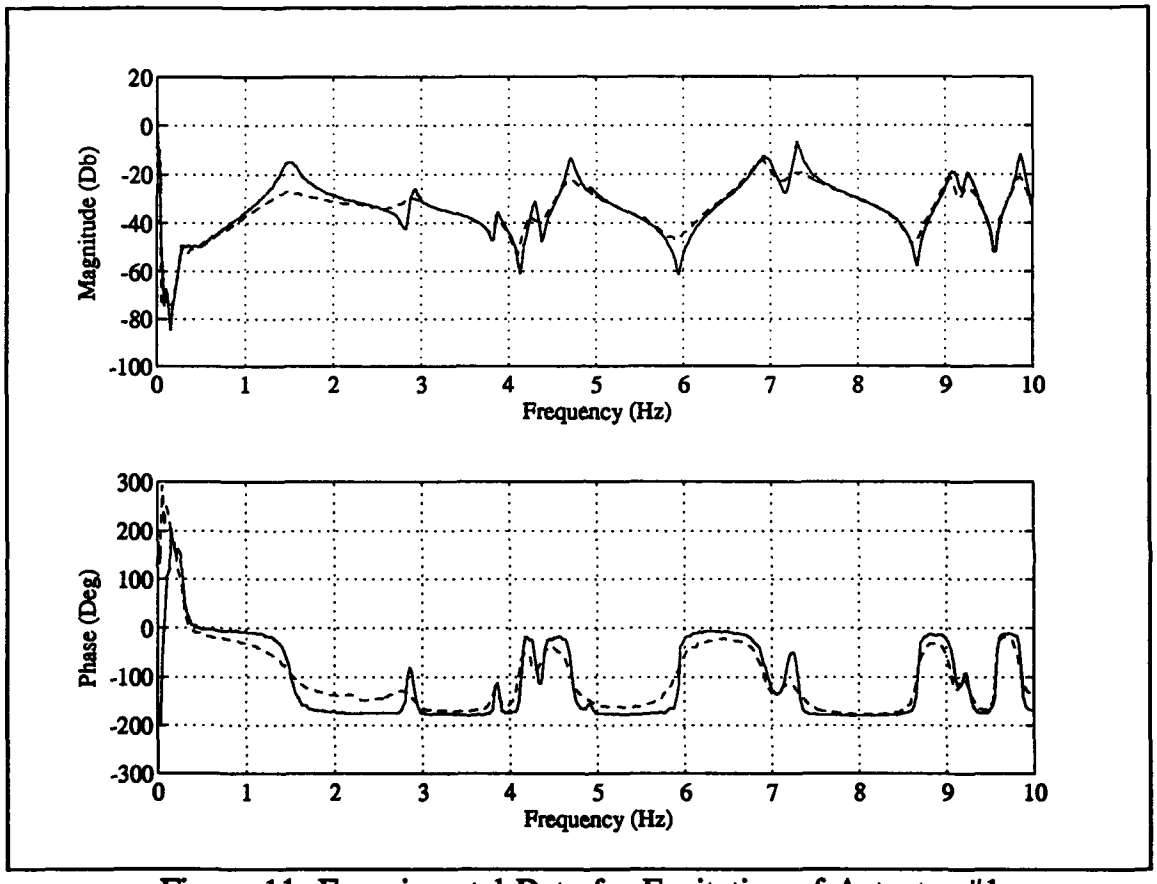

Figure 11: Experimental Data for Excitation of Actuator #1 and Measurement at Actuator #1 (Open Loop ——— Closed Loop -----)

indistinguishable from the open loop data. For these values of gain, the theoretical model predicts a nominal change in the closed loop damping ratios as well.

Figure 11 displays the experimental frequency response data for the direct rate feedback control law against the open loop experimental data. The dashed

lines represent the closed loop system response. These curves are for the response generated from the accelerometer at the location of actuator #1.

Figure 12 displays this same information except that the response is

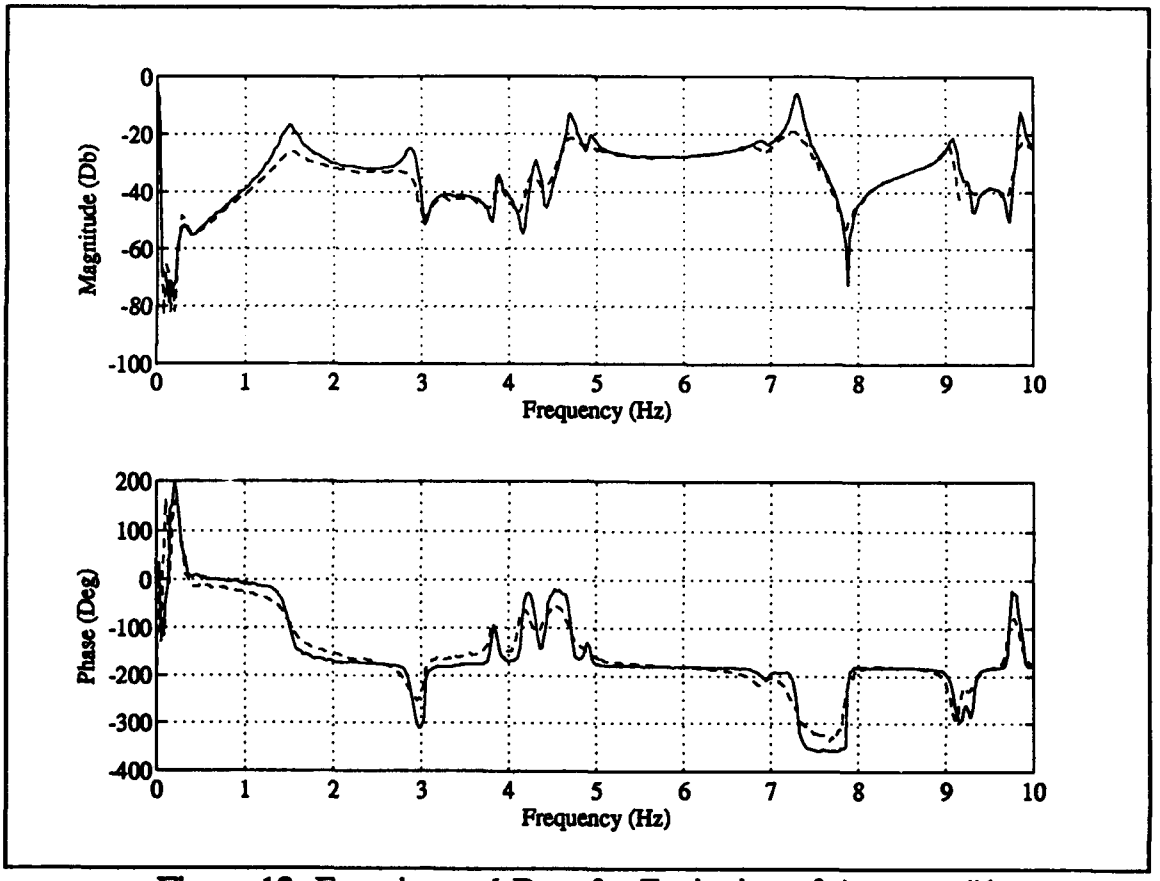

Figure 12: Experimental Data for Excitation of Actuator #1 and Measurement at Actuator #2 (Open Loop ——— Closed Loop -----)

measured at actuator #2. It is observed that in the frequency plot of Figure 12 the rigid body mode is beginning to become unstable as was predicted by the discussion on the low frequency behavior of systems of this class.

Figure 13 illustrates the theoretical and experimental closed loop response

for the accelerometer located at actuator #1. This plot represents the state space model prediction vs. the actual closed loop data. The theoretical data is represented by dashed lines.

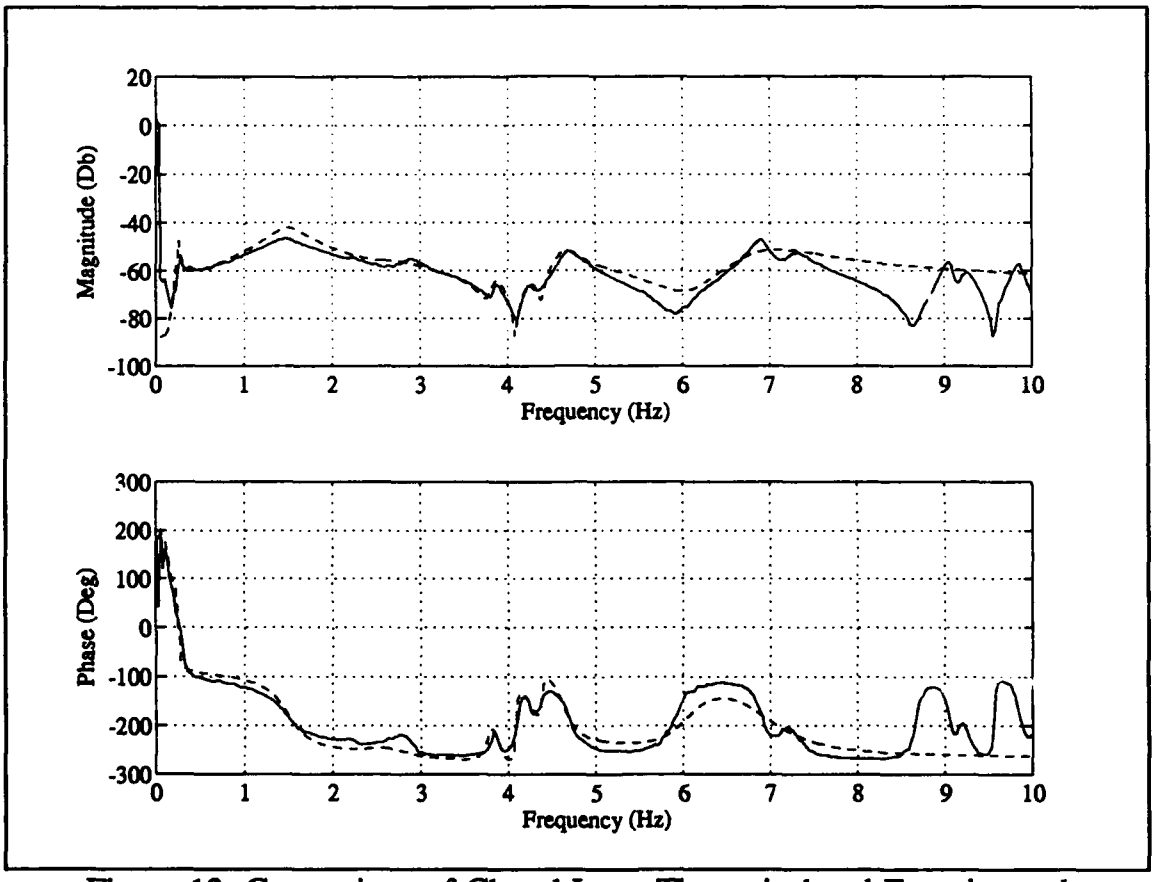

Figure 13: Comparison of Closed Loop Theoretical and Experimental Frequency Response Data for Excitation of Actuator #1 and Measurement #1 (Experimental Closed Loop Data ——— State Space Prediction -----)

It is observed that the mathematical model represented by dashed lines shows the beginnings of instability of the rigid body mode of the system. Also, the theoretical model is fairly close in its prediction of the closed loop damping values.

Figure 14 shows a plot of the errors of the two models that were created in the course of the research. These plots represent the maximum singular value of the error $\Delta(s)$ as a function of frequency. The dashed line is the error for the State

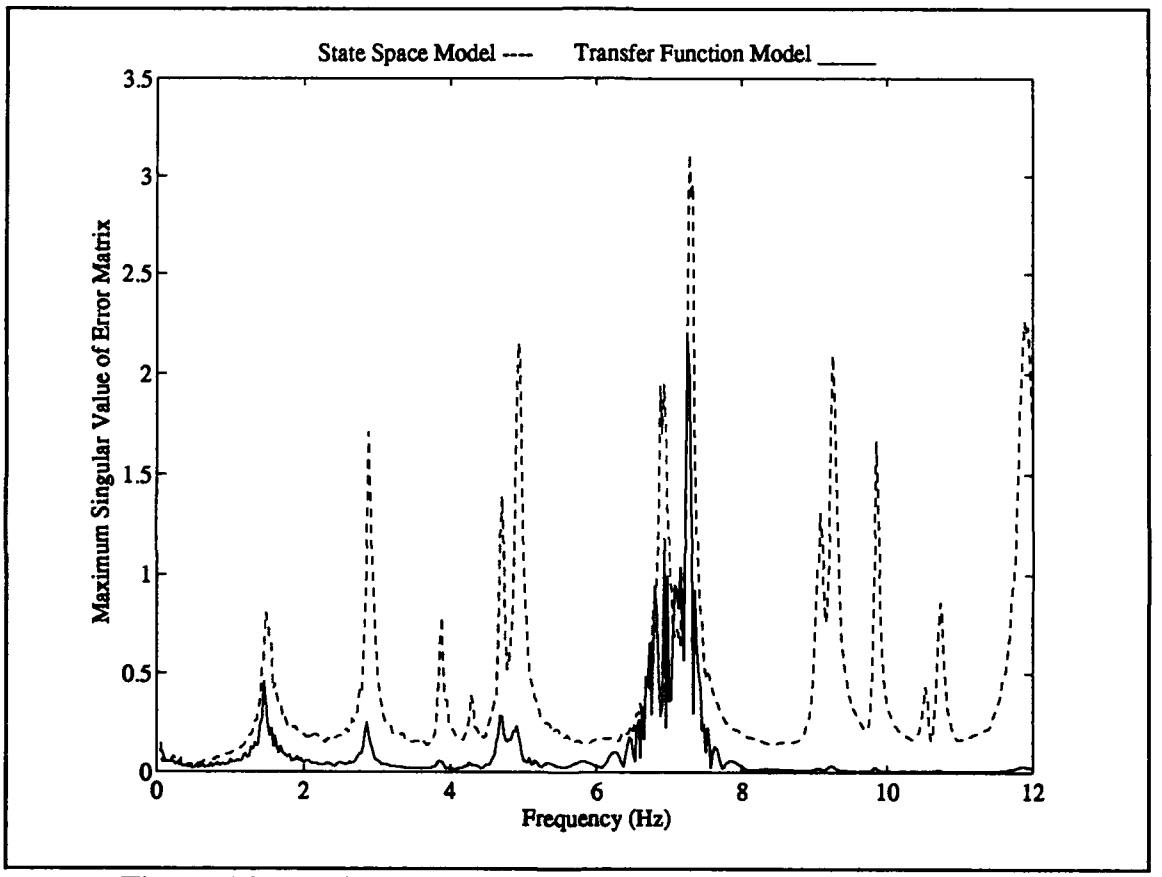

Figure 14: Maximum Singular Value Plot for Transfer Function Model and State Space Model

space model and the solid line is for the errors of the transfer function model. It can be seen that considerable error was generated by the method used to convert the transfer function model to state space.

For both the state space model and the transfer function model, it is seen

that the error is very large in the frequency range of 6 to 8 Hz. This is due to the nonlinear effects that were observed in this frequency range. These nonlinear effects that were present in the measurements can be observed in the plots of the data vs. the transfer function model included in Appendix B.

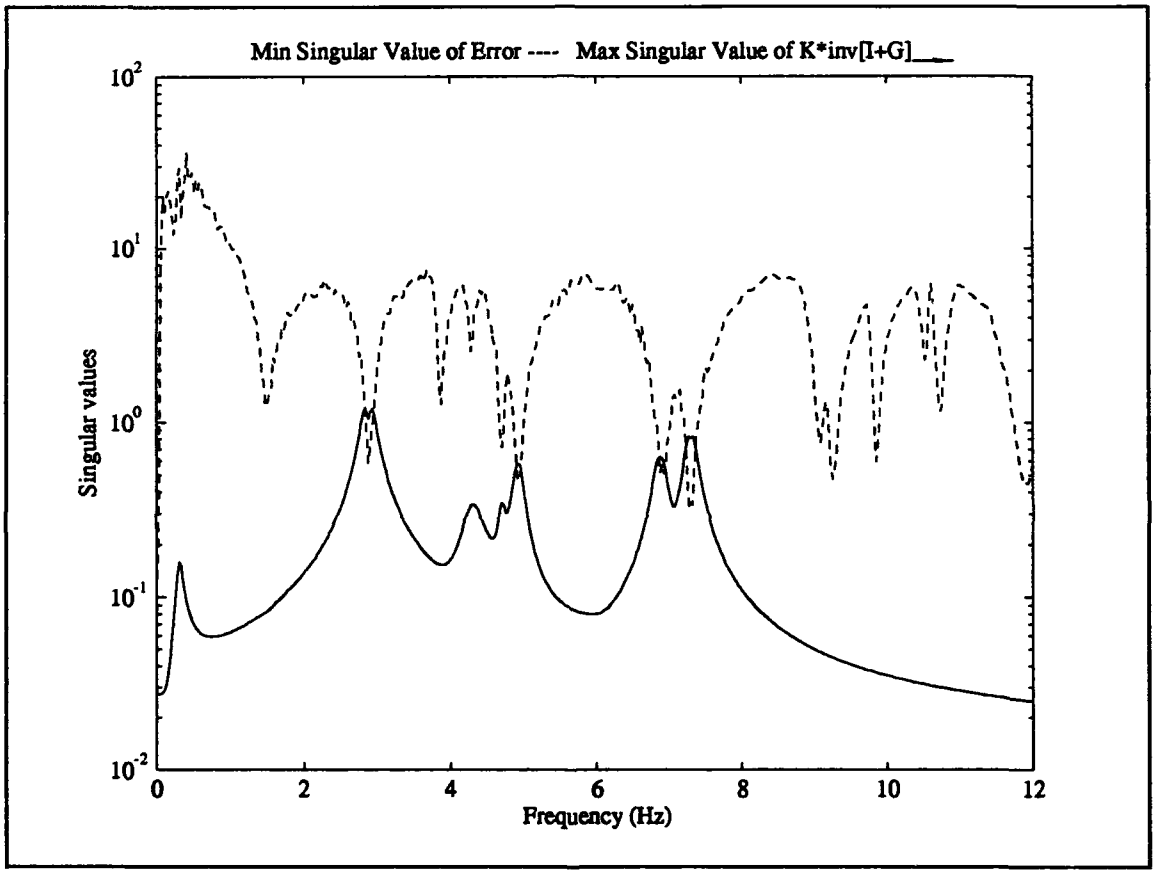

Figure 15: Plot Illustrating Stability Robustness Test

Figure 15 shows a plot of the stability robustness criteria for one of the unstable LQG controllers that were implemented. Again no data is available, but it can be seen that the controller does not pass this stability robustness test. The dashed lines represent the right hand side of Equation (34) or the minimum singular

values of $K[I+G_{model}(s)]^{-1}$. The solid lines represent the minimum singular values of the error matrix $\Delta(s)$. It can be seen that the robustness criteria has been violated in four spots. Thus, it is not surprising that this particular controller is unstable. Similar plots were done for the controllers that were stable and they passed this test. However, as stated before, the experimental frequency response curves for these controllers were indistinguishable from the open loop data due to their low gain. These plots are not included in this report.

VI. Recommendations and Conclusions

The goals of the research performed in this thesis were to create a mathematical model of the PACOSS Dynamic Test Article and apply active control techniques using the mathematical model. For the most part these goals have been achieved. The mathematical model in transfer function form describes the dynamics of the system very well. However, much of this model fidelity was lost in the attempt to find a state space realization that could be used to design a controller that could be employed on the Optima/3.

It was possible to design and implement a direct rate feedback controller that gave good results by increasing damping ratios significantly. The LQG controller on the other hand, did not yield any appreciable damping before the system became unstable. These results for the LQG controller stem from basically one source: modeling error.

There were two main sources of modeling error in the mathematical model. The first was the unmodeled dynamics of the system. Since very large order compensators are sometimes impossible or impractical to create, there will always be the problem of unmodeled dynamics, or the truncation of infinite transfer function series. The second source of error was inherent in the model identification technique used. The conversion of the model from transfer

function form to state space introduced considerable error in the overall mathematical model.

These results for the LQG controller were not entirely unexpected. According to the Martin Marietta documentation, the presence of the damping materials that were designed into the DTA at that time kept their modern control systems from becoming unstable (3:265). The absence of these damping treatments in the DTA as it currently exists allows little error in the model when modern control techniques are used. Without the presence of internal damping even small errors in the mathematical model will cause the closed loop system to destabilize.

With the difficulty encountered in creating a mathematical model of the system it is recommended that research pursuing better model identification techniques continue. An algorithm for identifying the dynamics of structures that are lightly damped and have high modal density is necessary if purely active control of structures is to be attempted. A second recommendation is that purely active control of this class of structure should not be attempted in the first place. The structure should be designed with passive damping built into the system and should only be controlled actively to augment the inherent damping characteristics that already exist.

Designing a structure with this in mind, can greatly aid the control system designer. Passive damping allows more modes to be removed from the

mathematical model which reduces the order of the compensator used (3:264). Also, as stated before, uncertainties in the plant model will be less likely to destabilize the closed loop system when passive damping is present in the system.

The nonlinear effects that were observed in the data in the frequency range of 6 to 8 Hz is believe to be due to the instrumentation wires that are connected to the structure. Recall that the DTA is instrumented with 151 accelerometers. Each of these accelerometers requires a wire to communicate with the measurement system. Quantifying the effect of these wires is difficult and it is suspected that they add mass and stiffness in a nonlinear manner. If continuing control work is to be done, it is recommended that the wires that are not being used be disconnected from the structure to minimize the impact on the plant dynamics.

Bibliography

1. Gehling, R.N., Morgenthaler, D.R., Arrajj, B.M. Passive and Active Control of Space Structures: Quarterly Report, April 1989 - June 1989. CDRL 13, Contract #F33615-82-C-3222. Denver, CO: Martin Marietta Astronautics Group, 30 Jun 1989.

2. Gehling, R.N., Morgenthaler, D.R., Wobschall, N. Passive and Active Control of Space Structures: Quarterly Report, January 1988 - March 1988. CDRL 13, Contract #F33615-82-C-3222. Denver, CO: Martin Marietta Astronautics Group, 31 March 1988.

3. Gehling, R.N., Morgenthaler, D.R., Richards, K.E. Passive and Active Control of Space Structures: Final Report, November 1988 - April 1991. CDRL 14, Contract #F33615-82-C-3222. Denver, CO: Martin Marietta Astronautics Group, 5 June 1991.

4. George, Capt Scott E. Modal Analysis and Modeling of a Lightly Damped Large Space Structure. MS Thesis. AFIT/GA/ENY/92J-01. School of Engineering, Air Force Institute of Technology (AU). Wright-Patterson AFB OH, June 1992.

5. Morgenthaler, D.R. Passive and Active Control of Space Structures Volume #1: Damping Design Methodology, Final Report, September 1987 - November 1988. CDRL 14, Contract #F33615-82-C-3222. Denver, CO: Martin Marietta Astronautics Group, September 1990.

6. Kwakernaak, Huber and Sivan, Raphael. Linear Optimal Control Systems. New York: Wiley Interscience, 1972.

7. Inman, D.J. "Control/Structure Interaction: Effects of Actuator Dynamics," in Mechanics and Control of Large Flexible Structures. Ed. John L. Junkins. Washington DC: American Institute of Aeronautics and Astronautics, Inc., 1990.

8. Reid, J. Gary. Linear System Fundamentals: Continuous and Discrete, Classic and Modern. New York: McGraw-Hill Publishing Company, 1983.

9. Junkins, John.L. and Kim, Y. "Minimum Sensitivity Design Method for Output Controllers," in Mechanics and Control of Large Flexible Structures. Ed. John L. Junkins. Washington DC: American Institute of Aeronautics and Astronautics, Inc., 1990.

10. Ridgely, Capt D. Brett and Banda, Siva S. Introduction to Robust Multivariable Control. Flight Dynamics Laboratory, Air Force Wright Aeronautical Laboratories, Air Force Systems Command, Wright-Patterson AFB, OH,1986.

11. Matlab Reference Guide. The Math Works Inc. Natik, MA, 1990.

12. 2600 Analyzer User's Guide. Tektronix Inc. Campbell, CA, 1987.

13. Gehling, R. N. Passive and Active Control of Space Structures: Volume #2: Dynamic Test Article Modal Survey: Test and Analysis Results. CDRL 14, Contract #F33615-82-C-3222. Denver, CO: Martin Marietta Astronautics Group, September 1990.

14. Kailath, Thomas. Linear Systems. Englewood Cliffs, NJ: Prentice-Hall, Inc.,1980.

15. Miller, D. W. and Crawley, E. F. Theoretical and Experimental Investigation of Space-Realizable Inertial Actuation for Passive and Active Structural Control. Journal of Guidance, Control, and Dynamics, Vol 11, No. 5, Sept-Oct 1989, pp. 449-458.

16. Yeh, Hsi-Han, Banda, Siva S. and Ridgely, Capt. D. Brett. Stability Robustness Measures Utilizing Structural Information. Journal of Control, Vol 41, No. 2, February 1985, pp. 365-387.

Appendix A: Accelerometer Calibration

Actuator Location	Serial Number	Calibration (mA/g)	Date
#1	1915	1.2397	23 NOV 88
#2	1576	1.3142	12 AUG 87
#3	1531	1.2484	10 AUG 87
#4	1564	1.3275	12 AUG 87
#5	1568	1.3217	12 AUG 87
#6	1516	1.2906	6 AUG 87
#9	1925	1.2473	1 DEC 88
#10	1924	1.3572	1 DEC 88

Appendix B: Transfer Function Model FRFs

This appendix contains the frequency response functions for all eight input points, to all eight output points (64 frequency response functions). The plots show both the transfer function model and the experimental data. The reader is reminded that the dashed line represents the transfer function model and the solid line represents the experimental data. The caption below each plot identifies the excitation point (or actuator that is being excited), and the output or measurement number (which corresponds to an actuator location at which the response is measured).

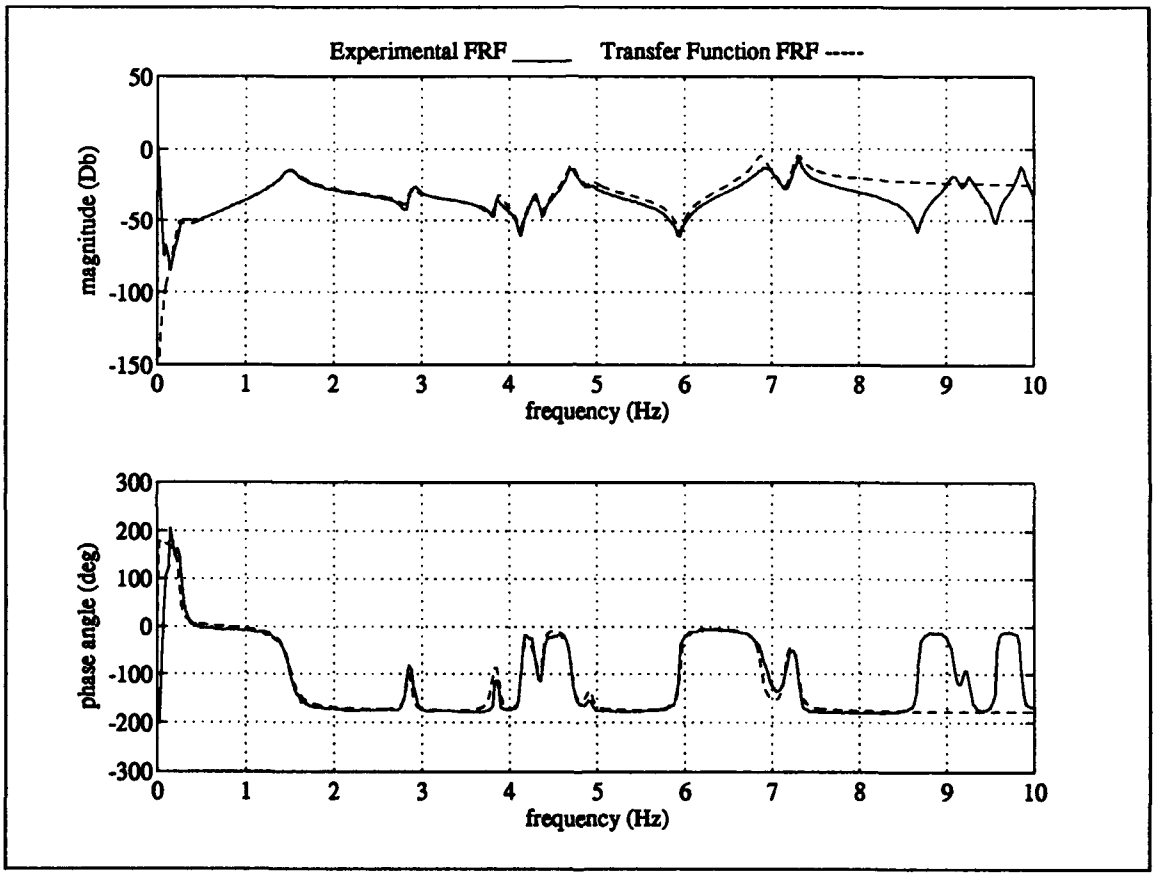

Excitation Actuator #1 Measurement #1

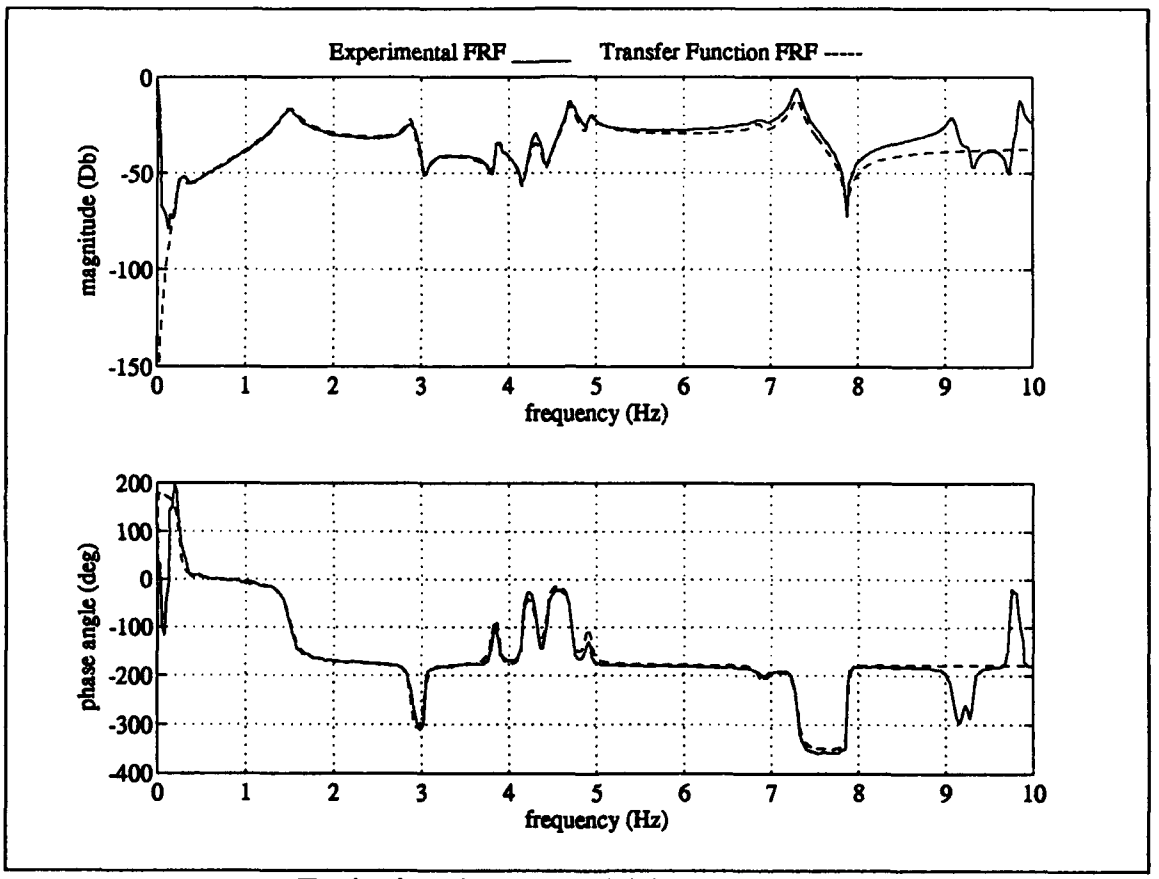

Excitation Actuator #1 Measurement #2

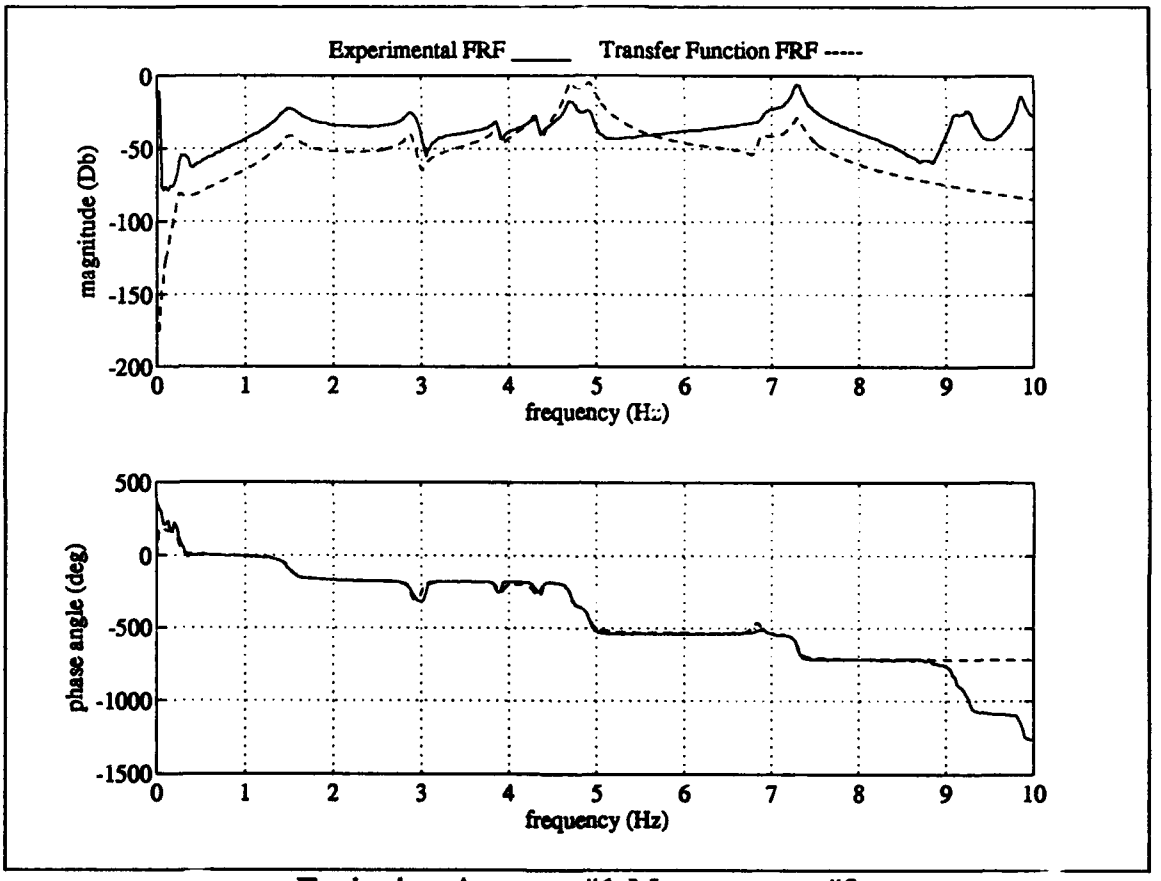

Excitation Actuator #1 Measurement #3

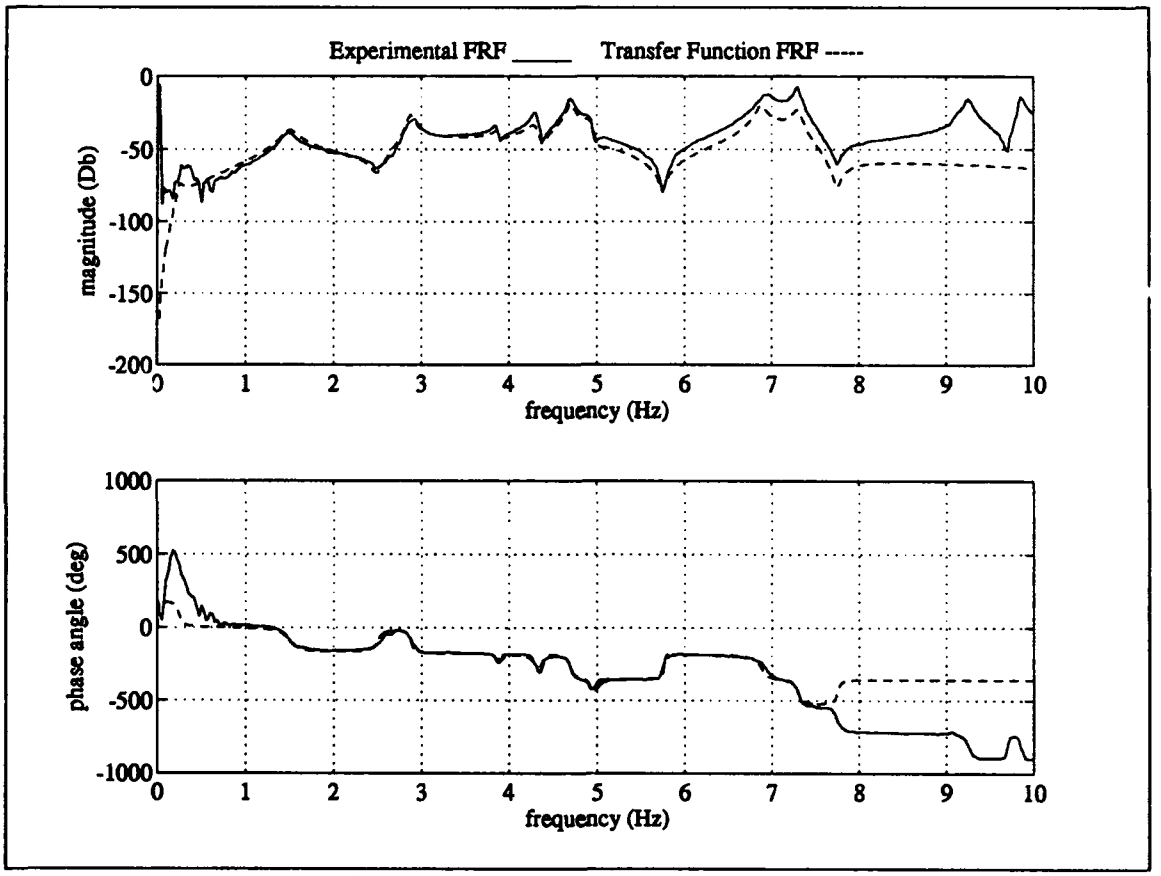

Excitation Actuator #1 Measurement #4

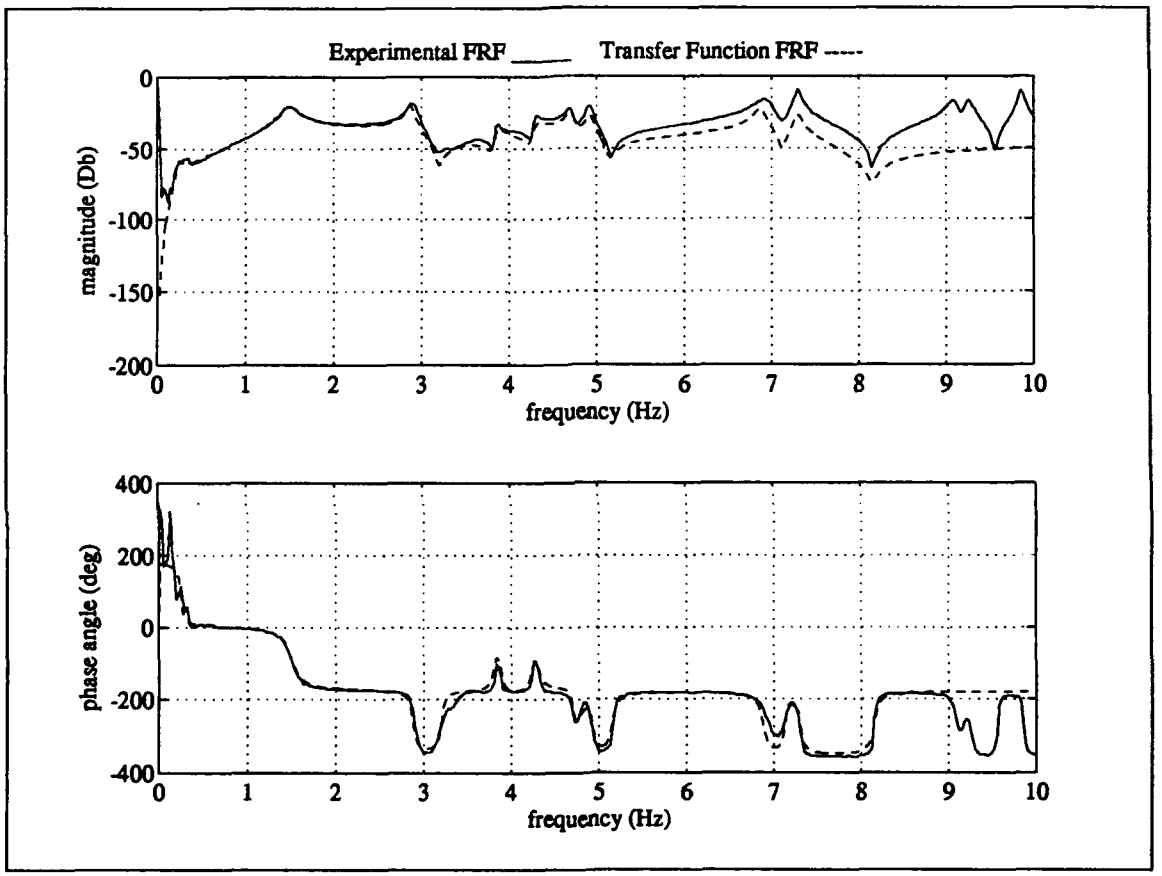

Excitation Actuator #1 Measurement #5

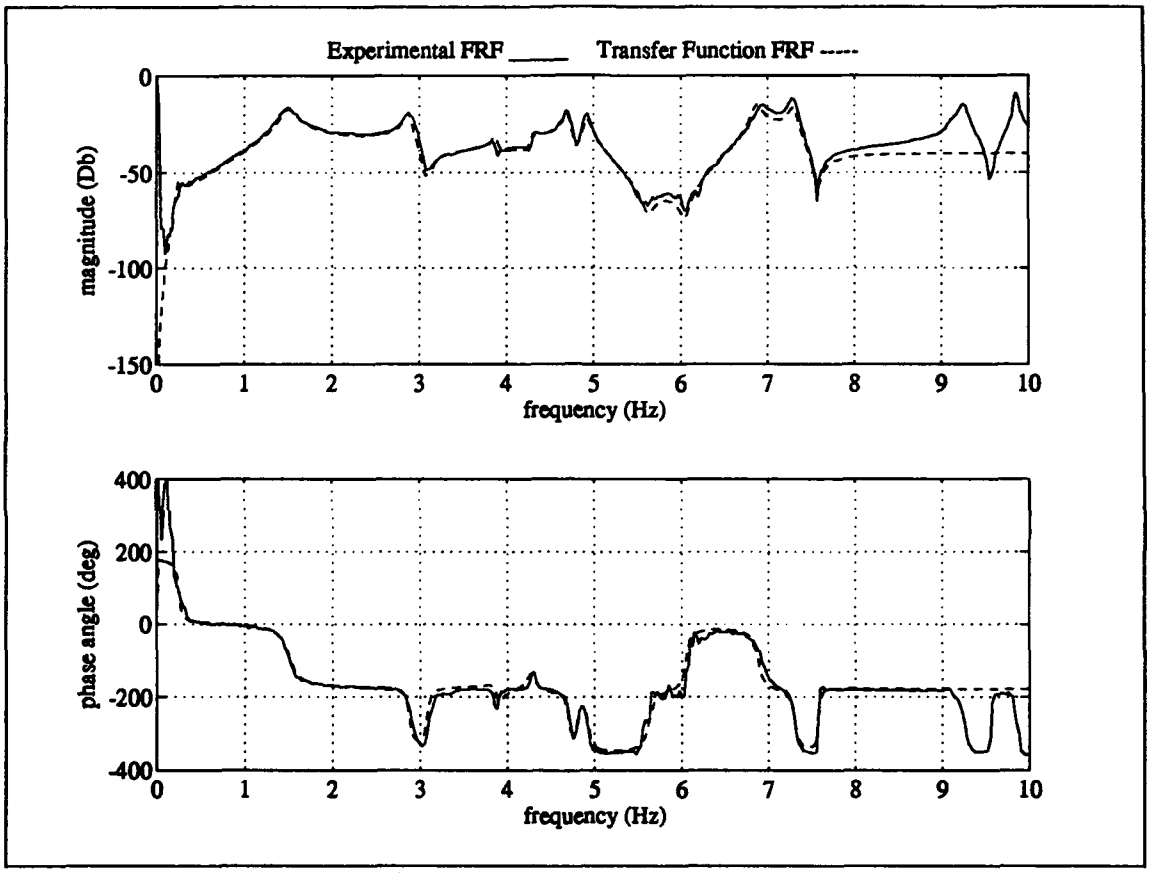

Excitation Actuator #1 Measurement #6

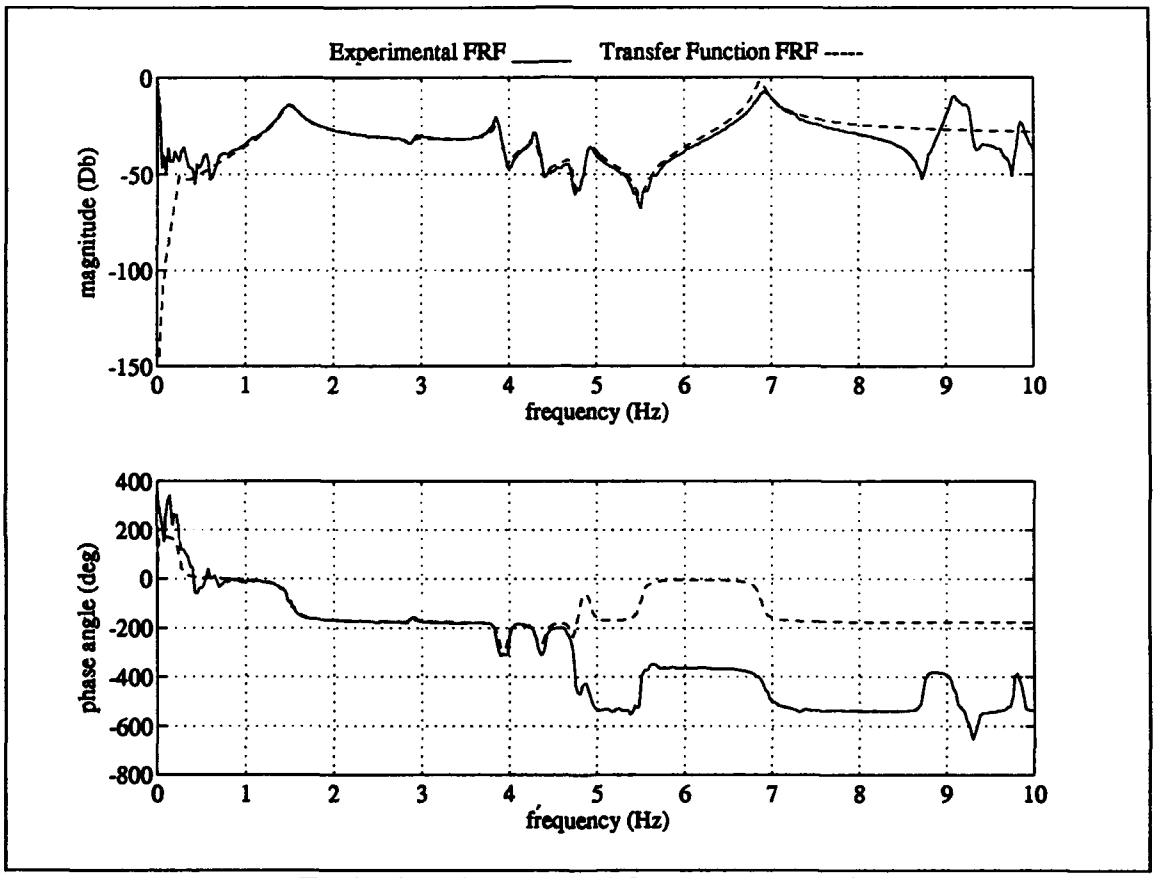

Excitation Actuator #1 Measurement #9

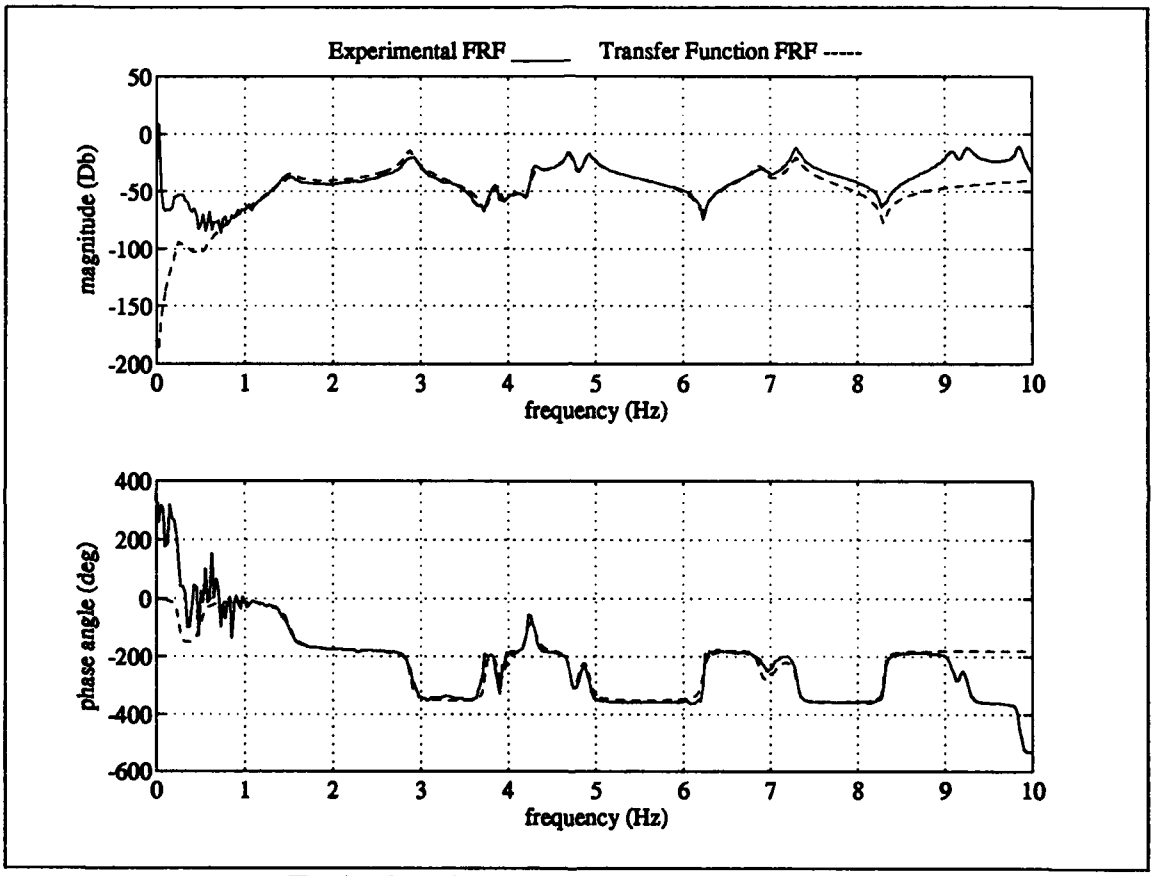

Excitation Actuator #1 Measurement #10

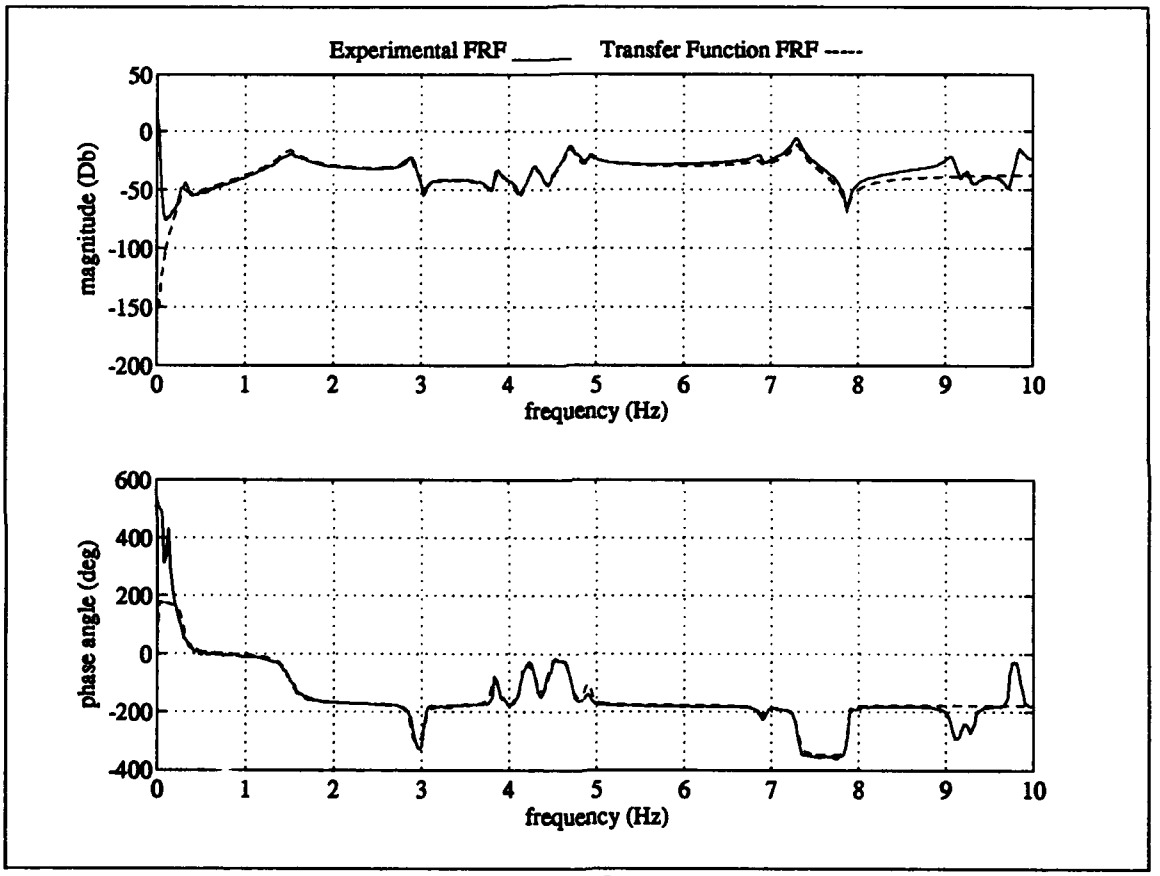

Excitation Actuator #2 Measurement #1

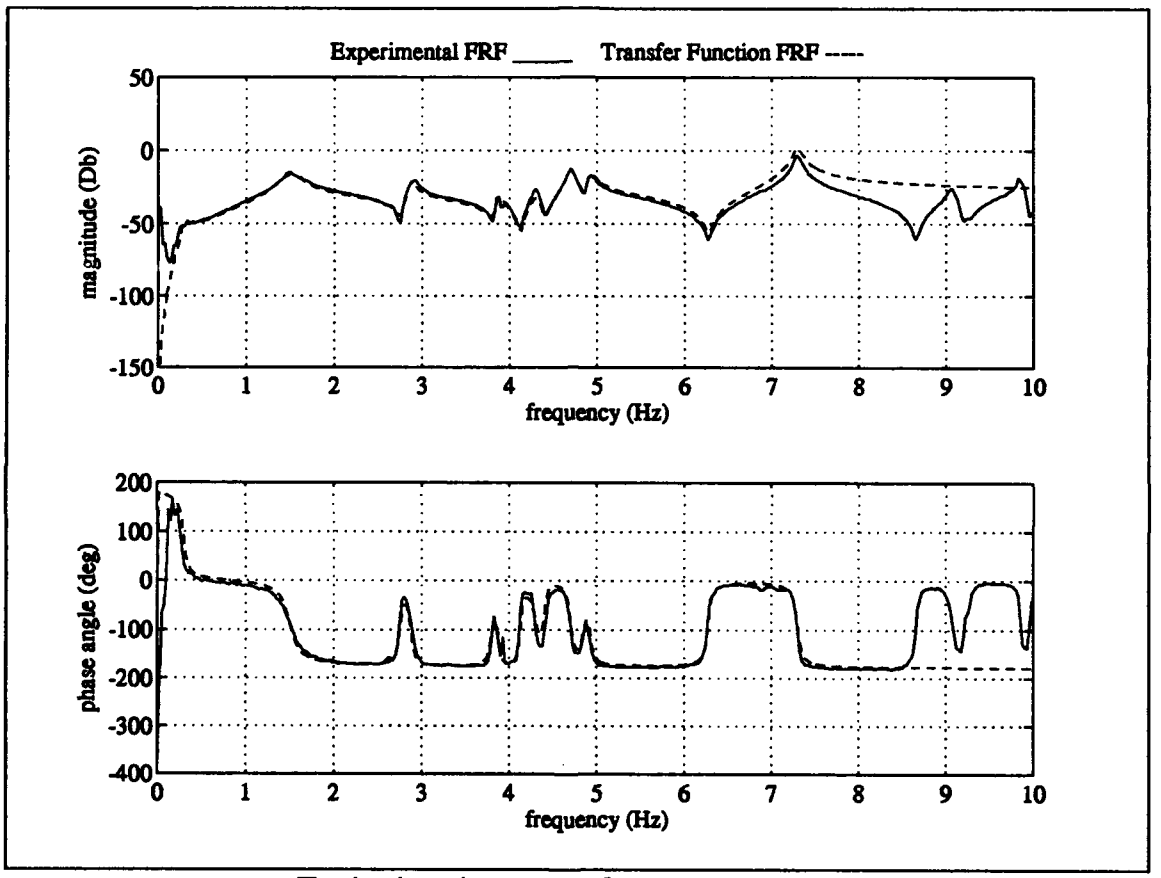

Excitation Actuator #2 Measurement #2

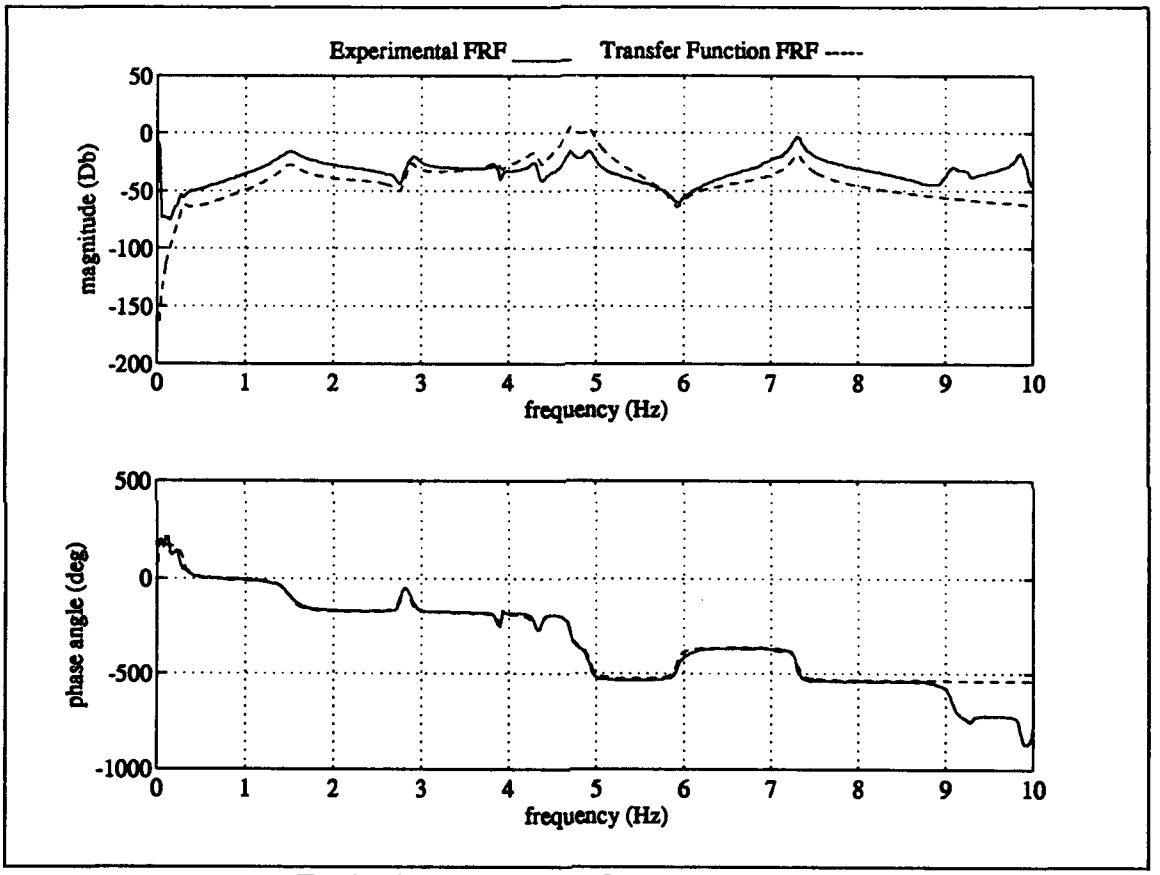

Excitation Actuator #2 Measurement #3

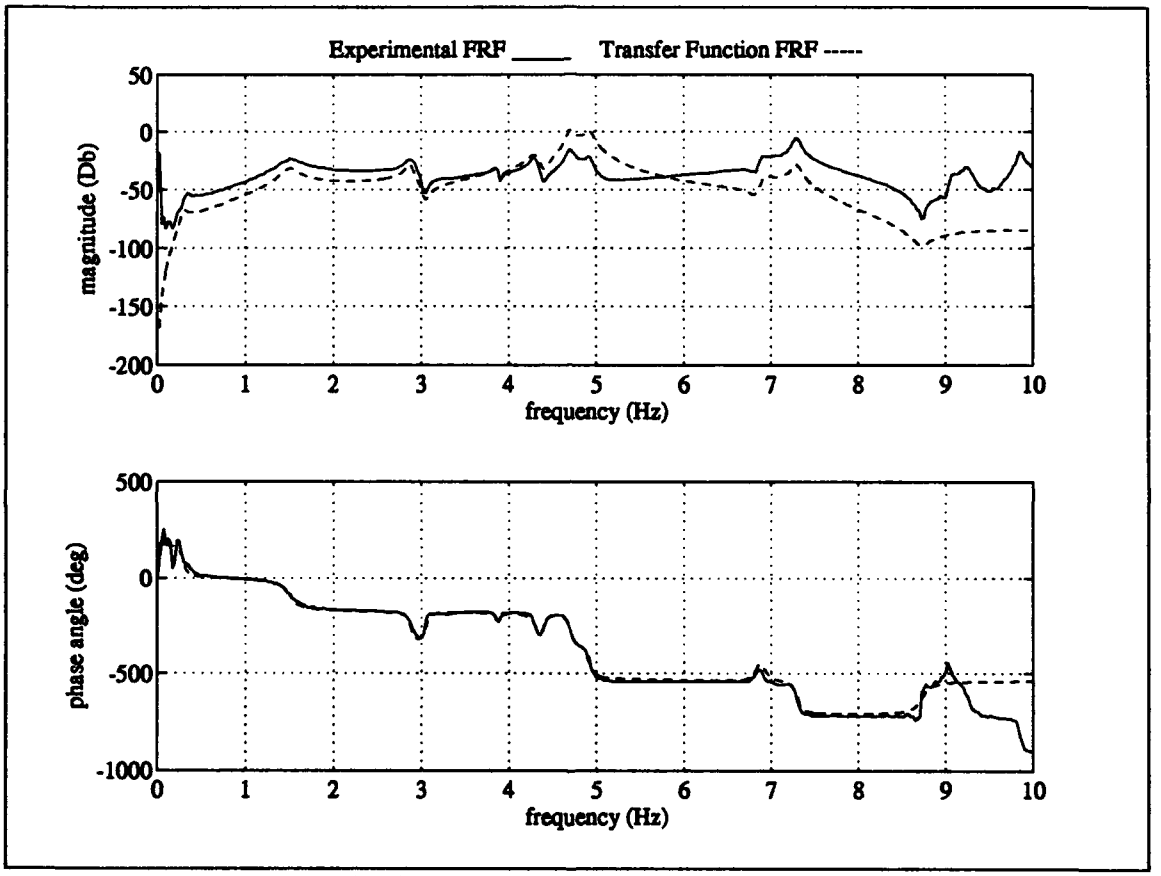

Excitation Actuator #2 Measurement #4

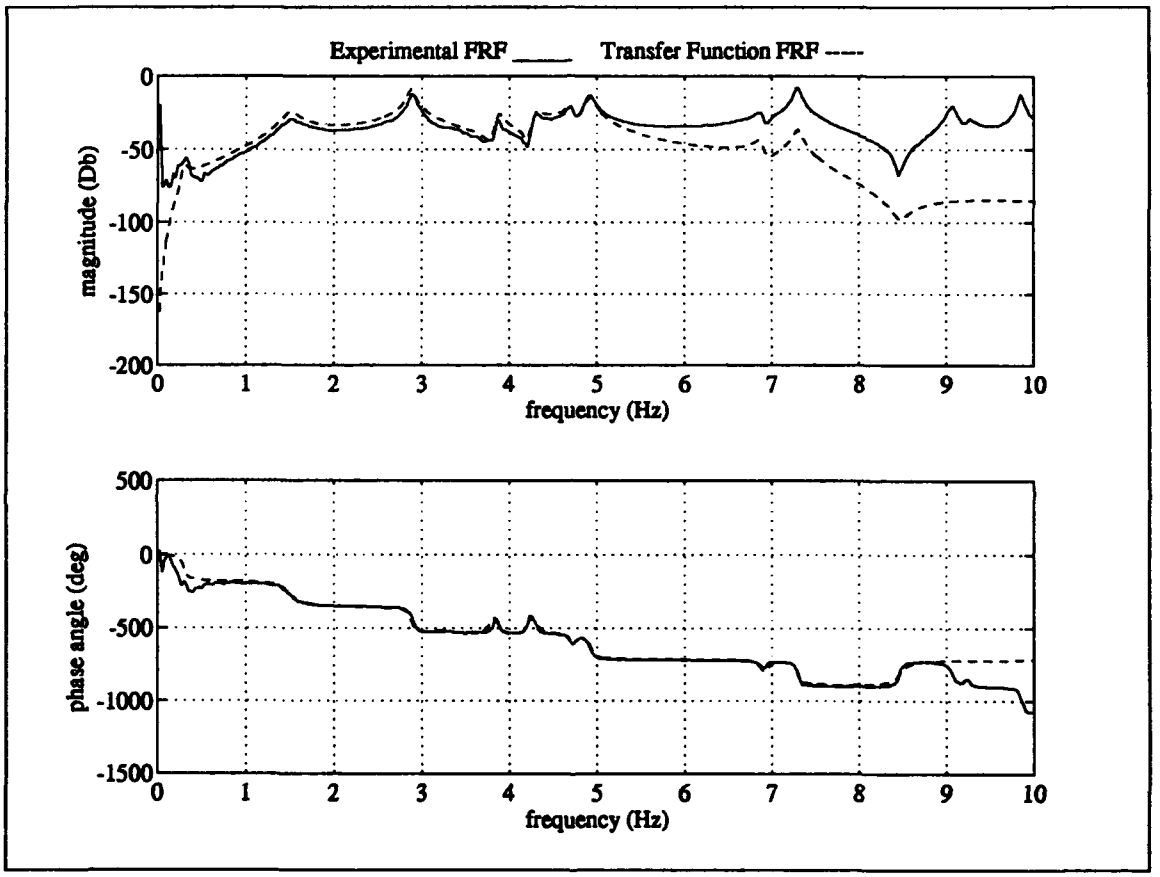

Excitation Actuator #2 Measurement #5

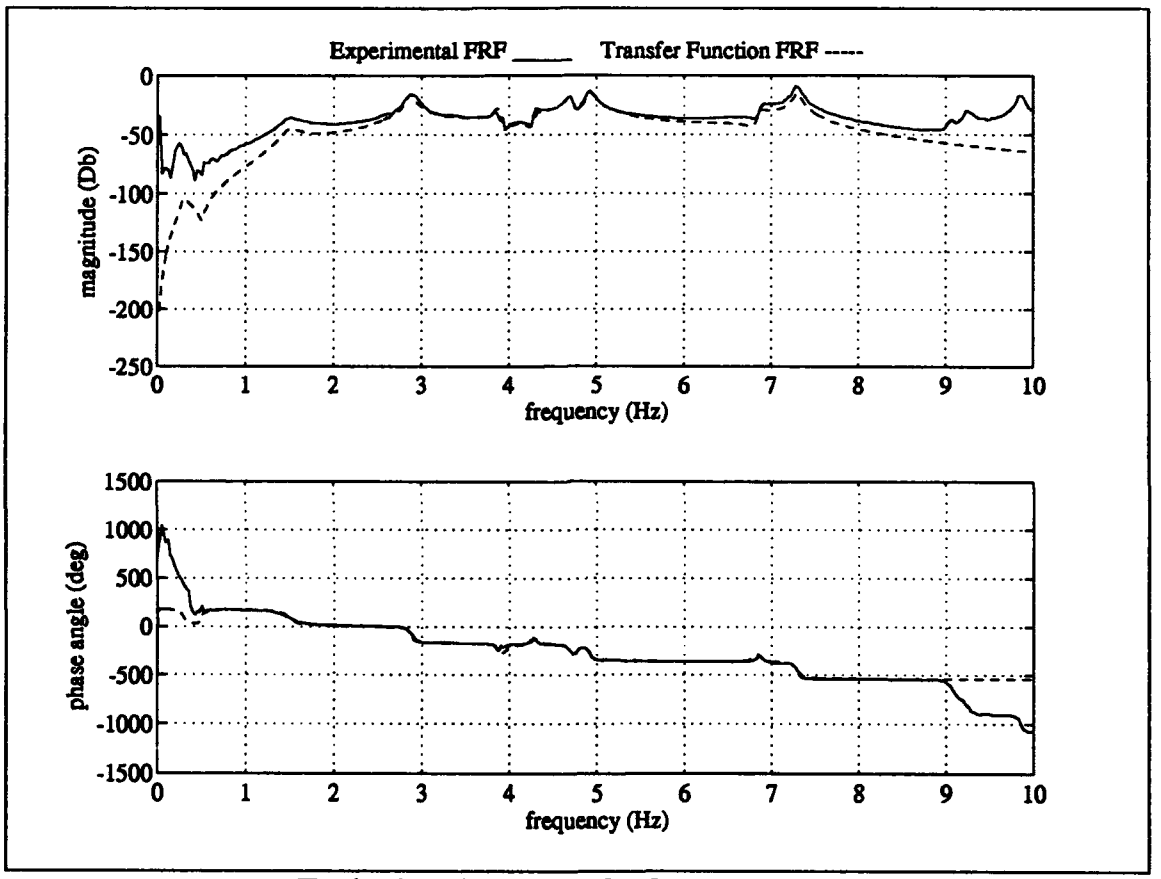

Excitation Actuator #2 Measurement #6

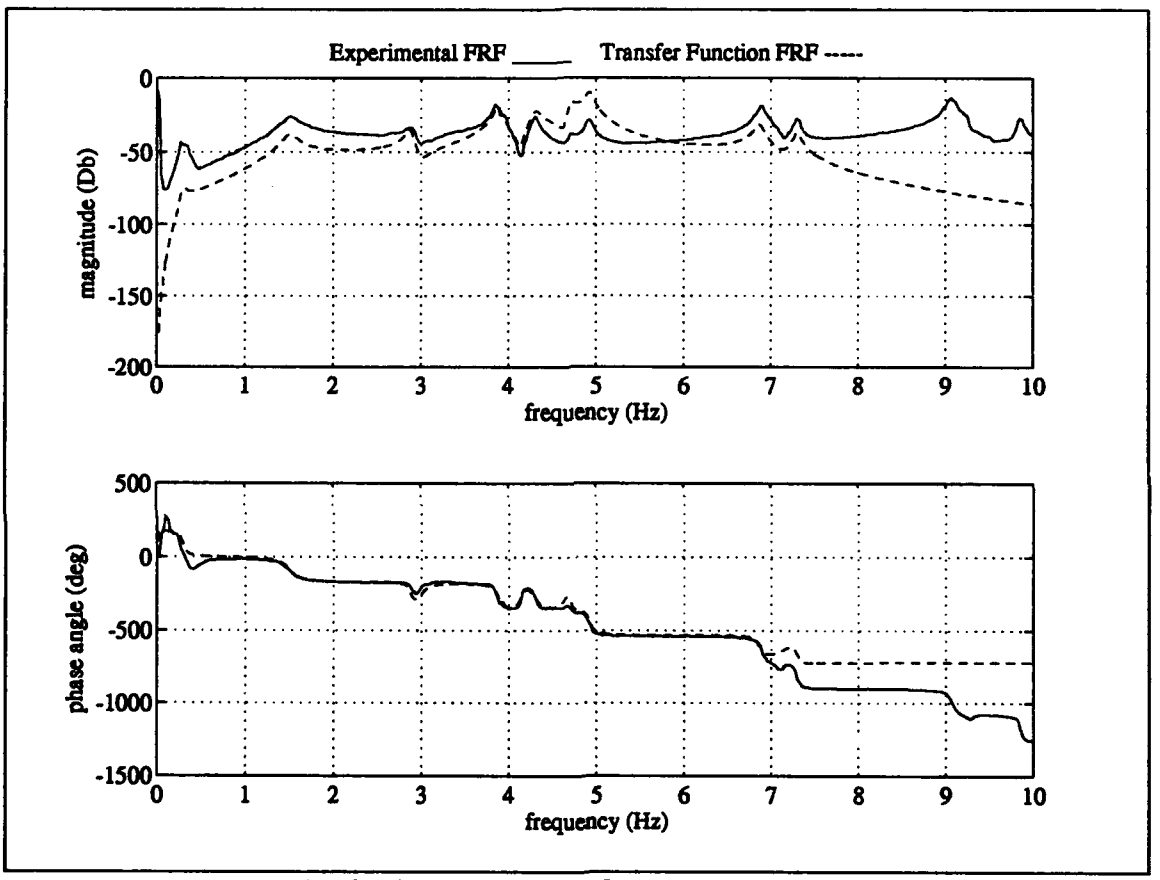

Excitation Actuator #2 Measurement #9

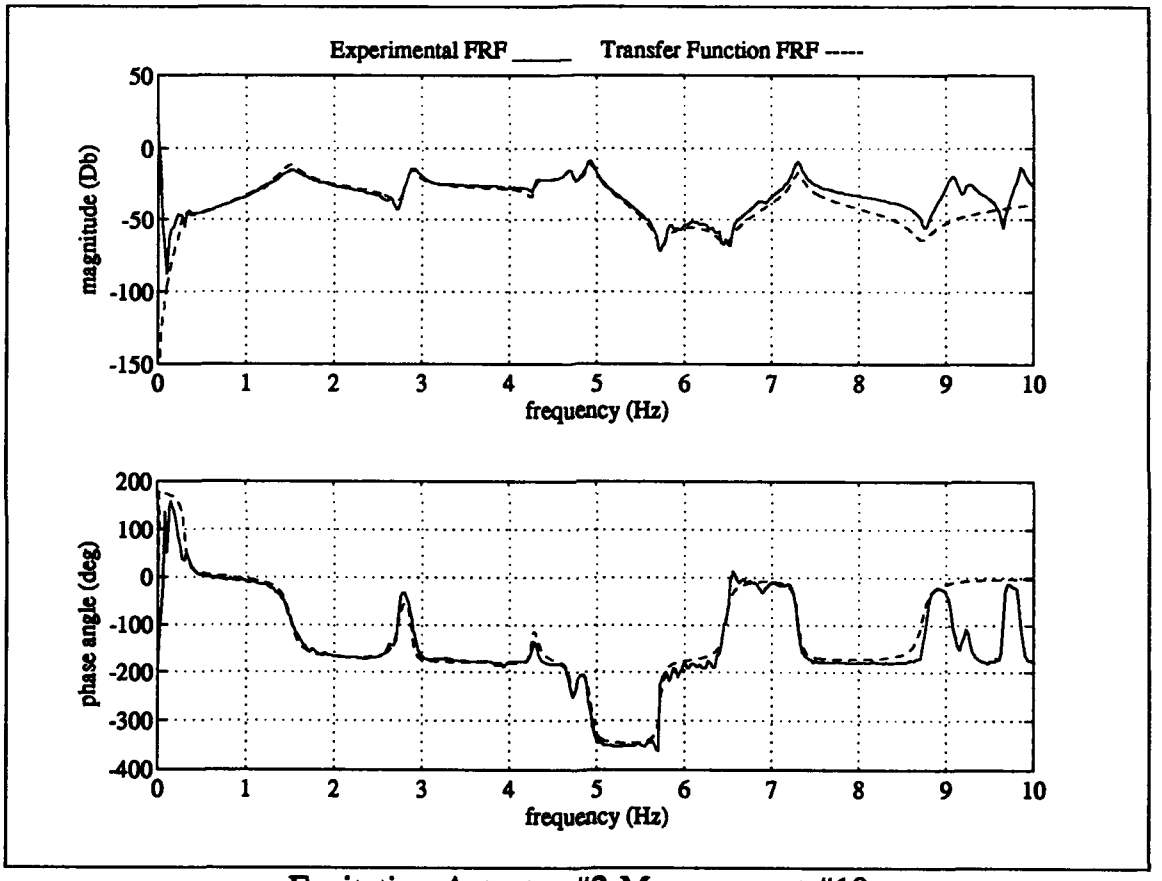

Excitation Actuator #2 Measurement #10

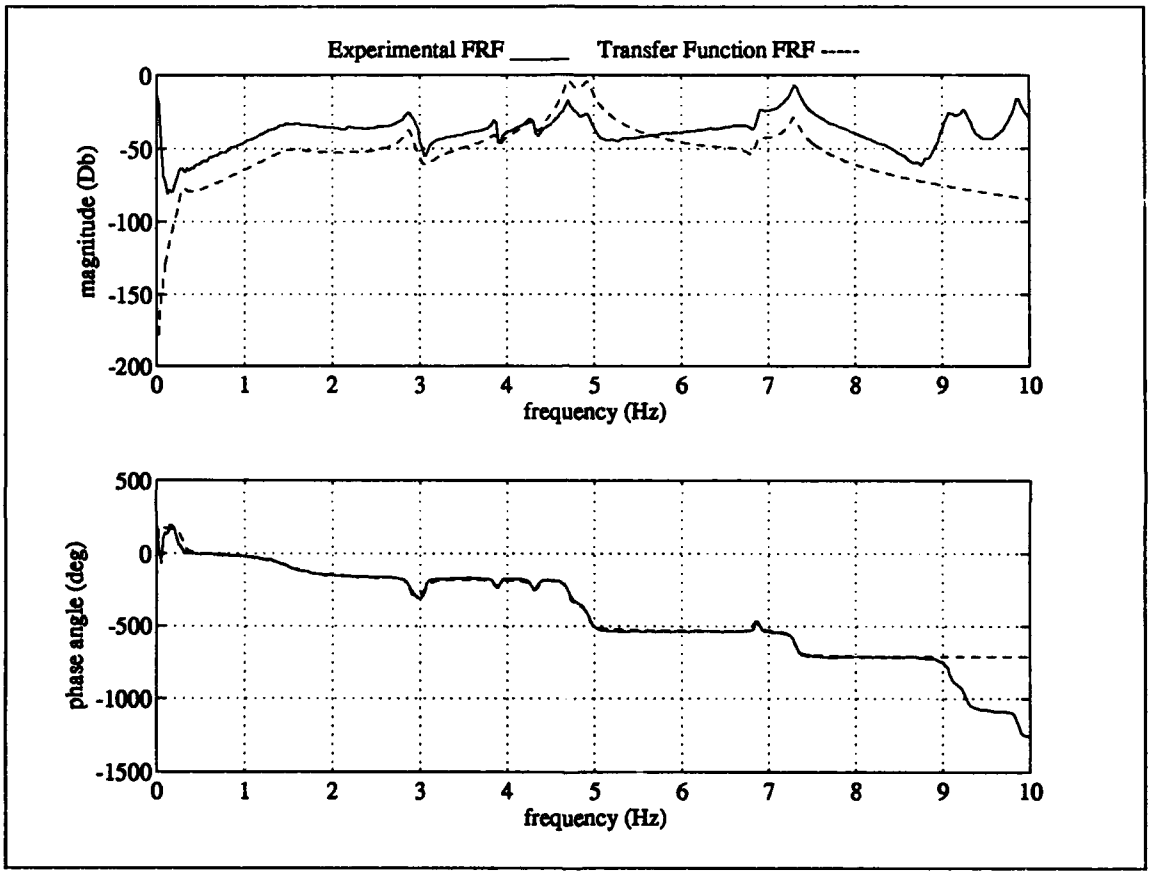

Excitation Actuator #3 Measurement #1

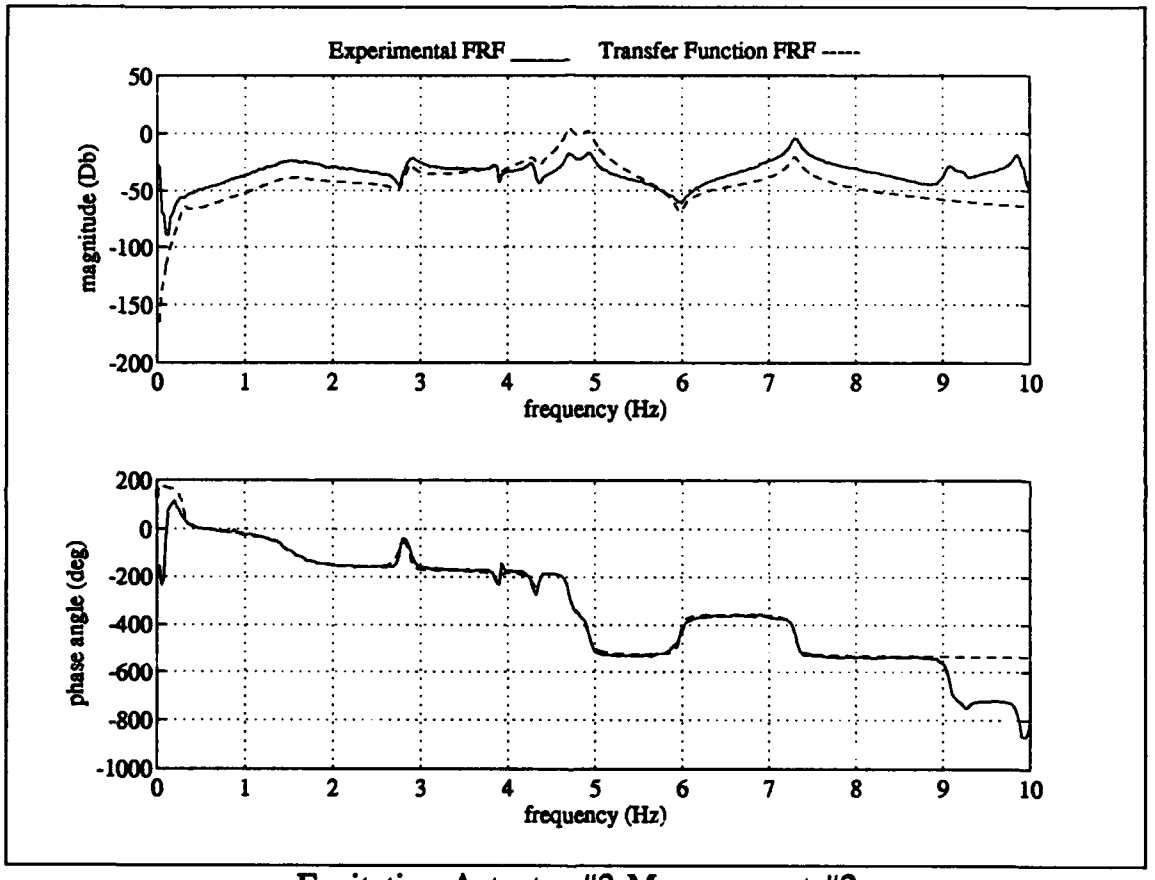

Excitation Actuator #3 Measurement #2

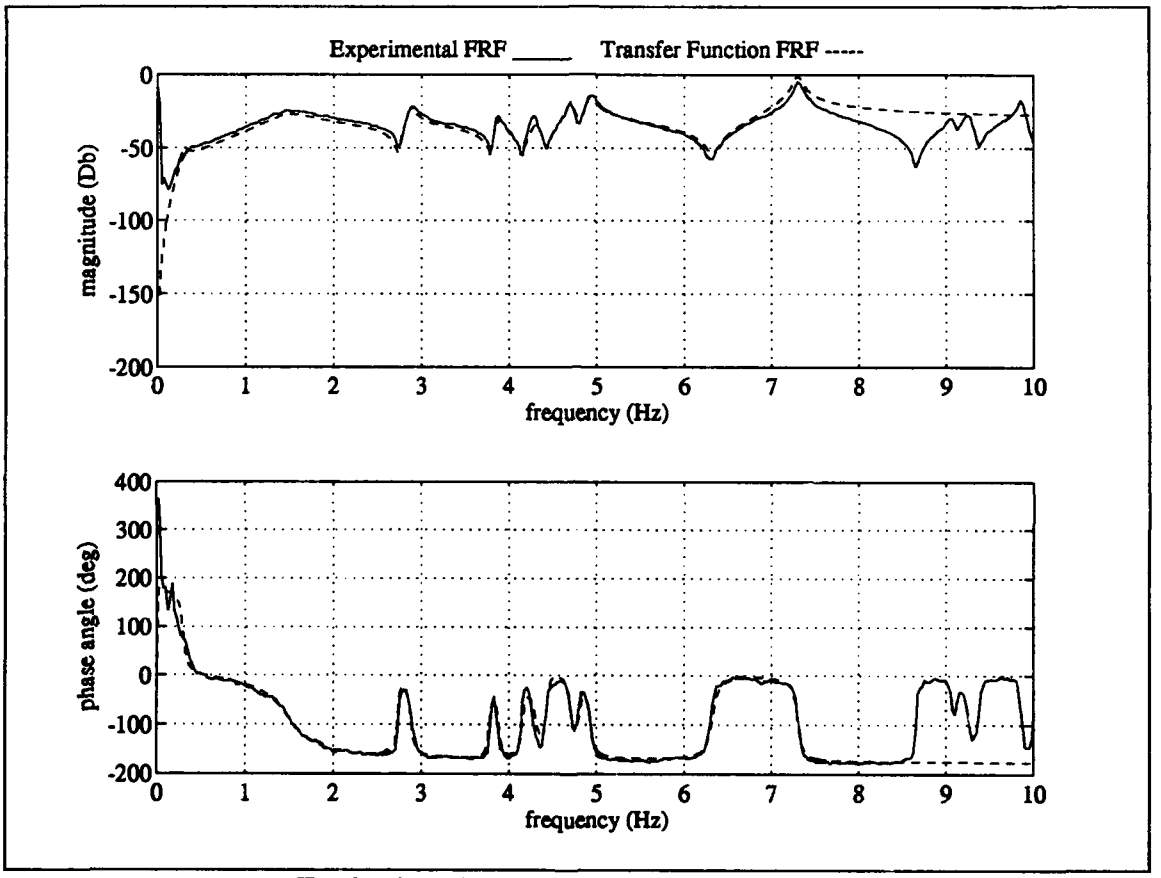

Excitation Actuator #3 Measurement #3

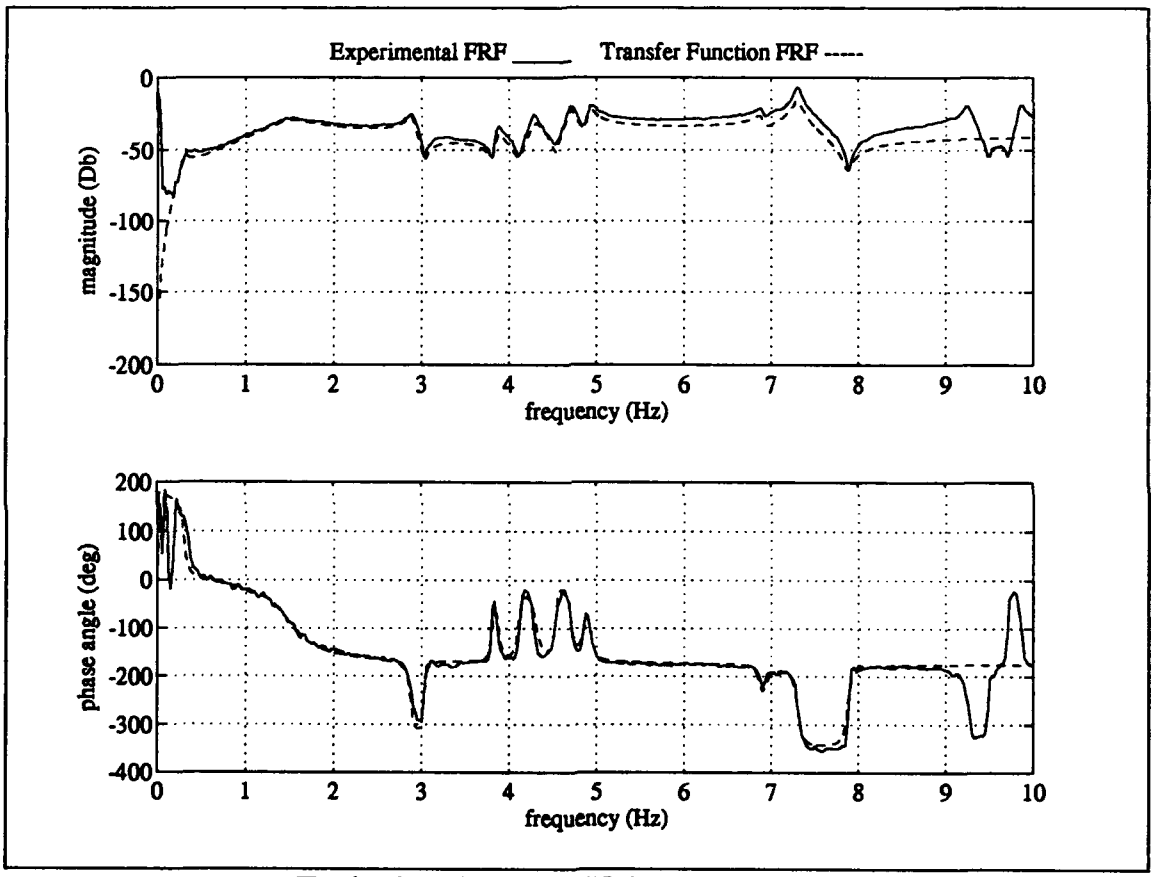

Excitation Actuator #3 Measurement #4

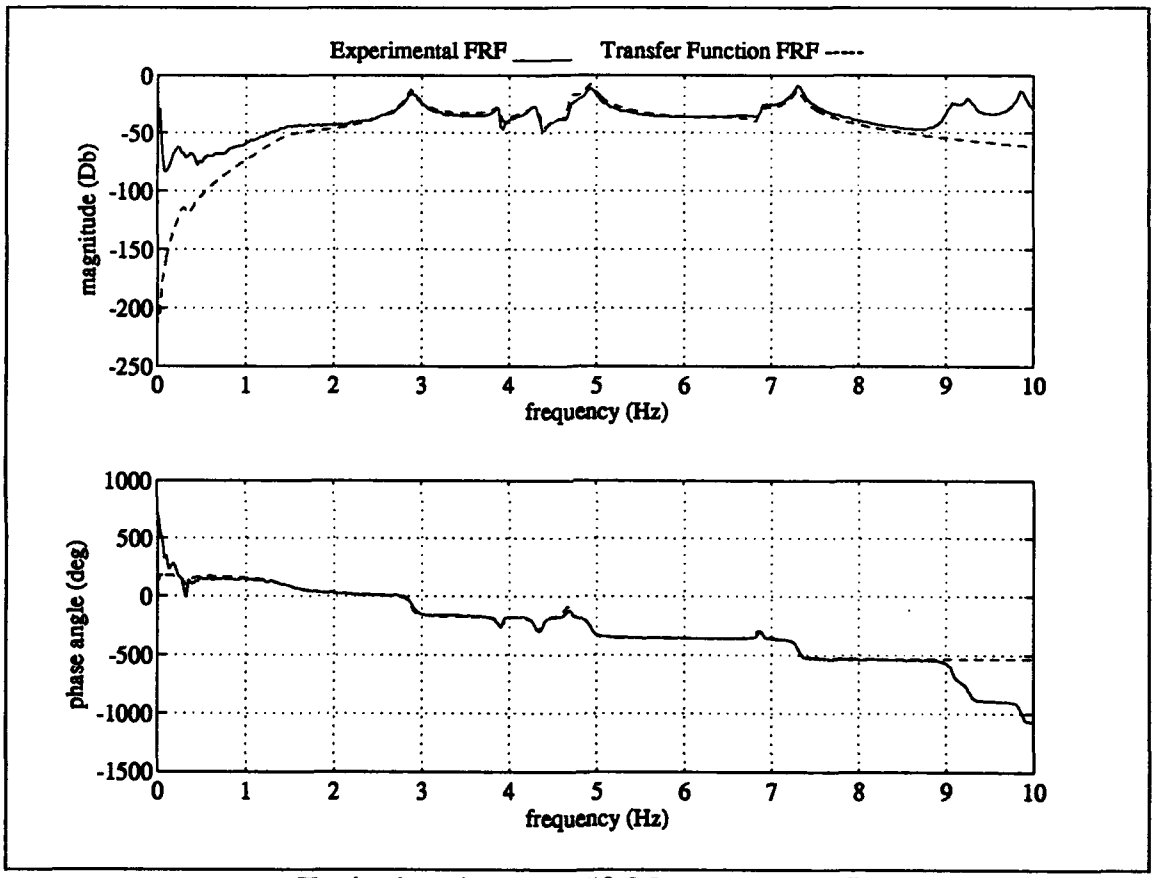

Excitation Actuator #3 Measurement #5

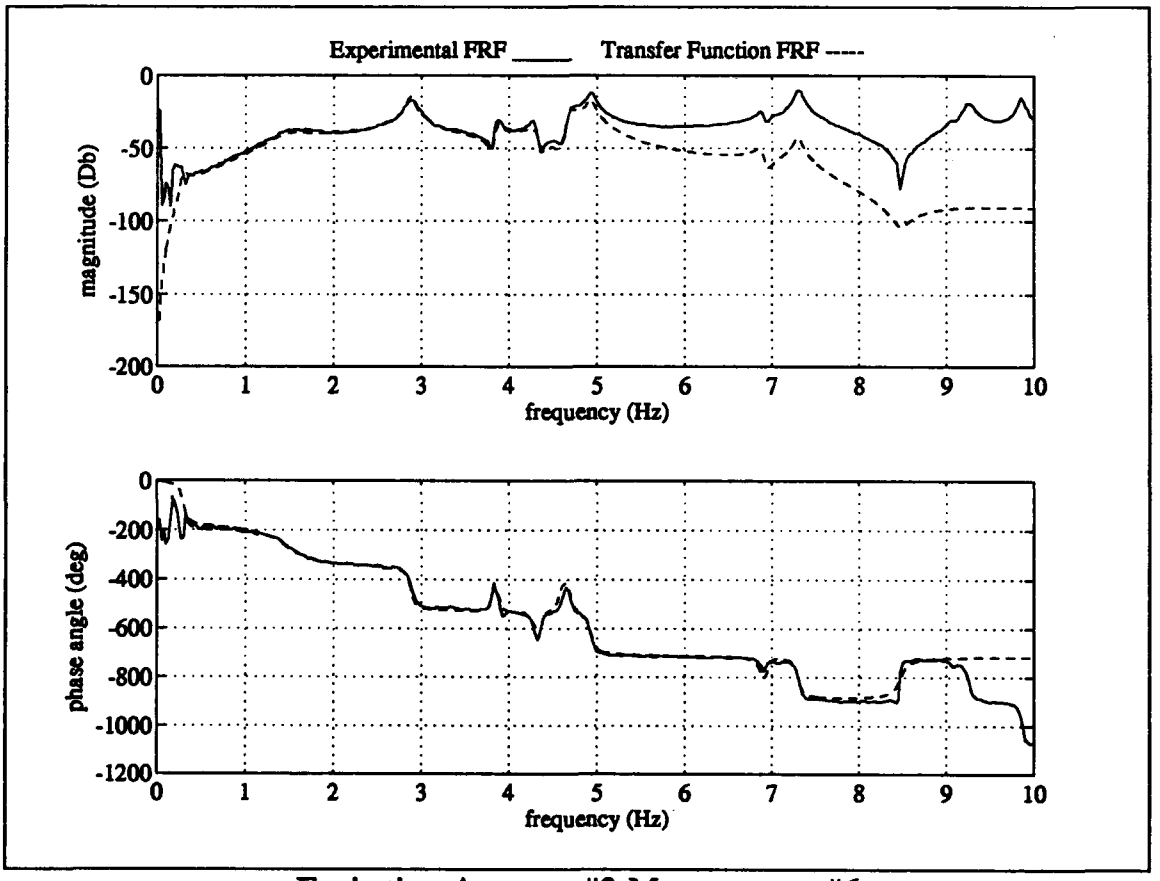

Excitation Actuator #3 Measurement #6

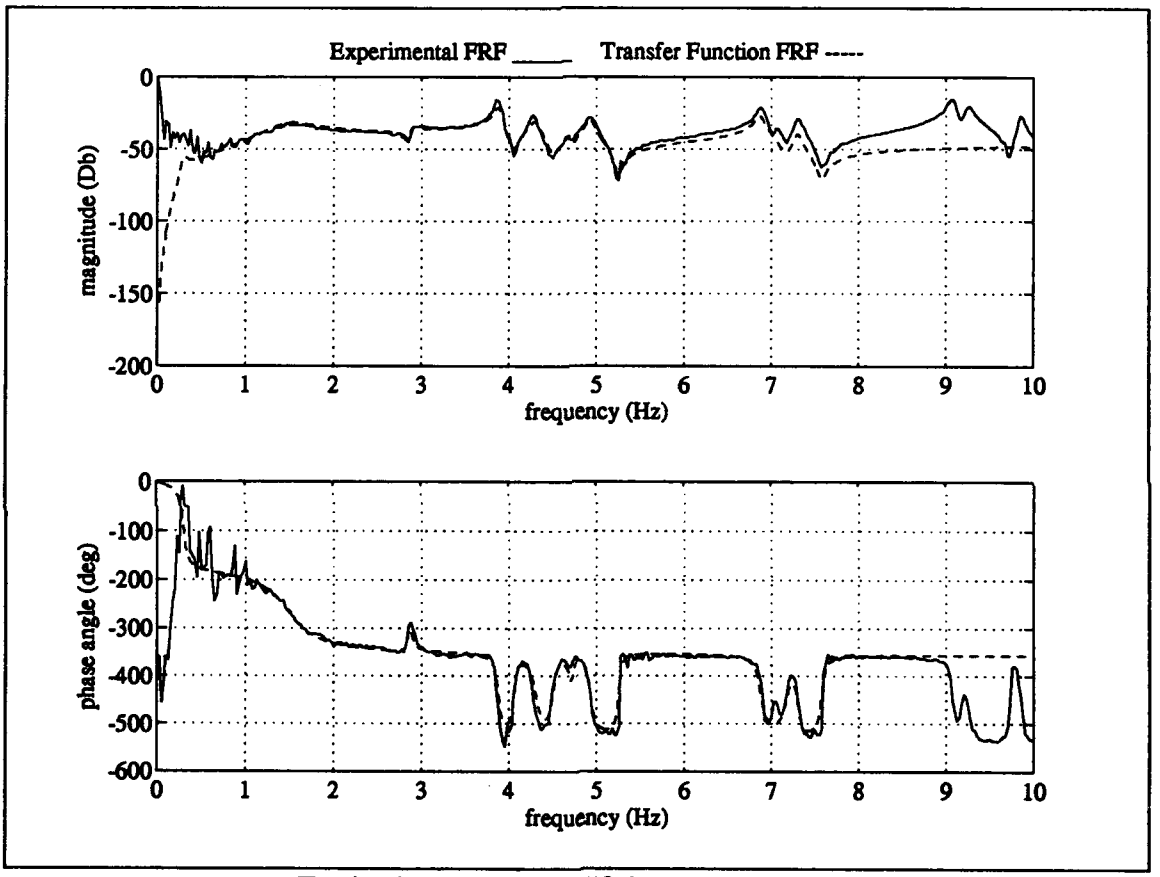

Excitation Actuator #3 Measurement #9

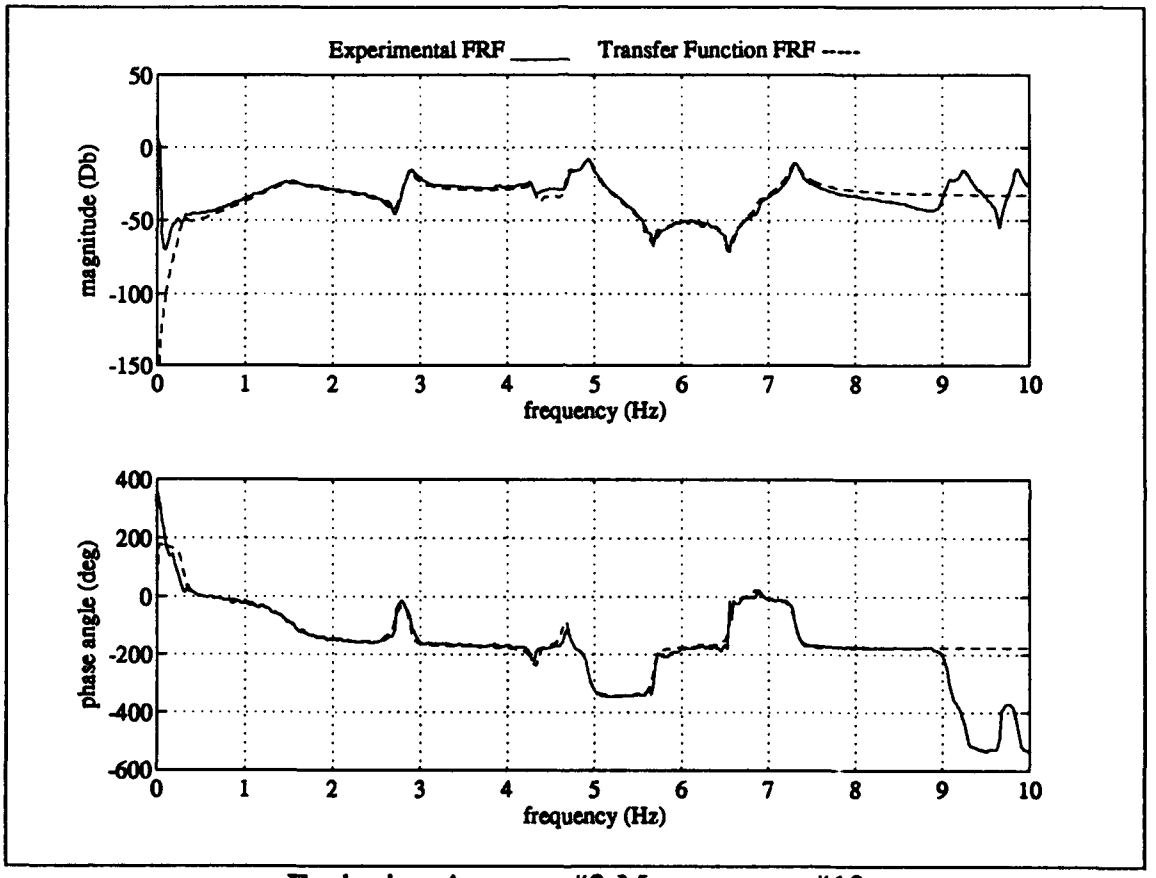

Excitation Actuator #3 Measurement #10

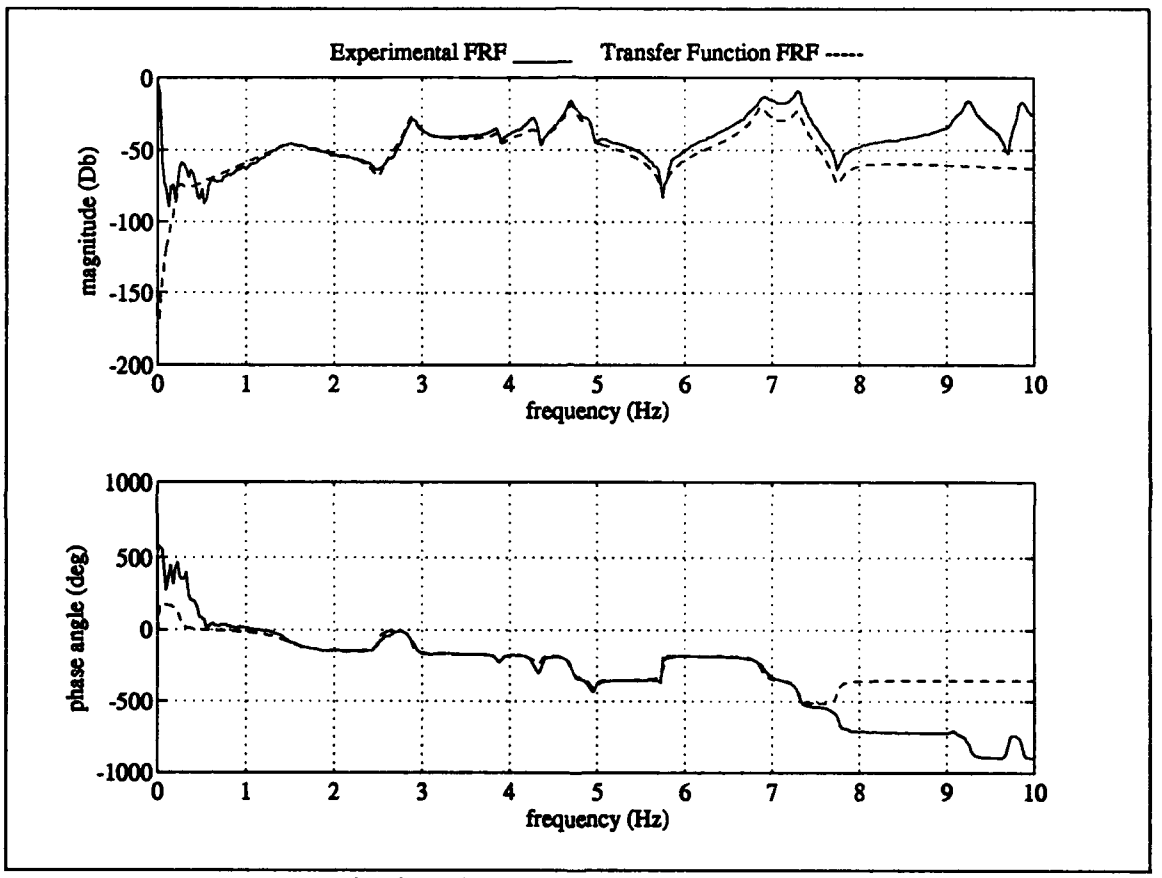

Excitation Actuator #4 Measurement #1

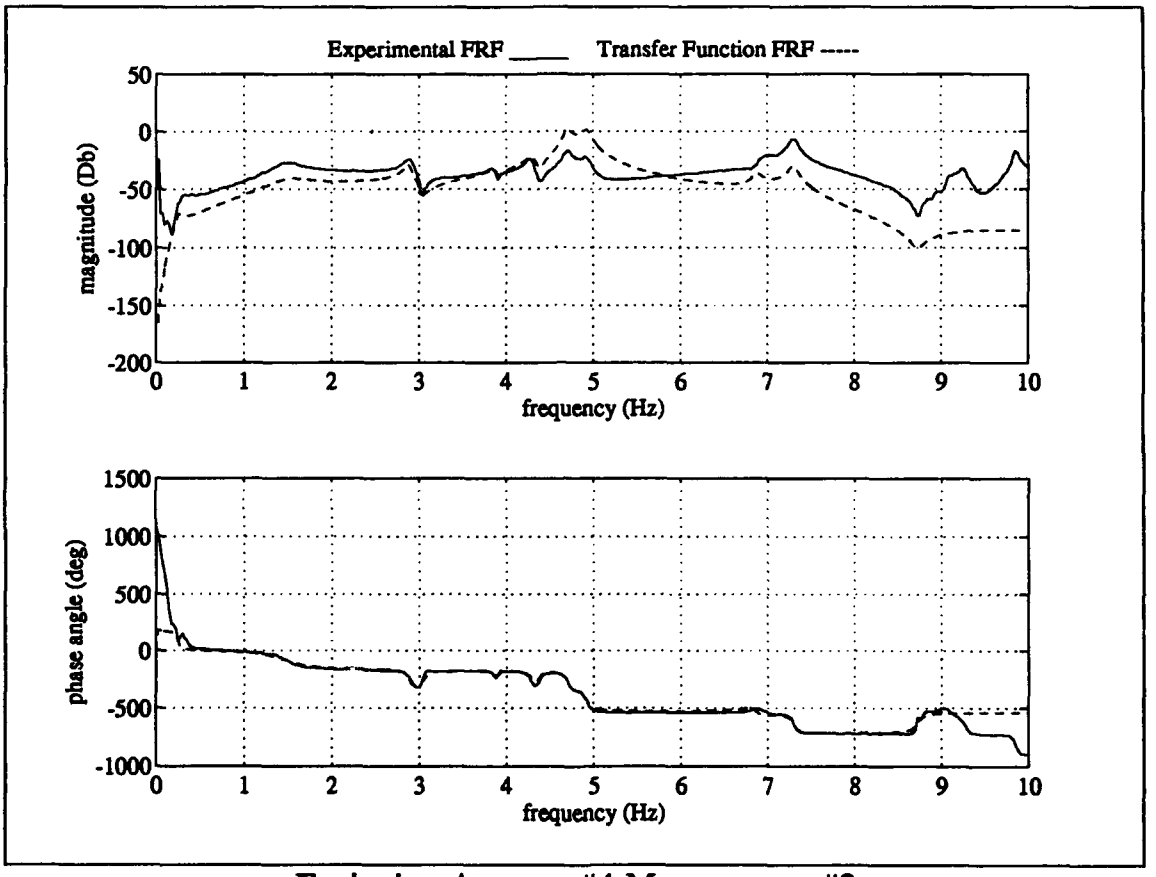

Excitation Actuator #4 Measurement #2

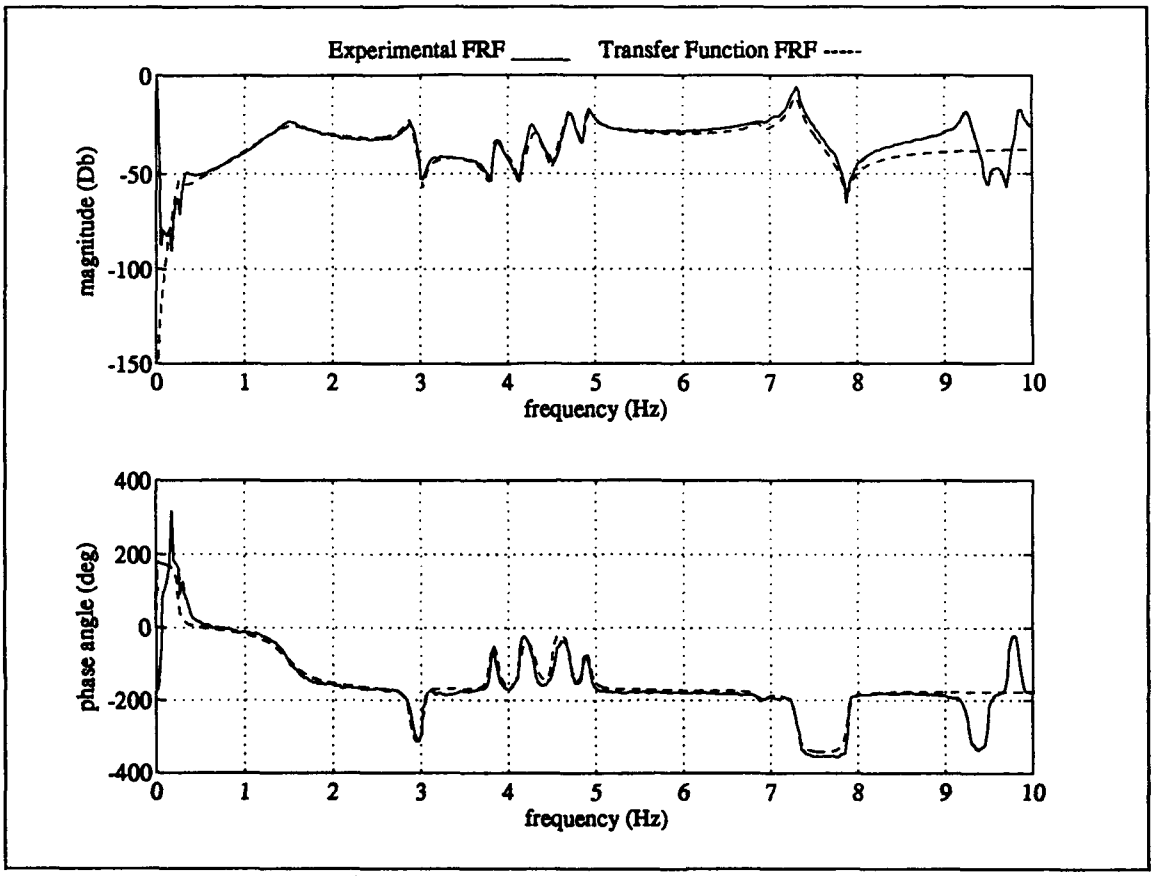

Excitation Actuator #4 Measurement #3

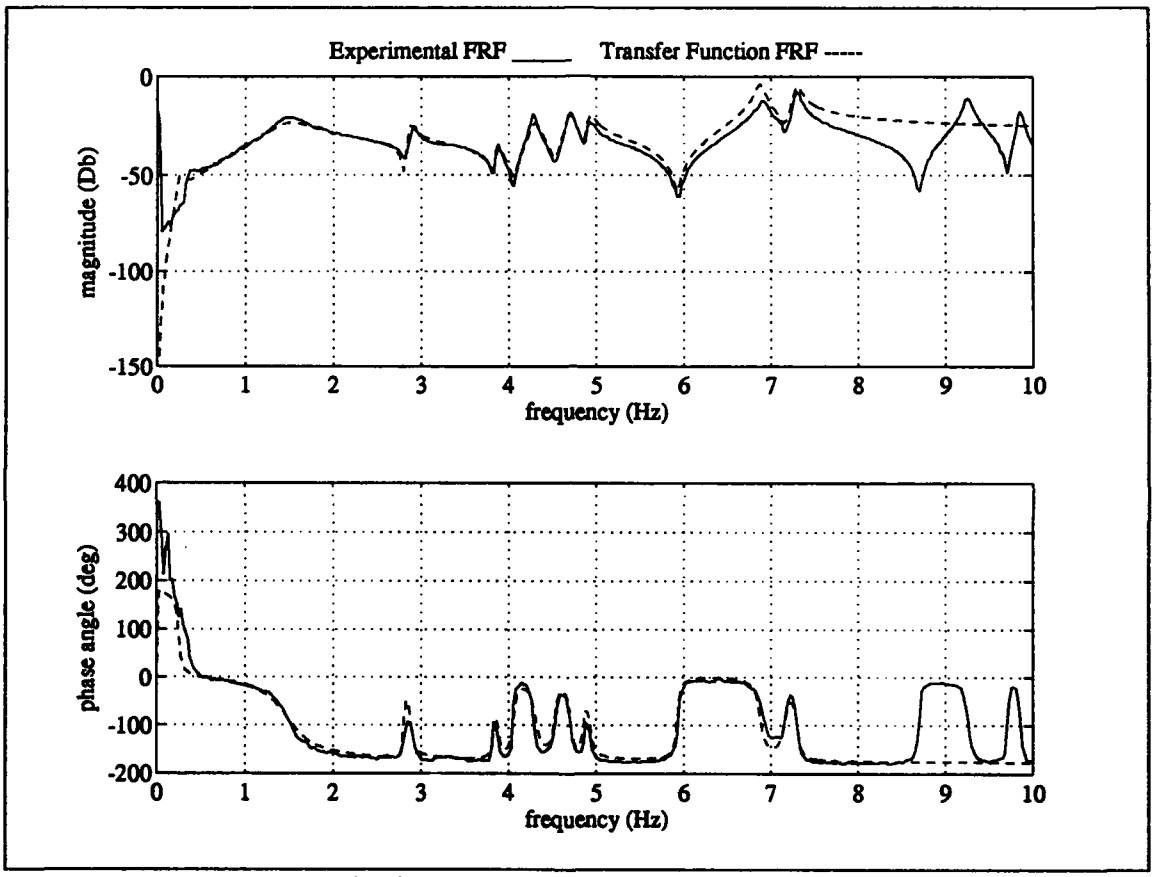

Excitation Actuator #4 Measurement #4

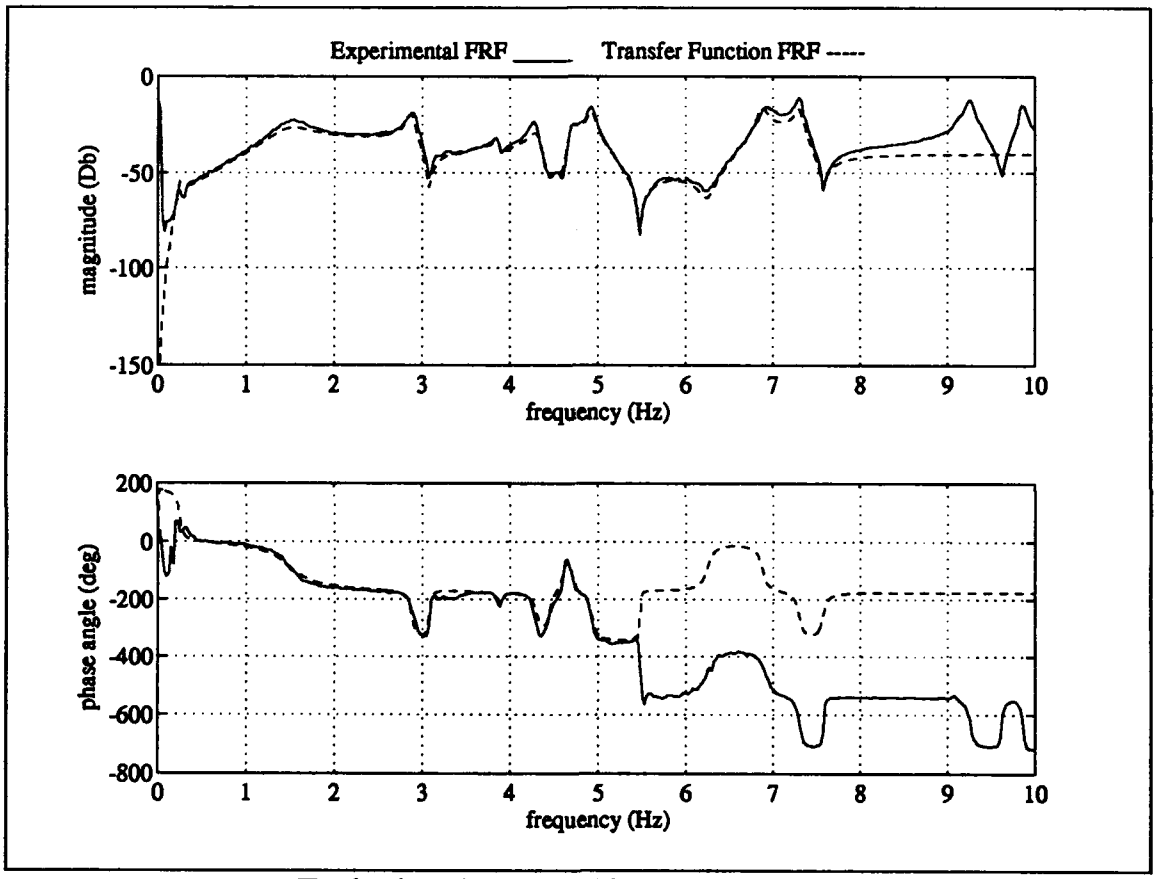

Excitation Actuator #4 Measurement #5

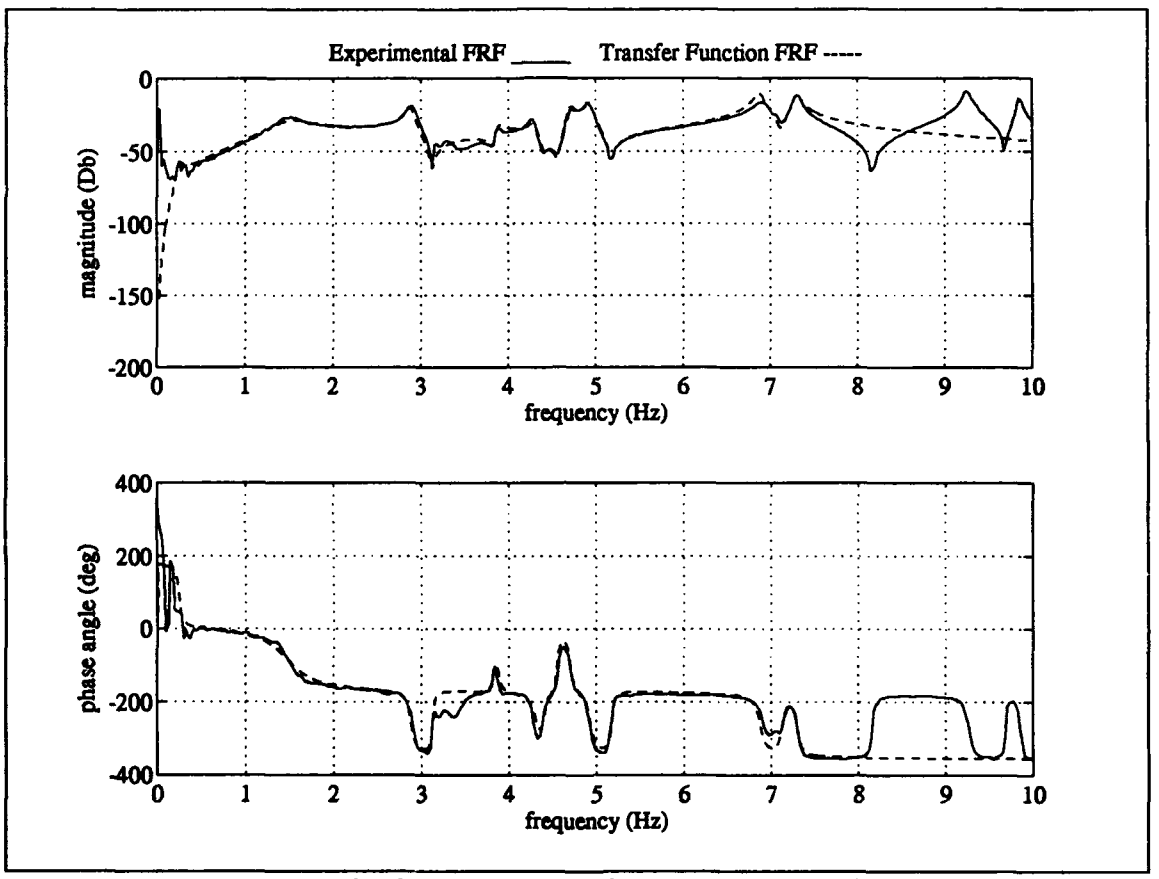

Excitation Actuator #4 Measurement #6

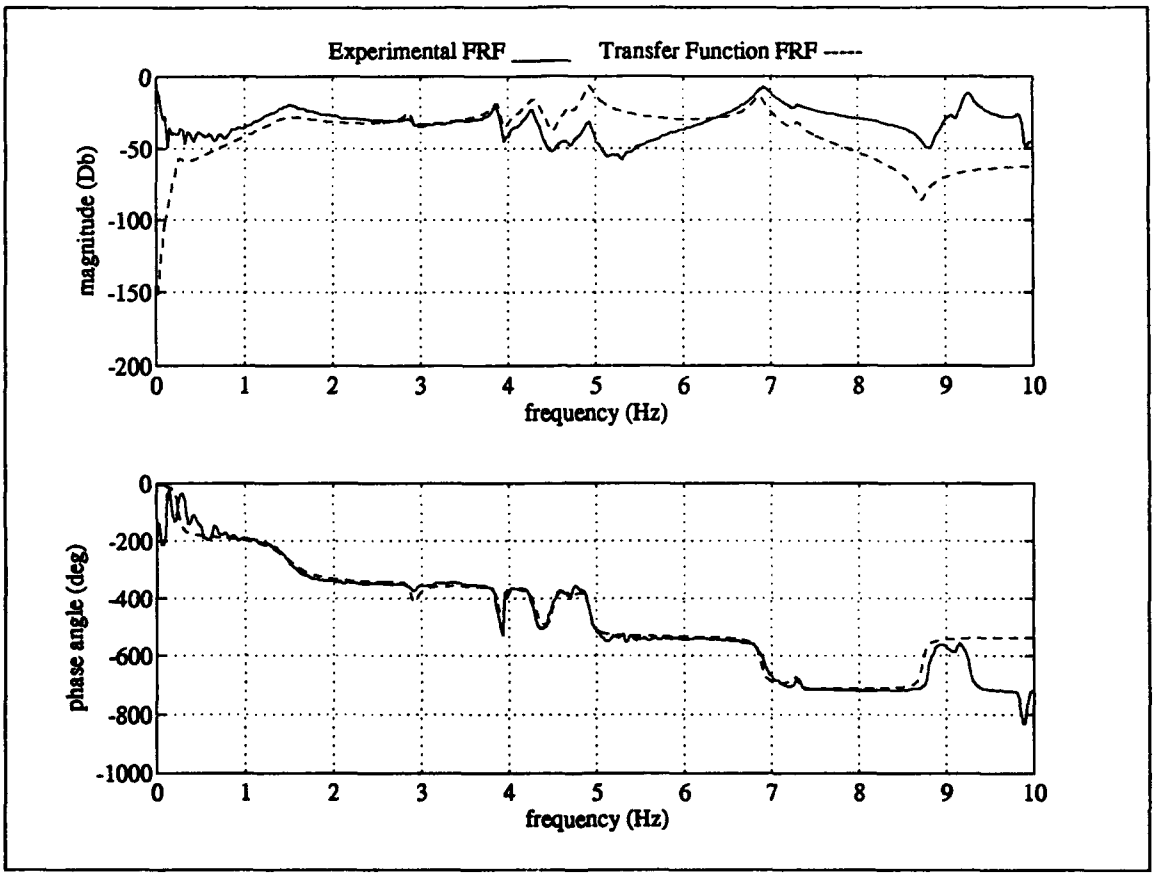

Excitation Actuator #4 Measurement #9

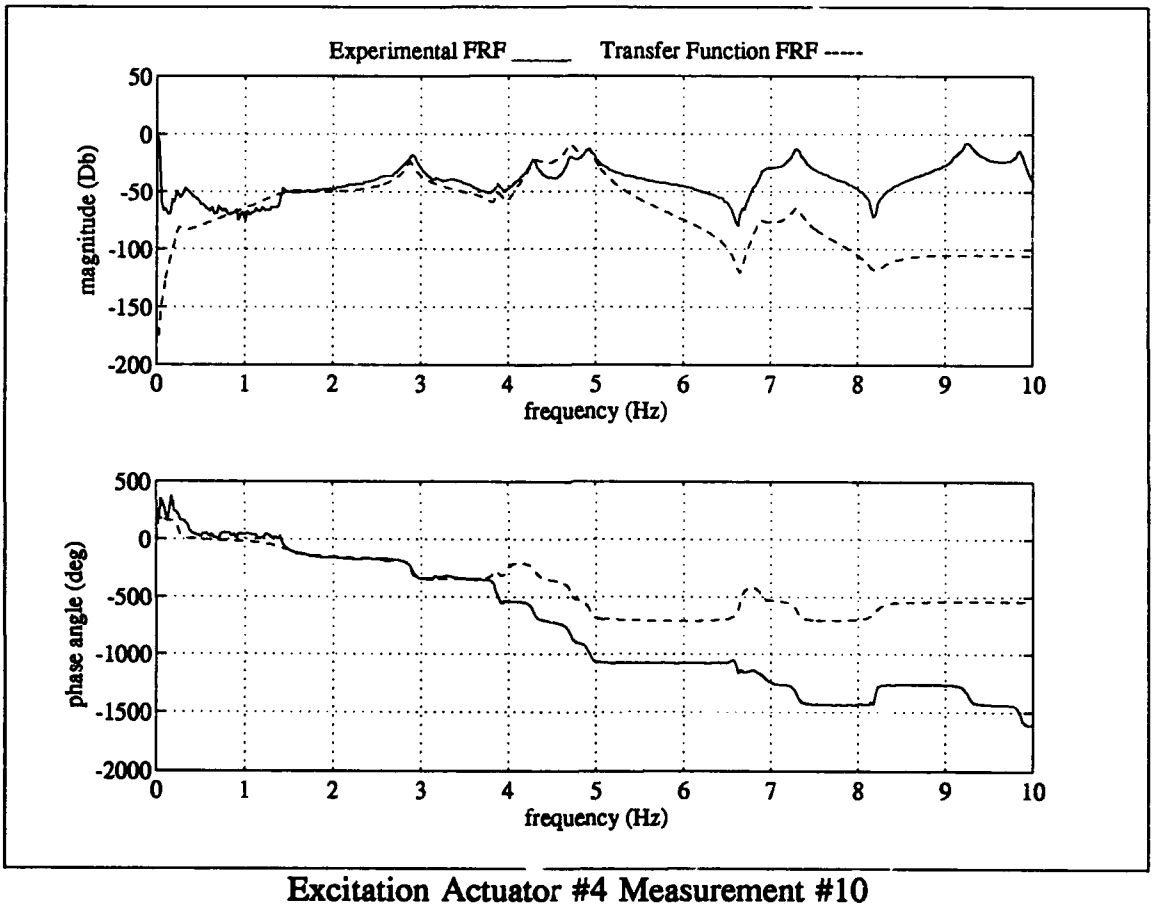

Excitation Actuator #4 Measurement #10

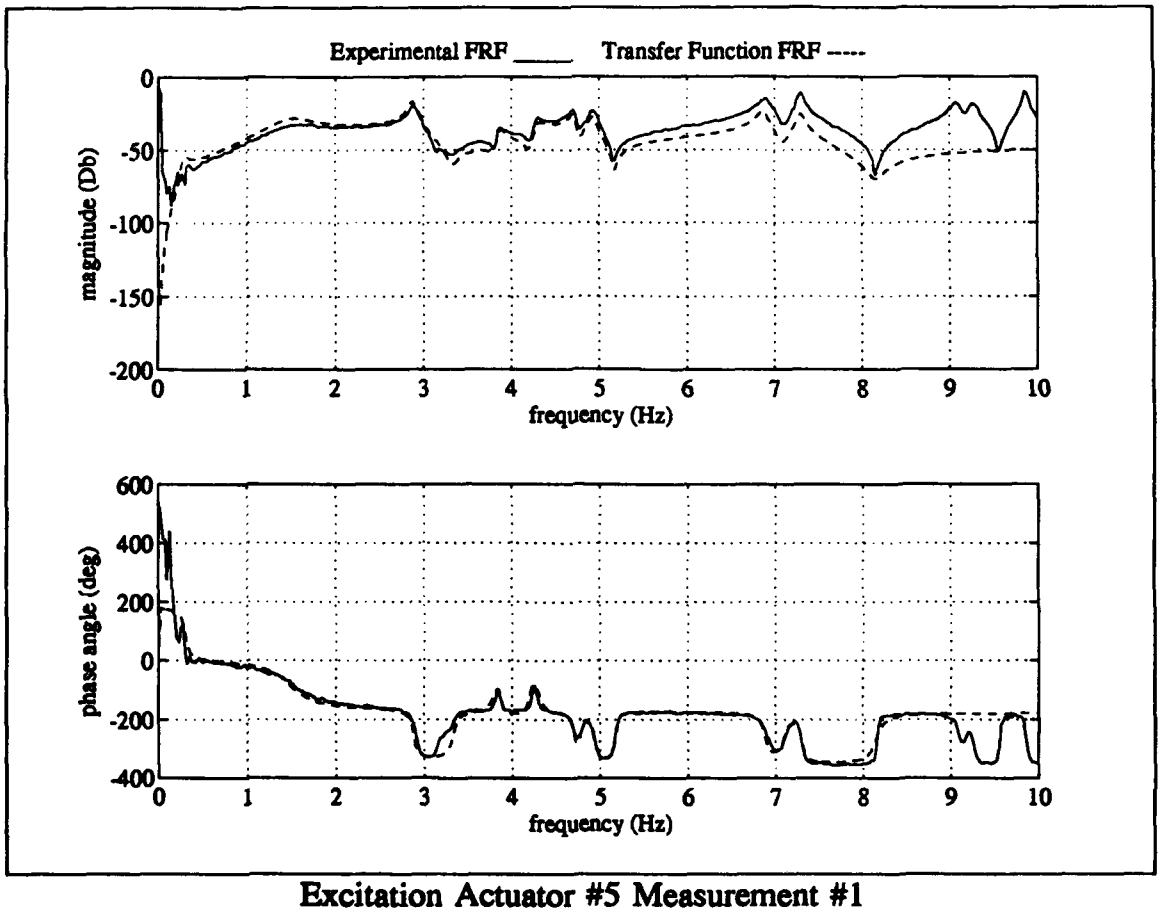

Excitation Actuator #5 Measurement #1

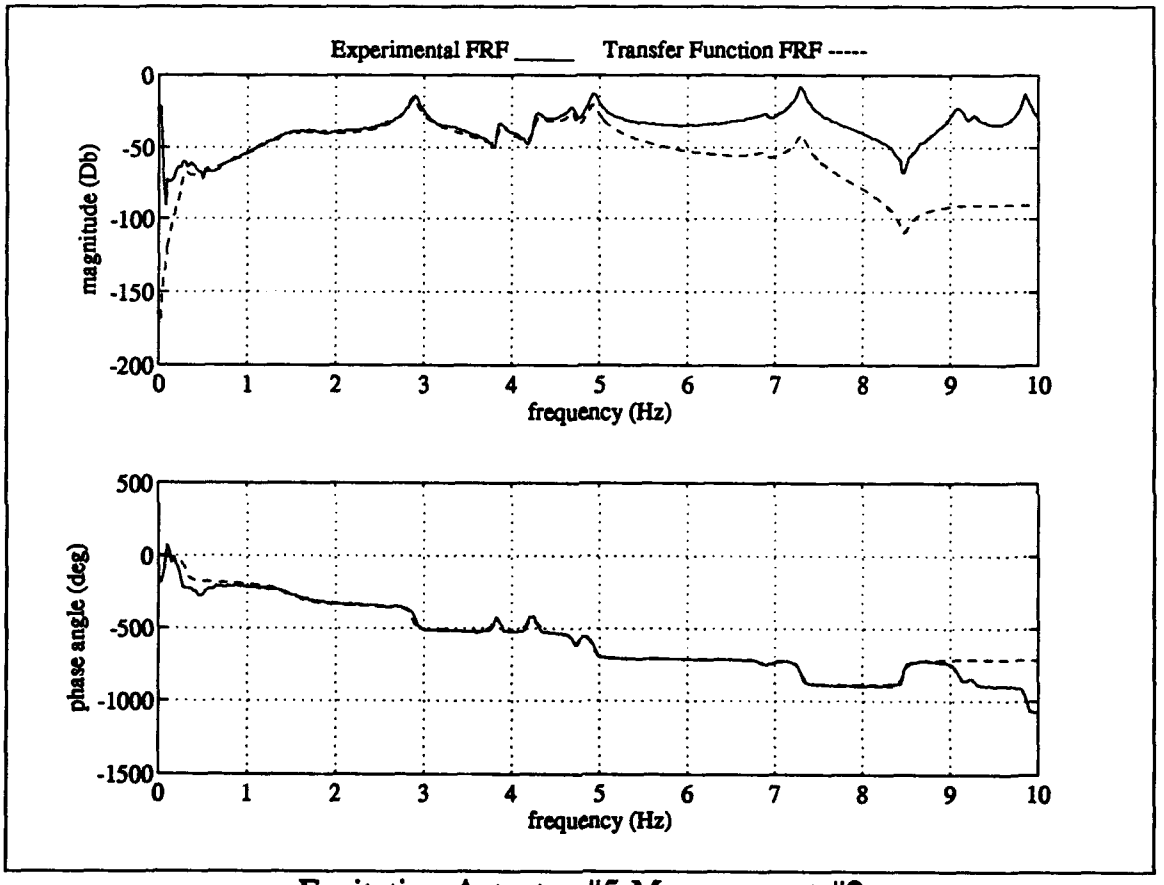

Excitation Actuator #5 Measurement #2

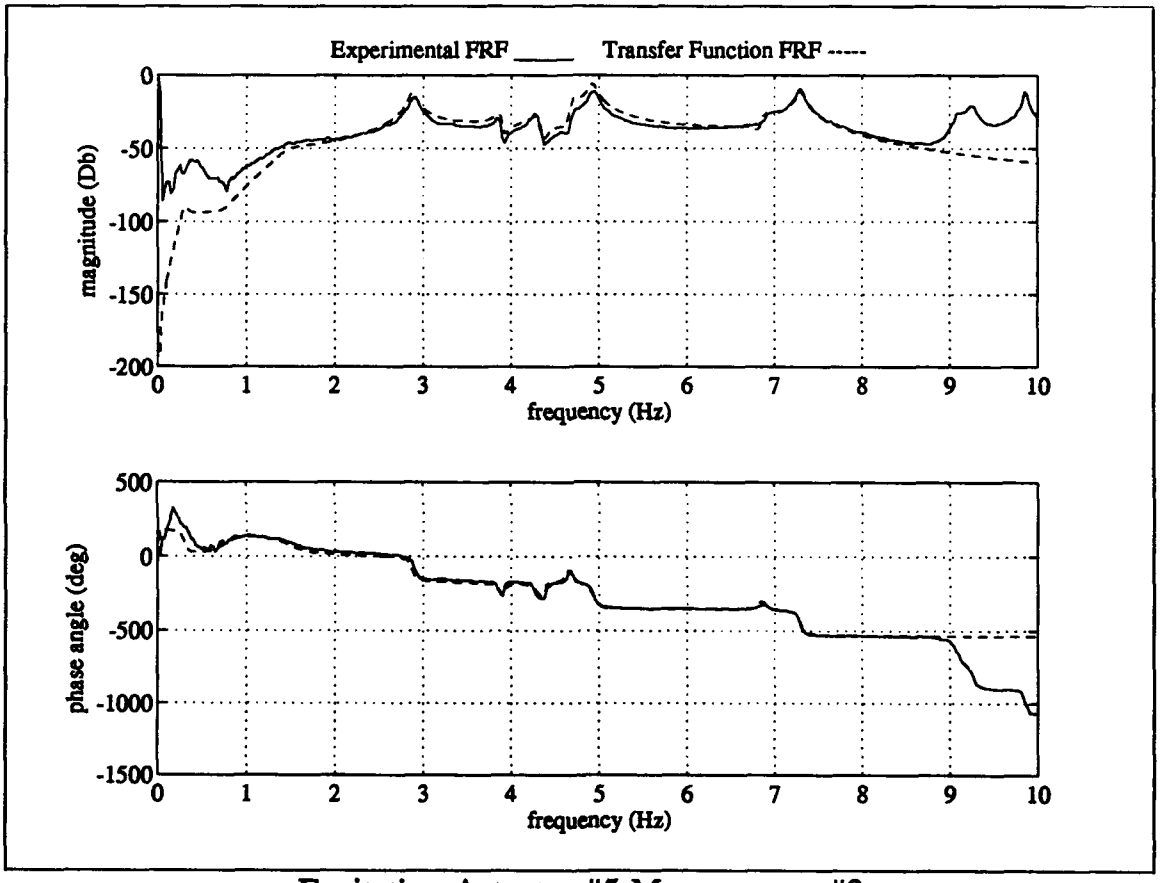

Excitation Actuator #5 Measurement #3

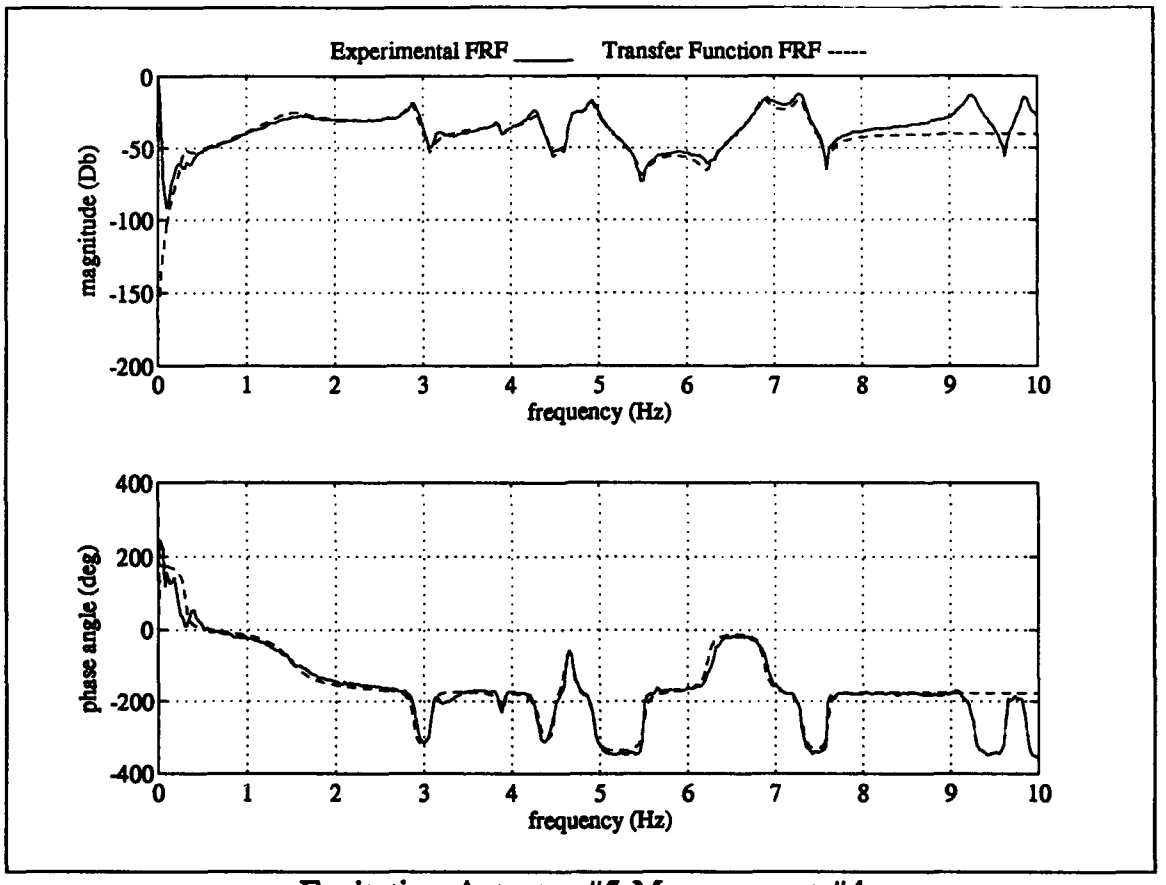

Excitation Actuator #5 Measurement #4

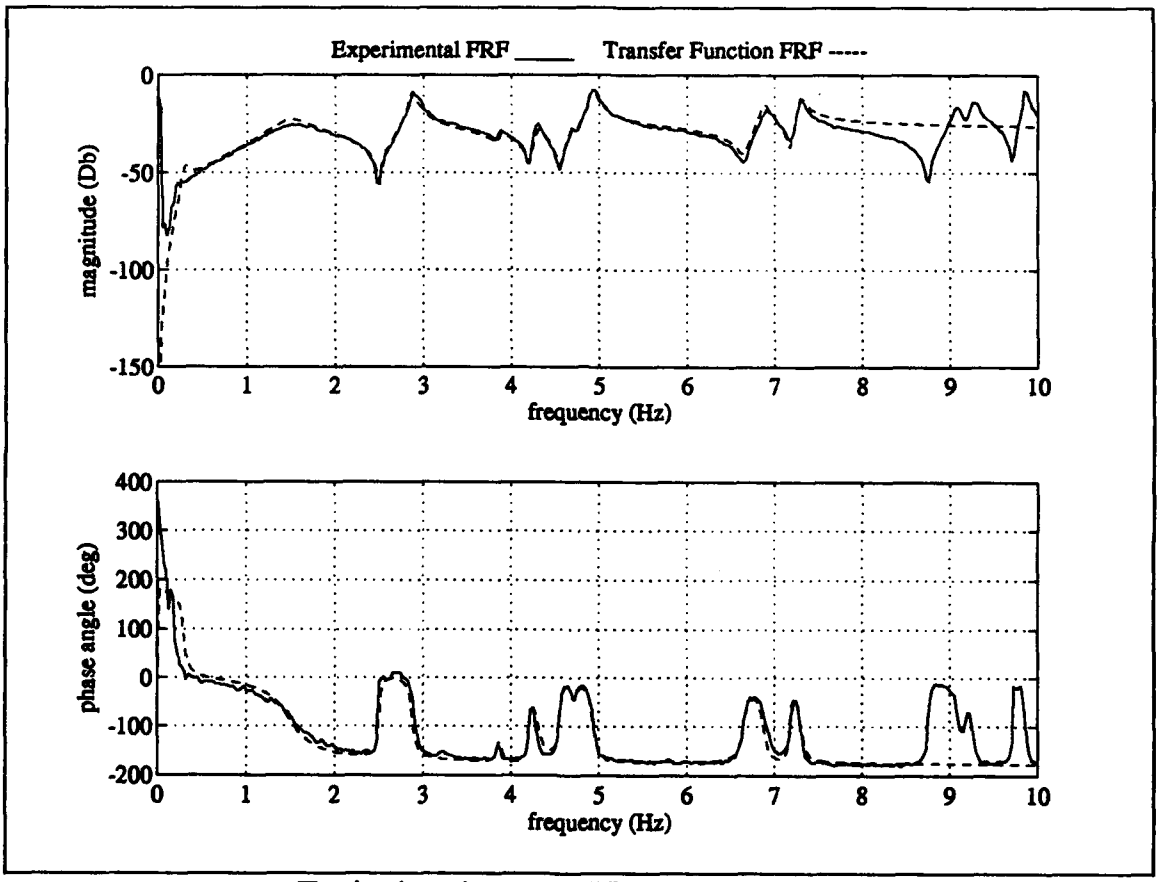

Excitation Actuator #5 Measurement #5

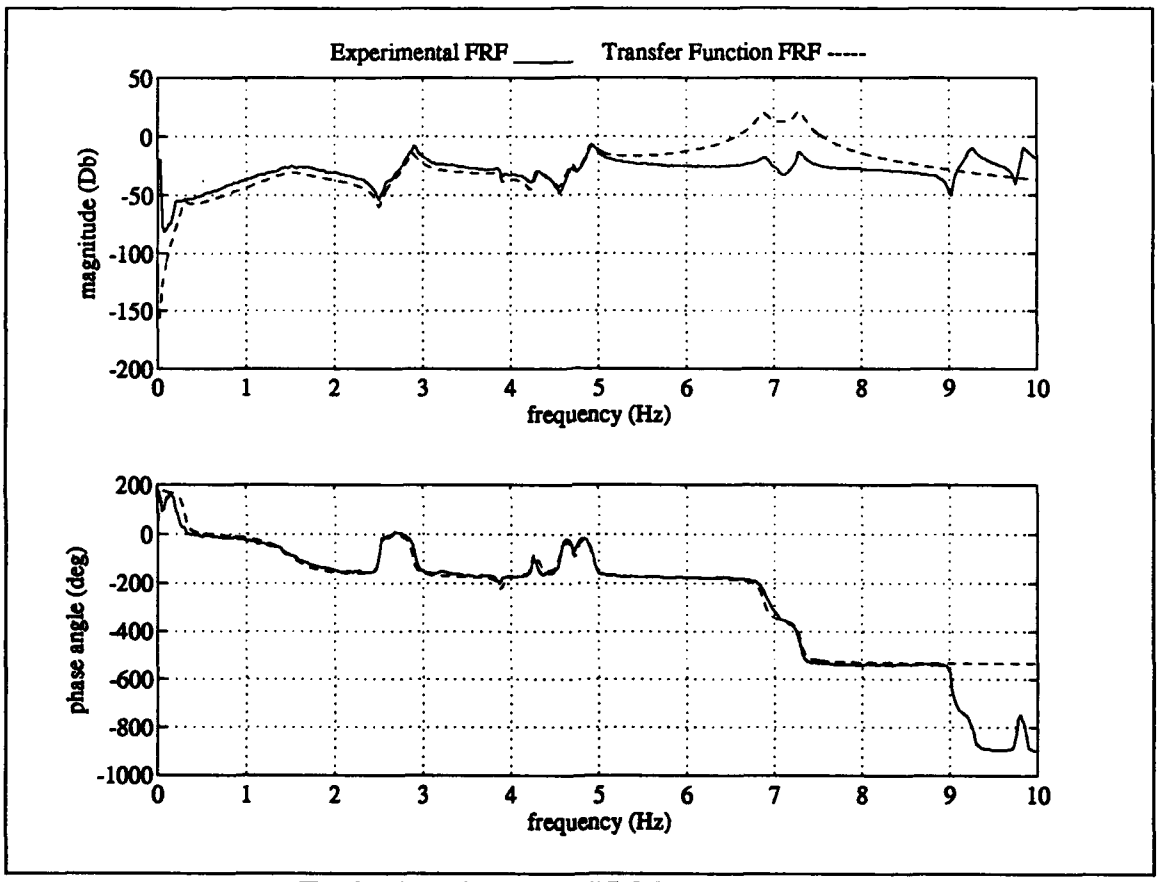

Excitation Actuator #5 Measurement #6

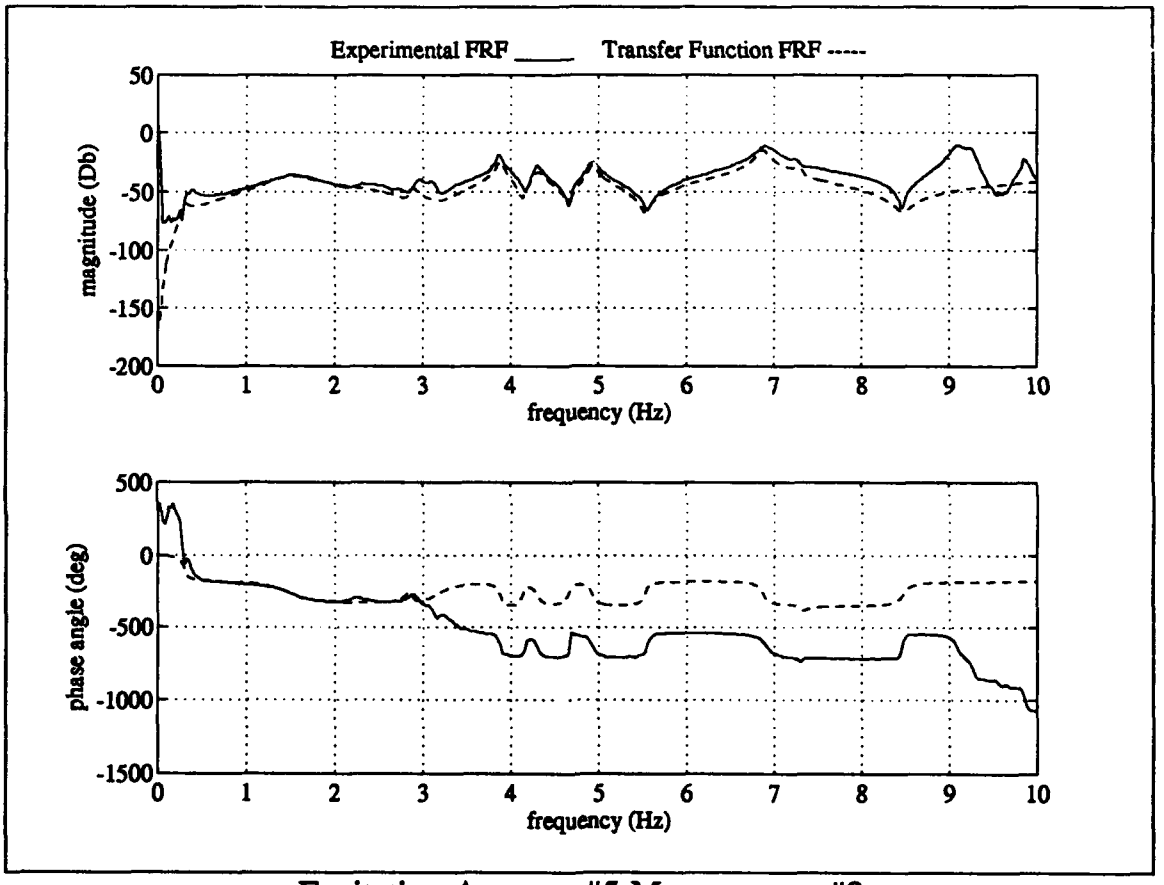

Excitation Actuator #5 Measurement #9

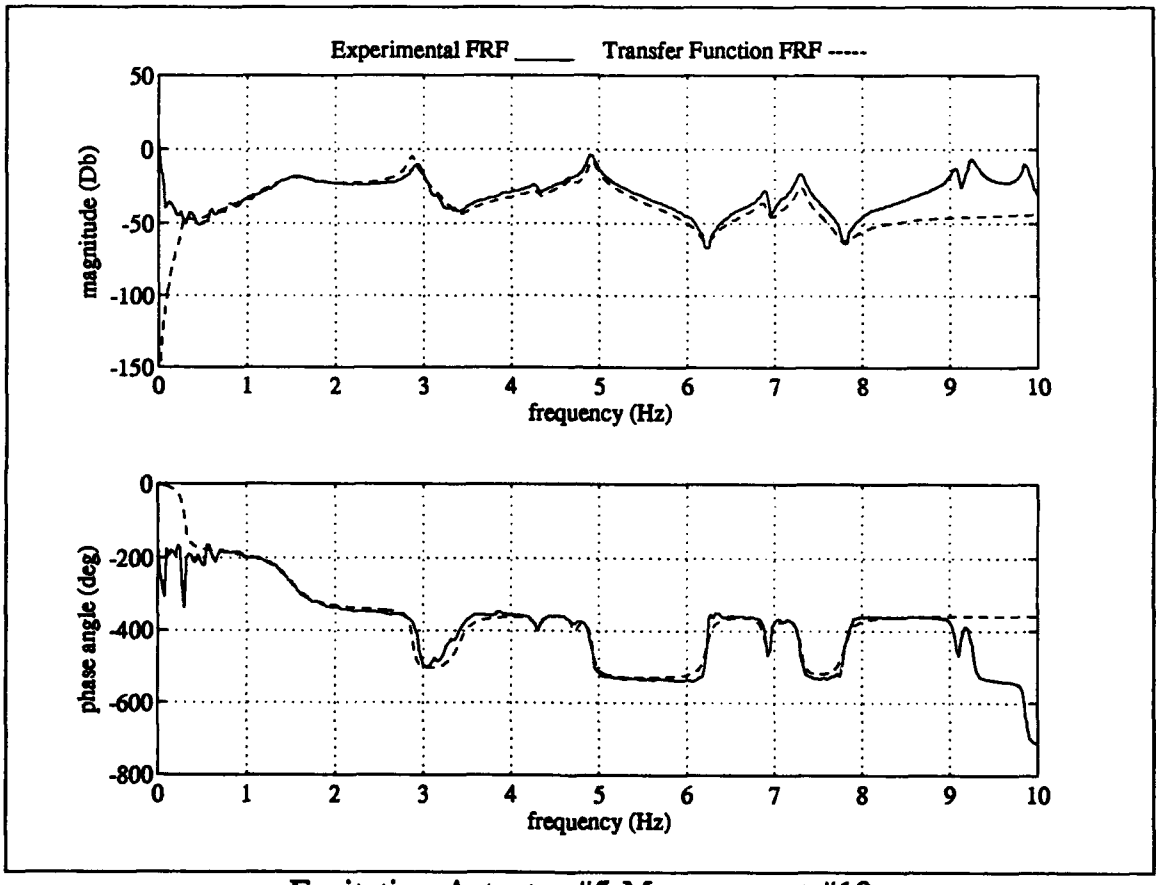

Excitation Actuator #5 Measurement #10

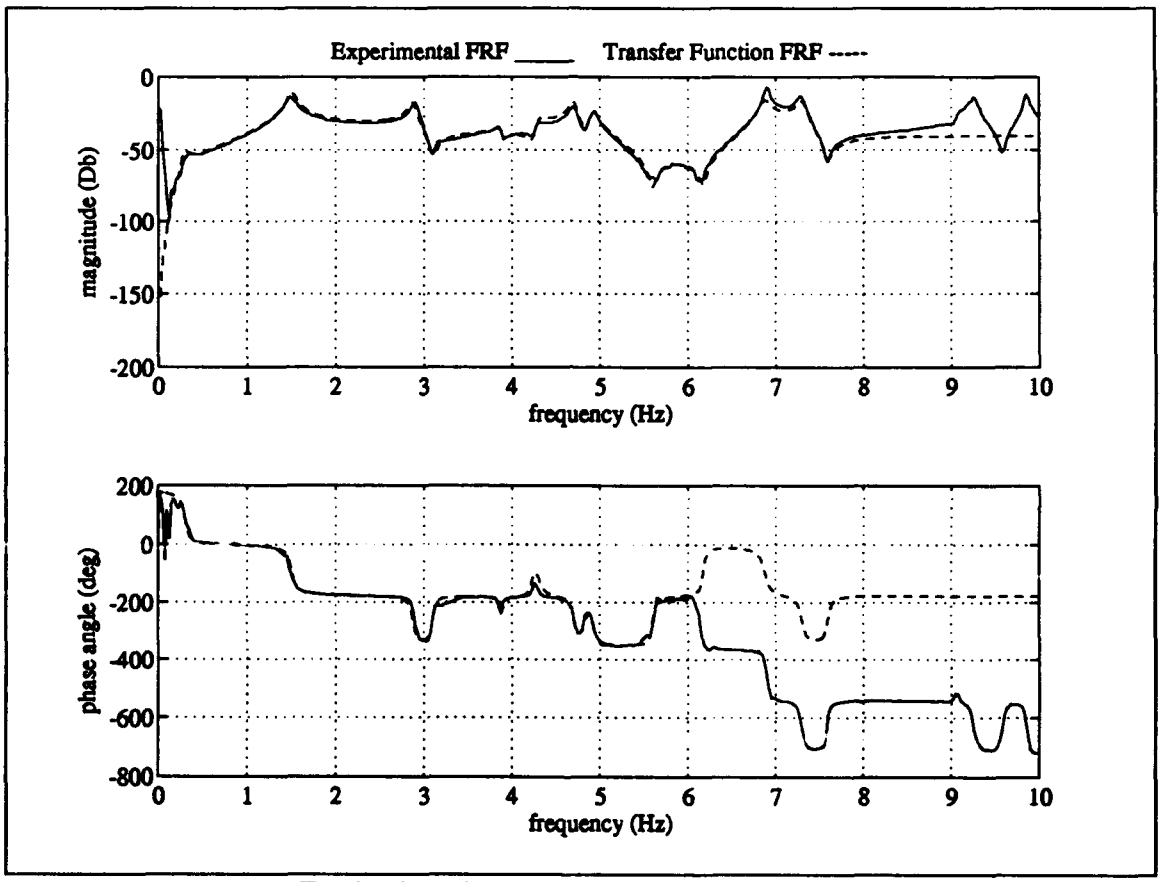

Excitation Actuator #6 Measurement #1

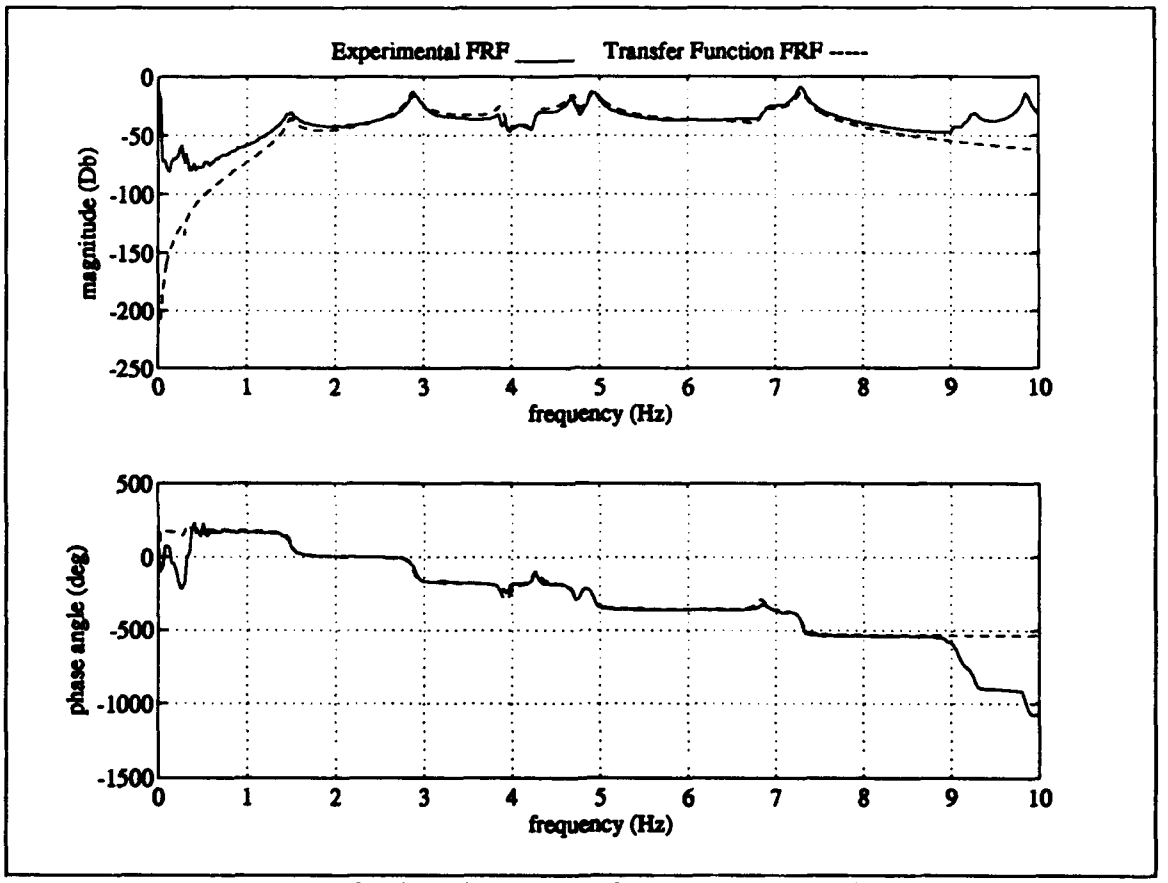

Excitation Actuator #6 Measurement #2

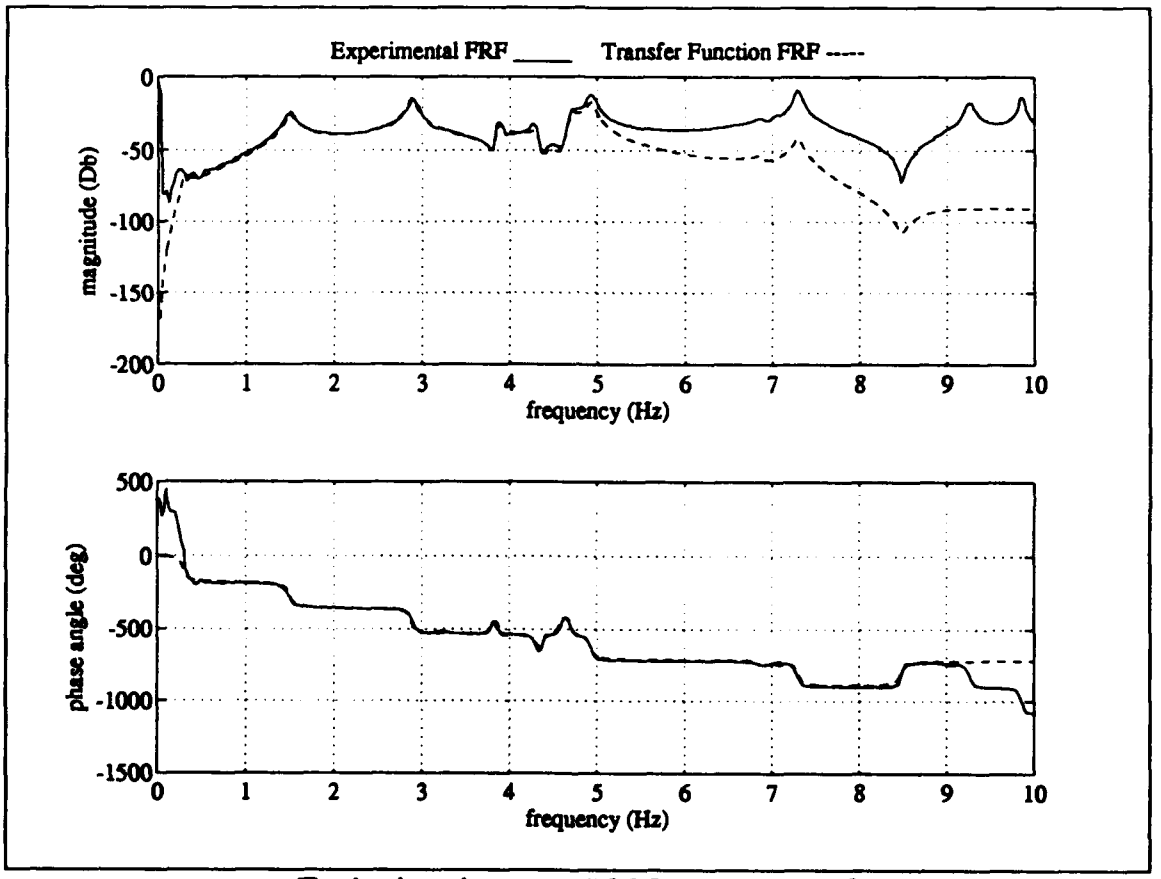

Excitation Actuator #6 Measurement #3

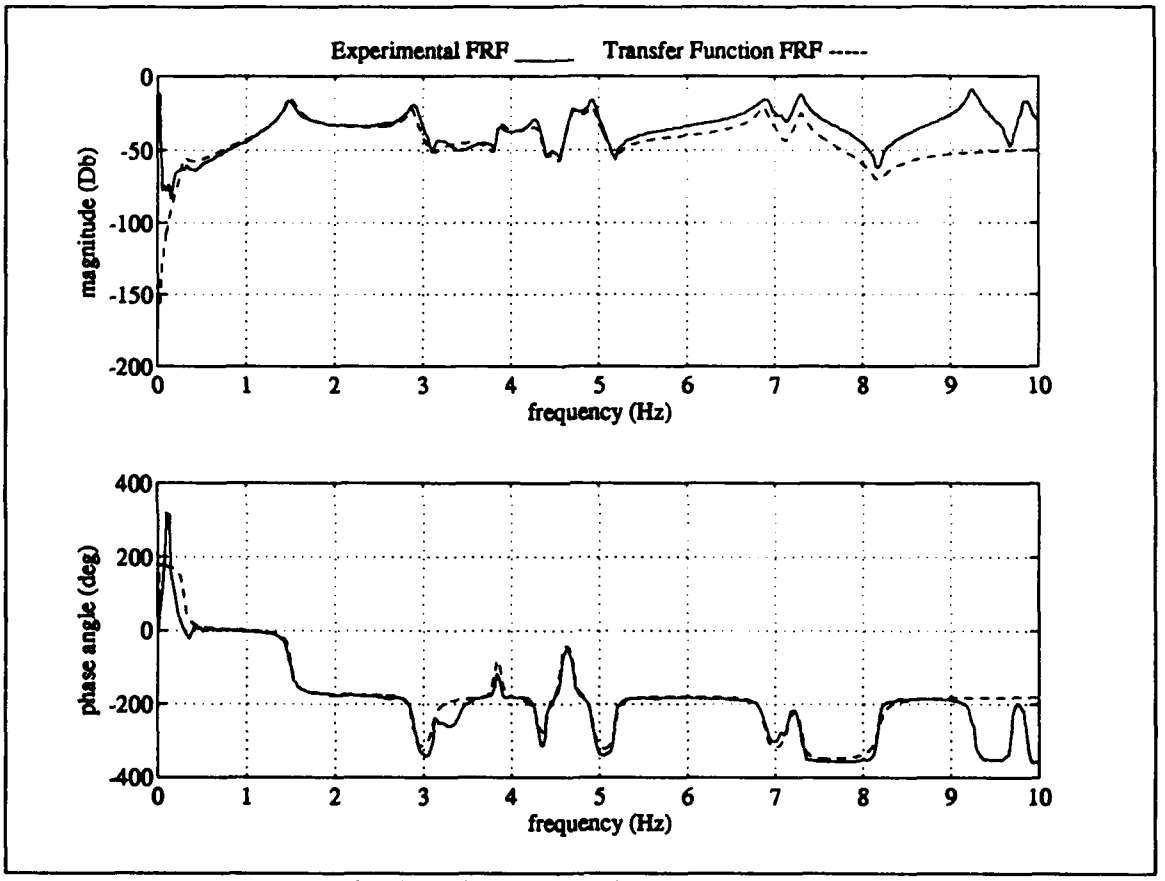

Excitation Actuator #6 Measurement #4

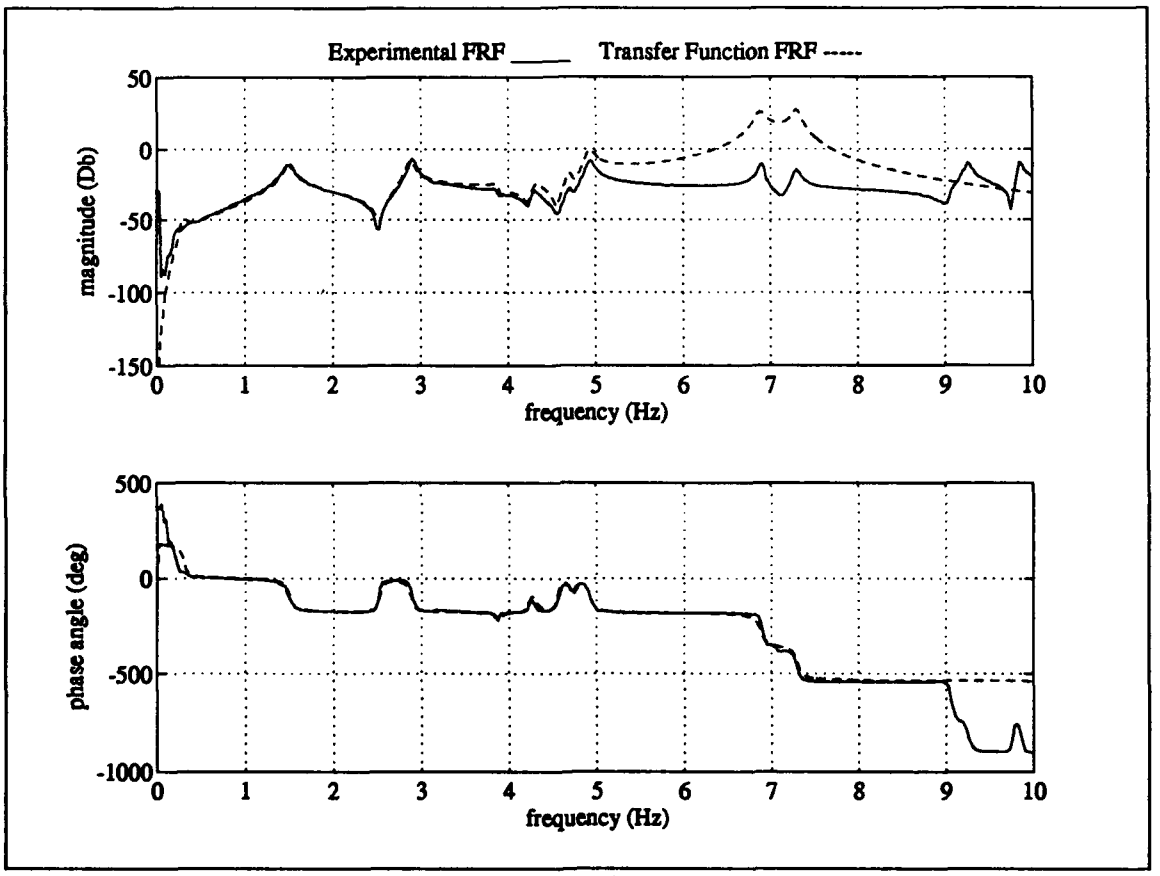

Excitation Actuator #6 Measurement #5

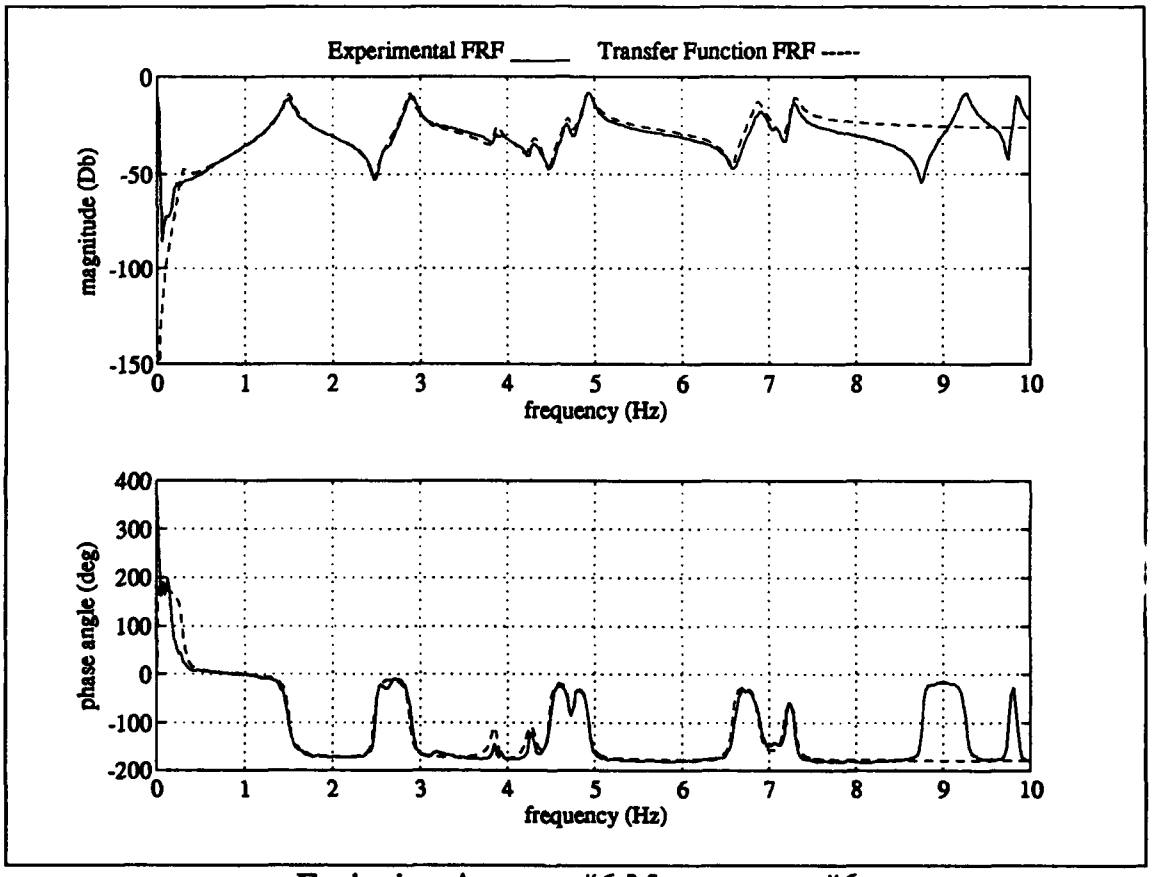

Excitation Actuator #6 Measurement #6

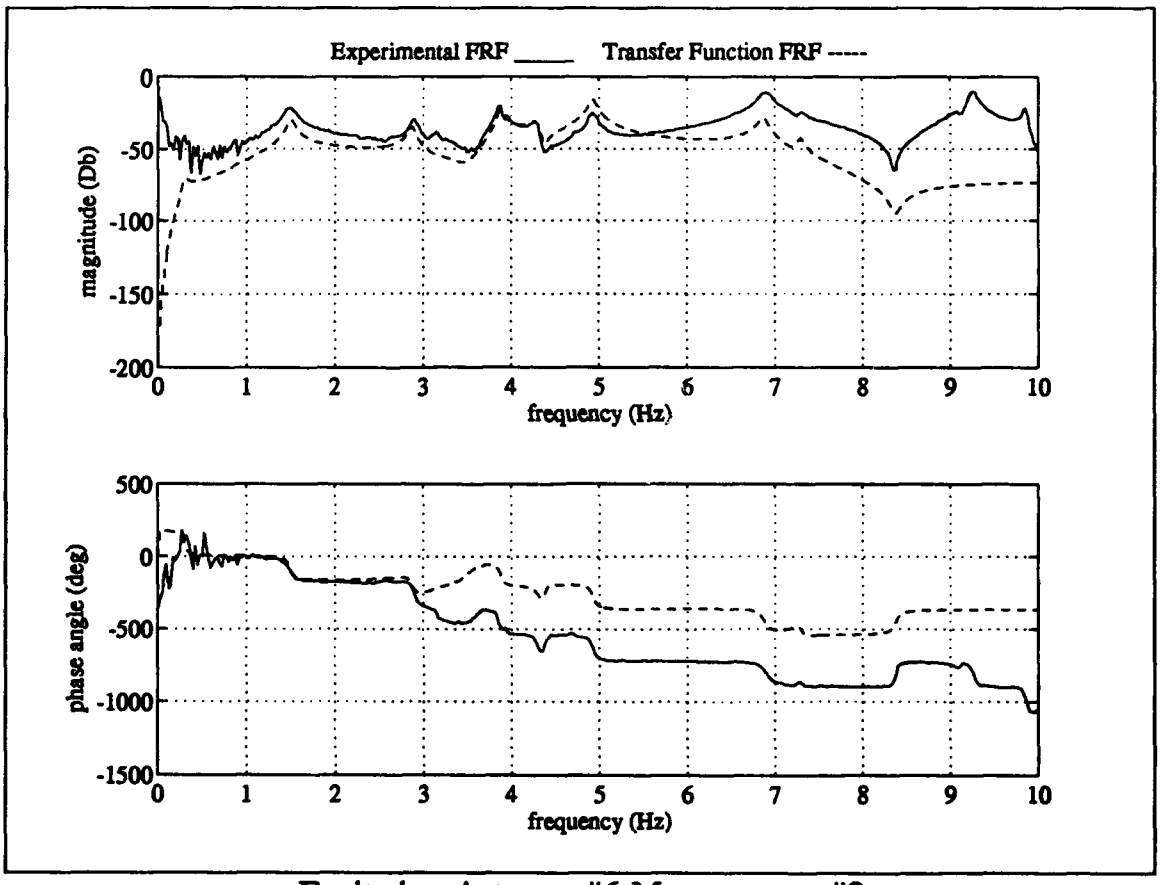

Excitation Actuator #6 Measurement #9

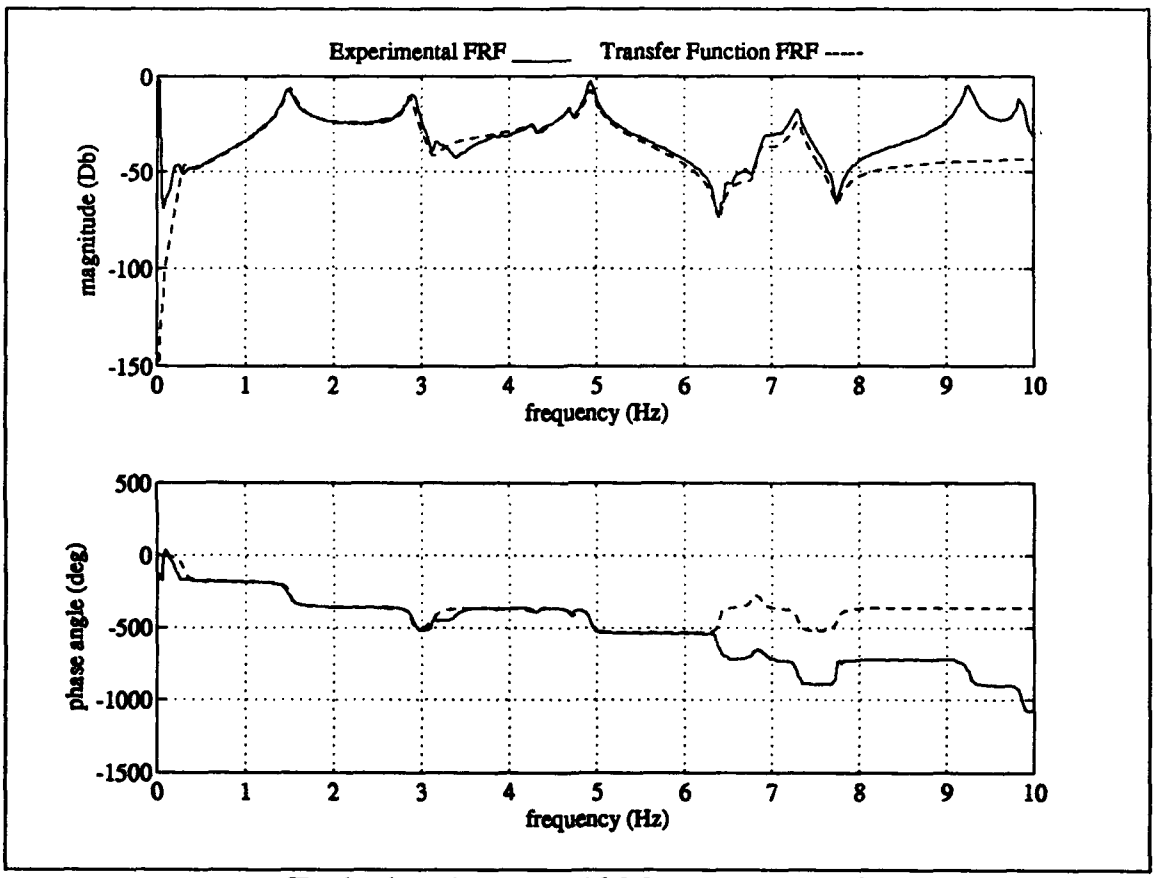

Excitation Actuator #6 Measurement #10

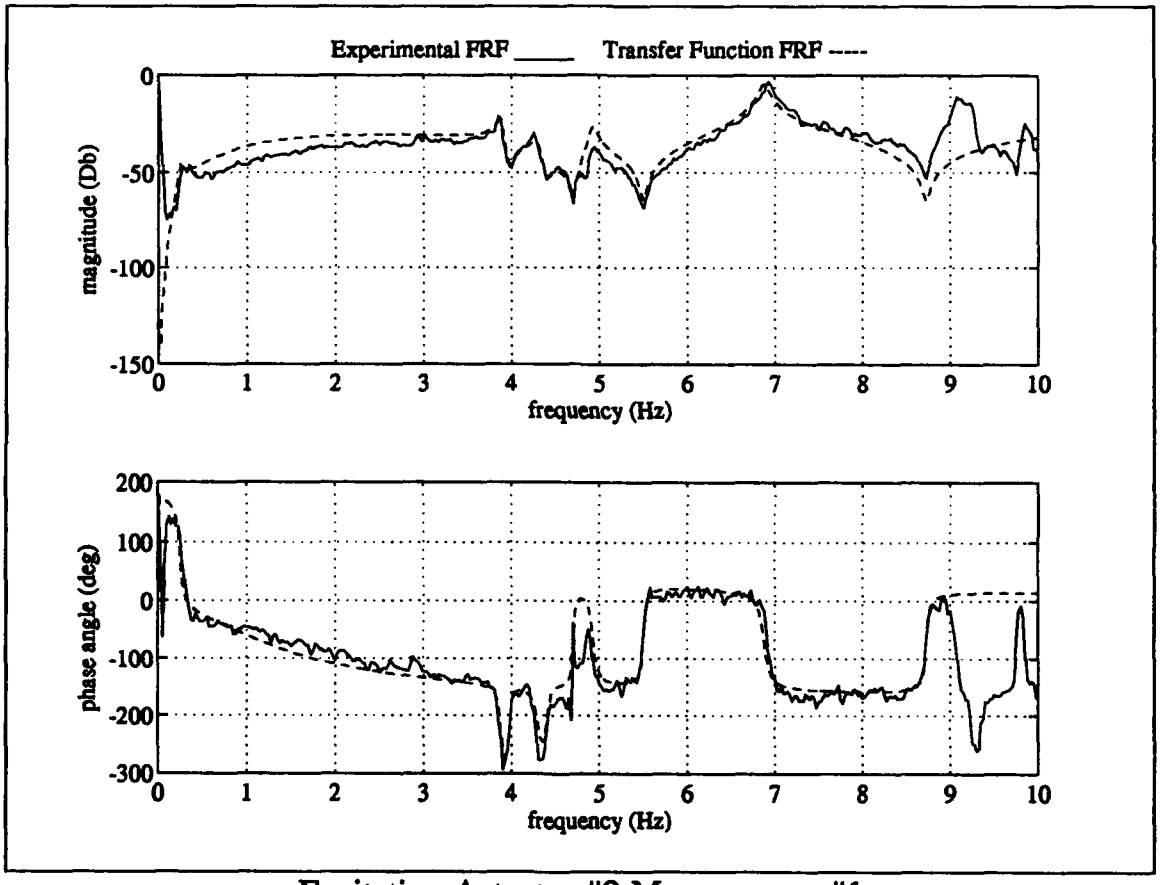

Excitation Actuator #9 Measurement #1

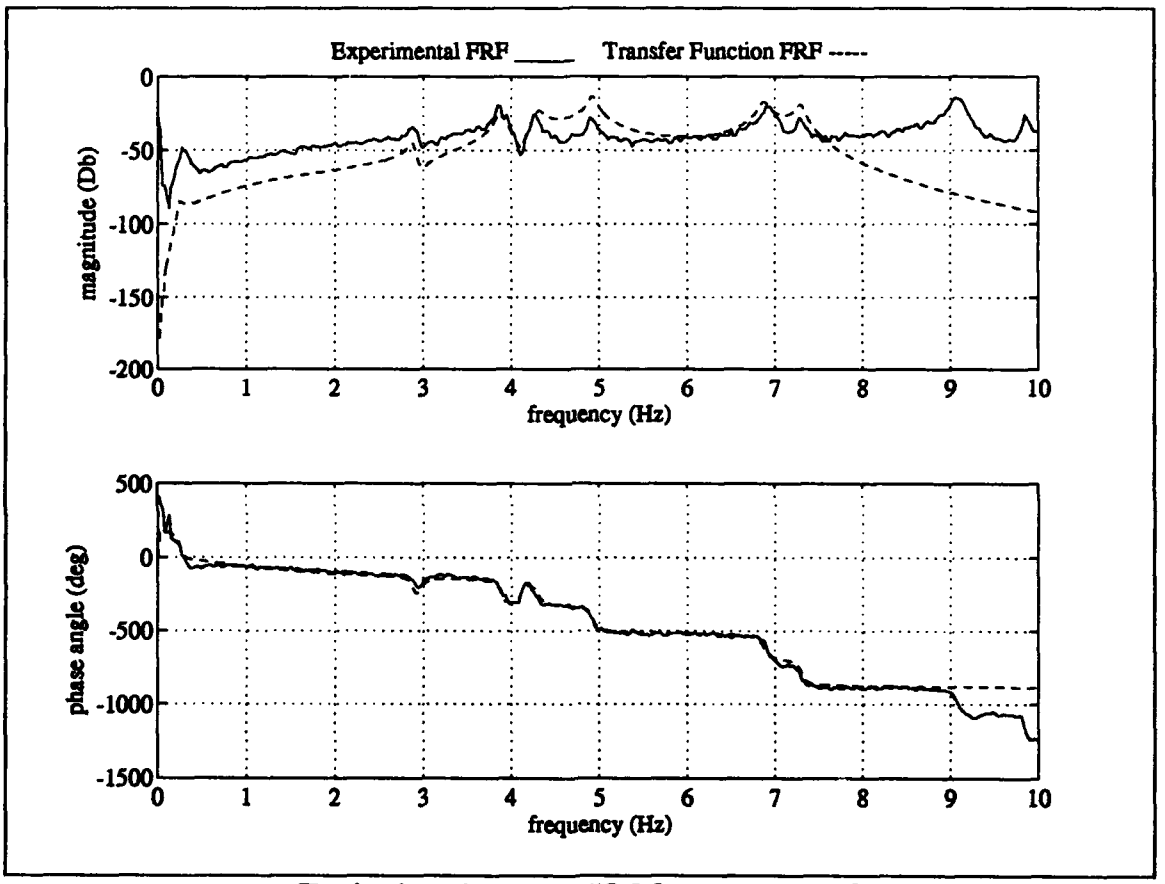

Excitation Actuator #9 Measurement #2

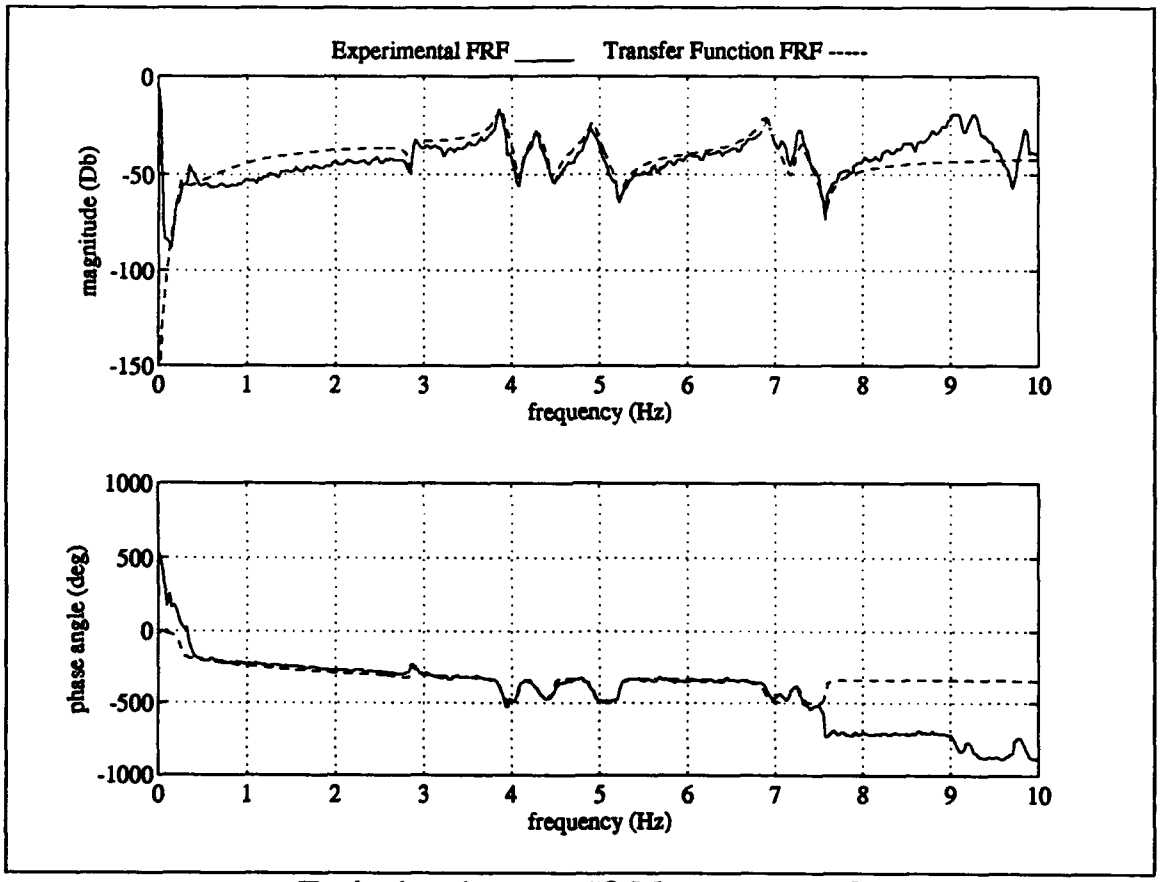

Excitation Actuator #9 Measurement #3

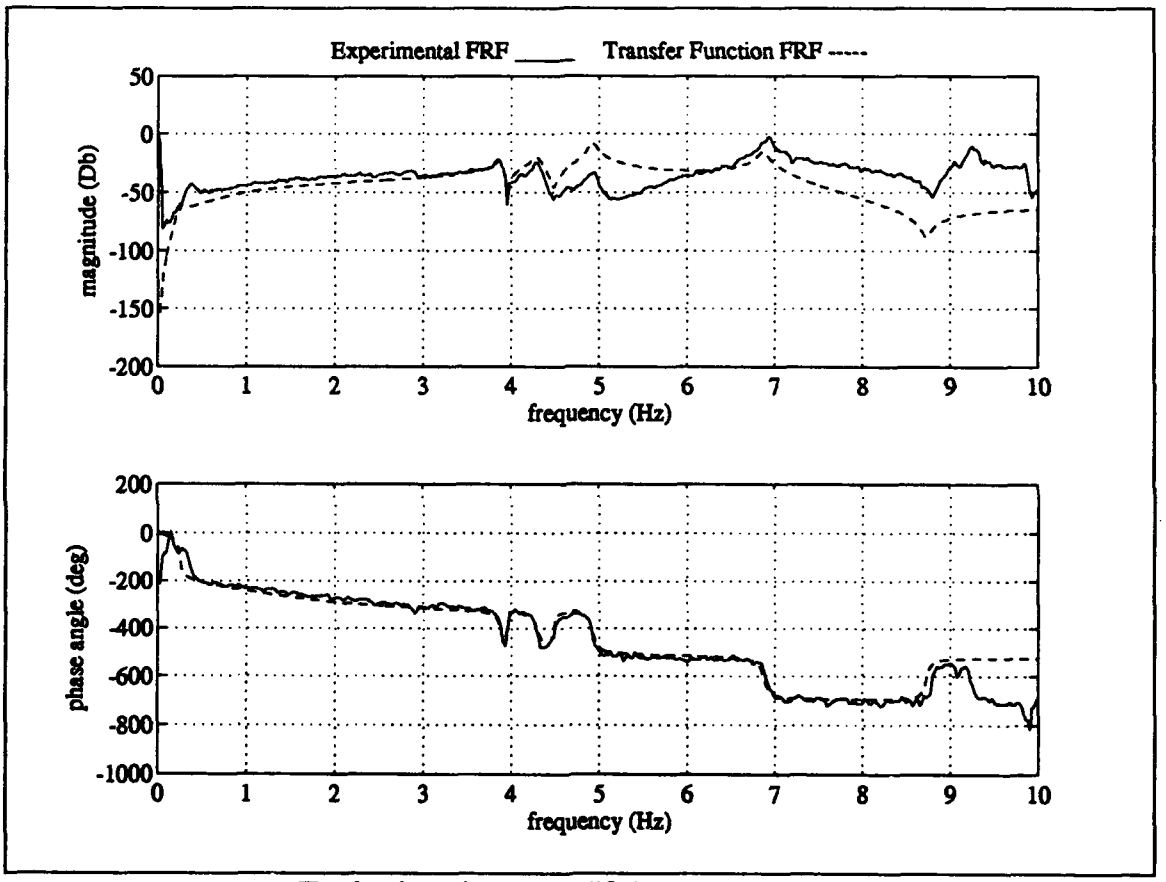

Excitation Actuator #9 Measurement #4

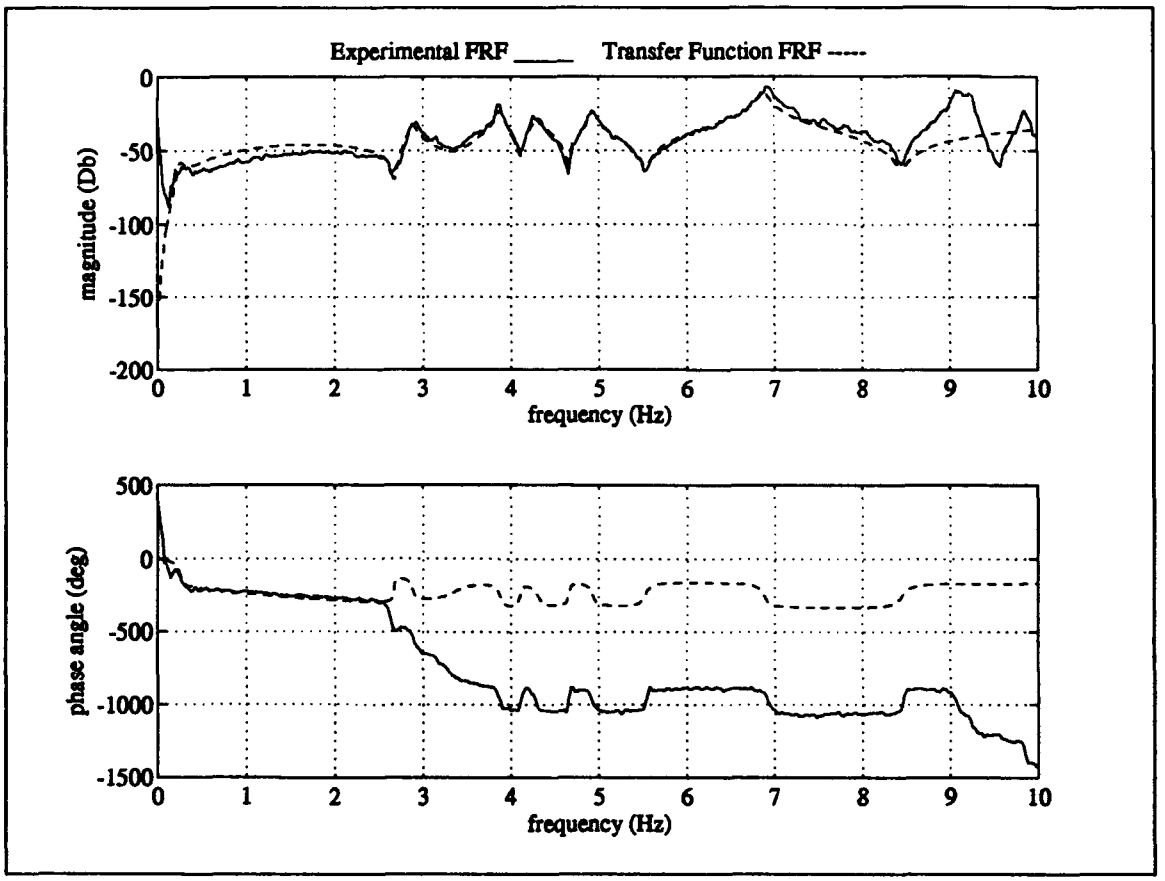

Excitation Actuator #9 Measurement #5

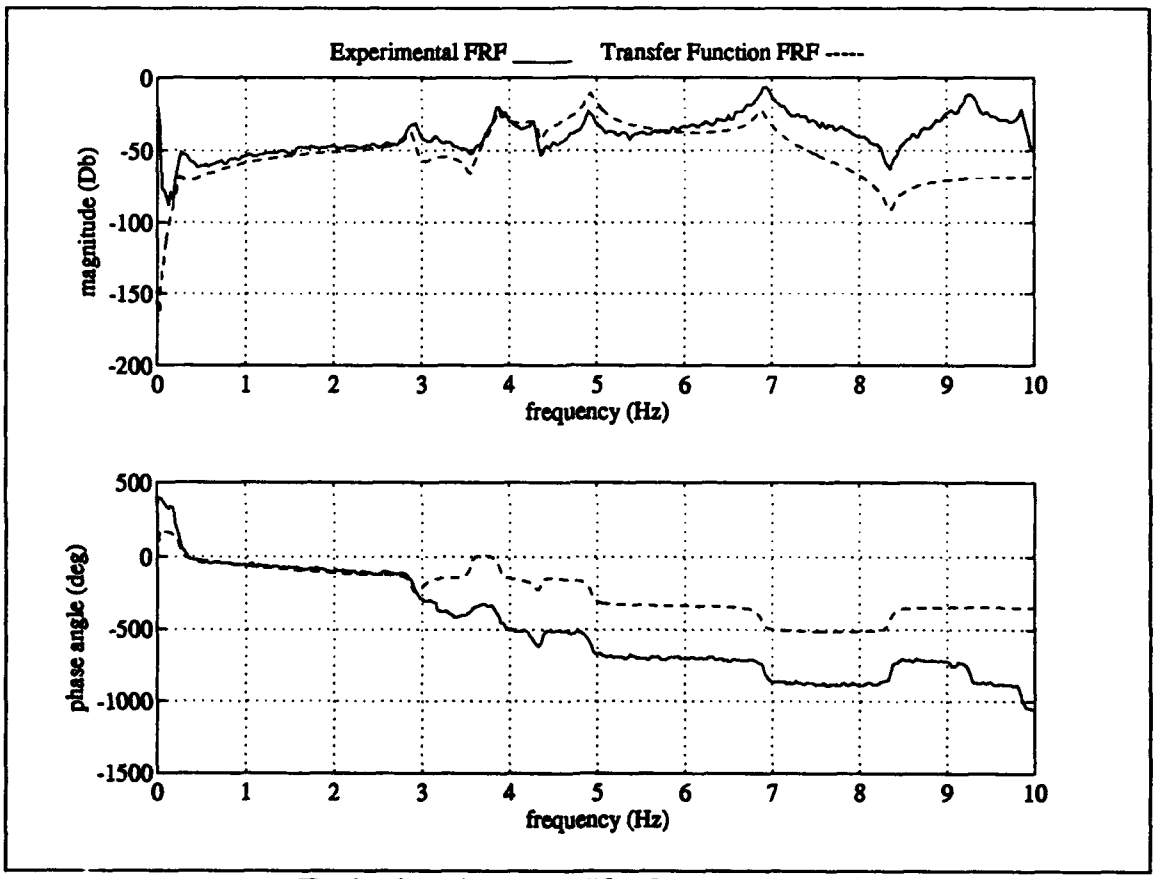

Excitation Actuator #9 Measurement #6

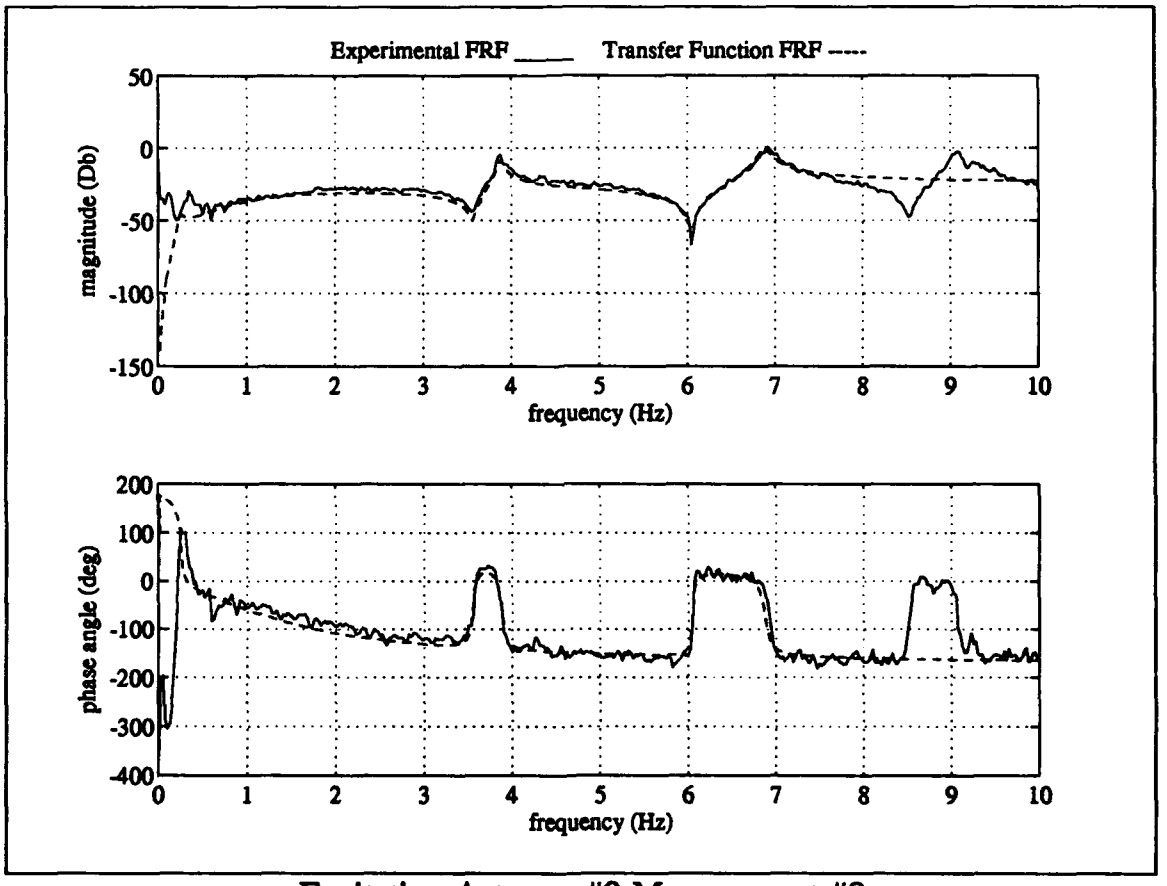

Excitation Actuator #9 Measurement #9

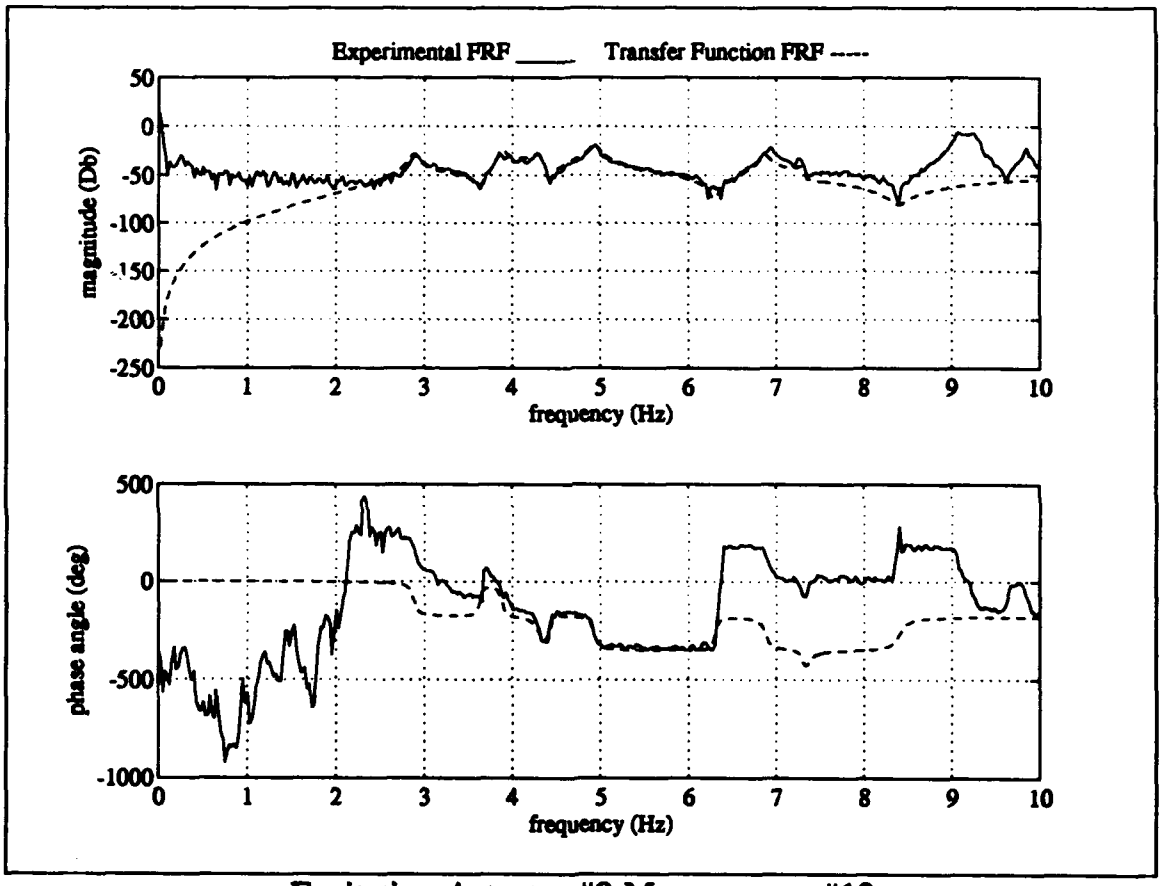

Excitation Actuator #9 Measurement #10

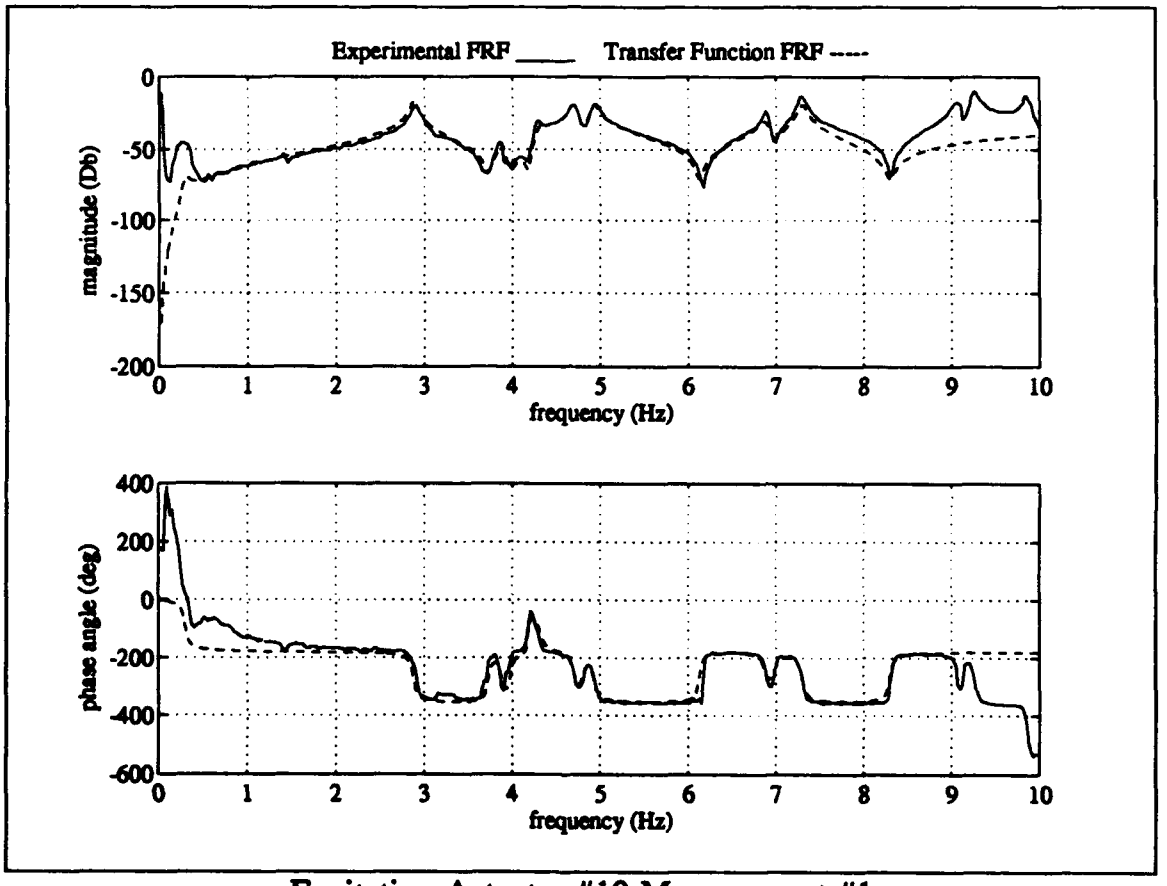

Excitation Actuator #10 Measurement #1

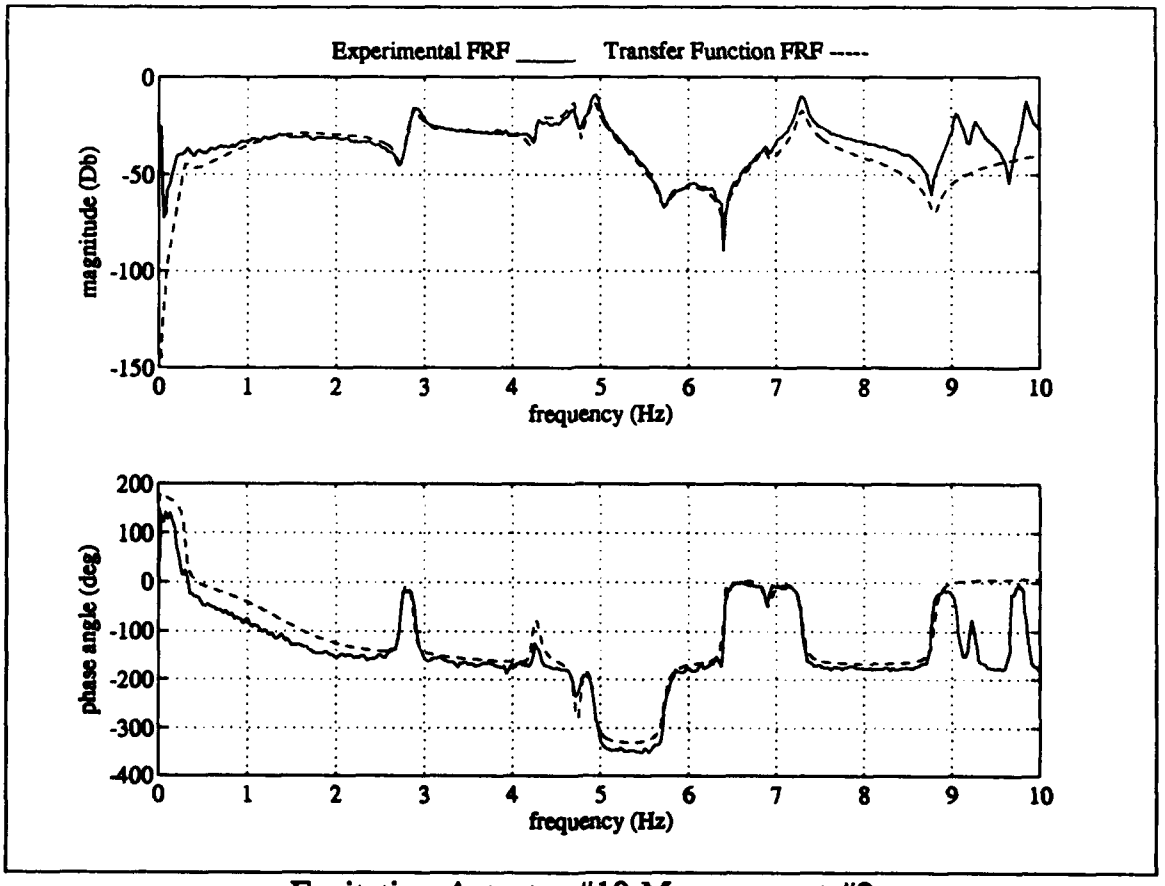

Excitation Actuator #10 Measurement #2

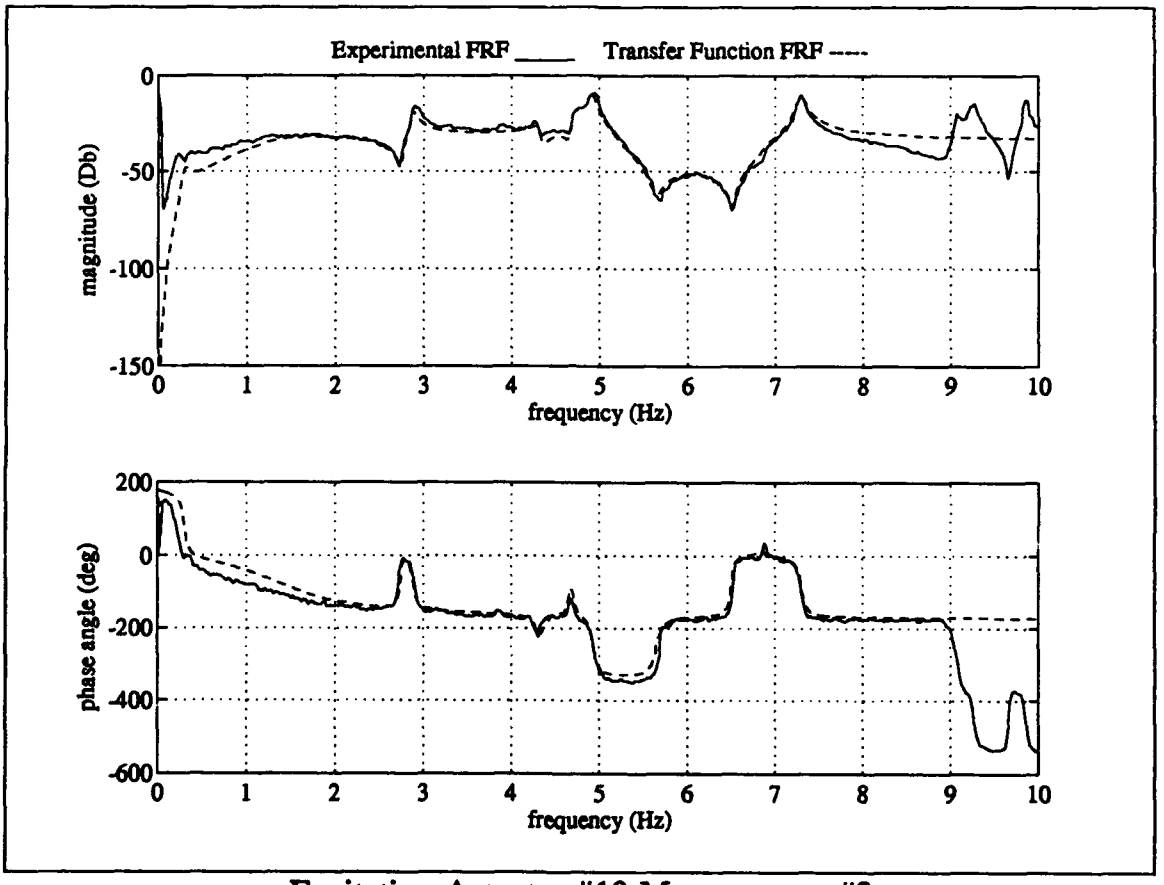

Excitation Actuator #10 Measurement #3

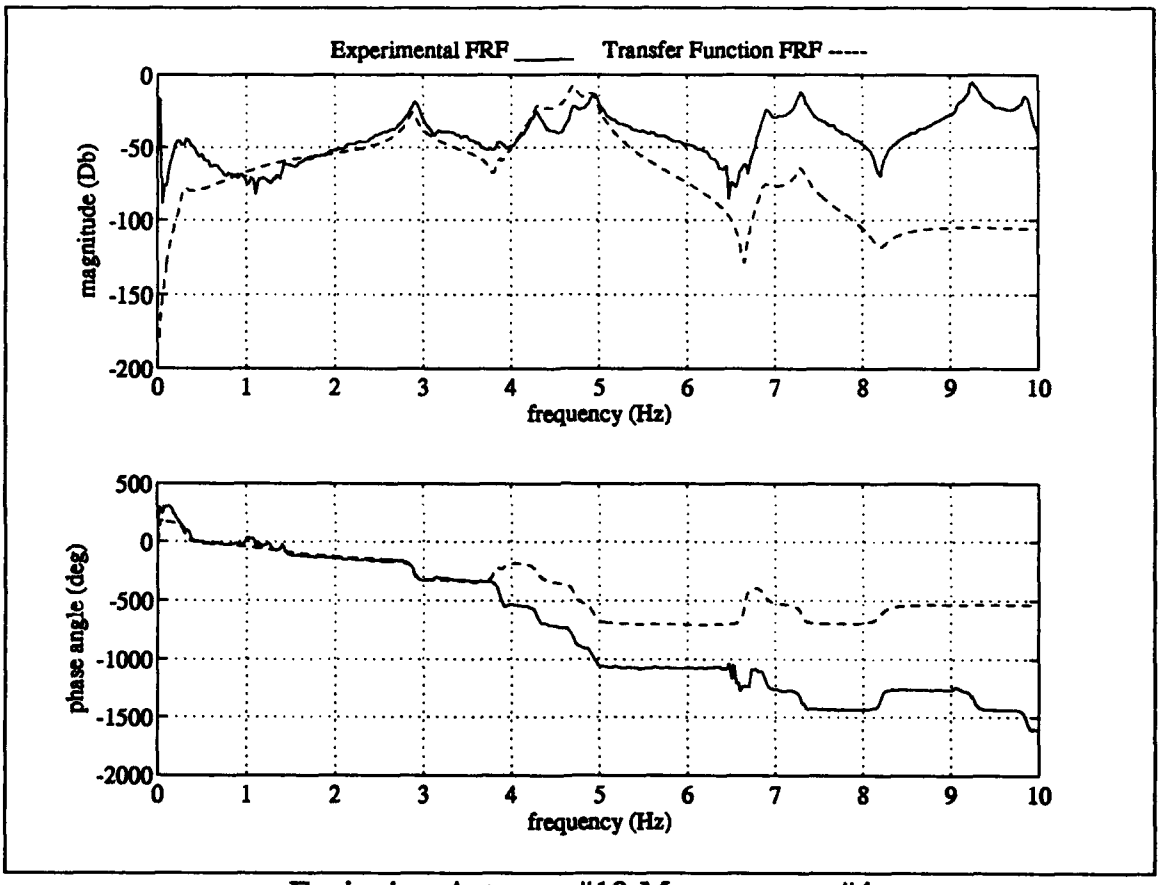

Excitation Actuator #10 Measurement #4

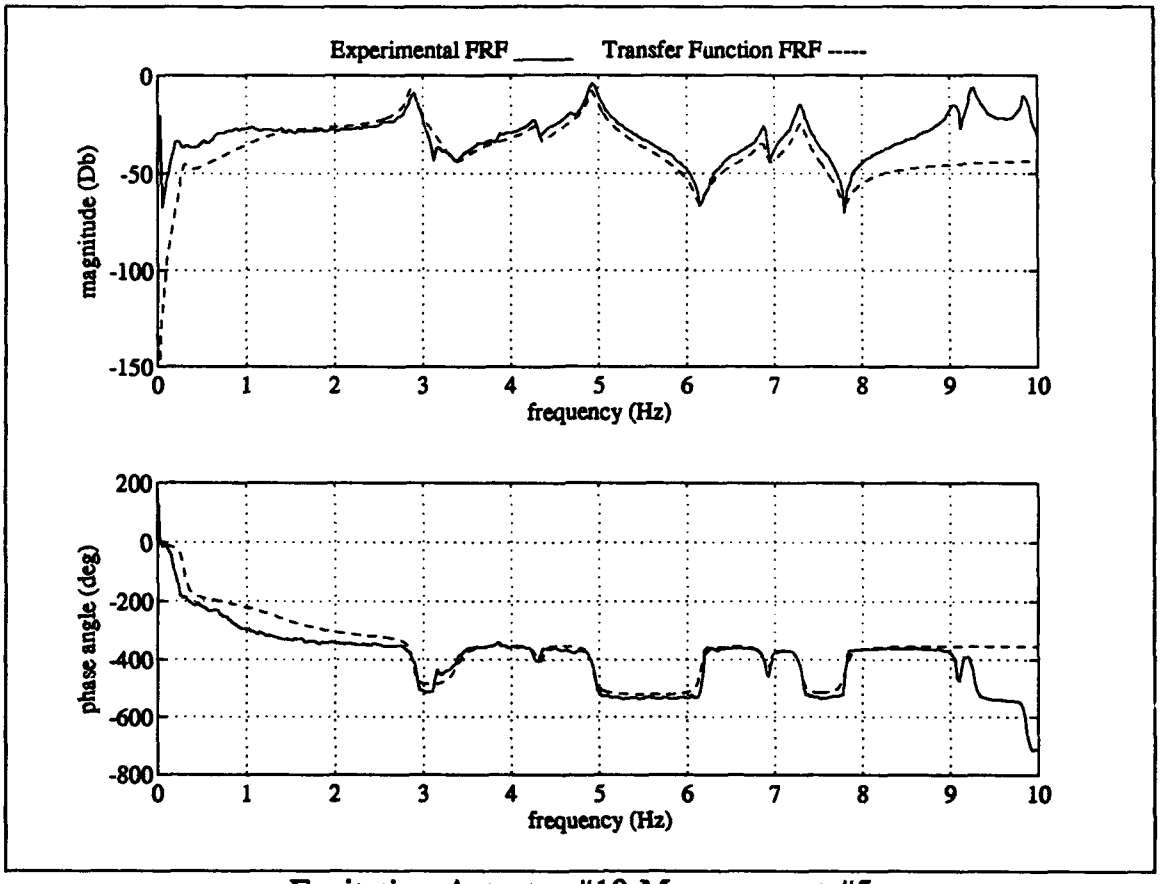

Excitation Actuator #10 Measurement #5

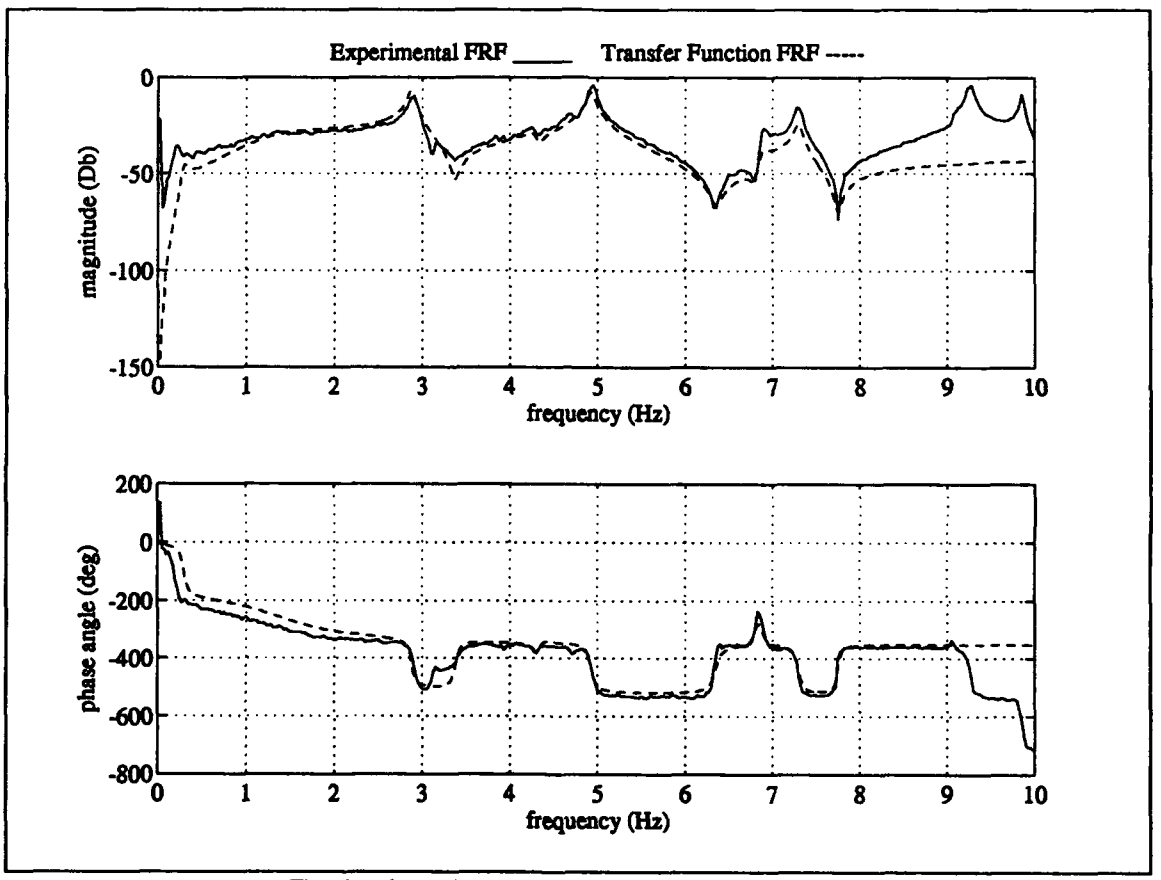

Excitation Actuator #10 Measurement #6

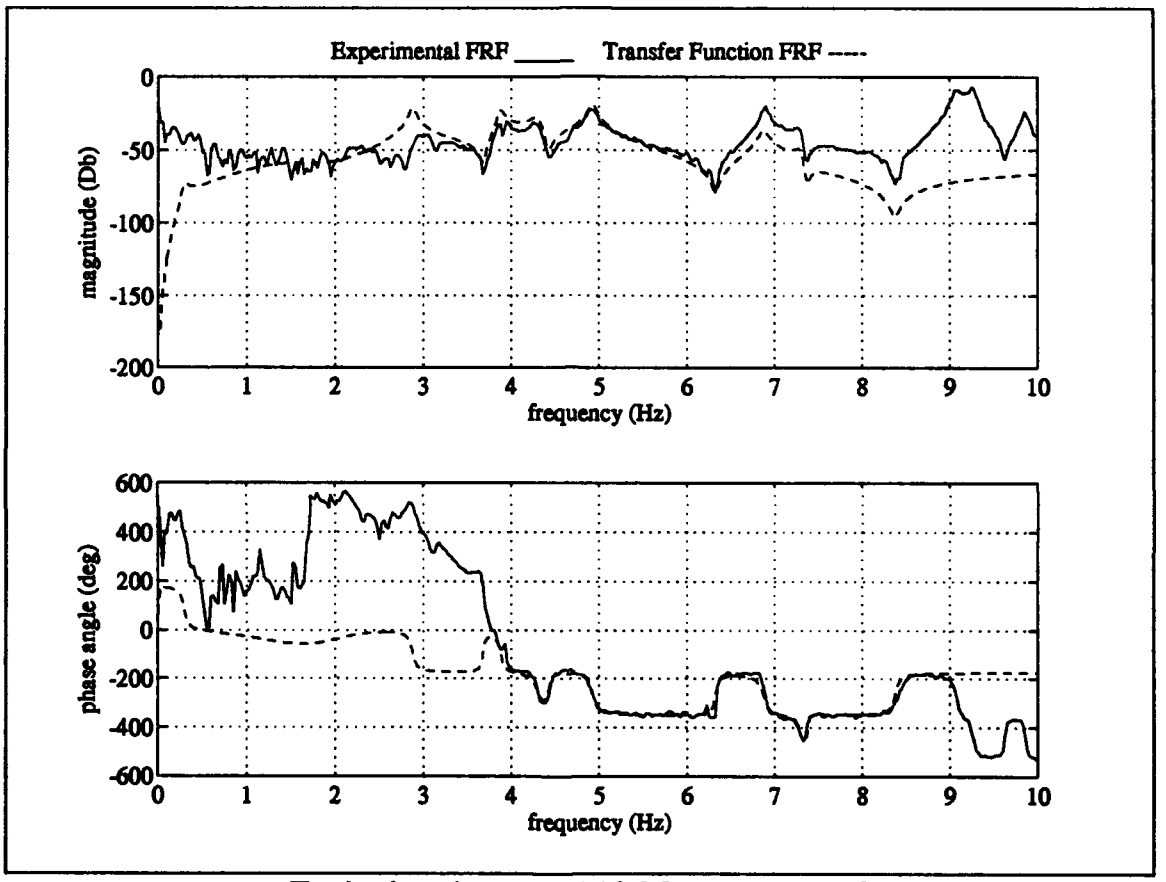

Excitation Actuator #10 Measurement #9

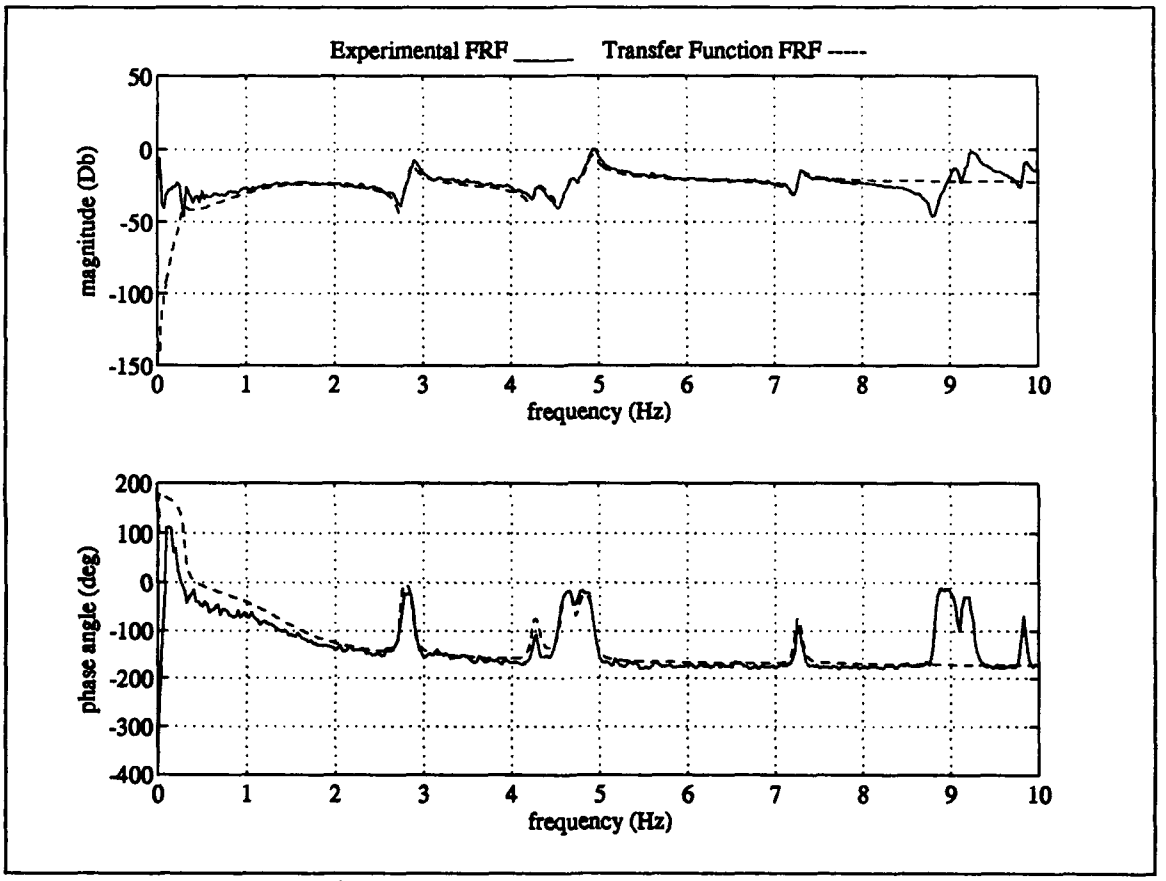

Excitation Actuator #10 Measurement #10

Appendix C: State Space Model FRFs

This appendix contains the frequency response functions for all eight input points, to all eight output points (64 frequency response functions). The plots show both the state space model and the experimental data. The reader is reminded that the dashed line represents the state space model and the solid line represents the experimental data. The caption below each plot identifies the excitation point (or actuator that is being excited), and the output or measurement number (which corresponds to an actuator location at which the response is measured).

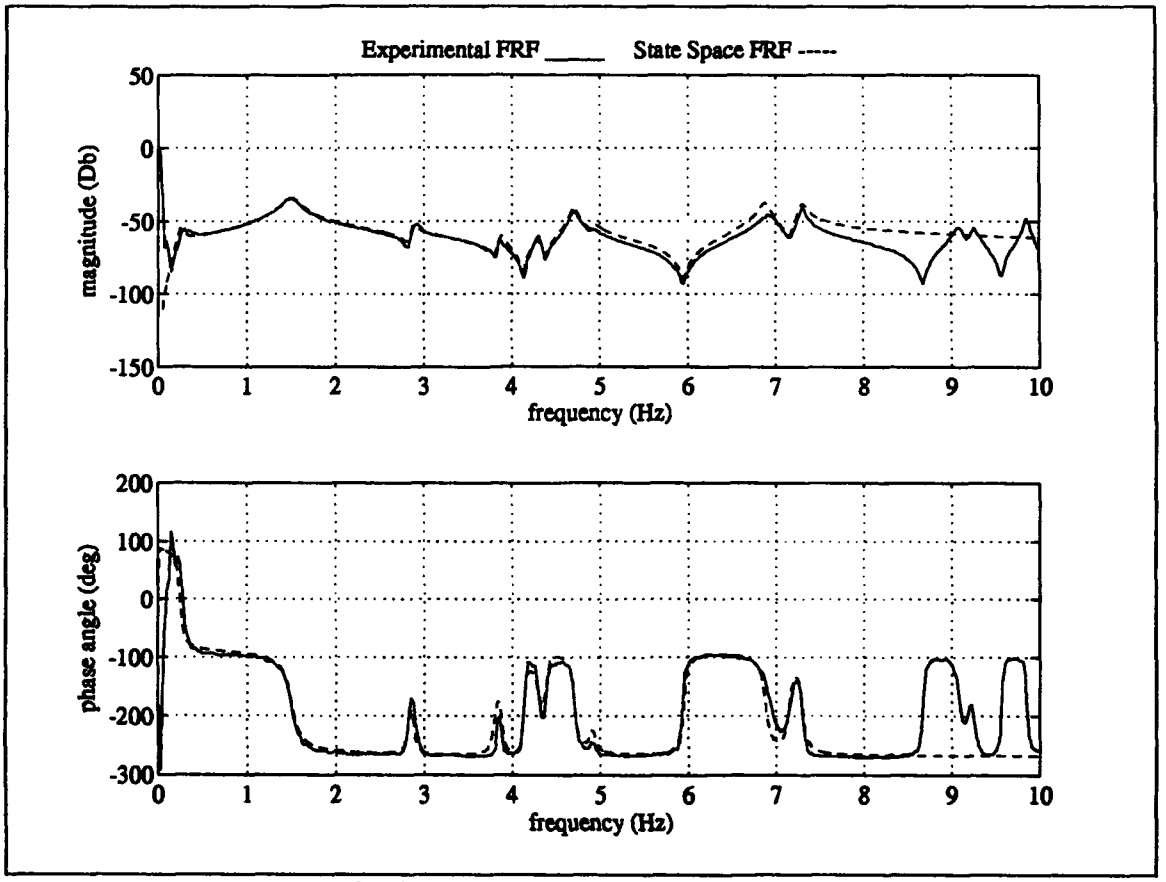

Excitation Actuator #1 Measurement #1

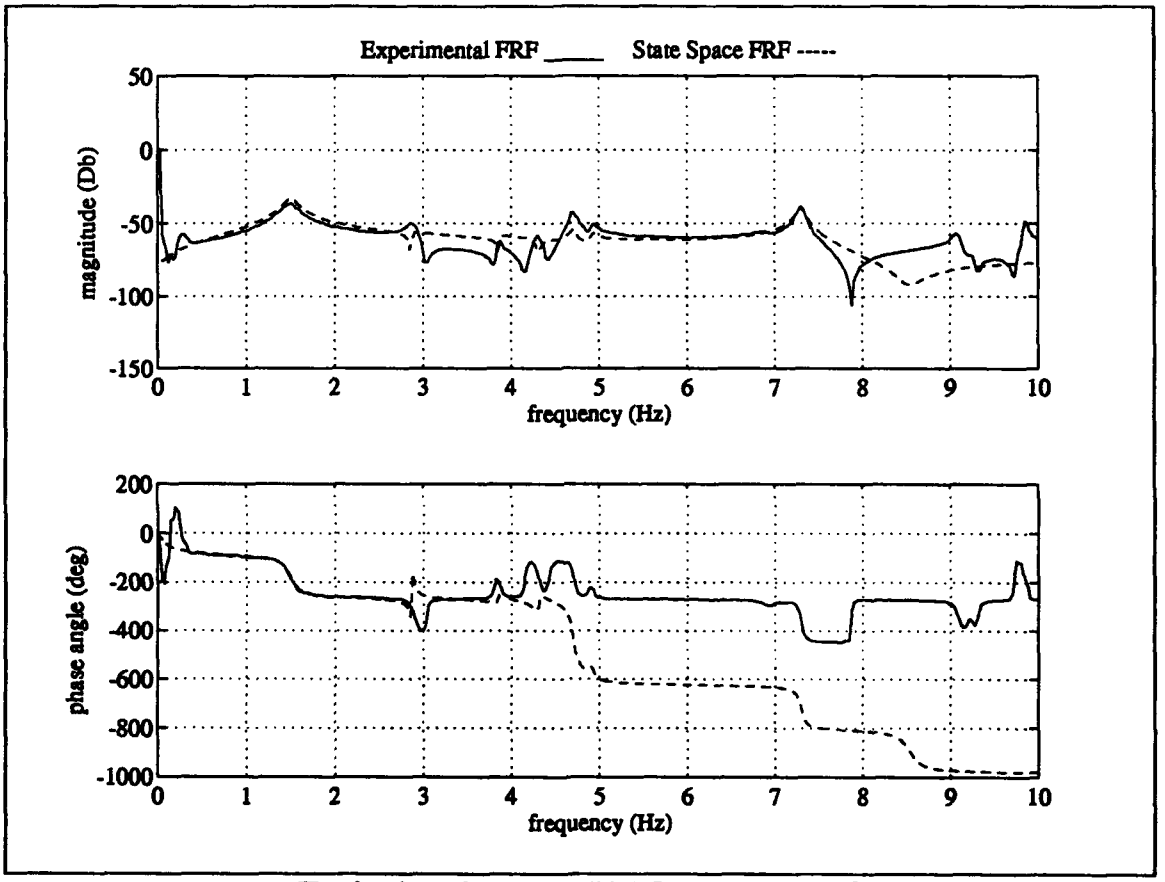

Excitation Actuator #1 Measurement #2

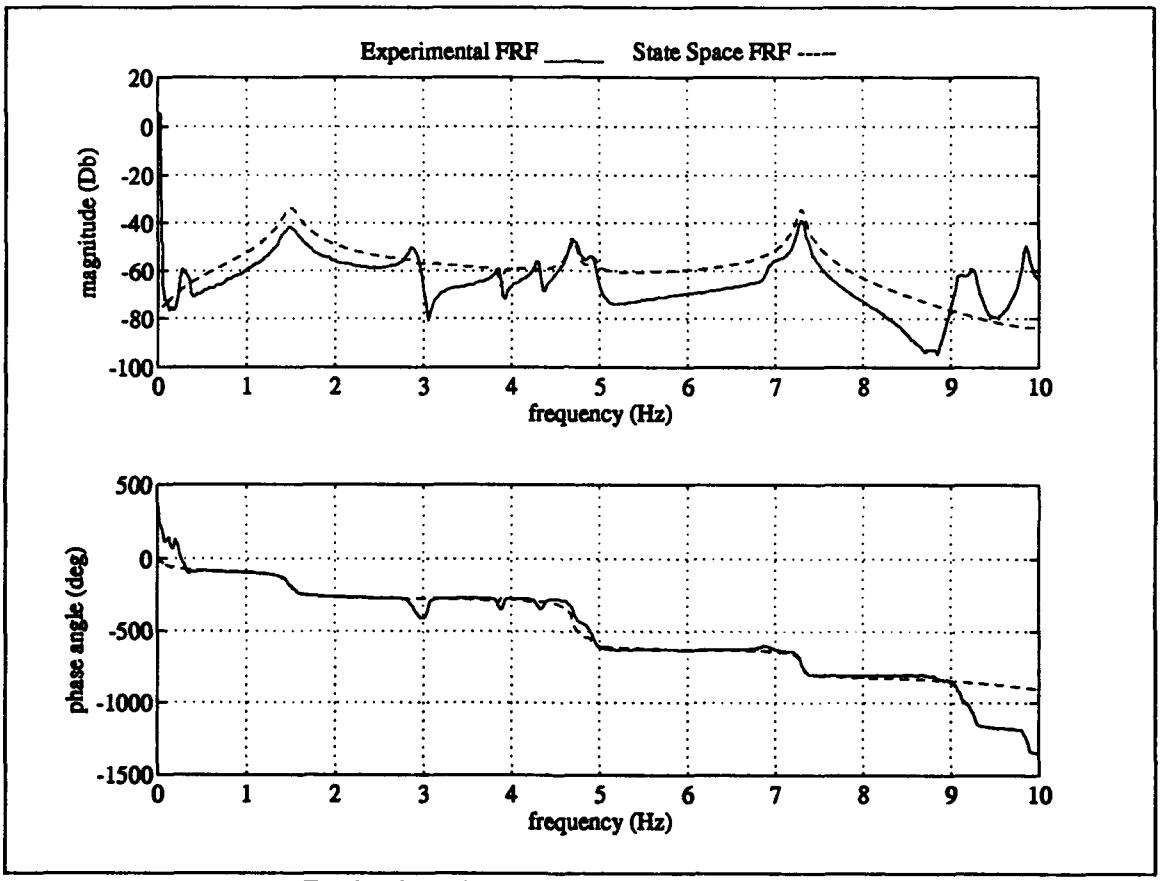

Excitation Actuator #1 Measurement #3

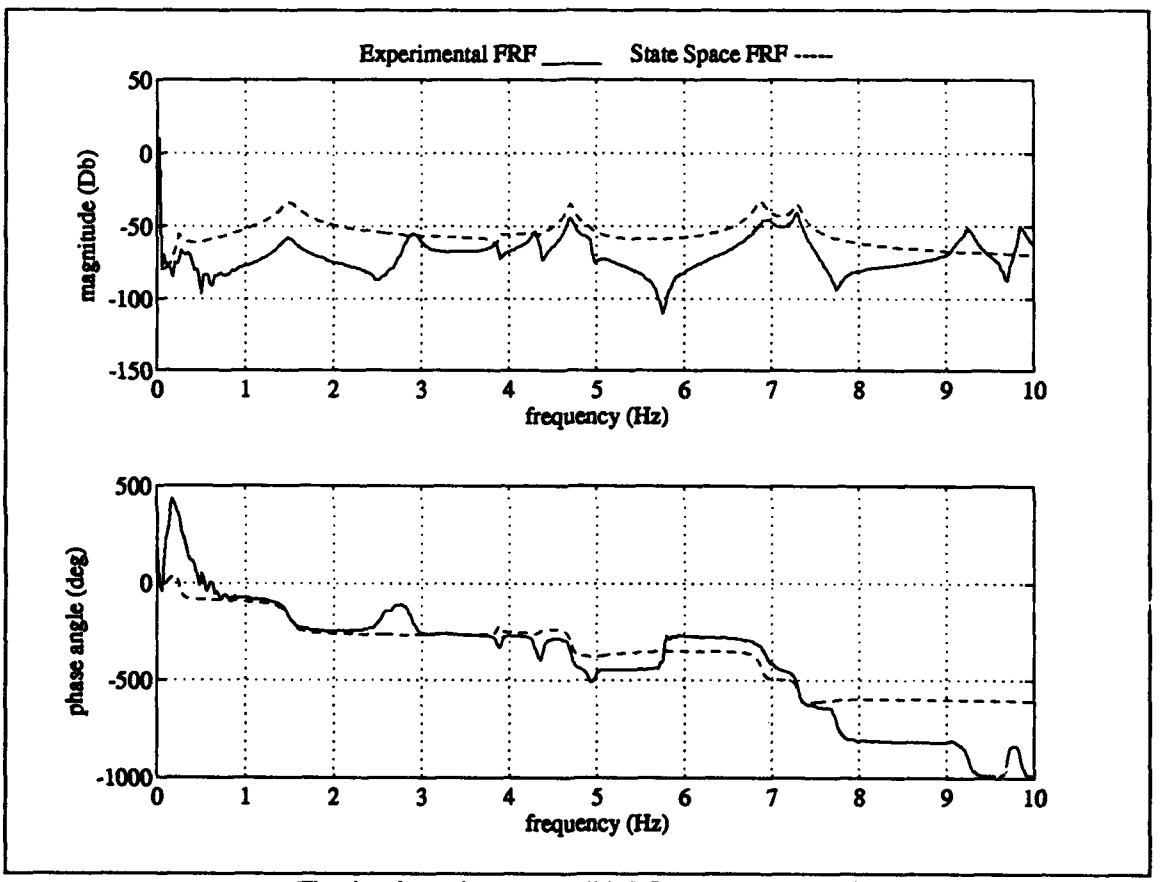

Excitation Actuator #1 Measurement #4

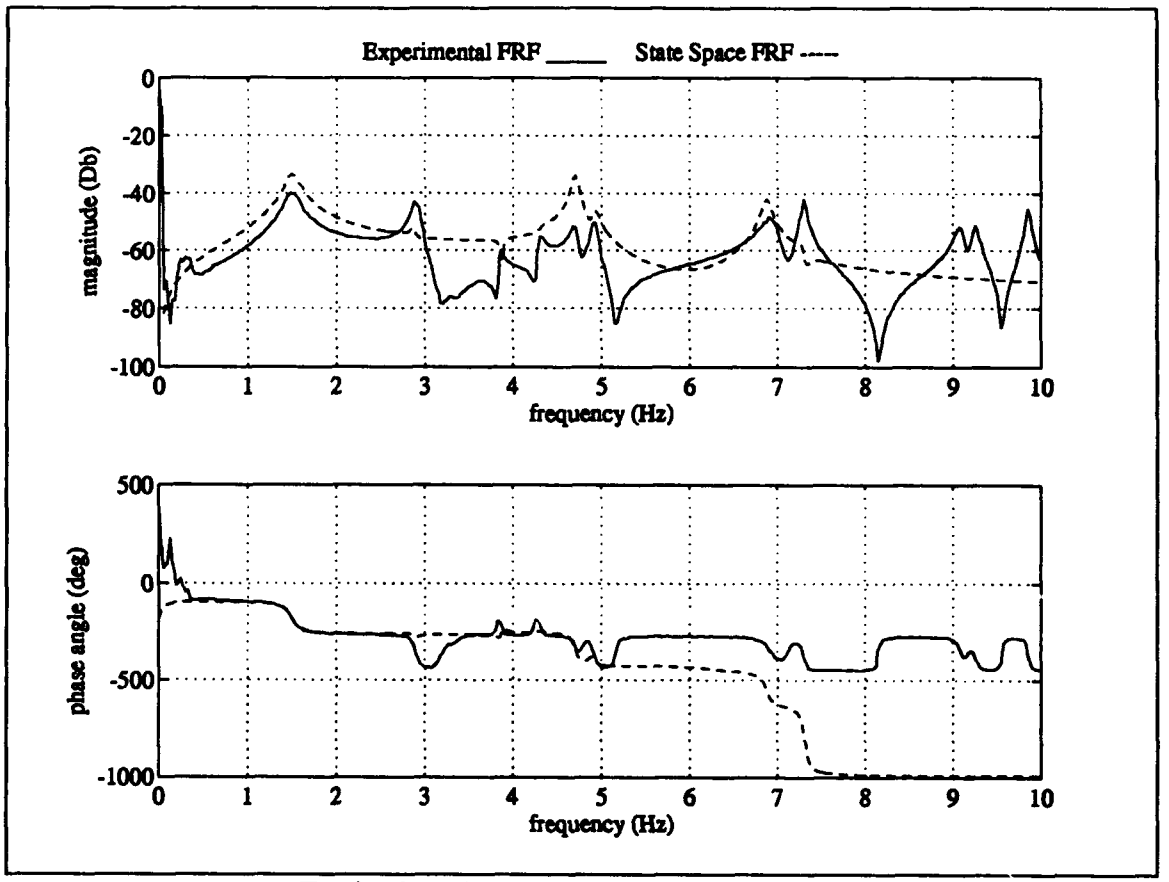

Excitation Actuator #1 Measurement #5

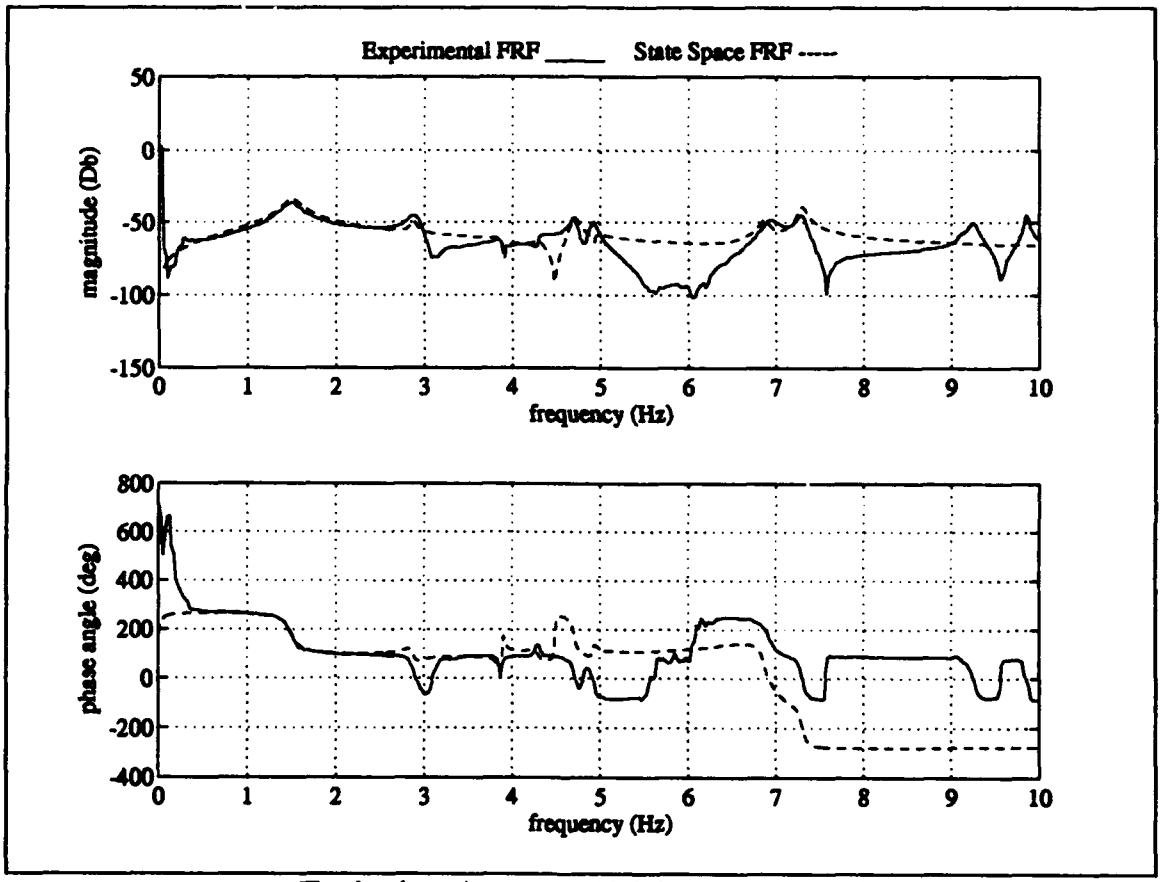

Excitation Actuator #1 Measurement #6

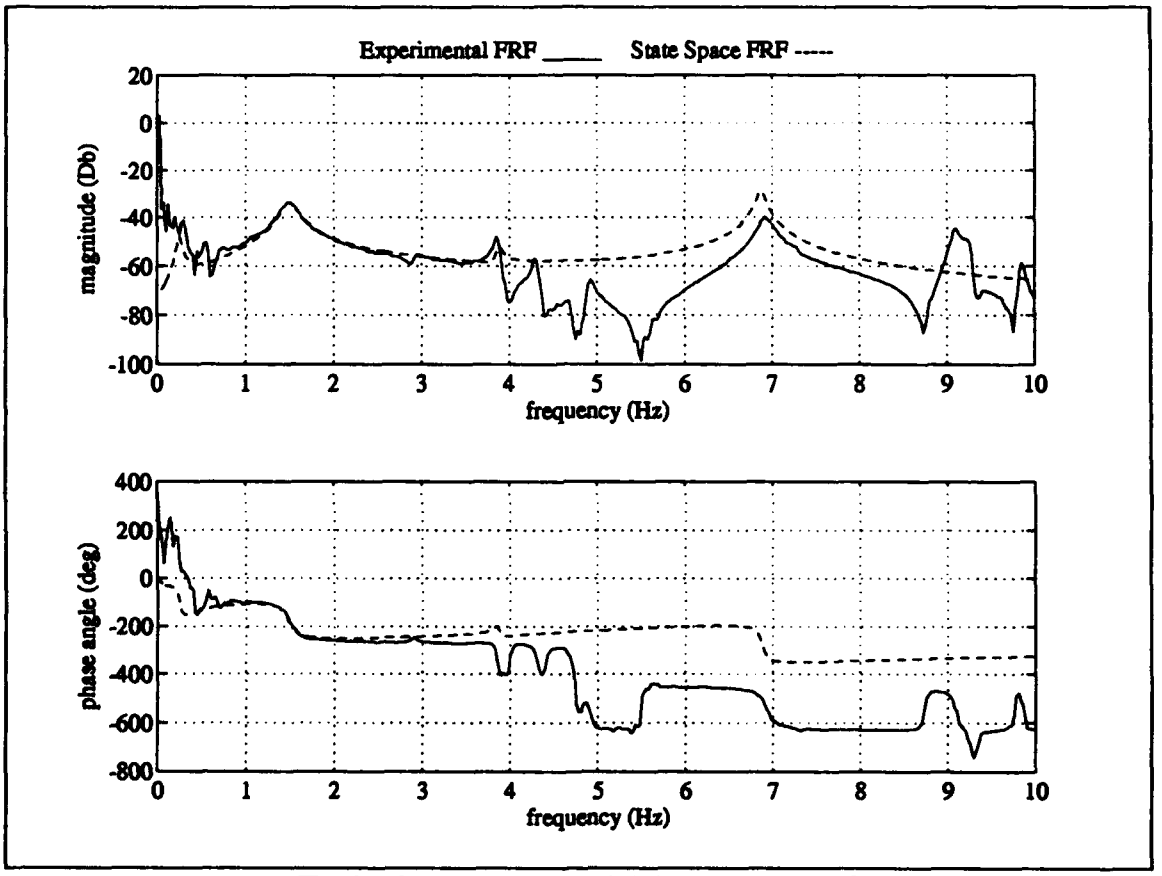

Excitation Actuator #1 Measurement #9

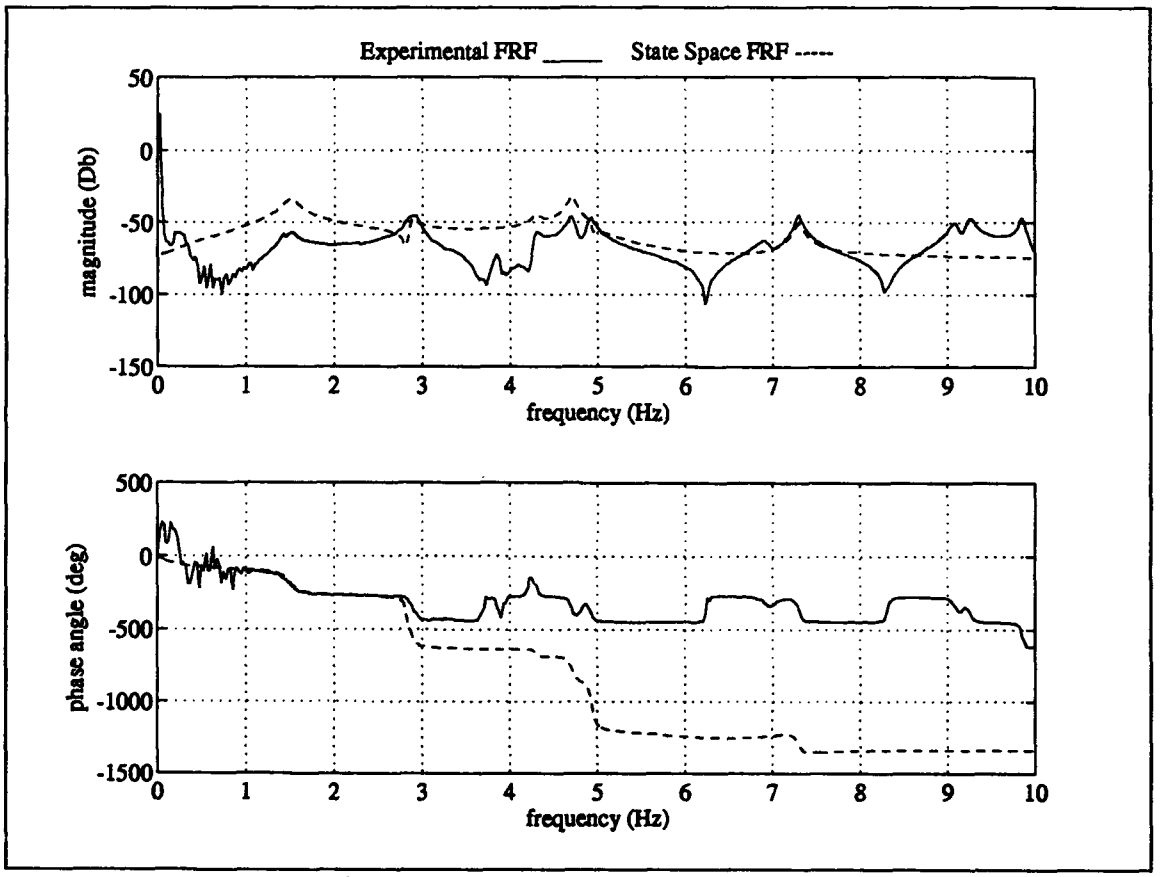

Excitation Actuator #1 Measurement #10

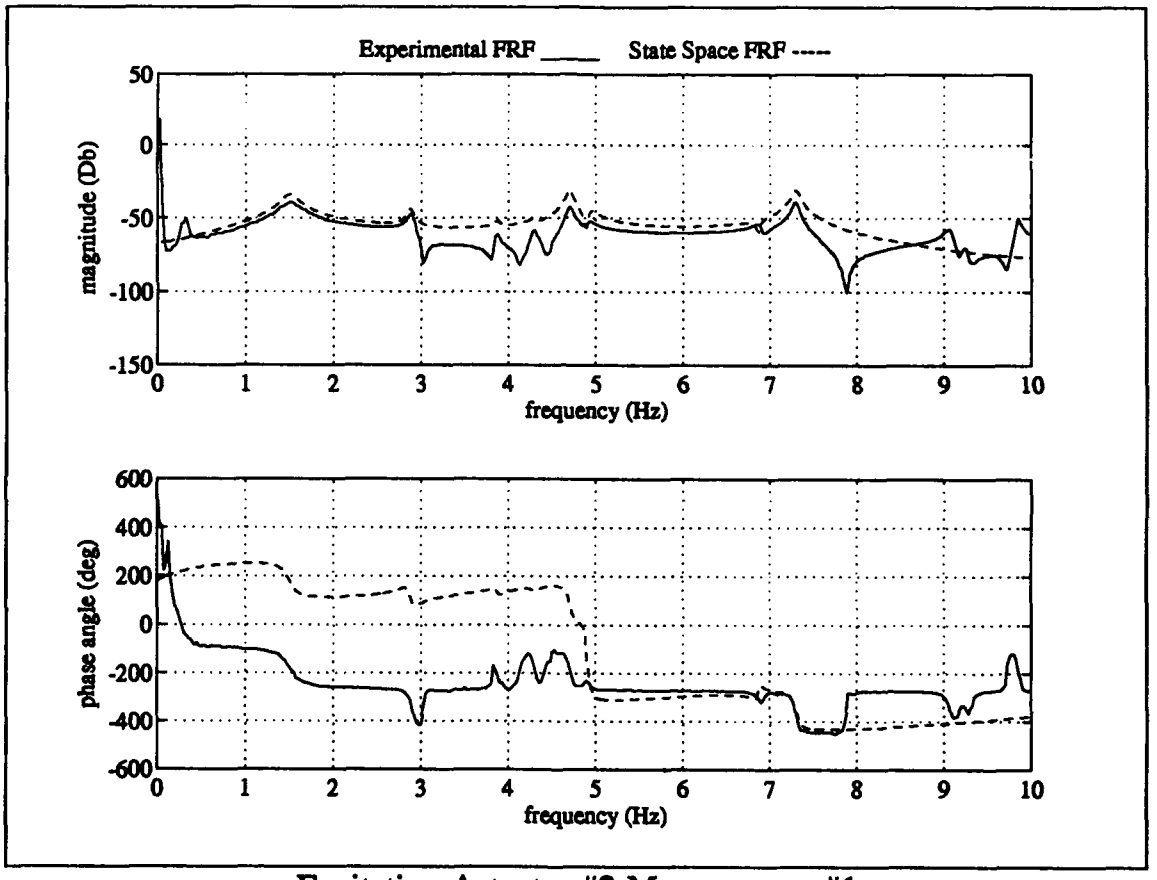

Excitation Actuator #2 Measurement #1

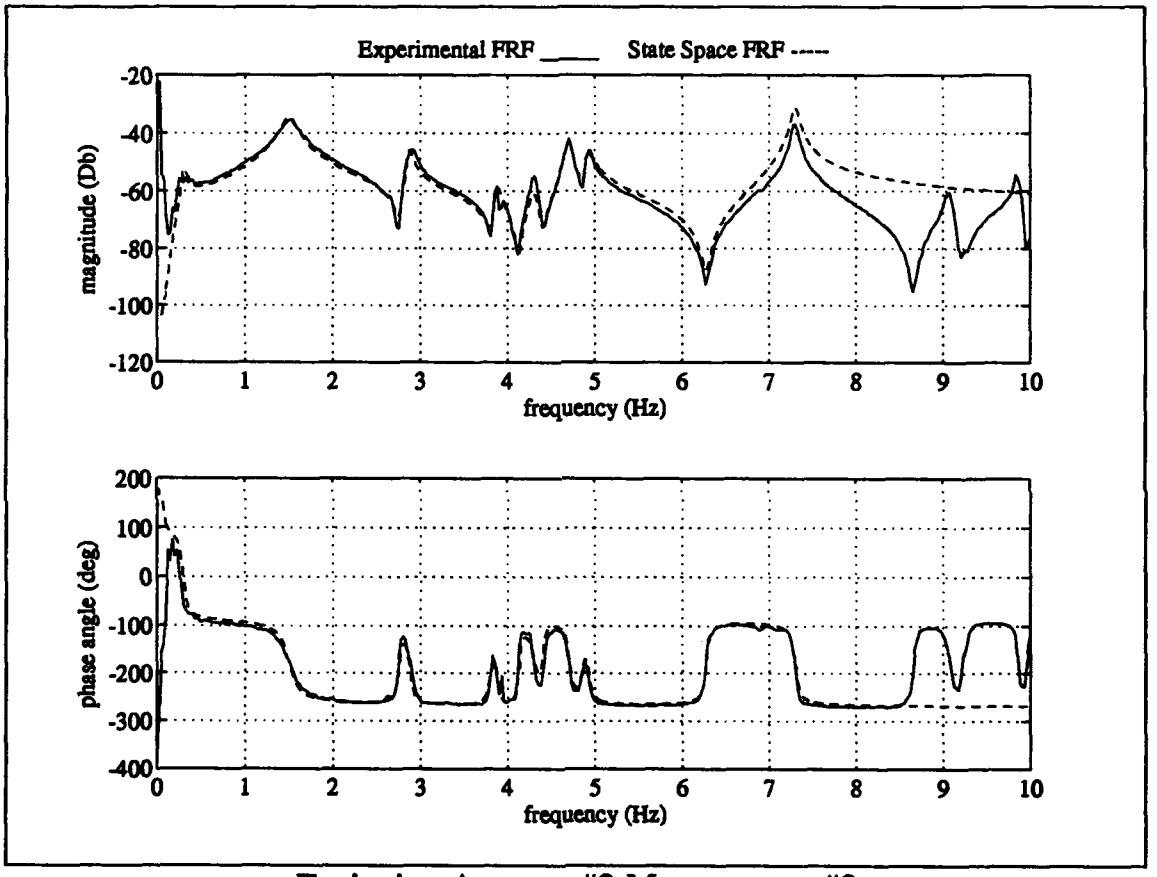

Excitation Actuator #2 Measurement #2

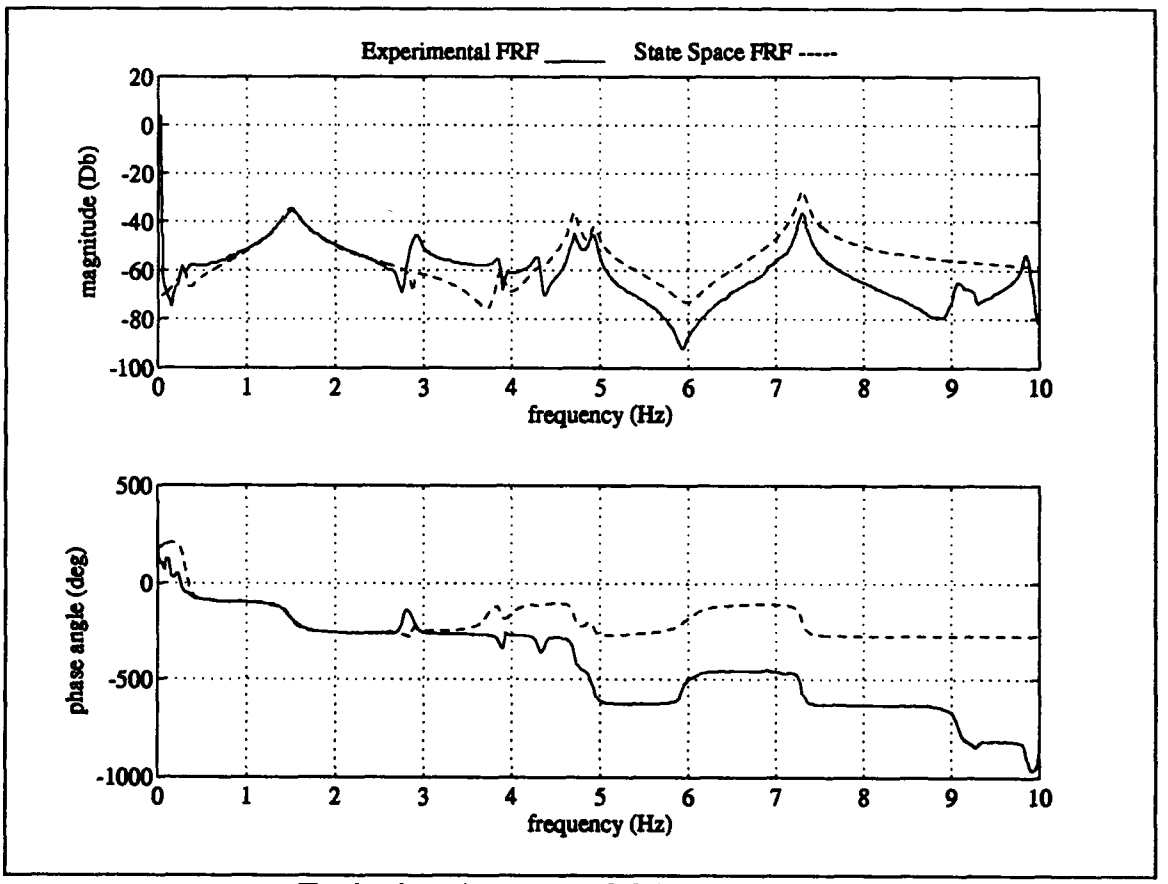

Excitation Actuator #2 Measurement #3

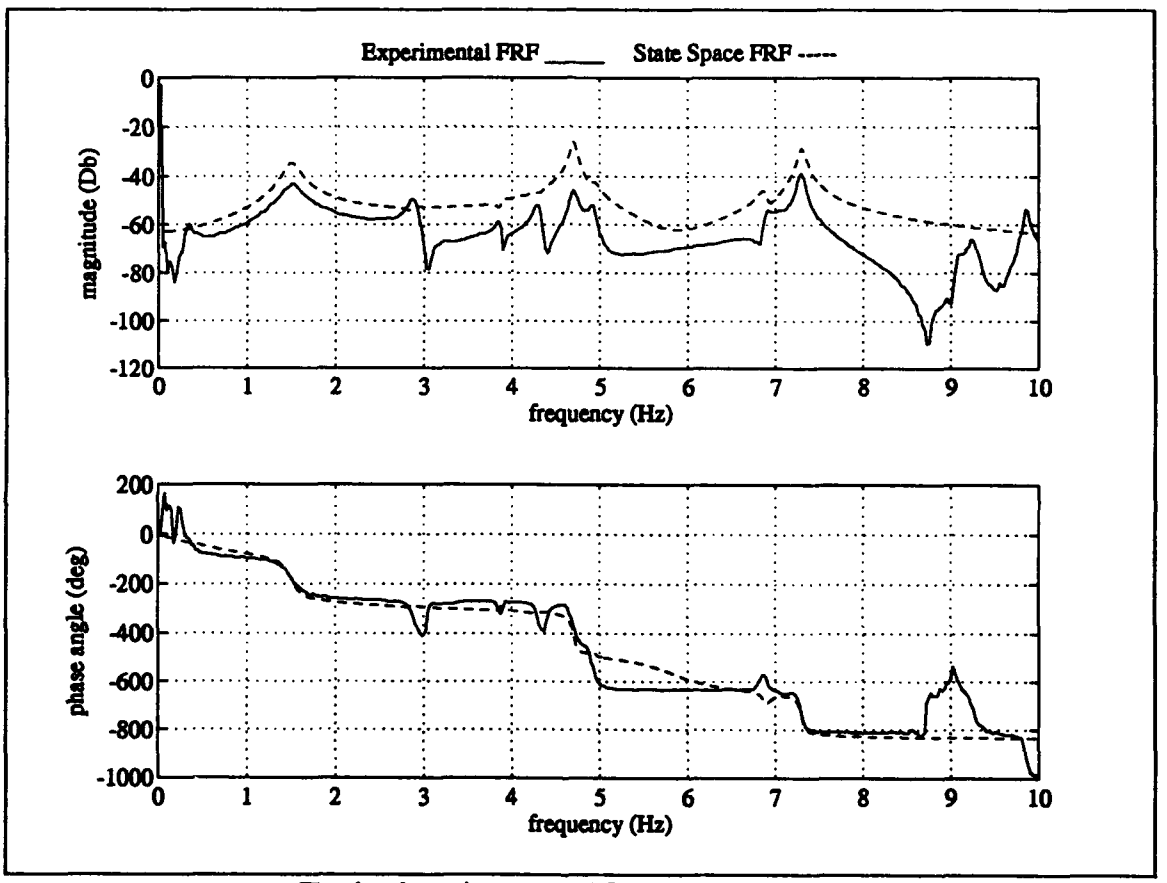

Excitation Actuator #2 Measurement #4

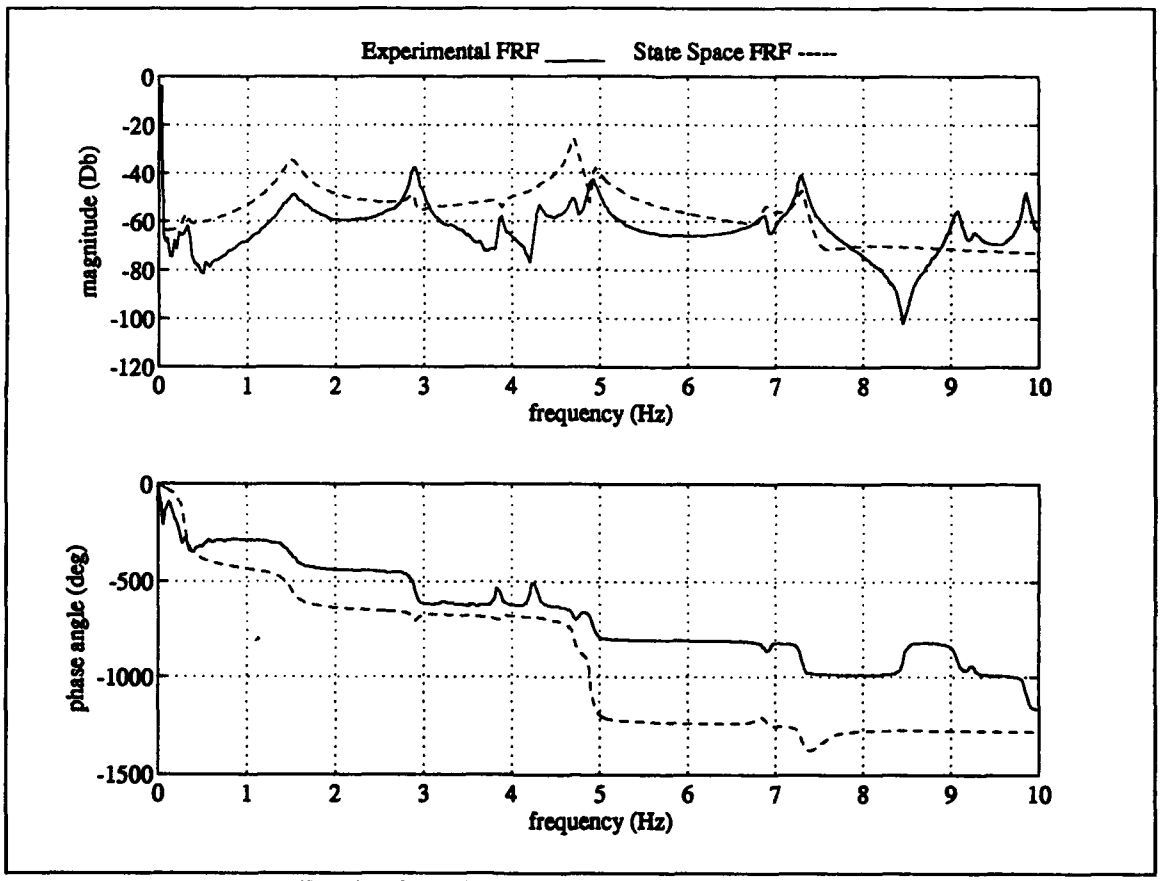

Excitation Actuator #2 Measurement #5

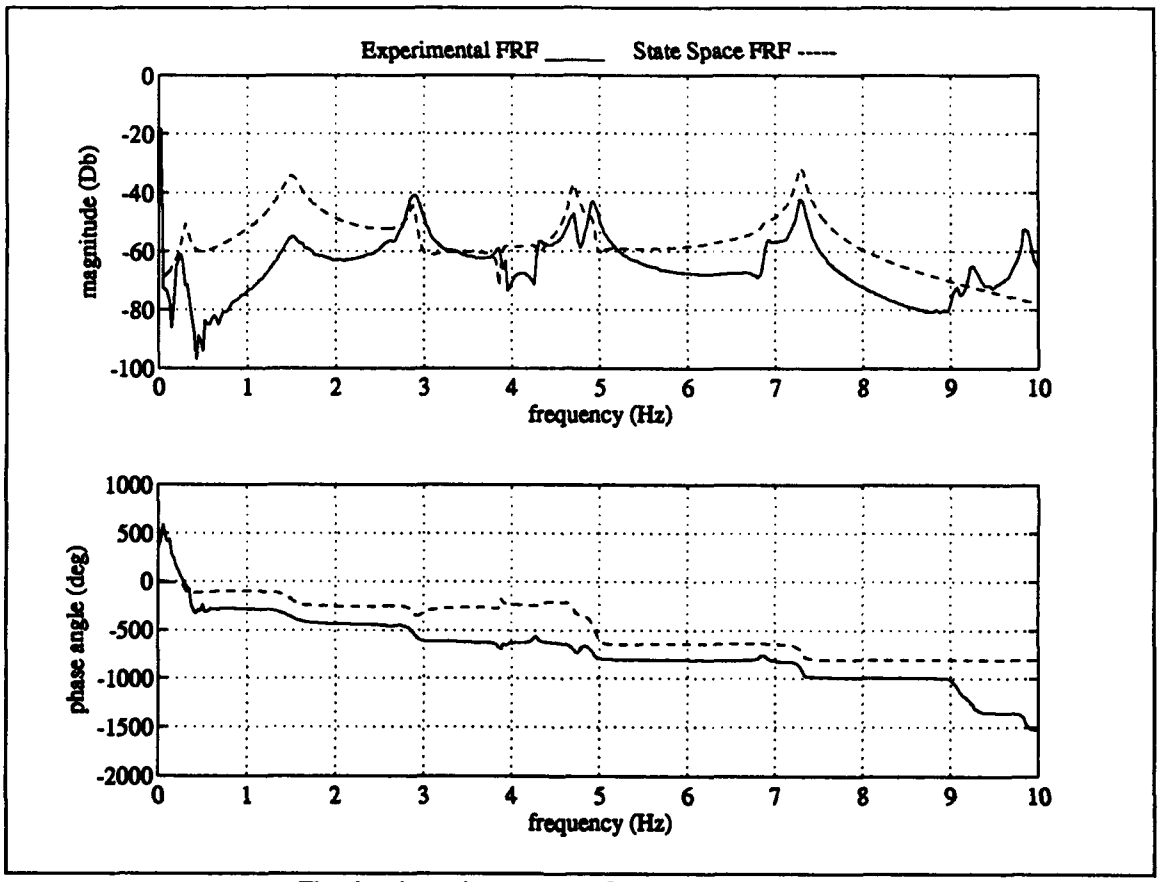

Excitation Actuator #2 Measurement #6

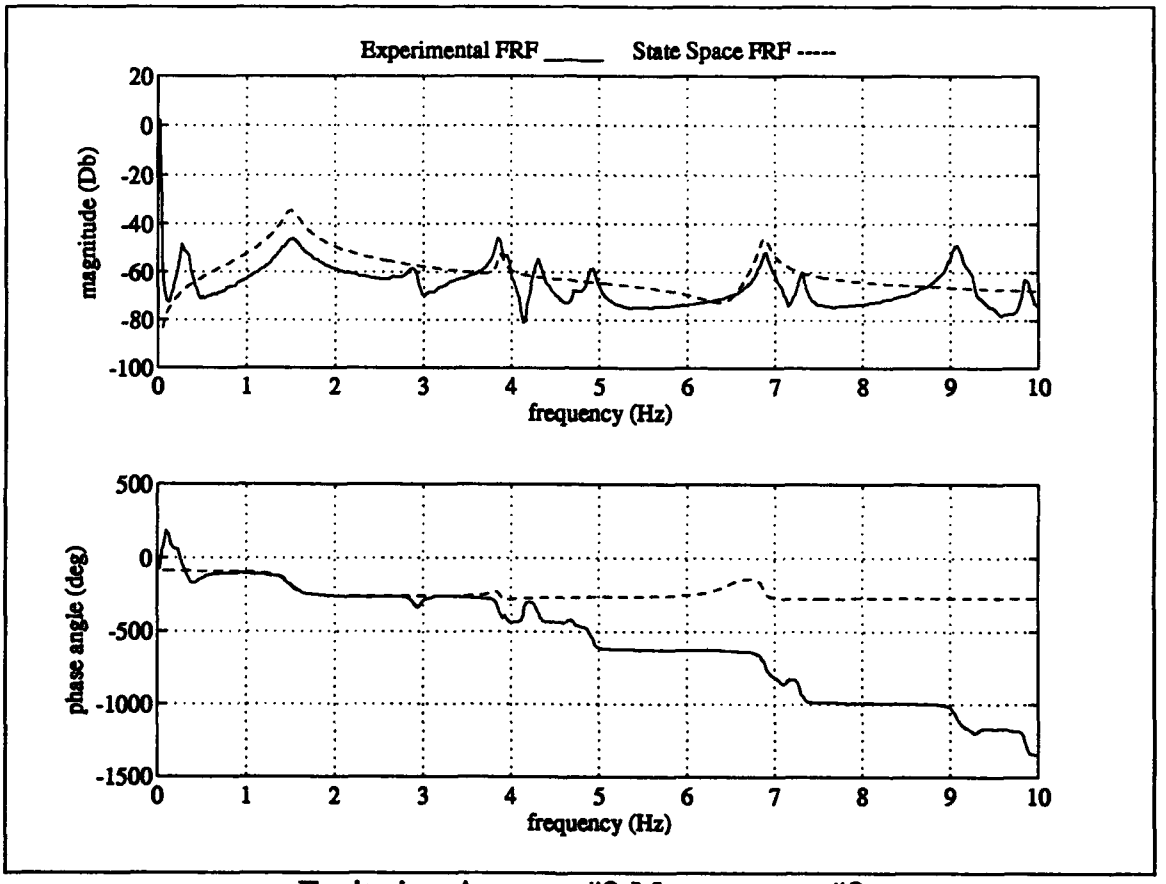

Excitation Actuator #2 Measurement #9

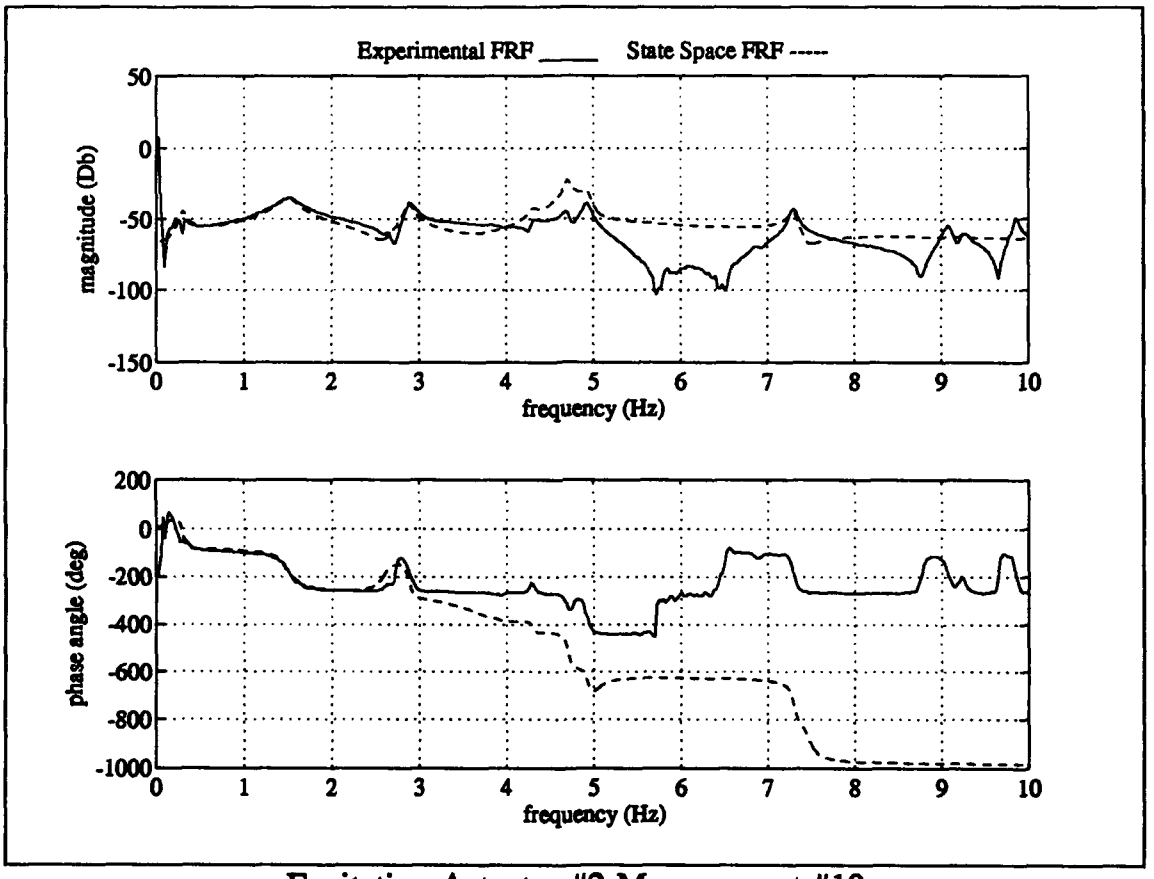

Excitation Actuator #2 Measurement #10

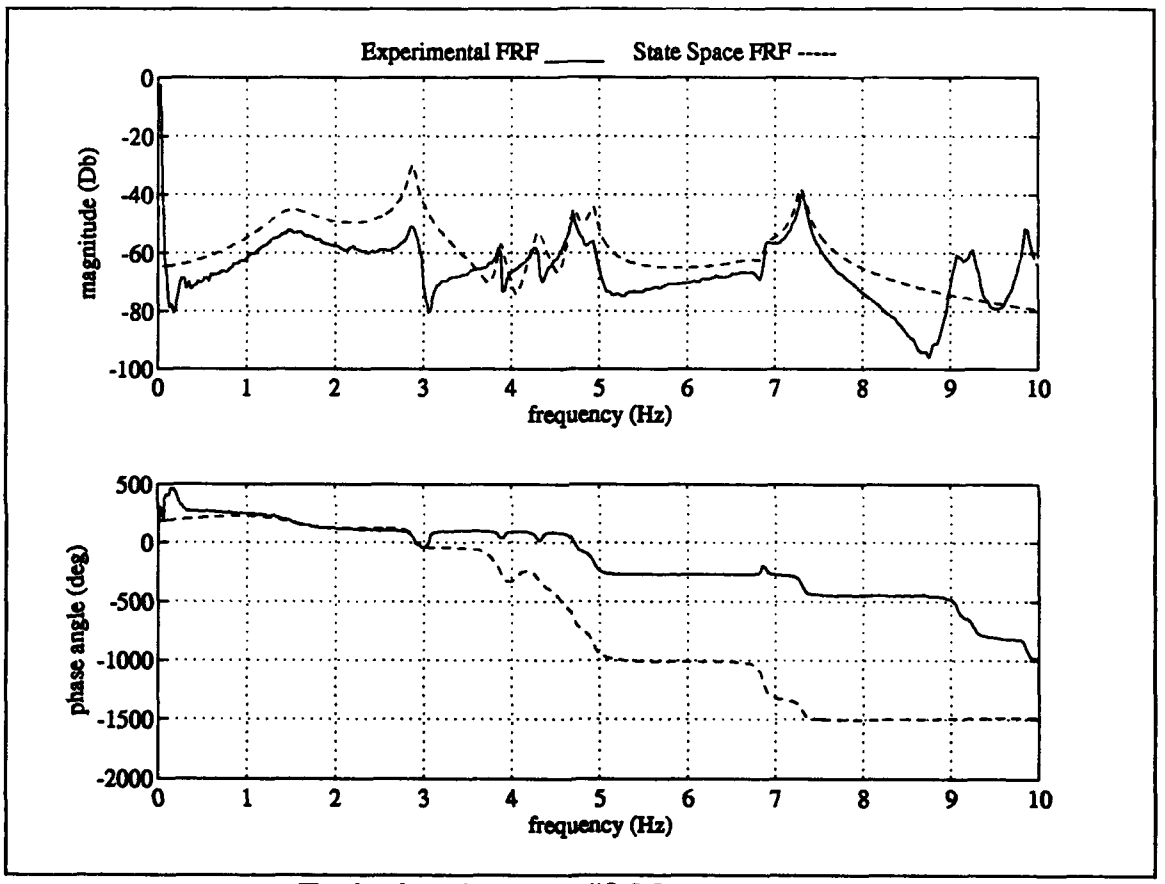

Excitation Actuator #3 Measurement #1

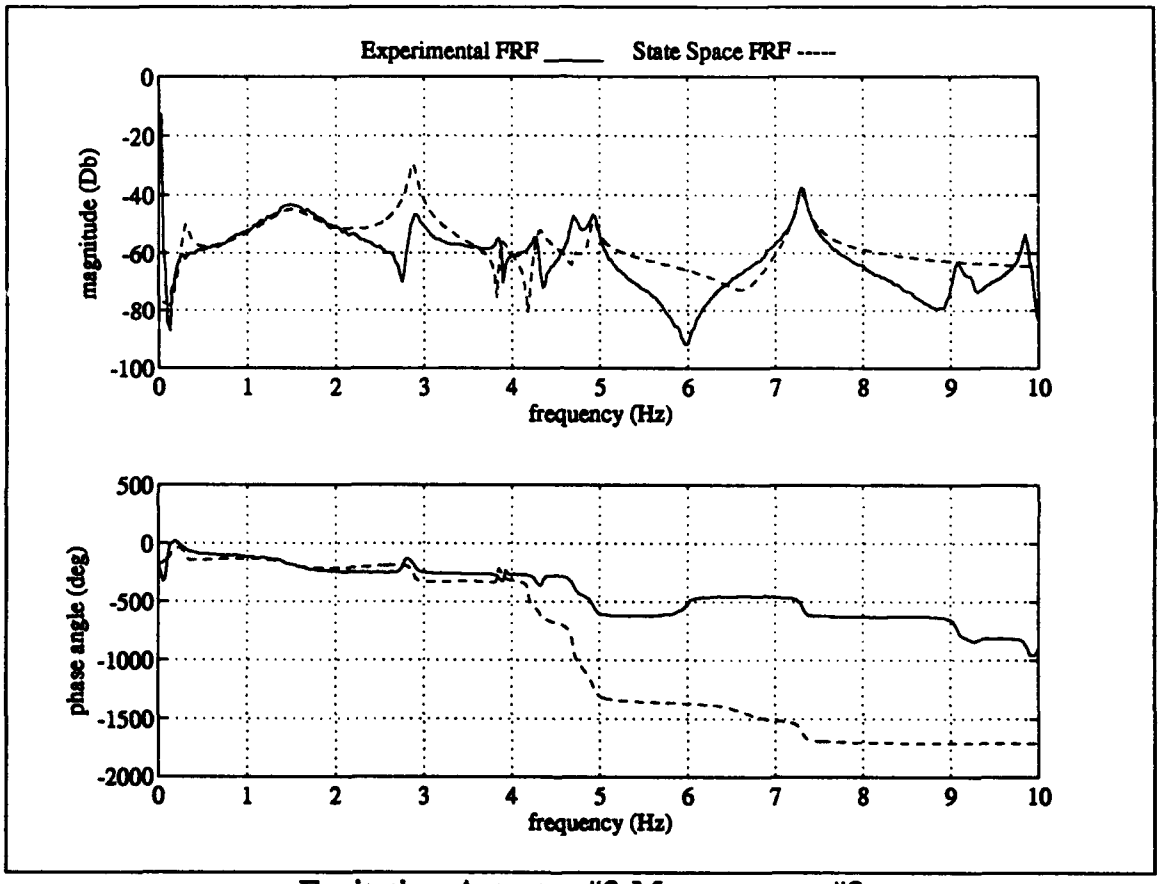

Excitation Actuator #3 Measurement #2

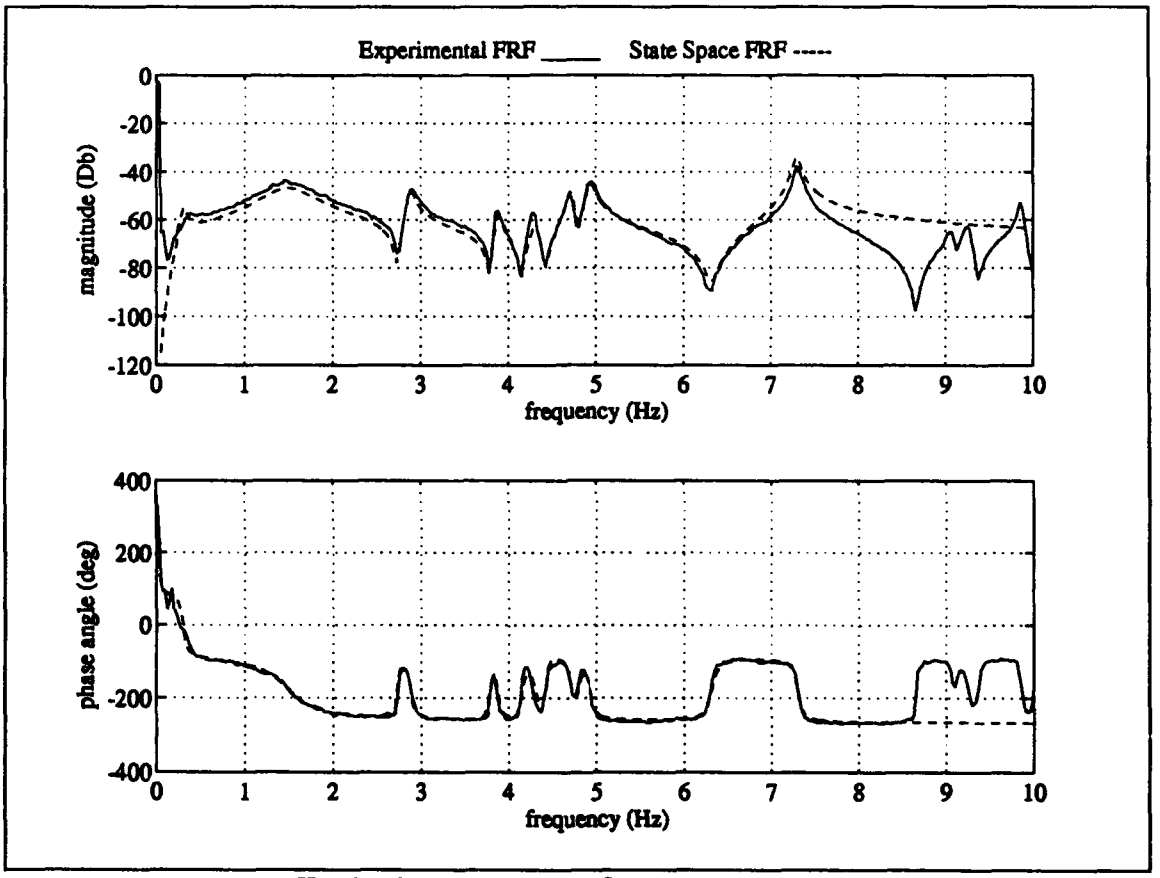

Excitation Actuator #3 Measurement #3

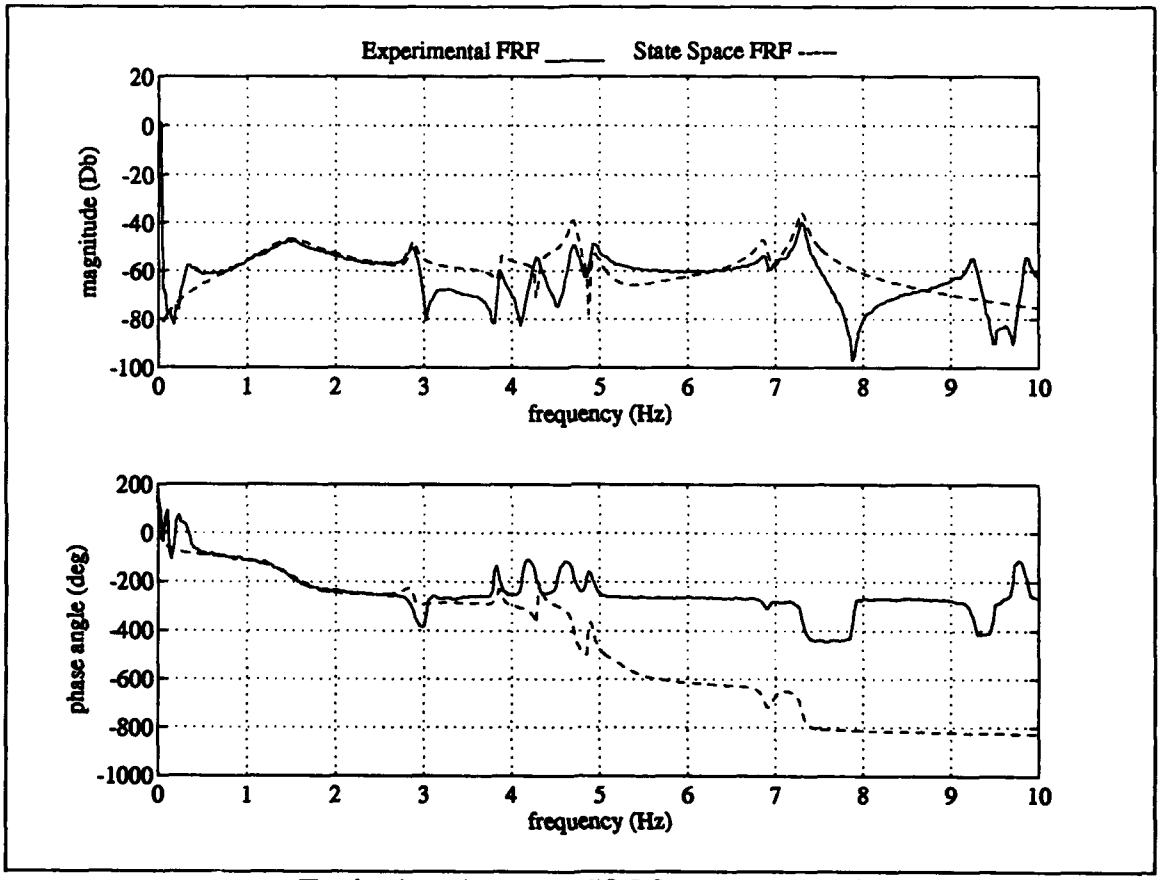

Excitation Actuator #3 Measurement #4

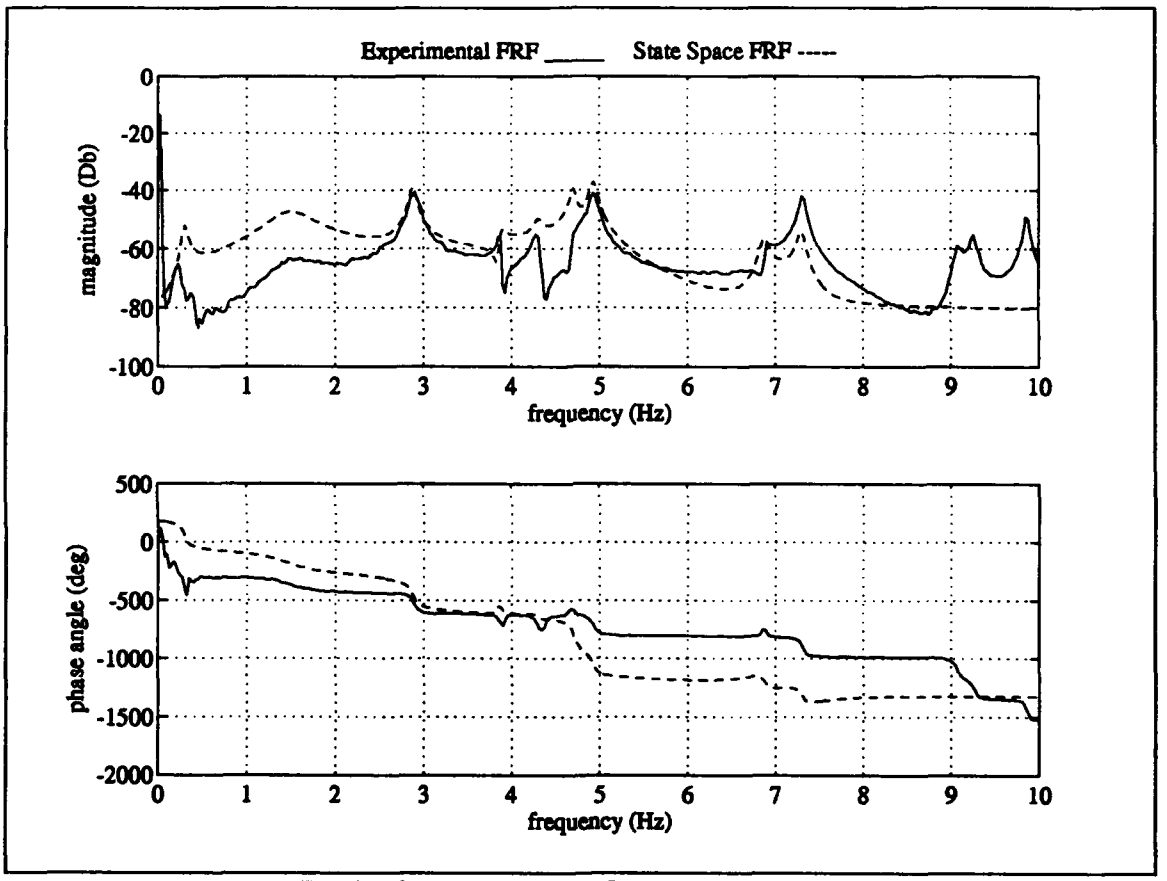

Excitation Actuator #3 Measurement #5

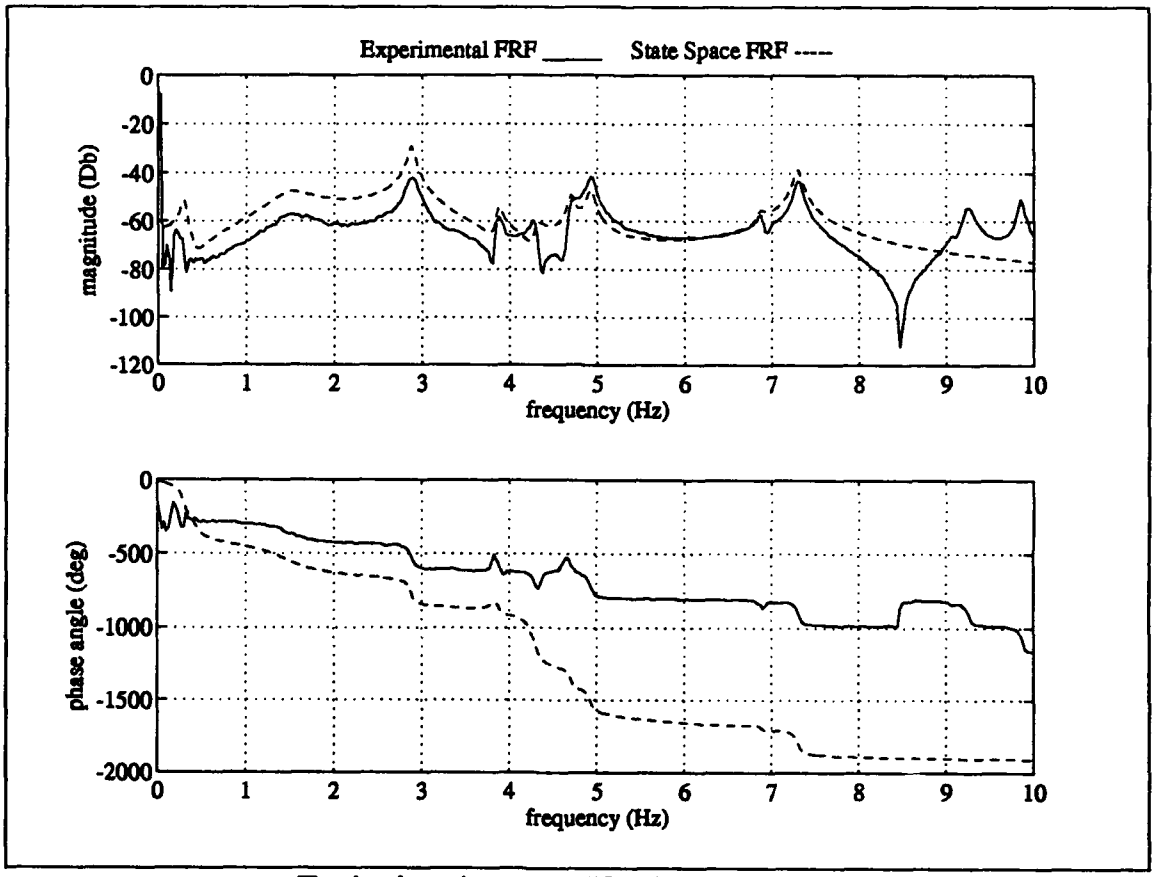

Excitation Actuator #3 Measurement #6

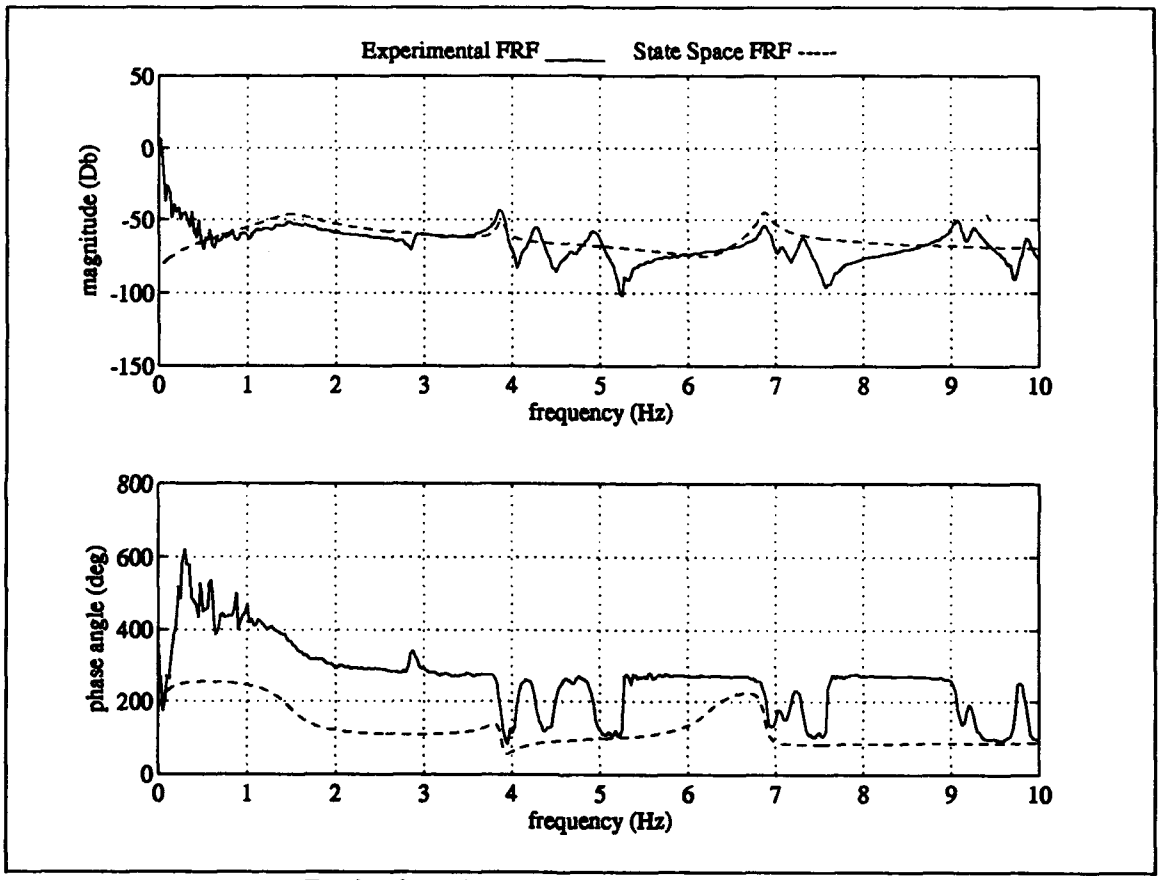

Excitation Actuator #3 Measurement #9

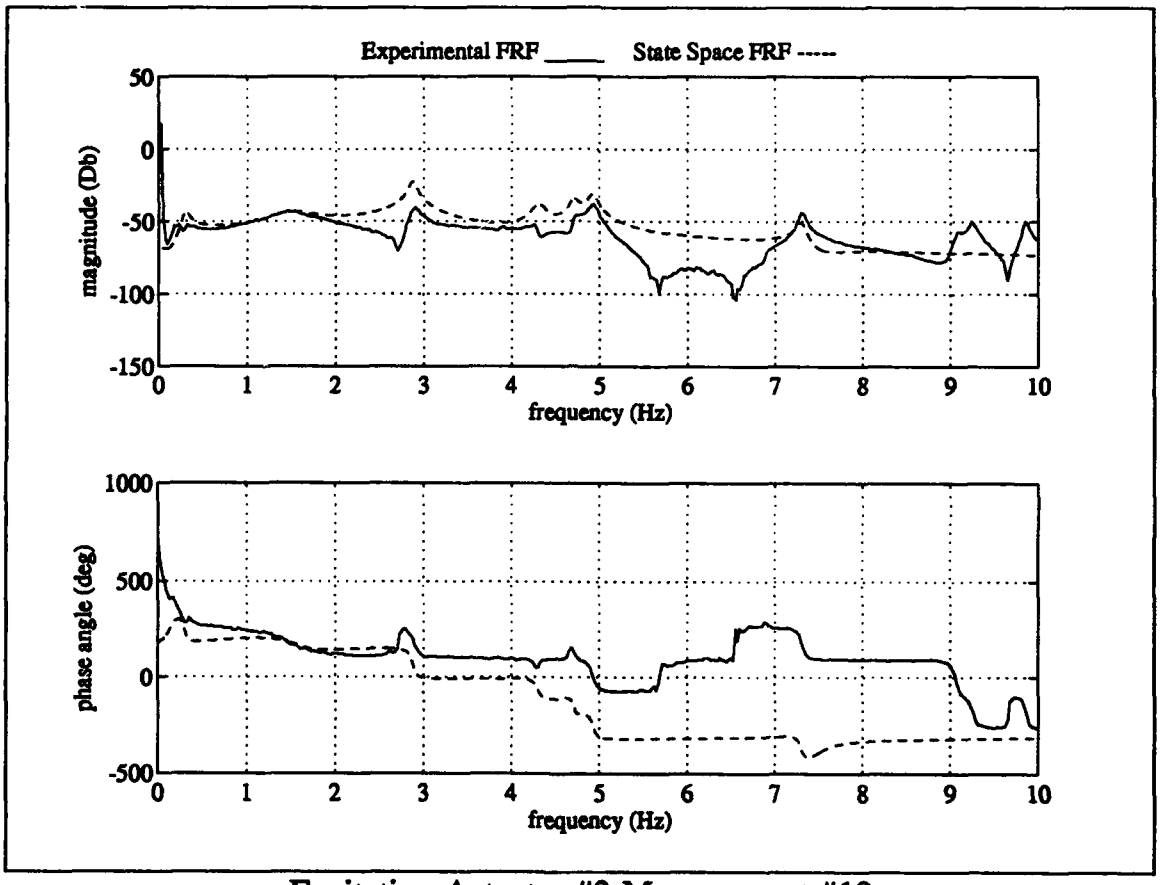

Excitation Actuator #3 Measurement #10

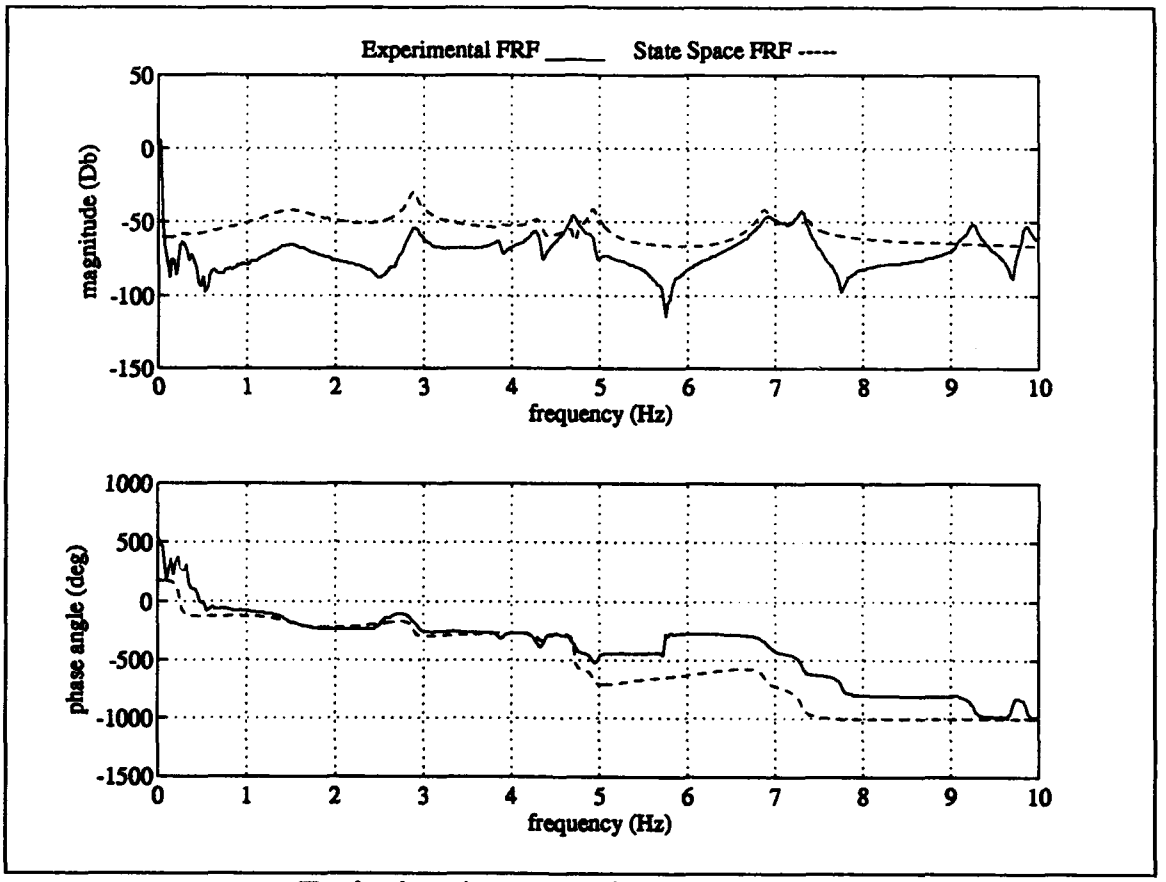

Excitation Actuator #4 Measurement #1

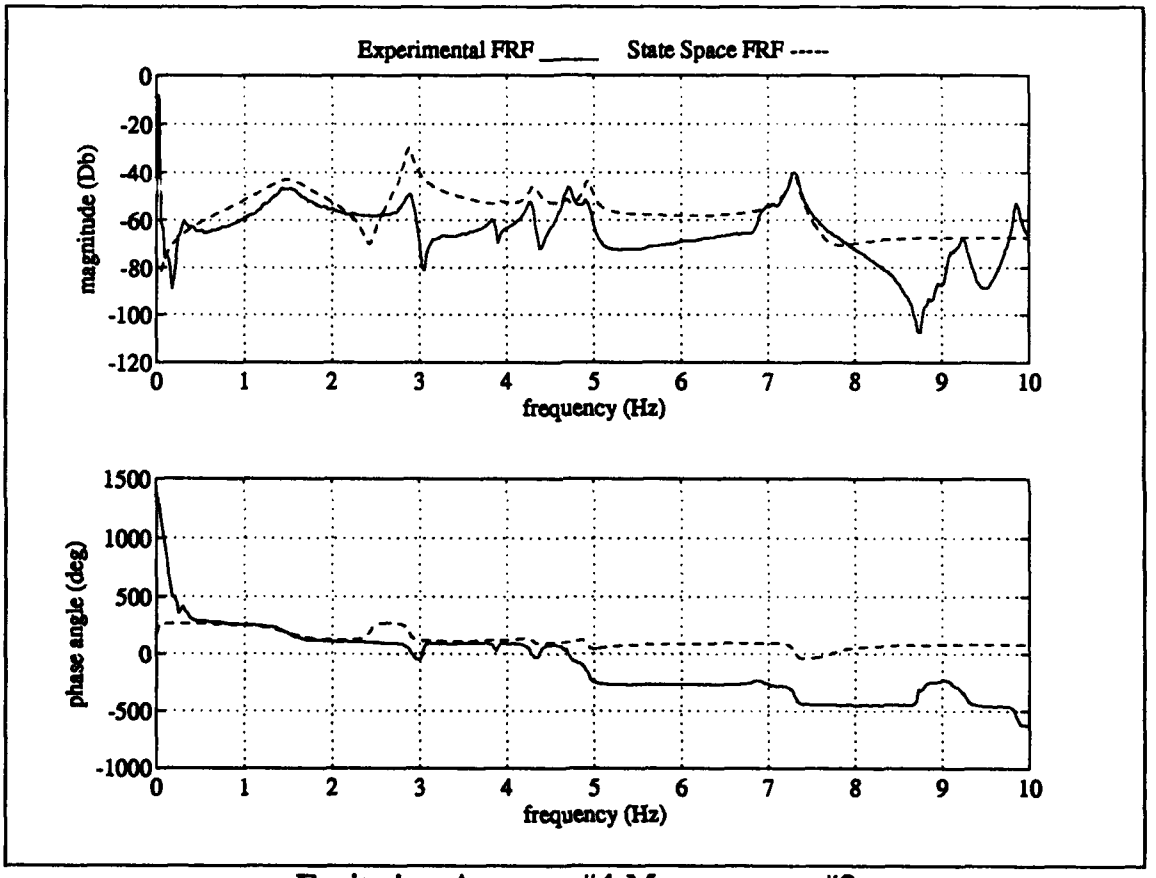

Excitation Actuator #4 Measurement #2

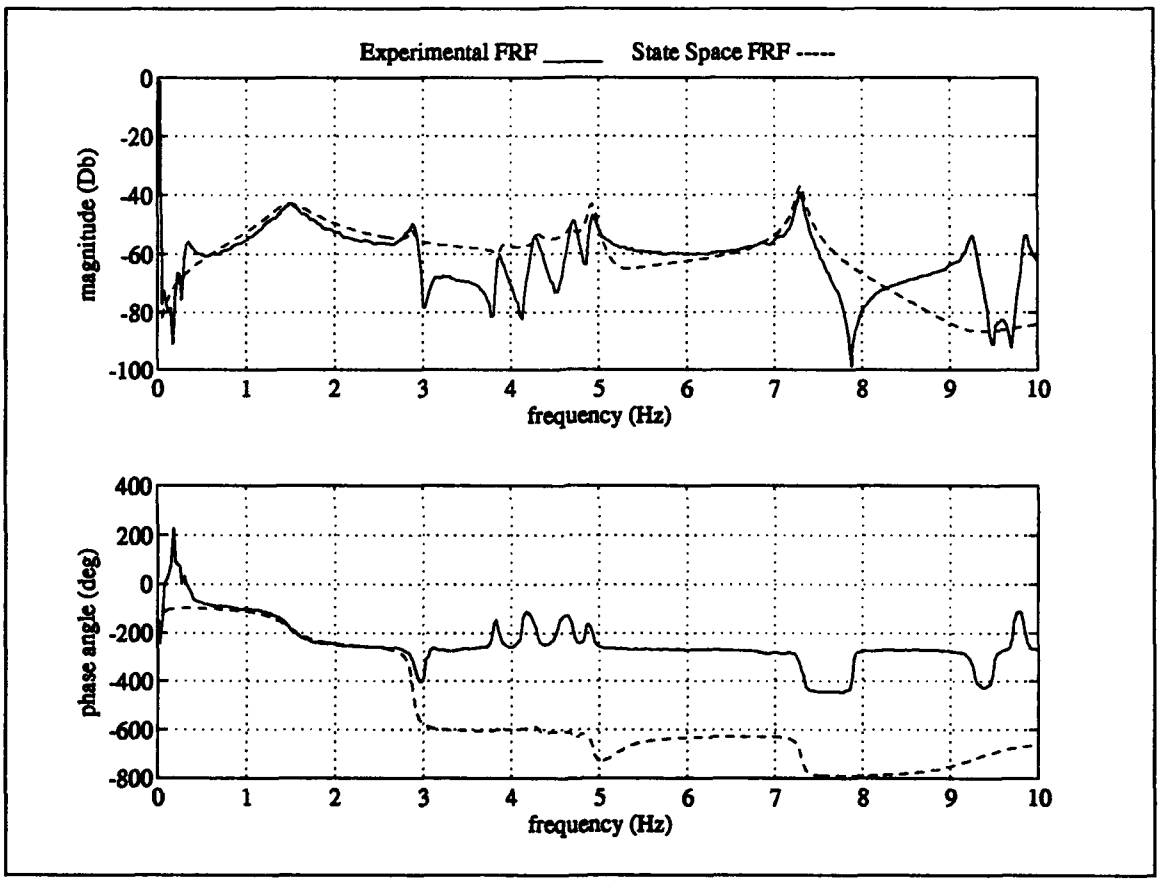

Excitation Actuator #4 Measurement #3

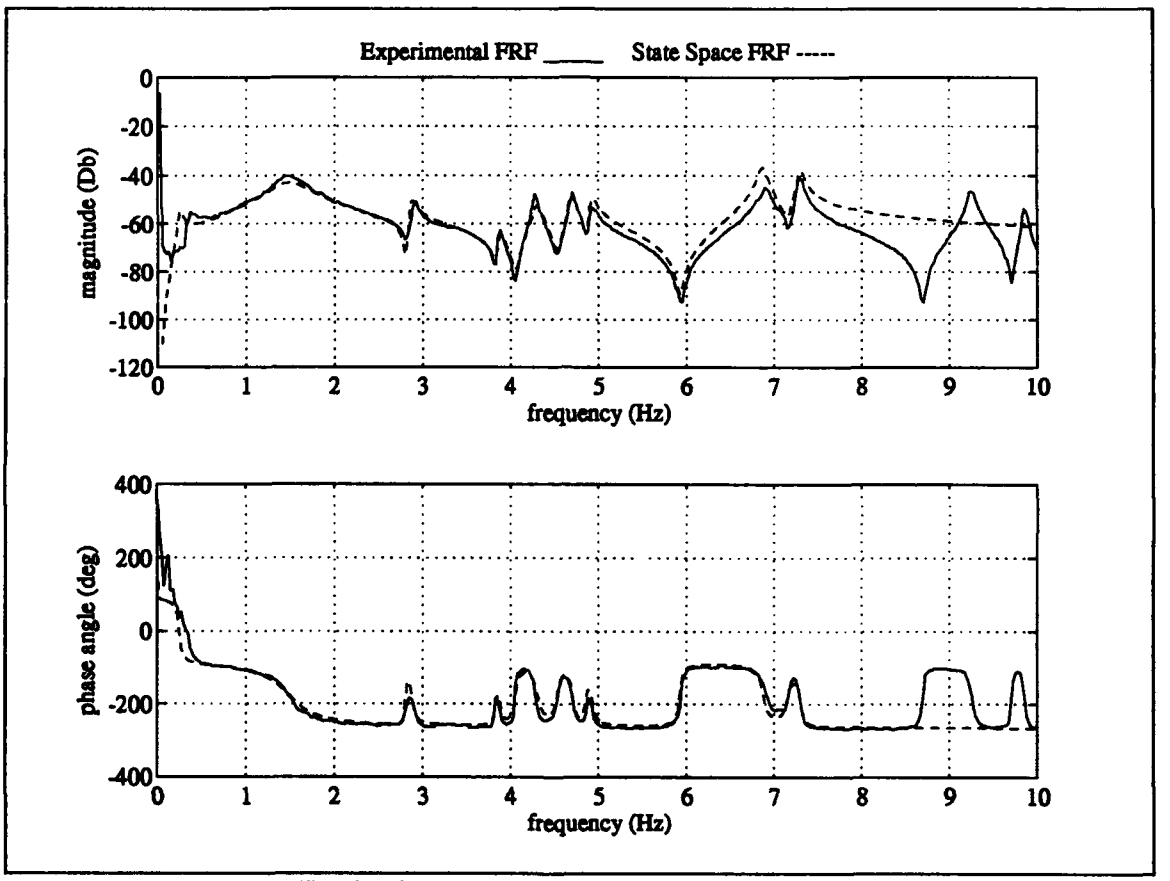

Excitation Actuator #4 Measurement #4

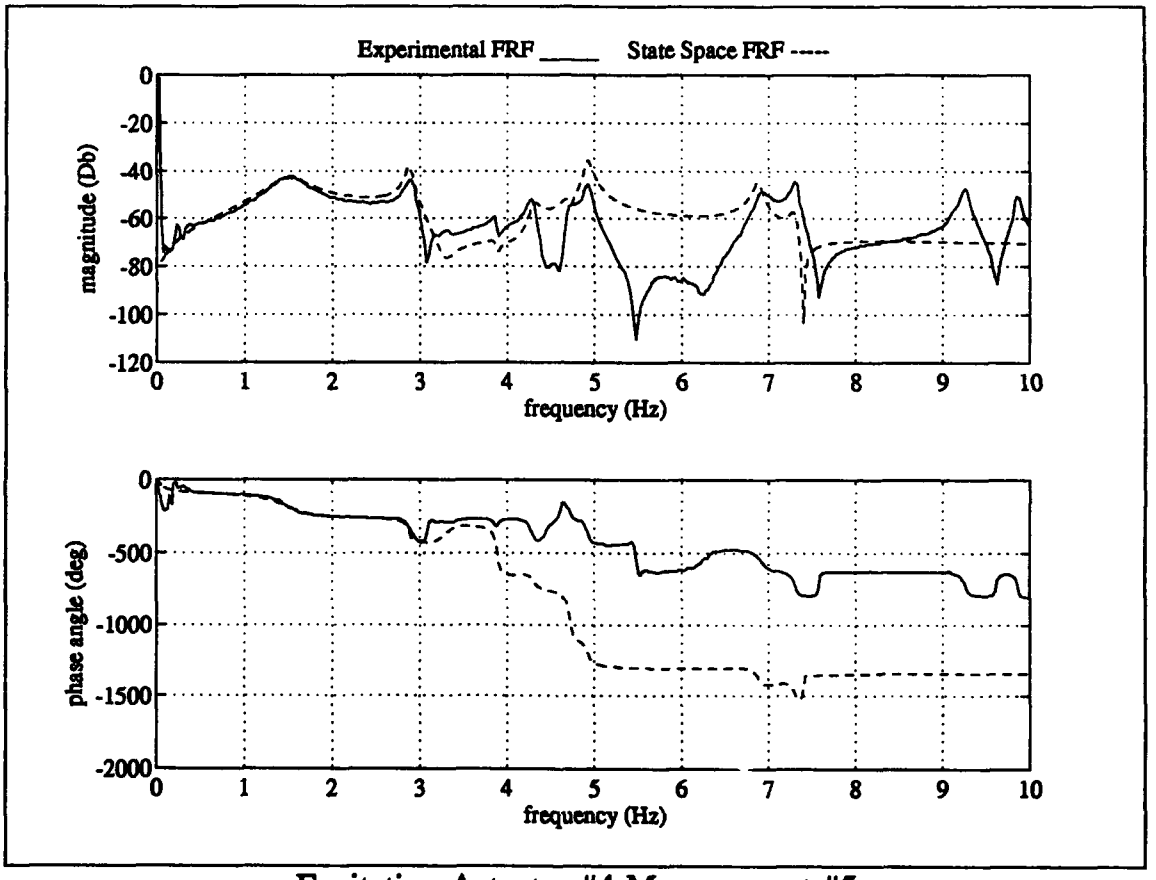

Excitation Actuator #4 Measurement #5

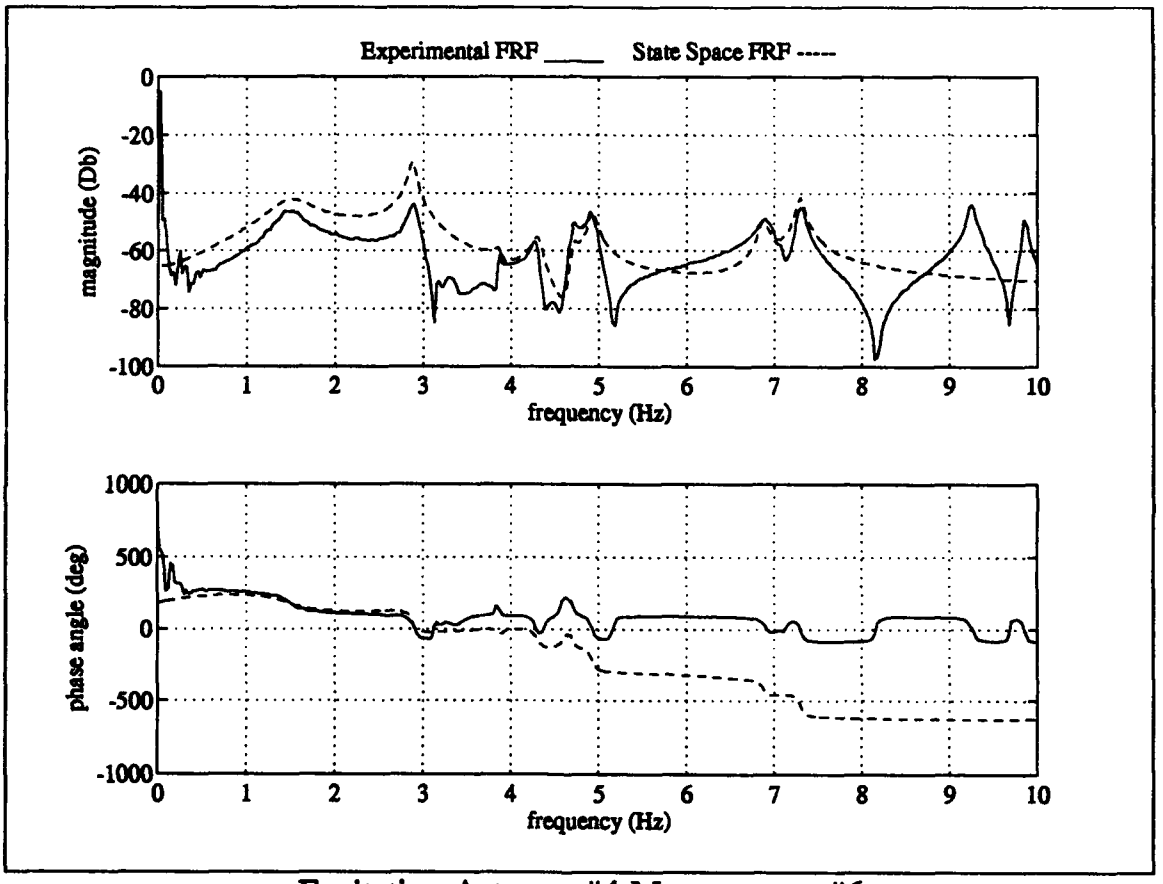

Excitation Actuator #4 Measurement #6

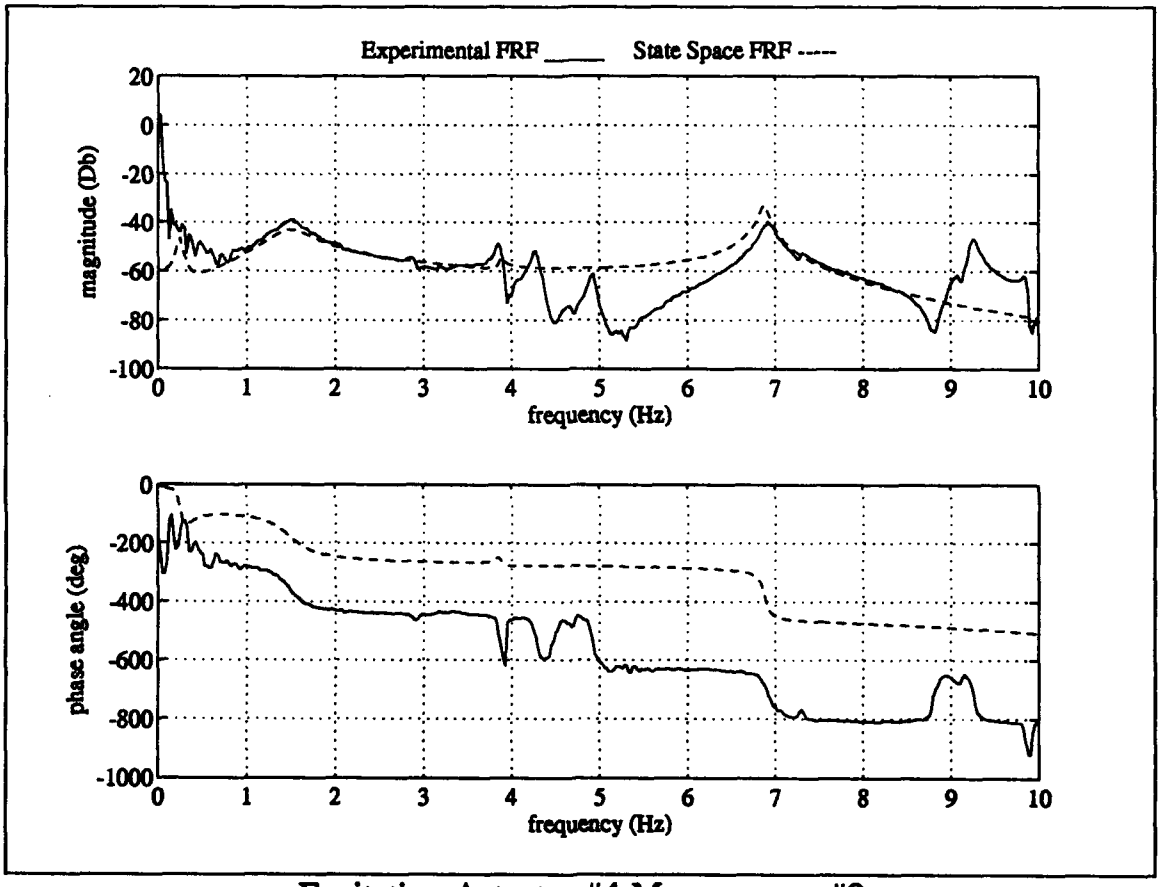

Excitation Actuator #4 Measurement #9

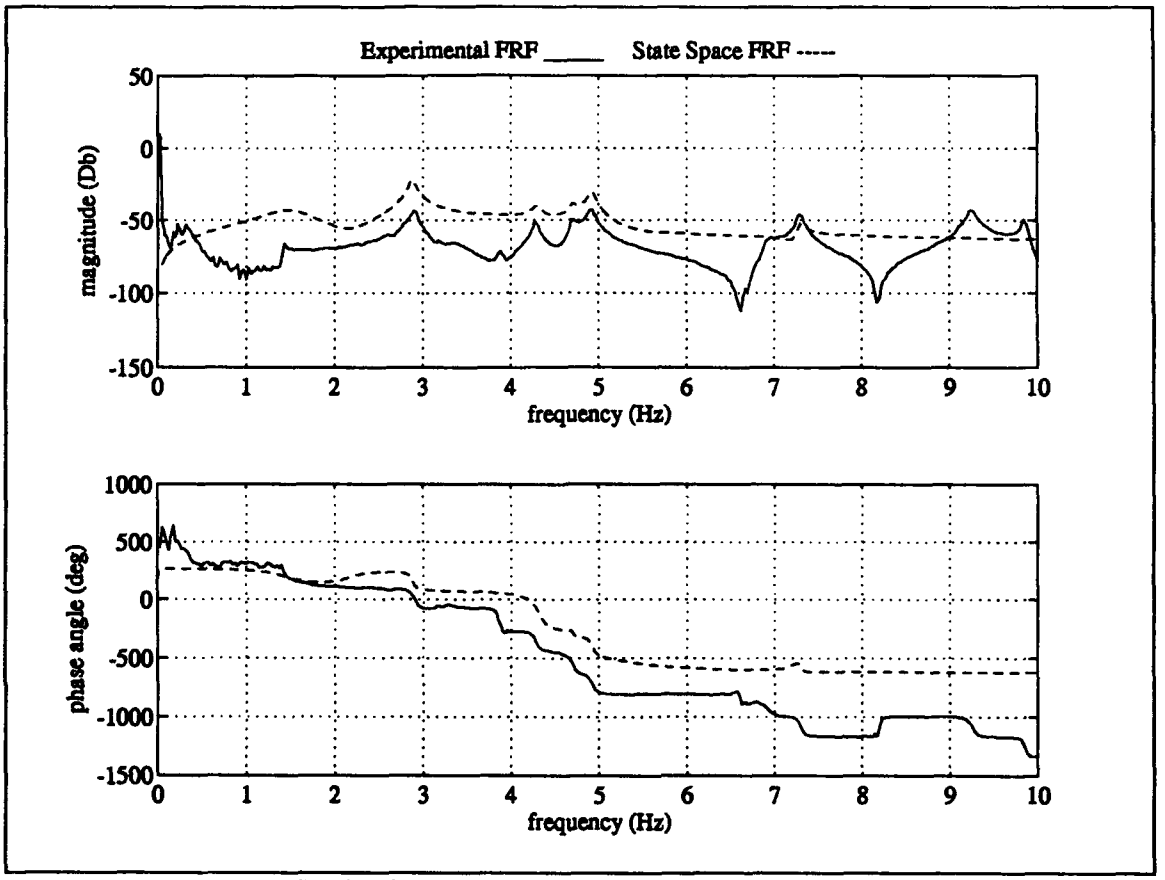

Excitation Actuator #4 Measurement #10

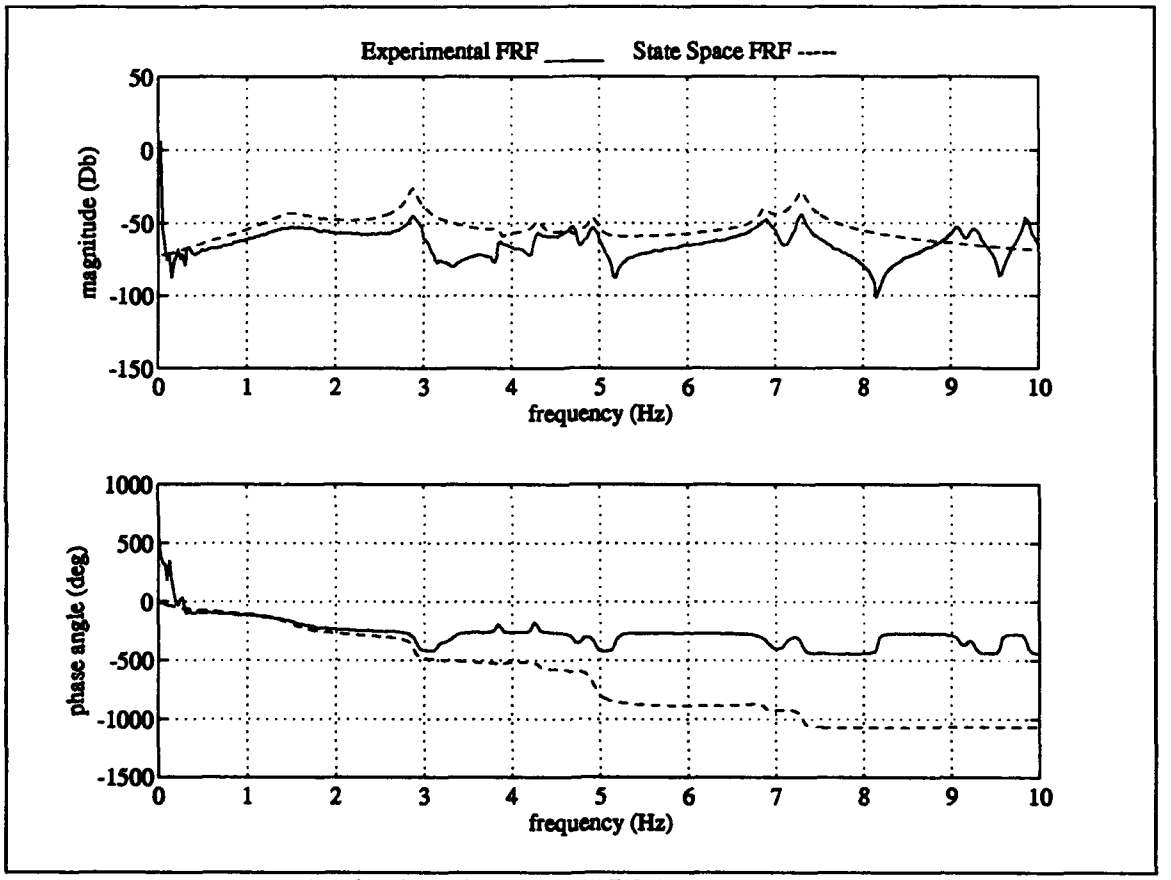

Excitation Actuator #5 Measurement #1

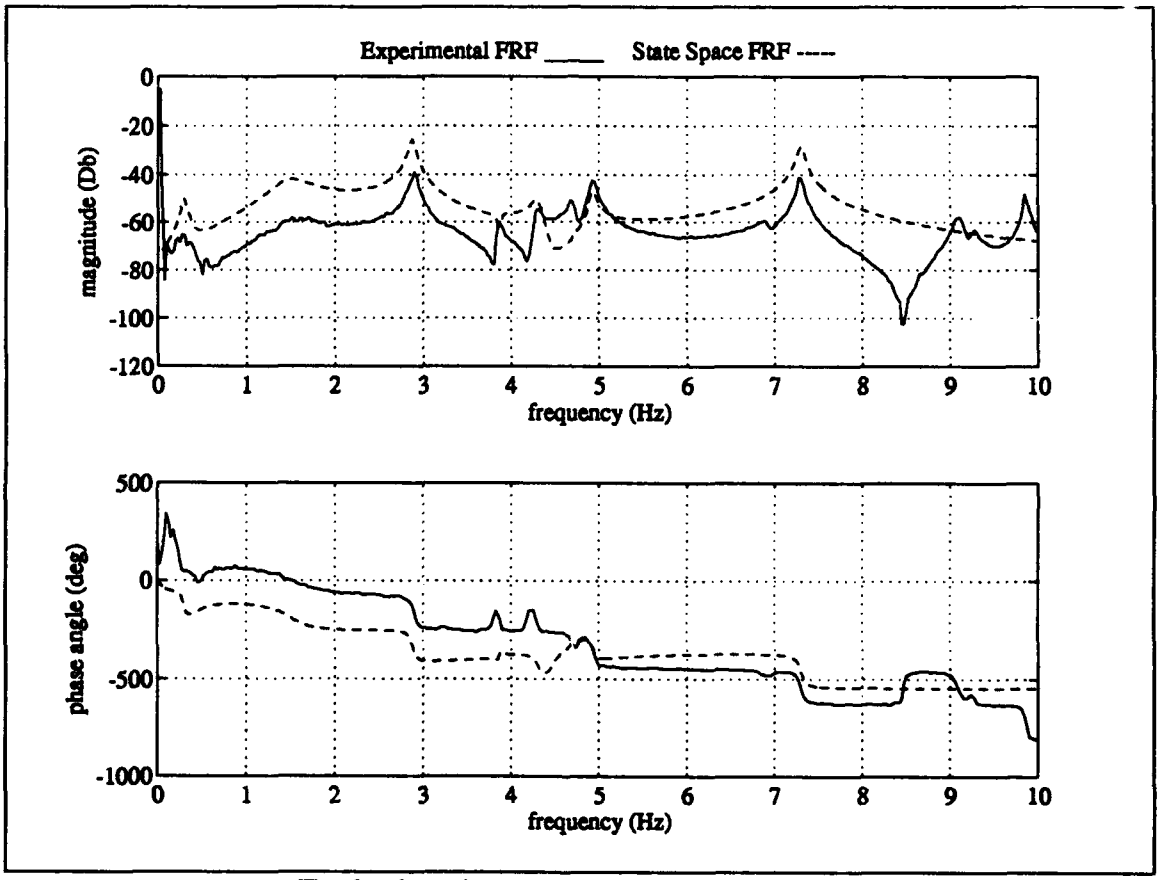

Excitation Actuator #5 Measurement #2

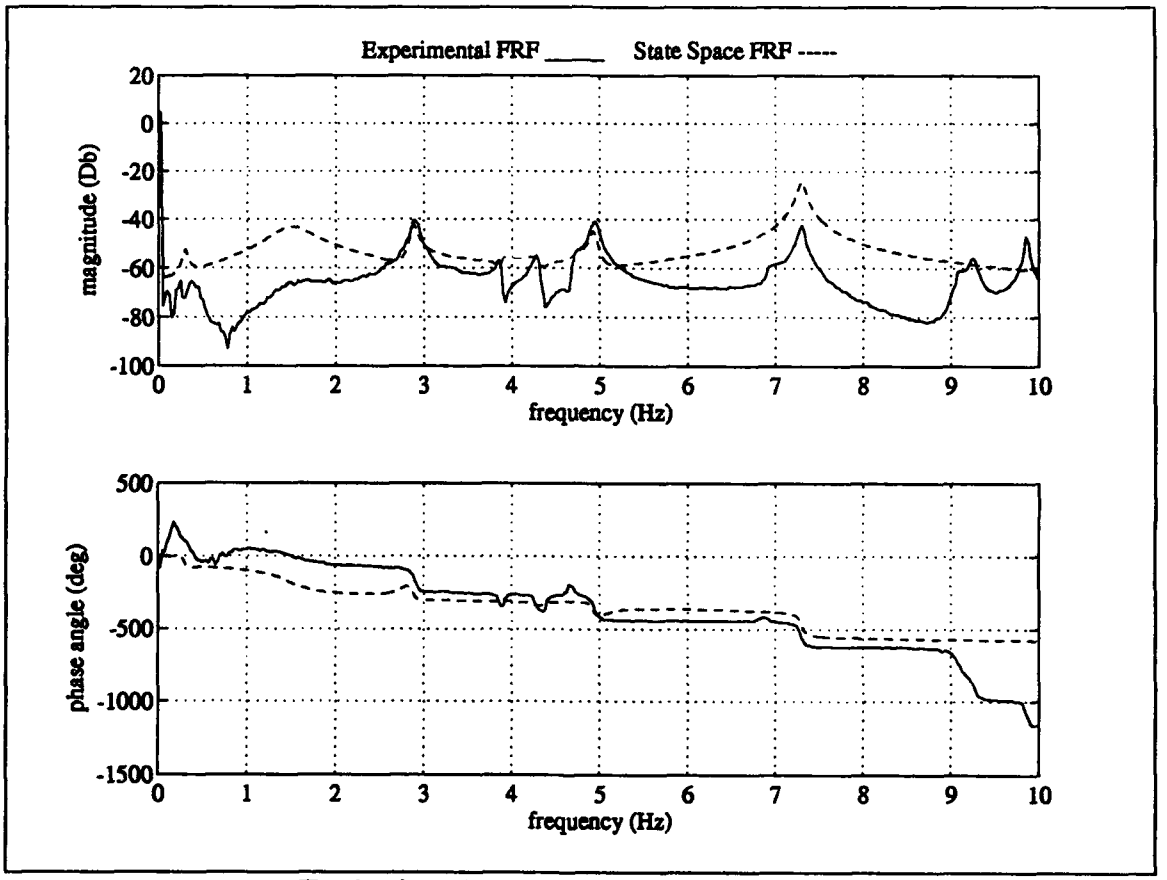

Excitation Actuator #5 Measurement #3

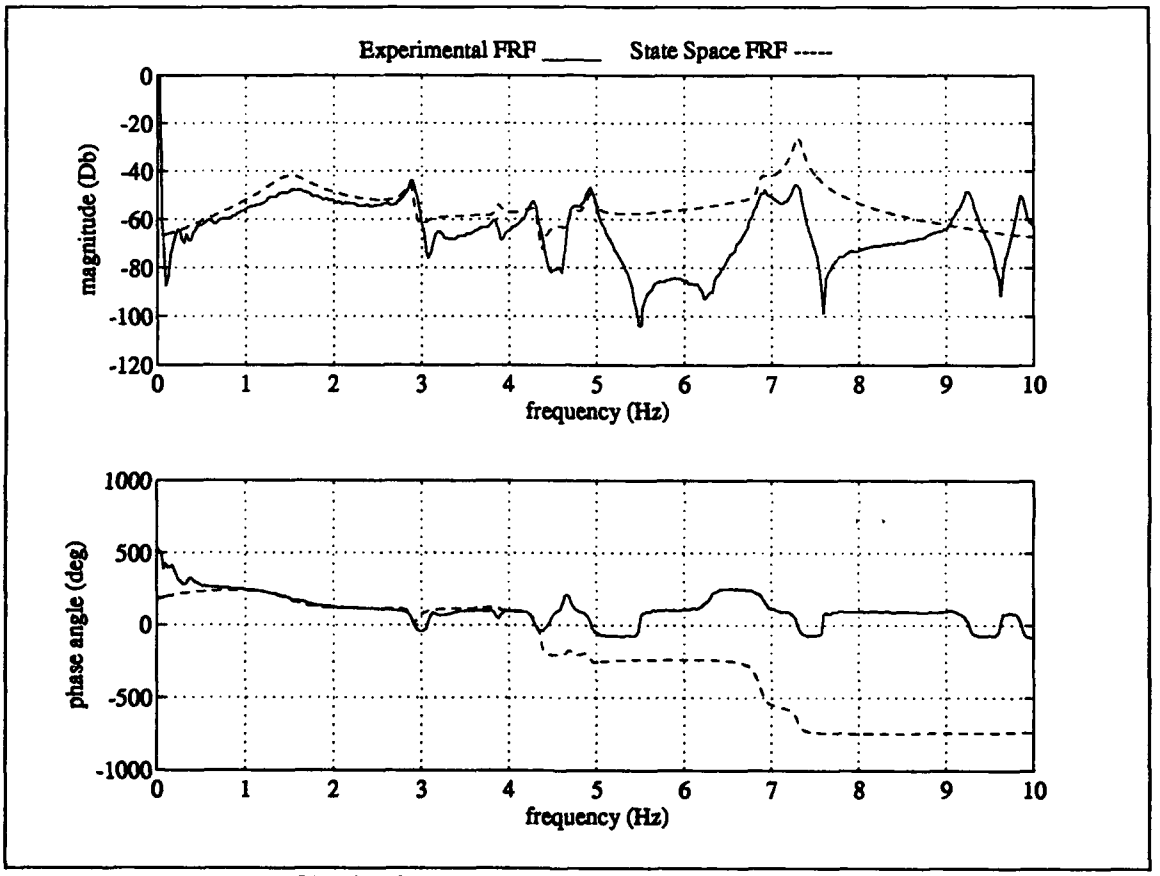

Excitation Actuator #5 Measurement #4

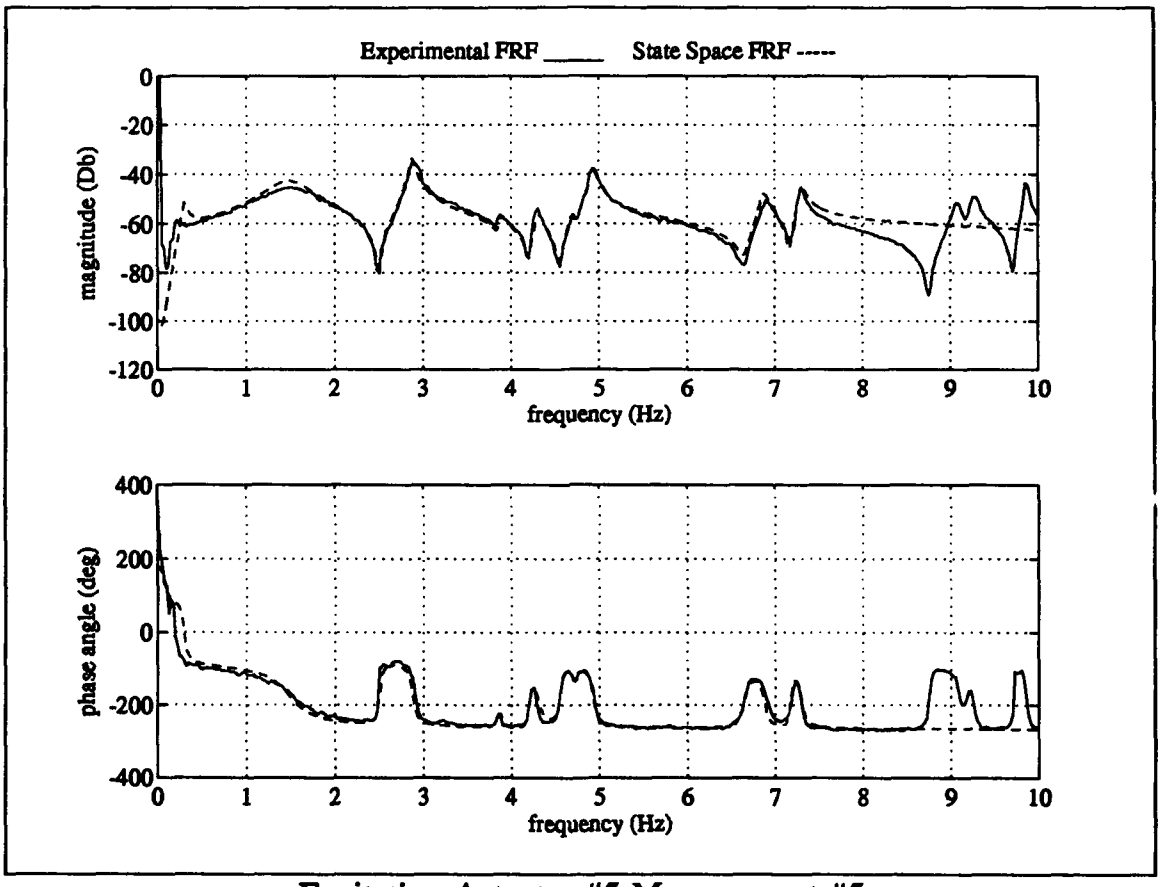

Excitation Actuator #5 Measurement #5

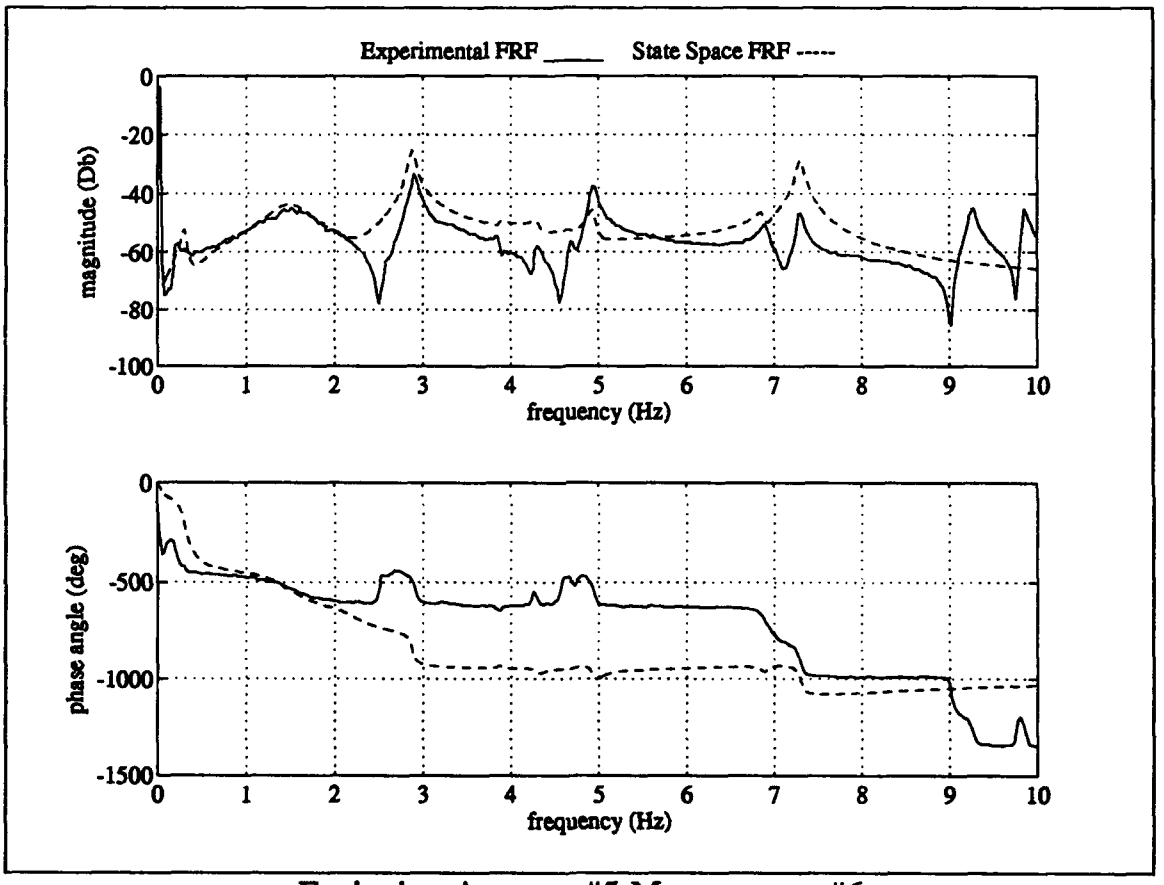

Excitation Actuator #5 Measurement #6

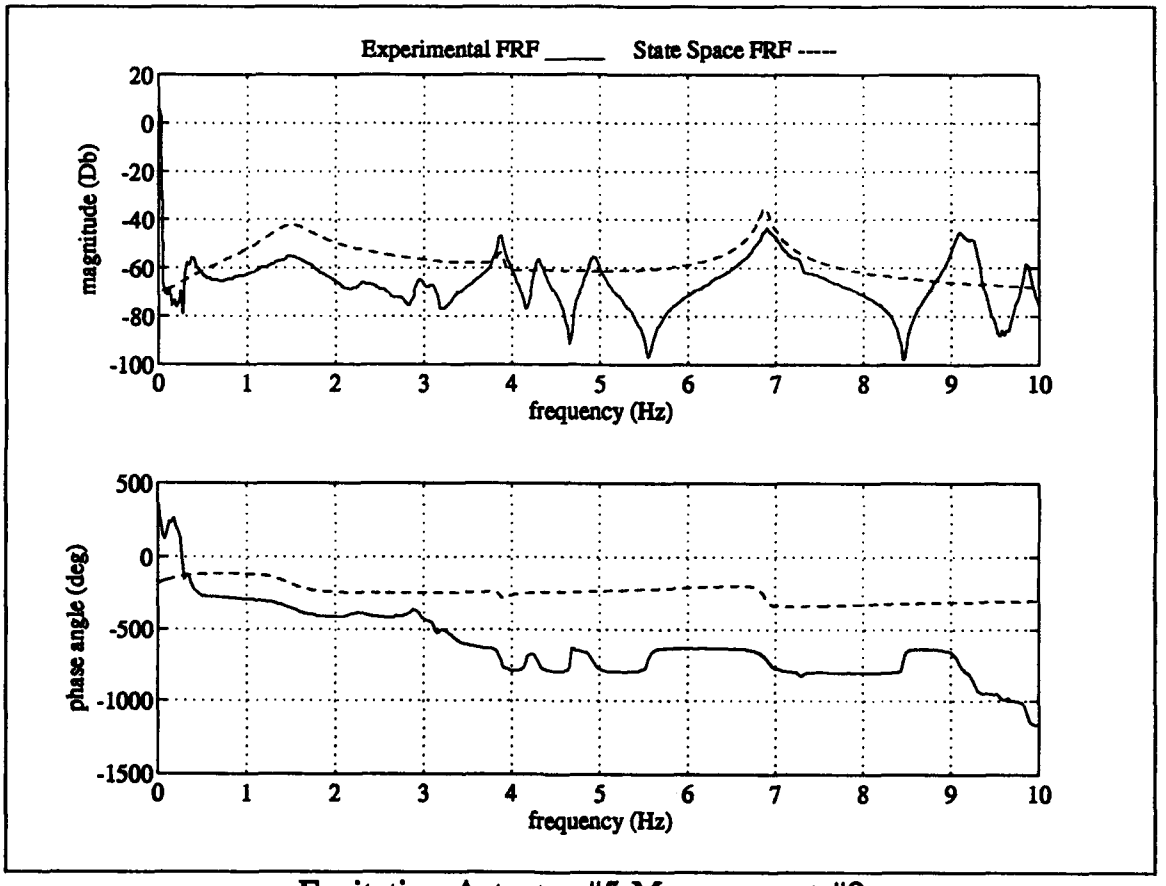

Excitation Actuator #5 Measurement #9

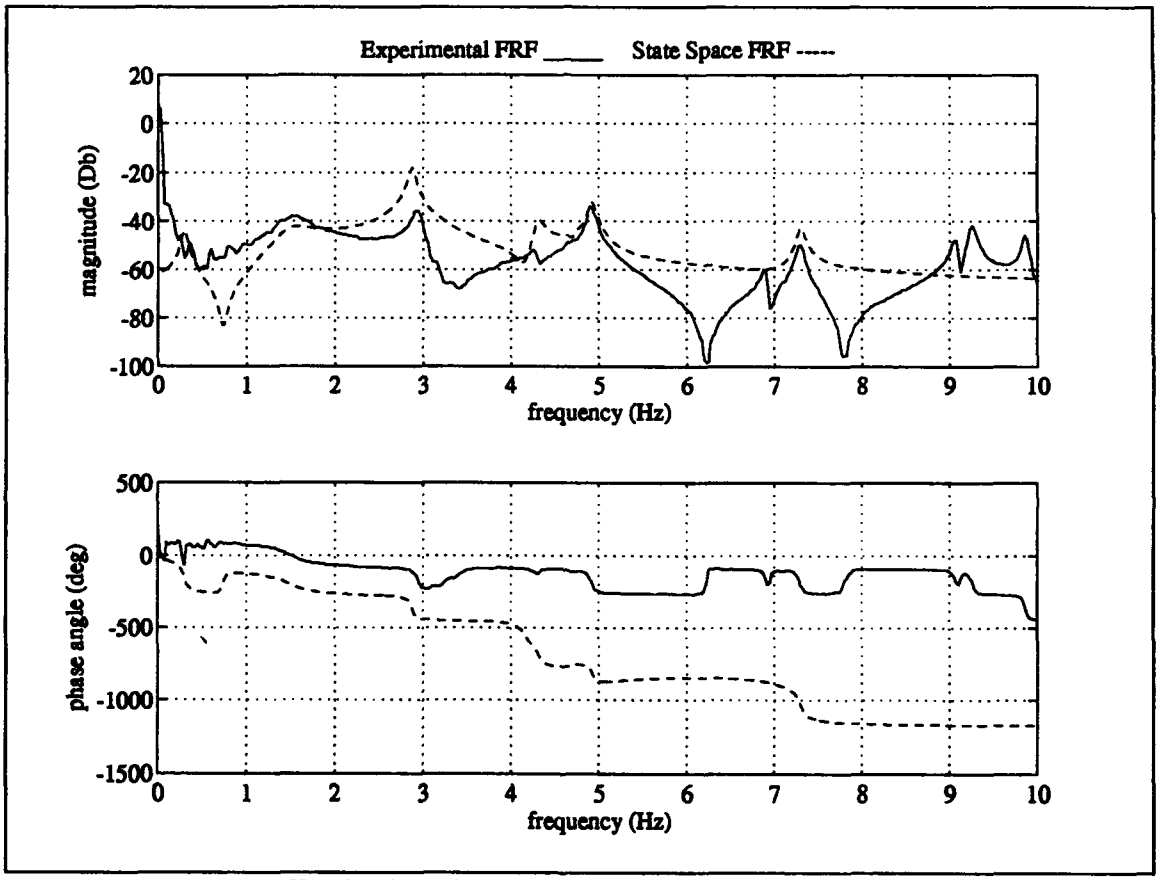

Excitation Actuator #5 Measurement #10

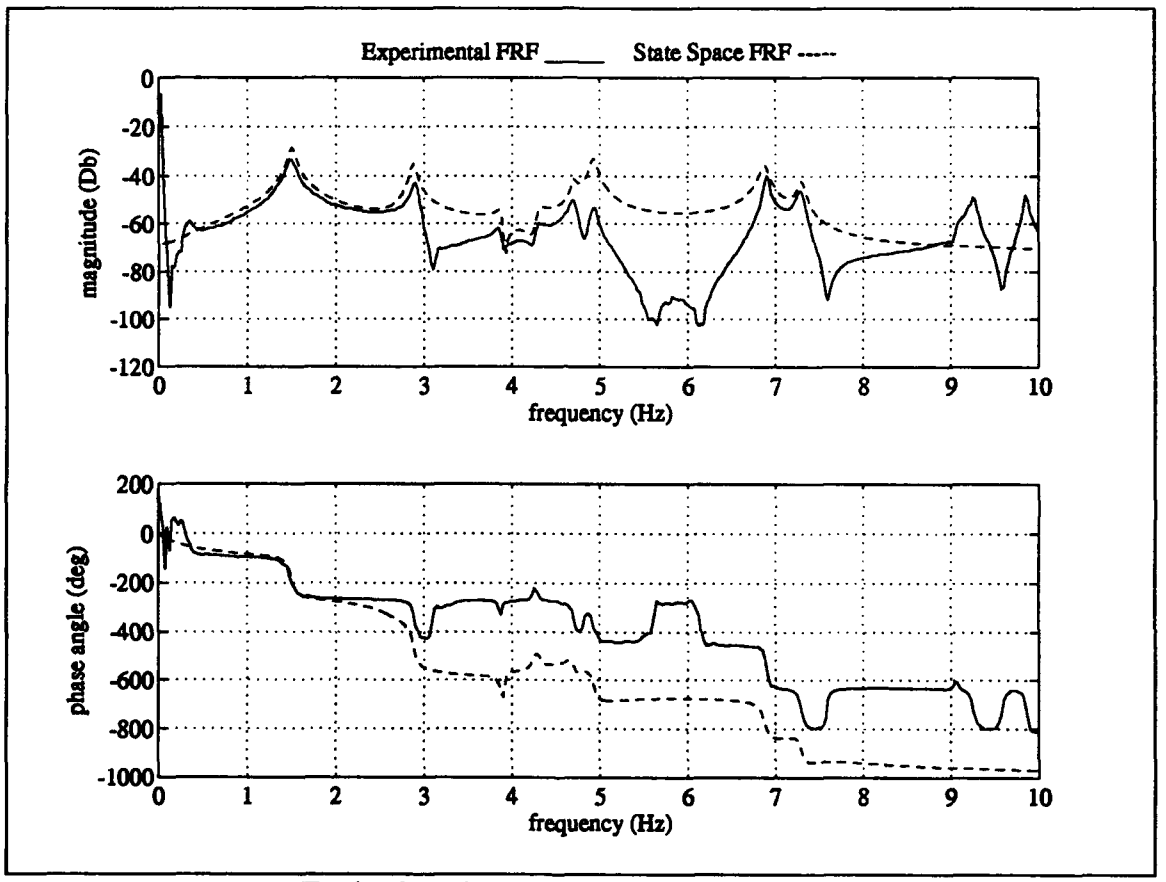

Excitation Actuator #6 Measurement #1

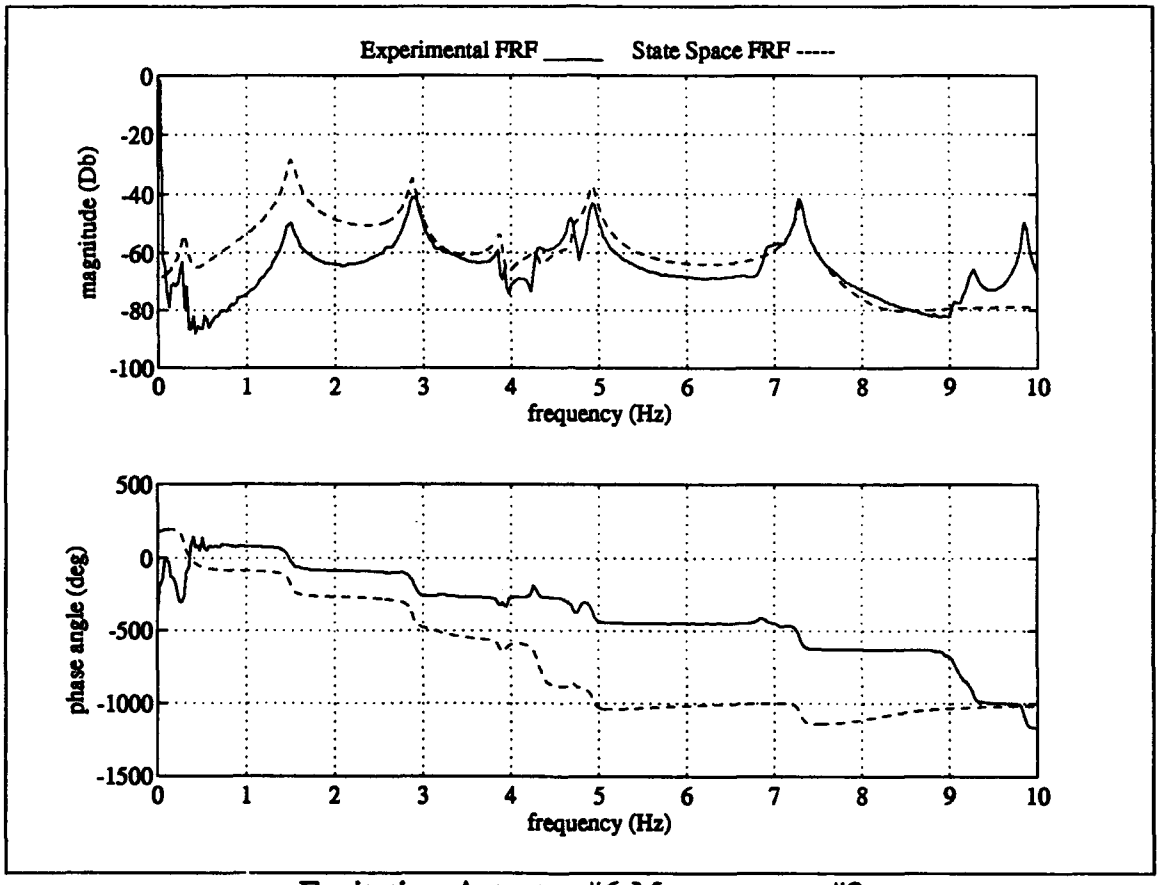

Excitation Actuator #6 Measurement #2

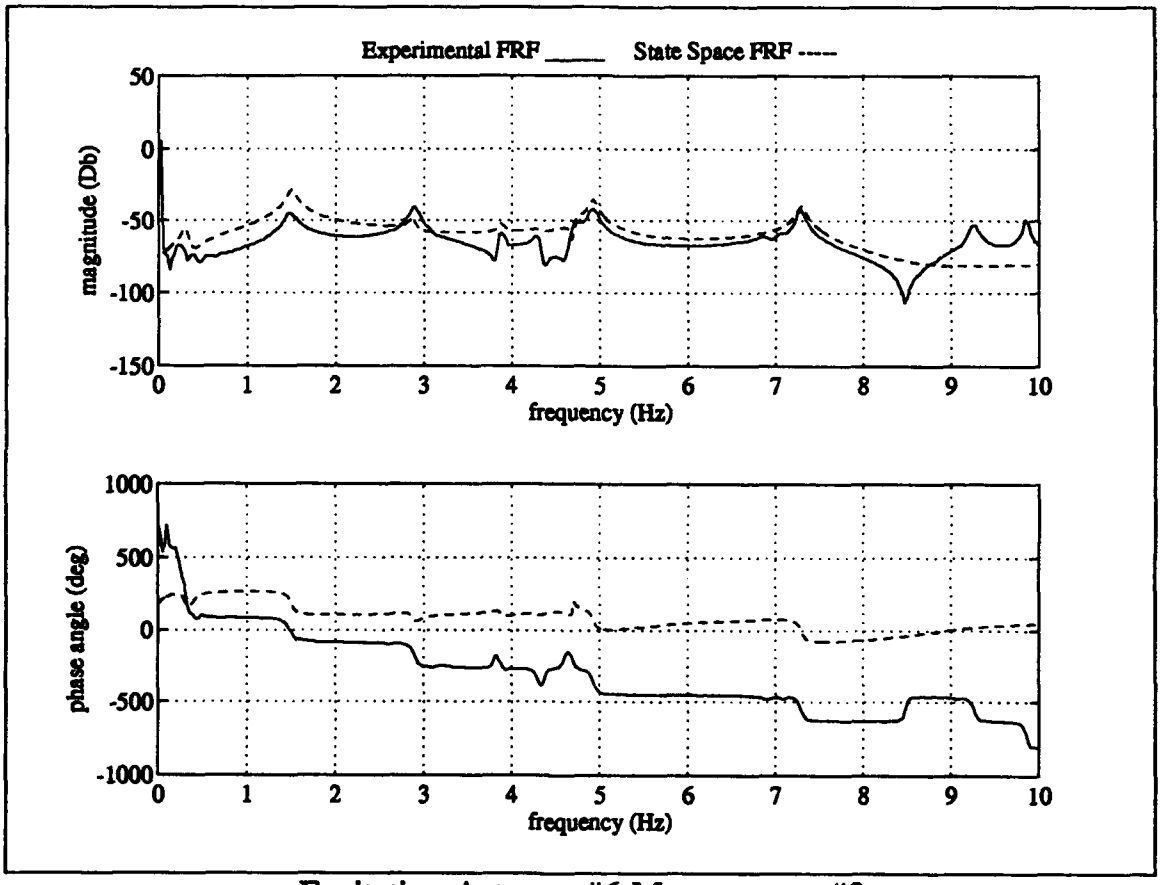

Excitation Actuator #6 Measurement #3

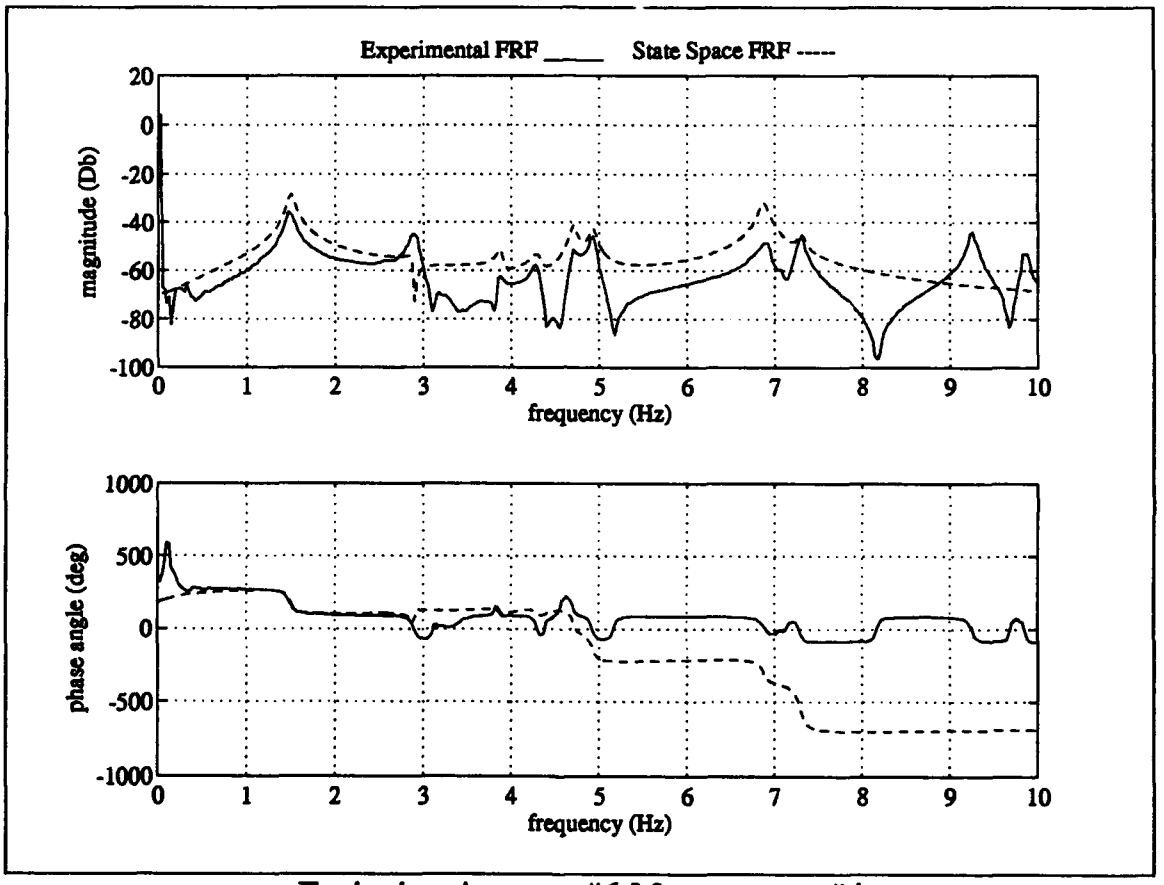

Excitation Actuator #6 Measurement #4

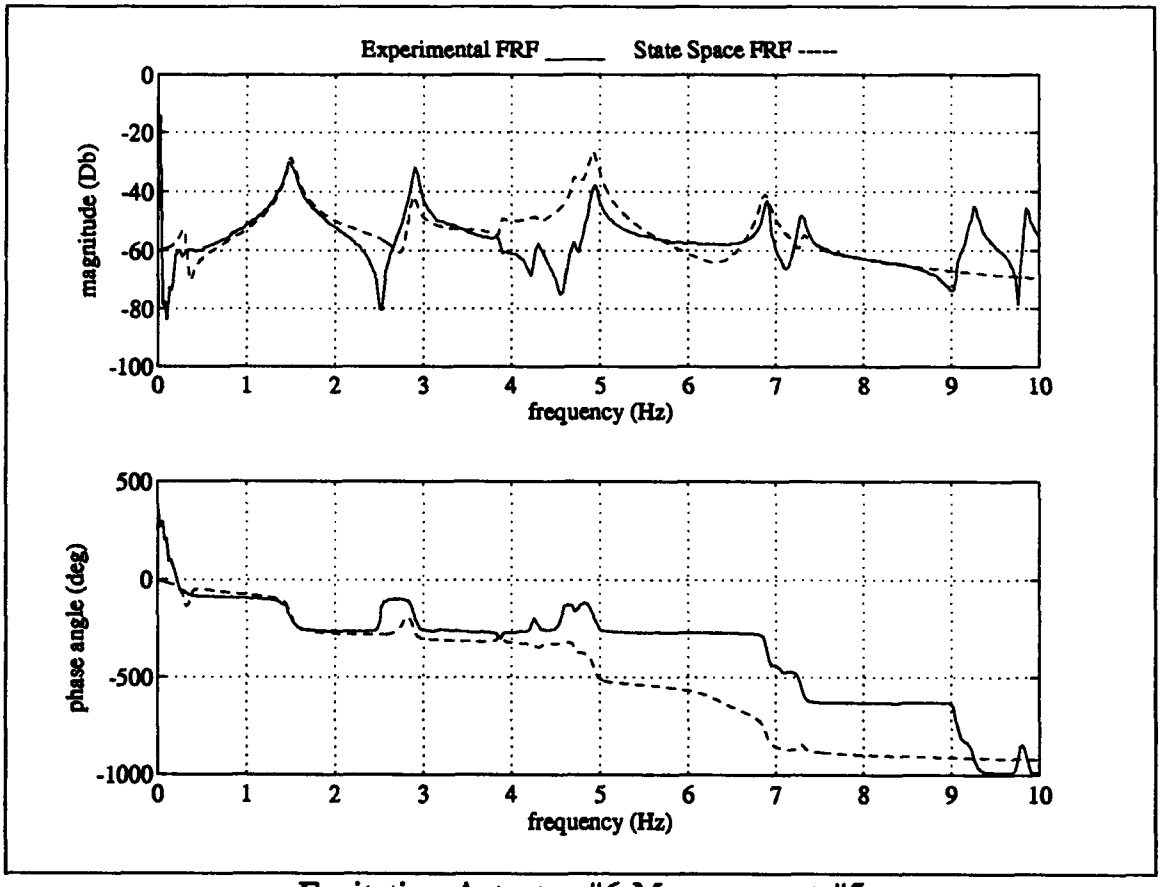

Excitation Actuator #6 Measurement #5

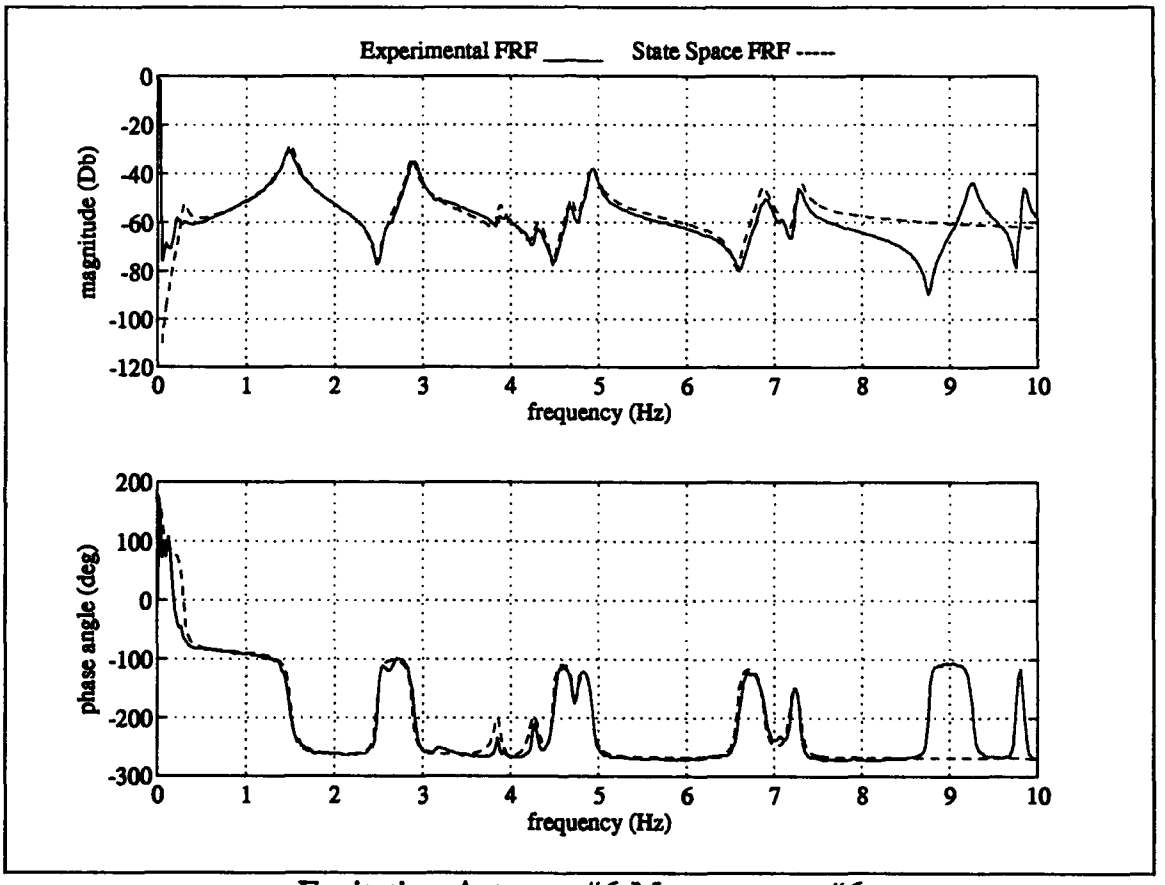

Excitation Actuator #6 Measurement #6

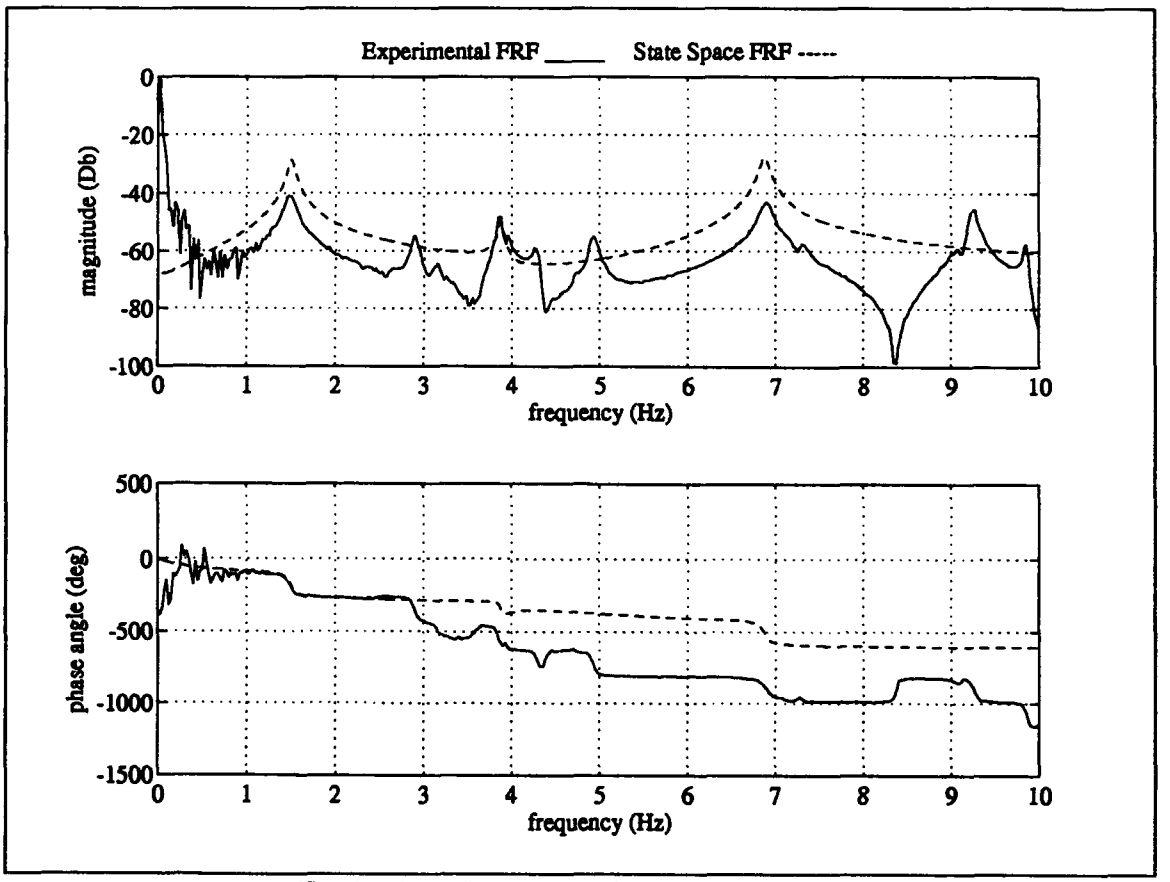

Excitation Actuator #6 Measurement #9

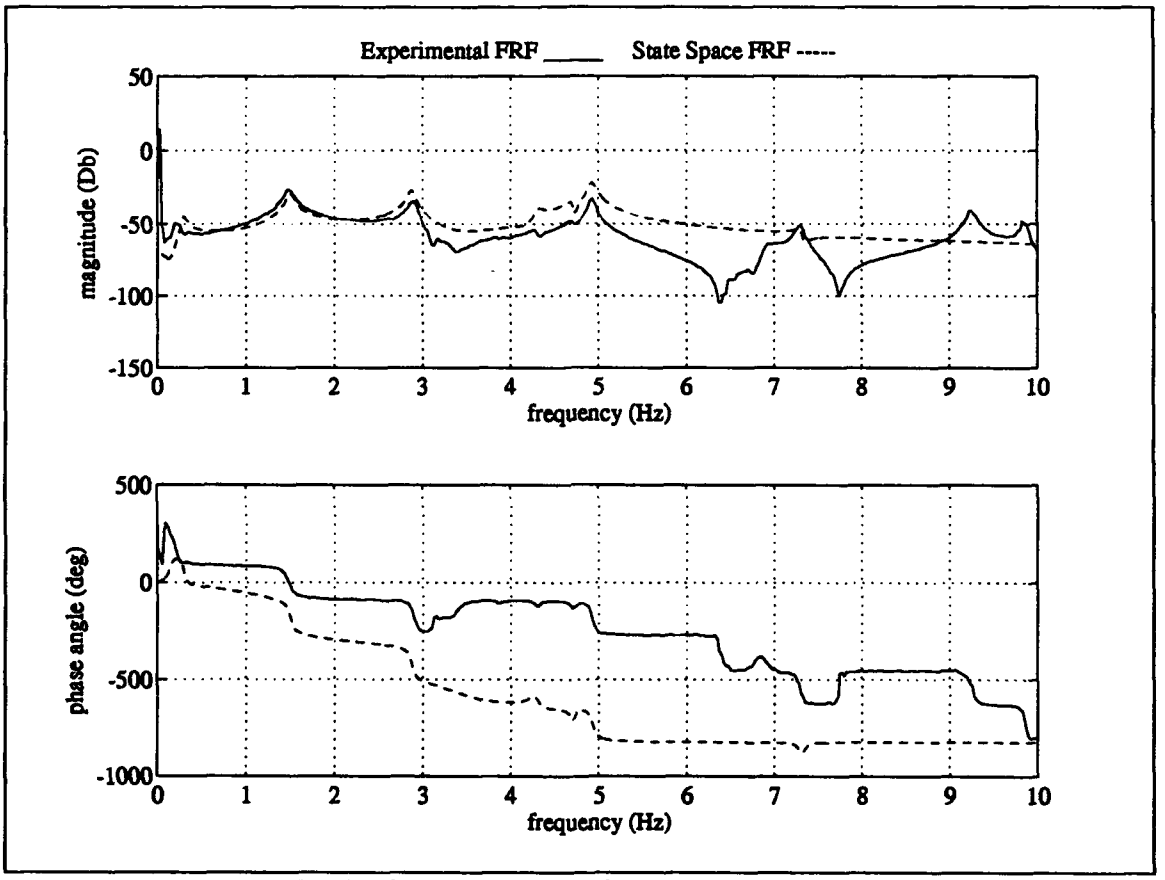

Excitation Actuator #6 Measurement #10

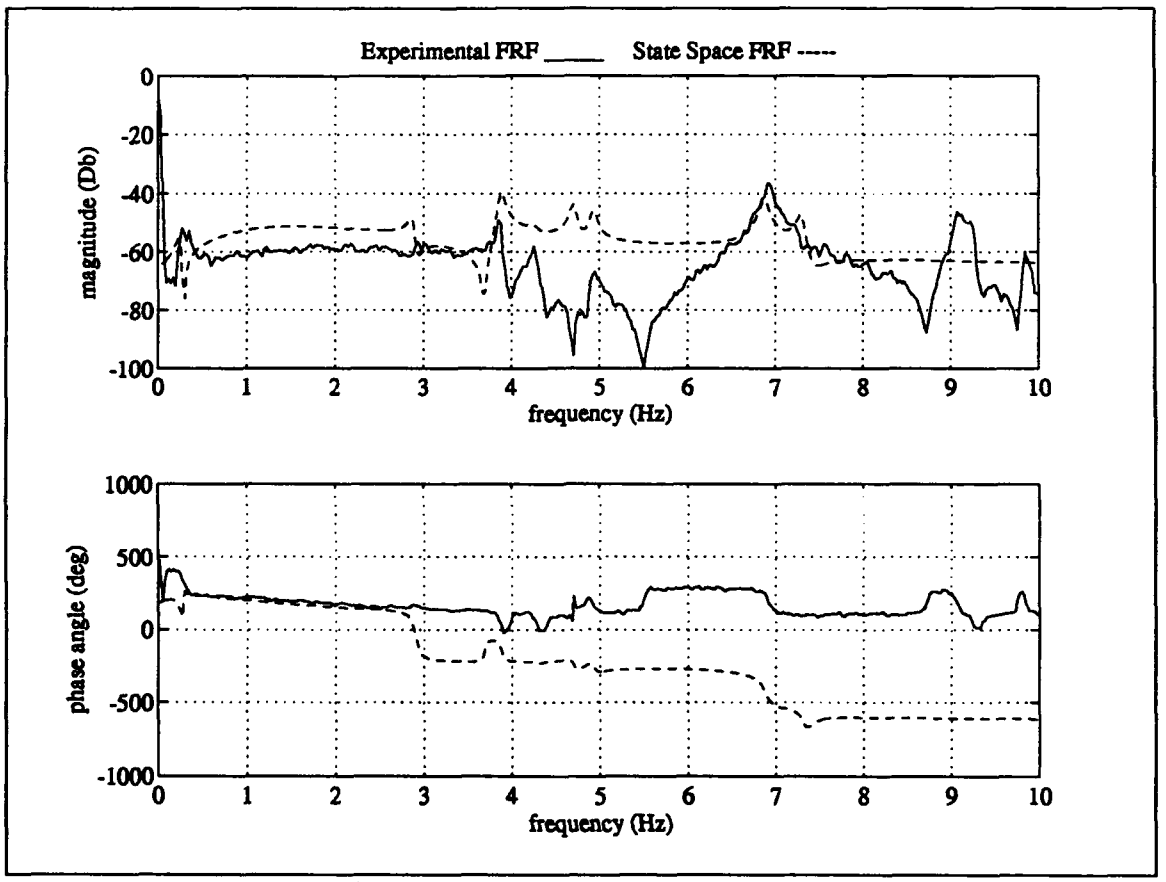

Excitation Actuator #9 Measurement #1

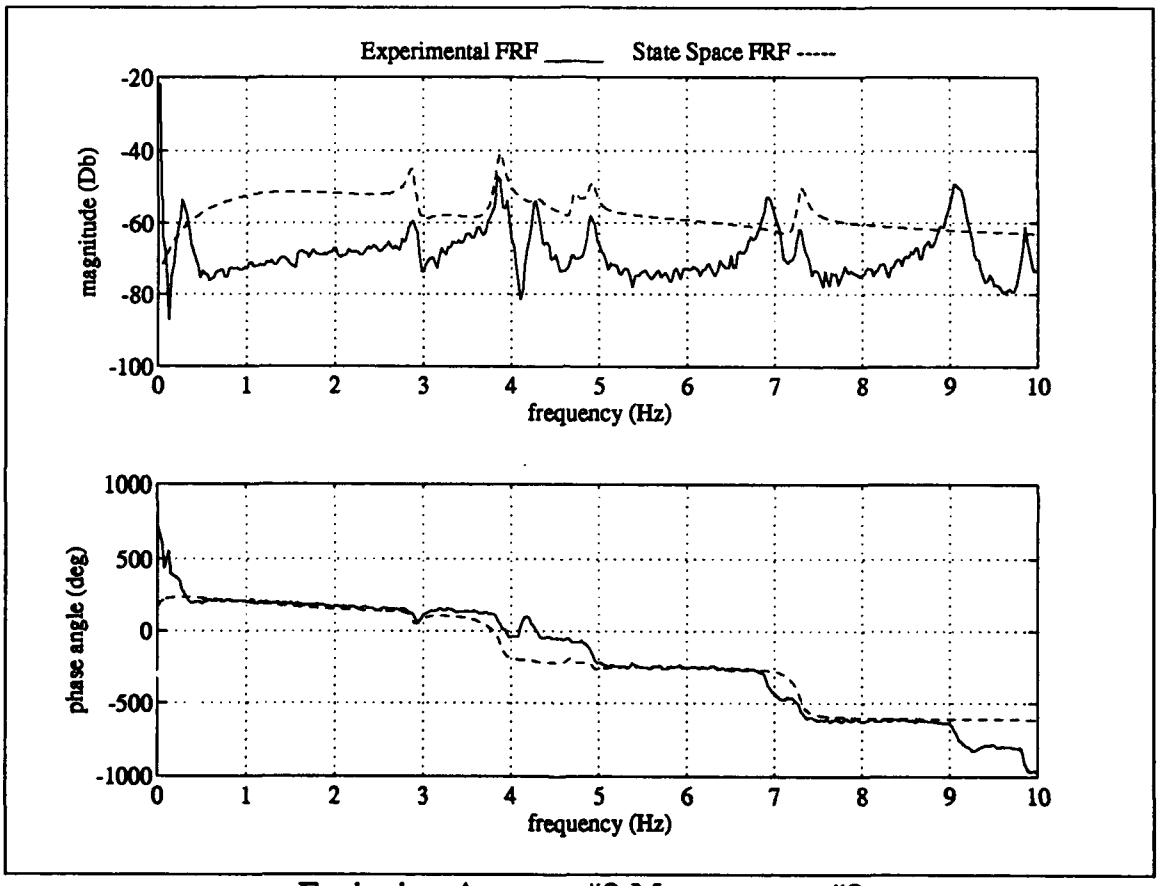

Excitation Actuator #9 Measurement #2

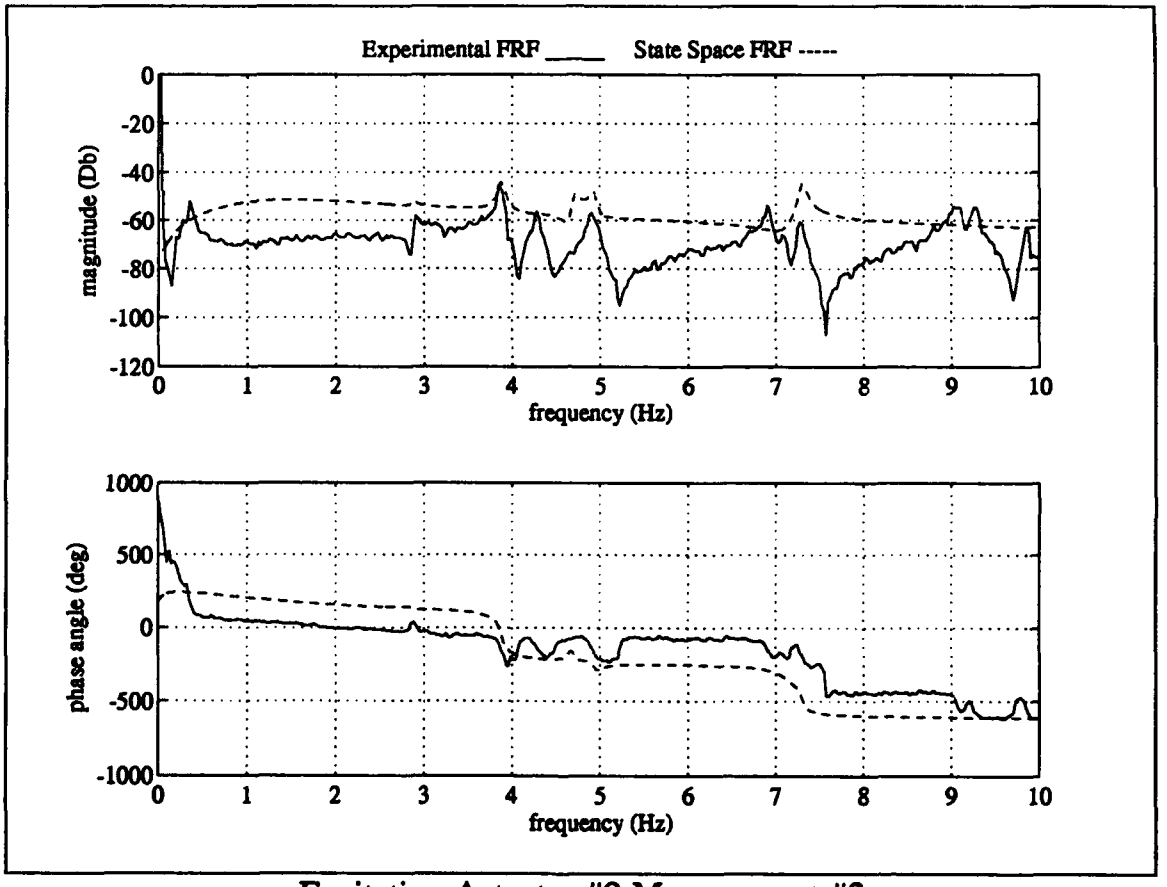

Excitation Actuator #9 Measurement #3

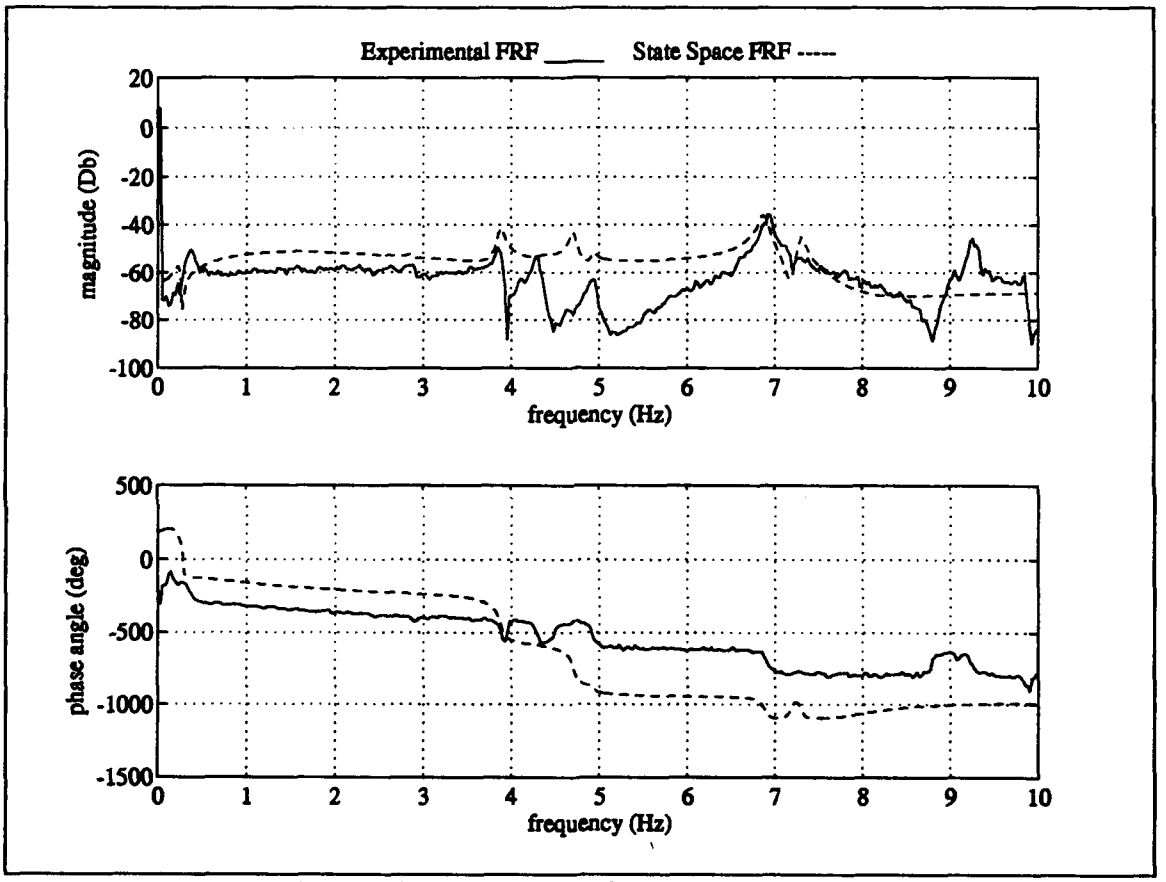

Excitation Actuator #9 Measurement #4

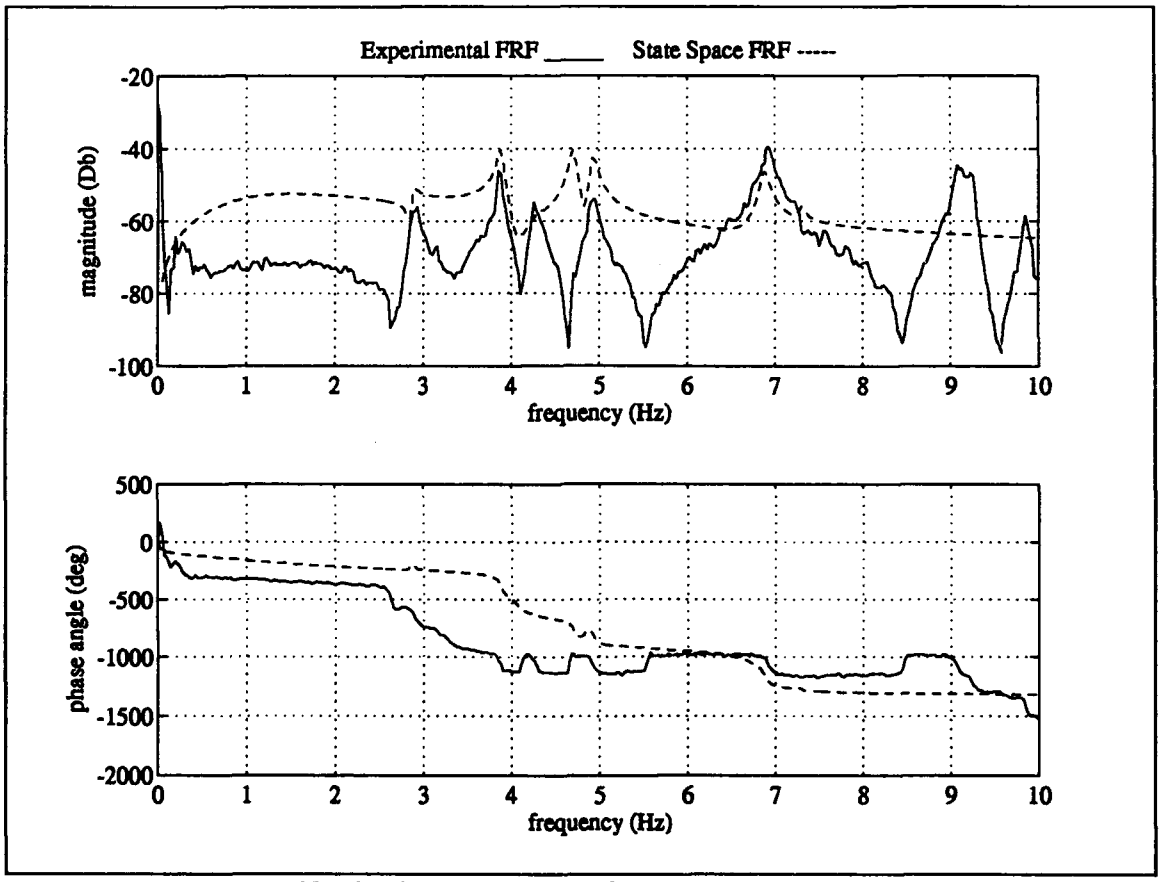

Excitation Actuator #9 Measurement #5

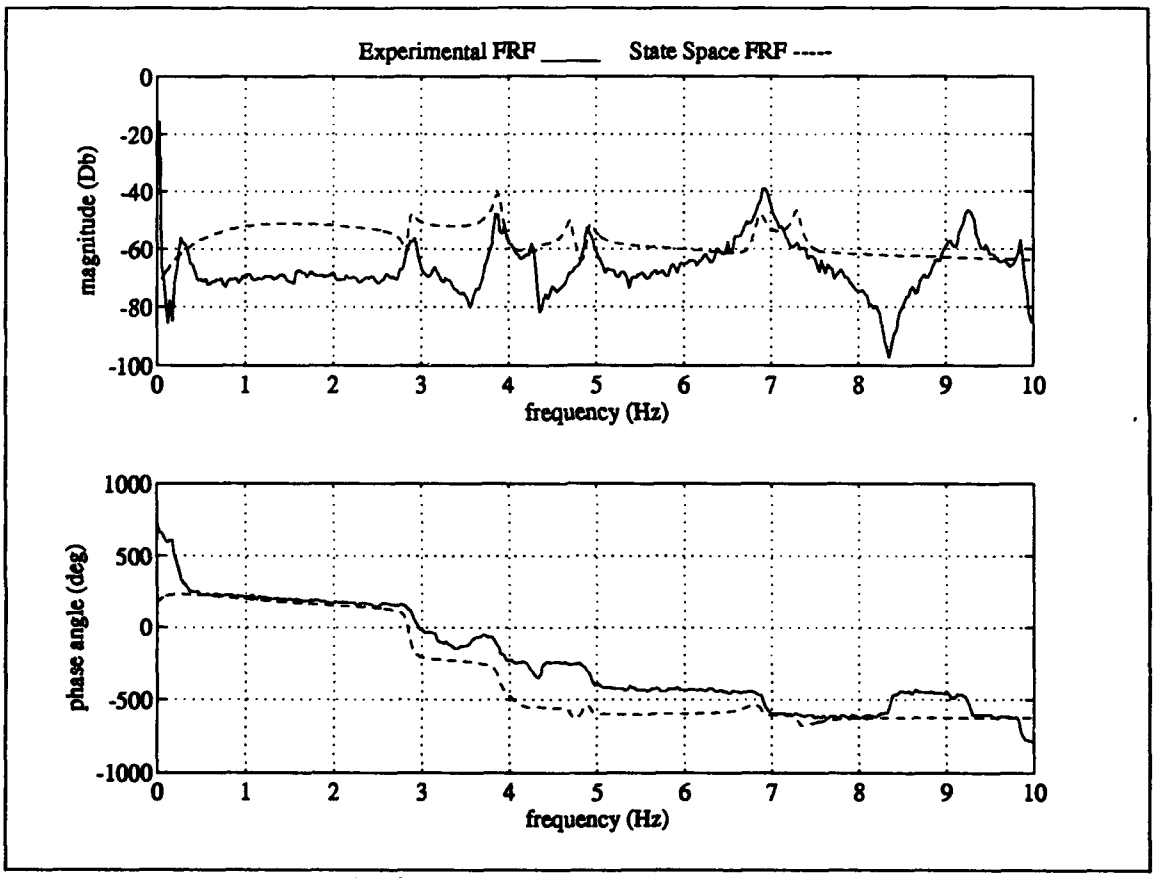

Excitation Actuator #9 Measurement #6

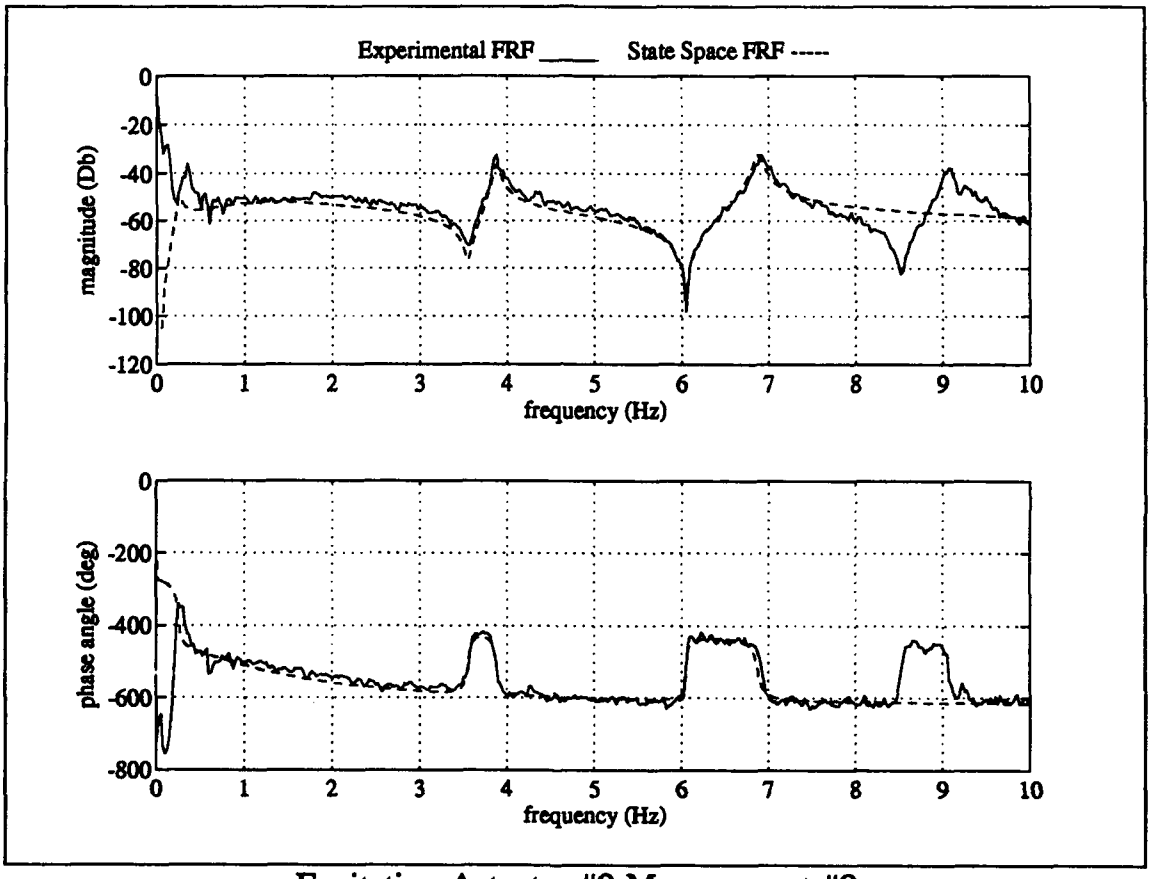

Excitation Actuator #9 Measurement #9

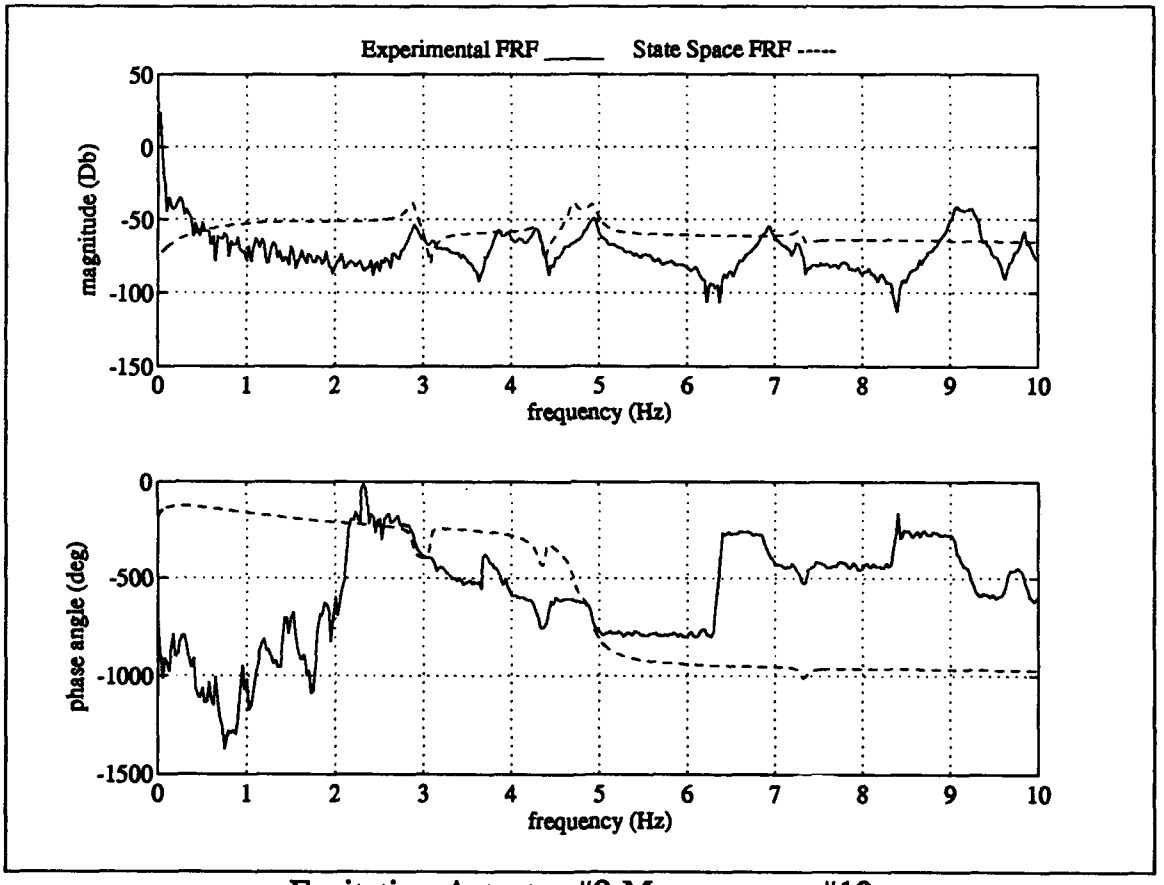

Excitation Actuator #9 Measurement #10

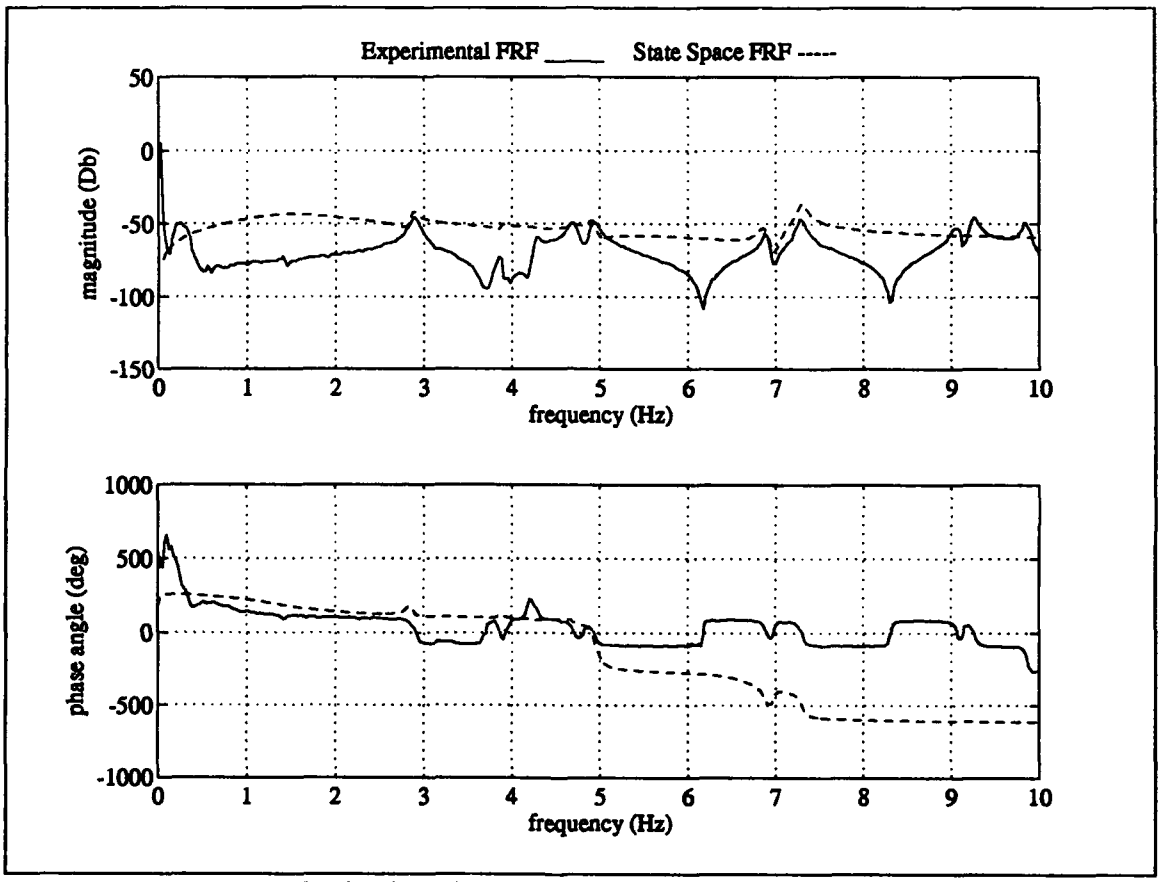

Excitation Actuator #10 Measurement #1

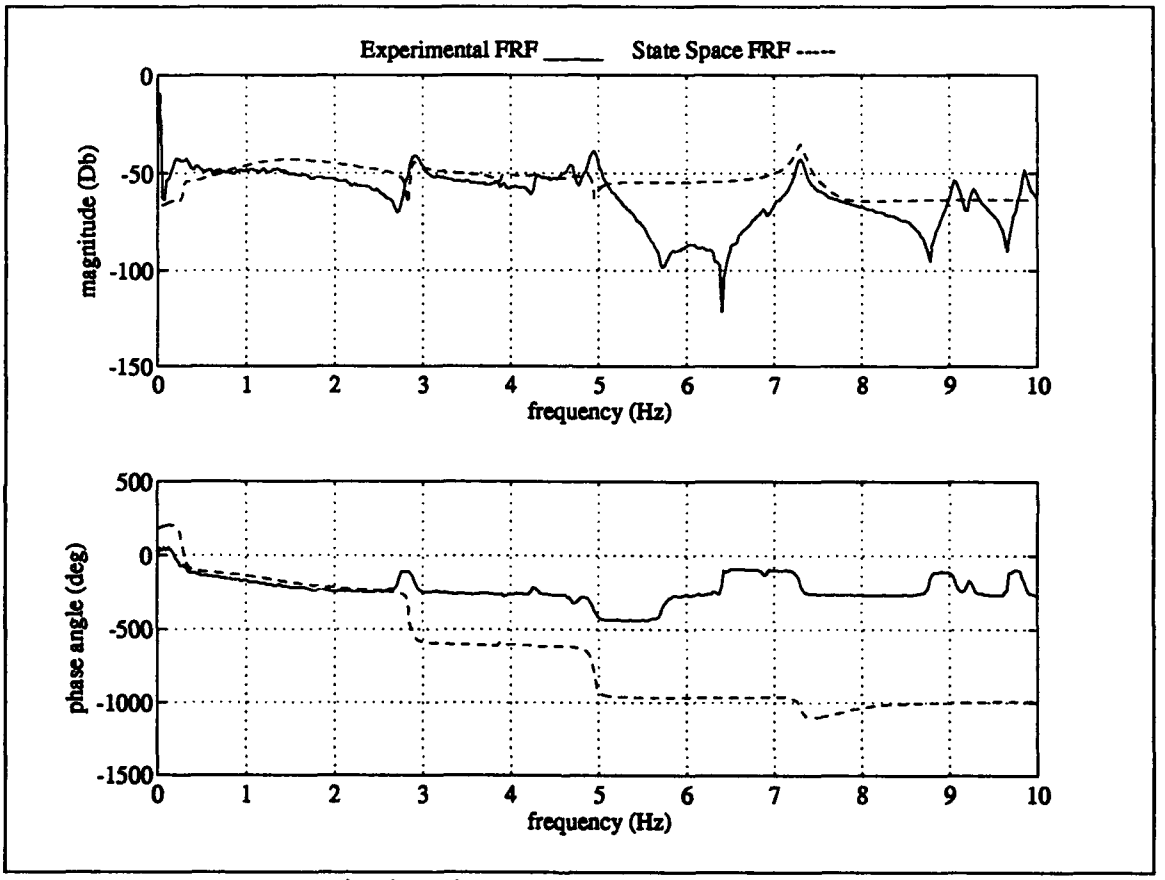

Excitation Actuator #10 Measurement #2

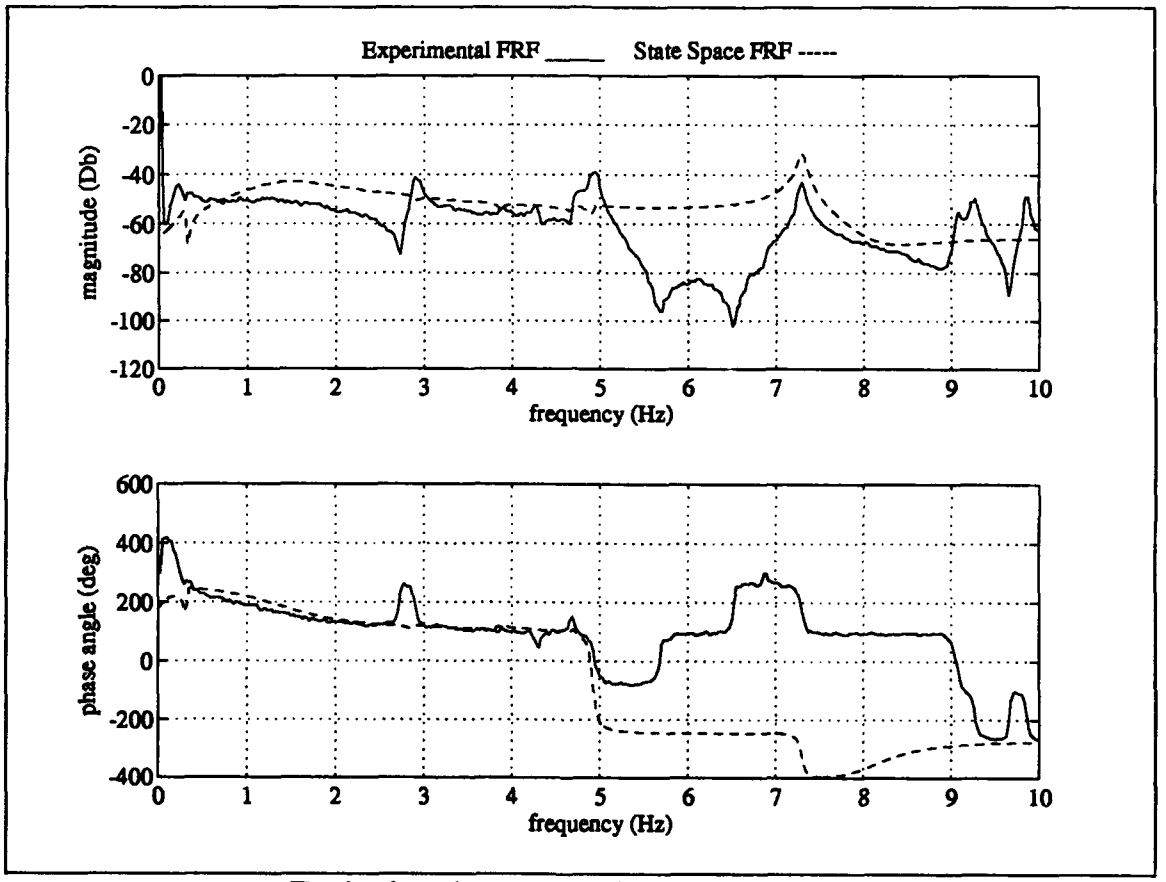

Excitation Actuator #10 Measurement #3

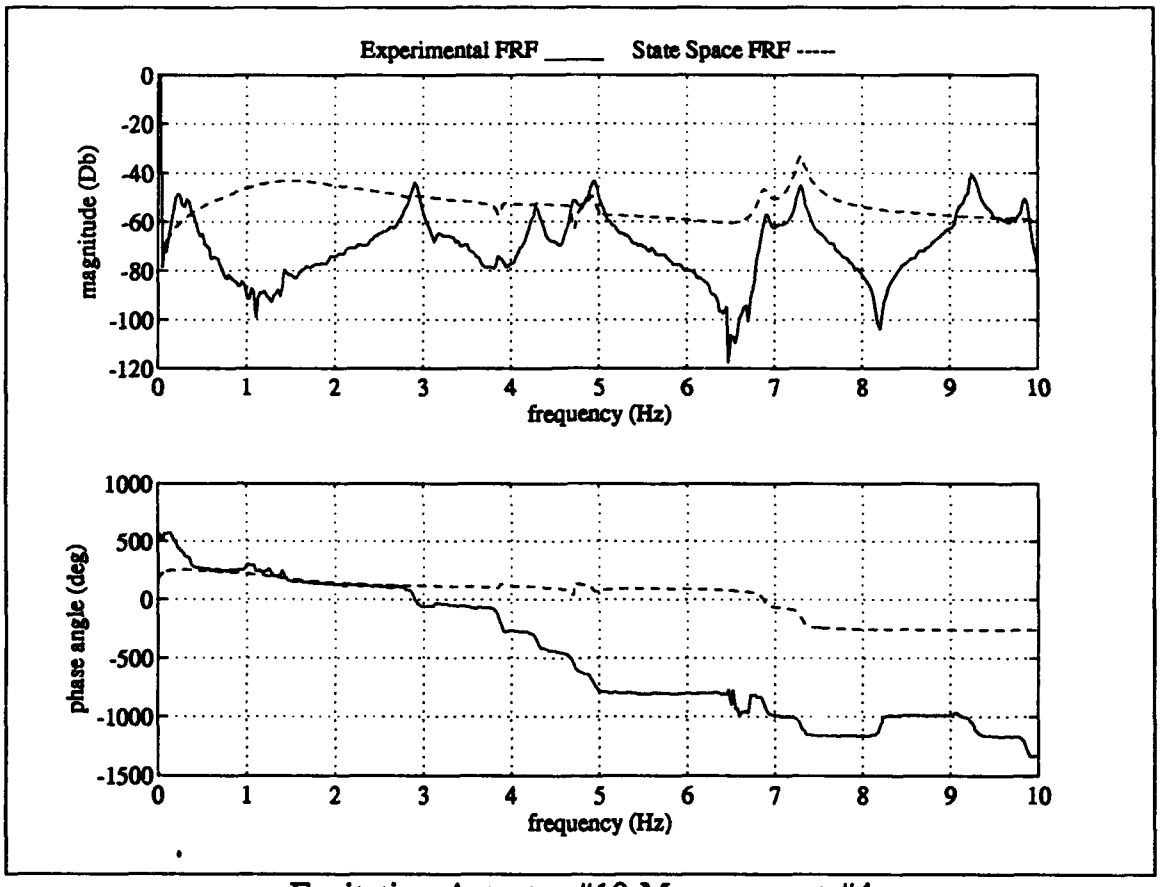

Excitation Actuator #10 Measurement #4

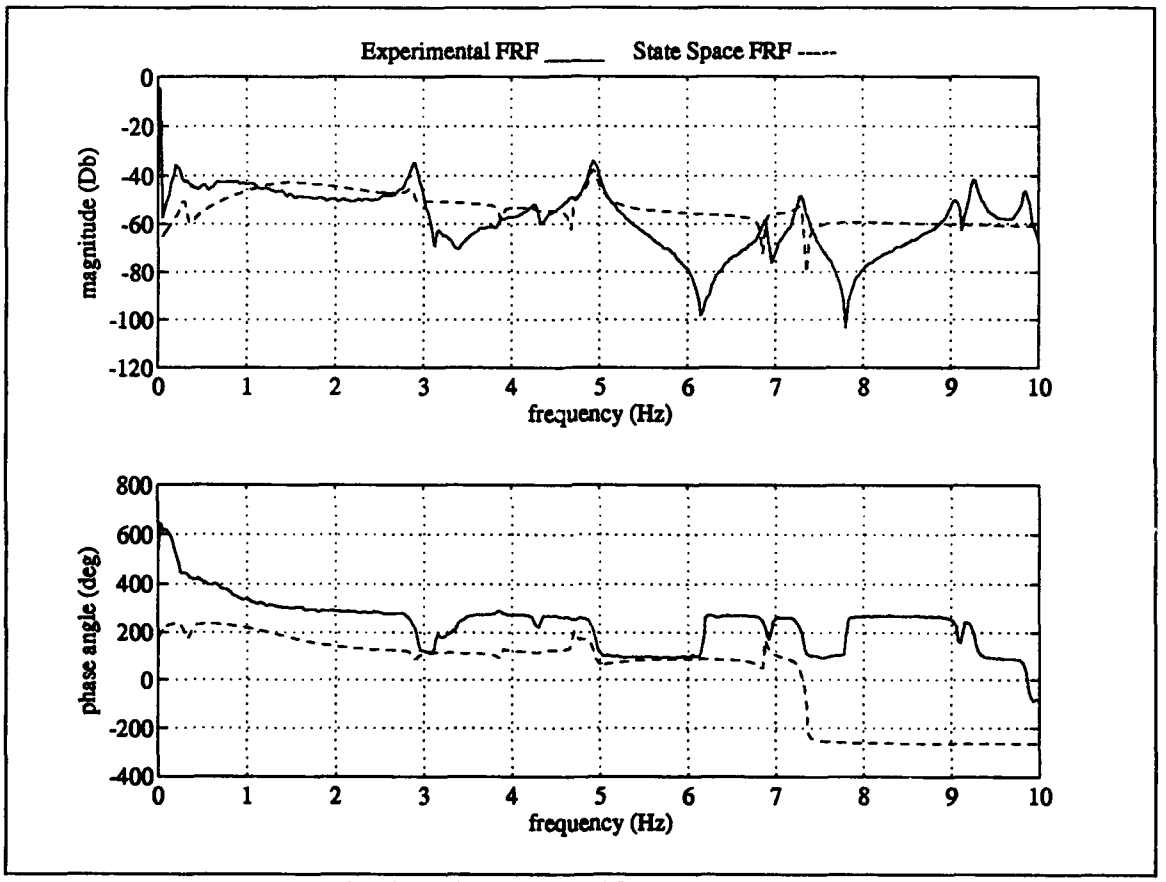

Excitation Actuator #10 Measurement #5

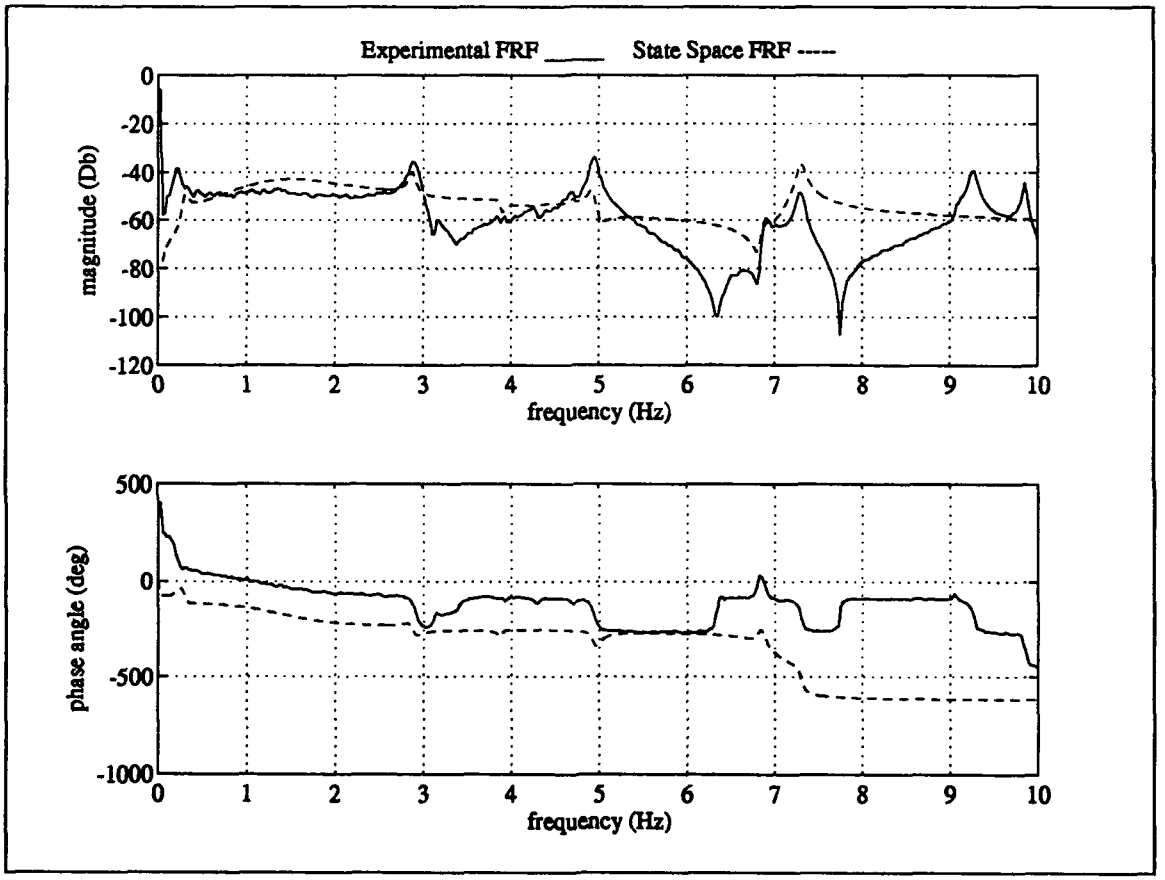

Excitation Actuator #10 Measurement #6

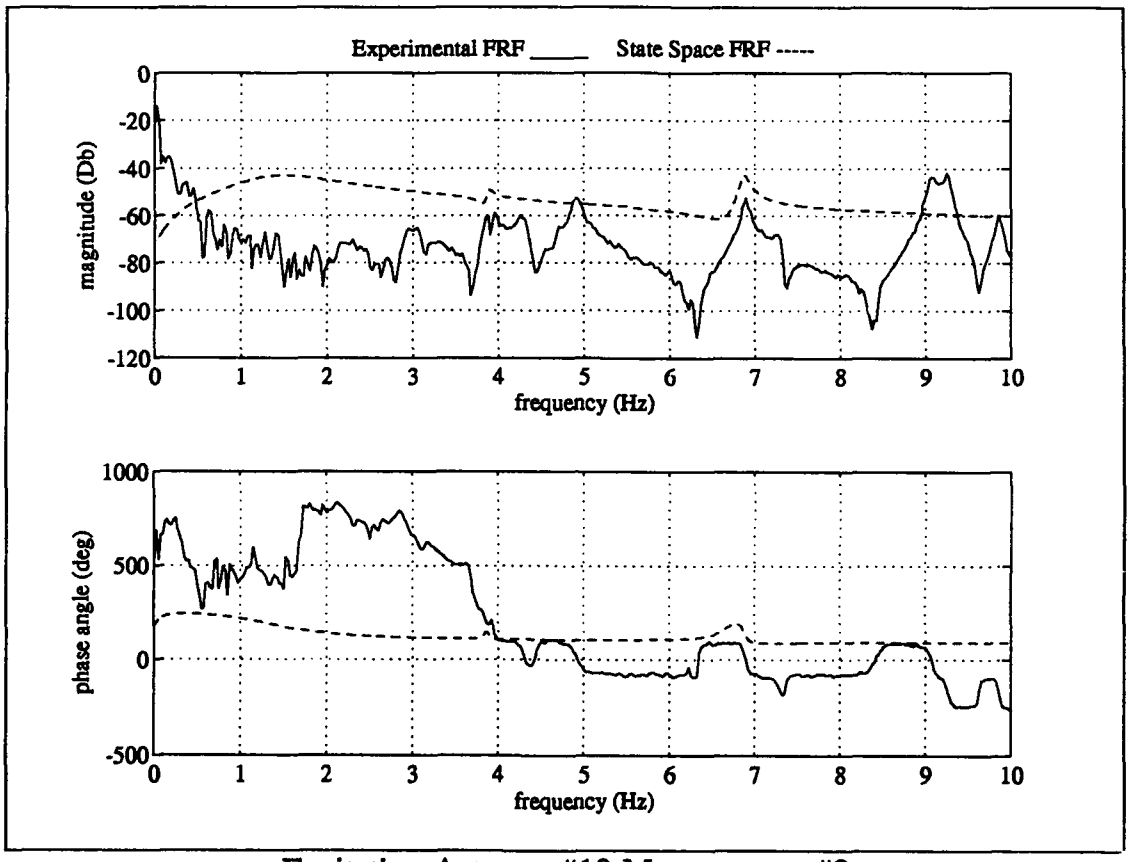

Excitation Actuator #10 Measurement #9

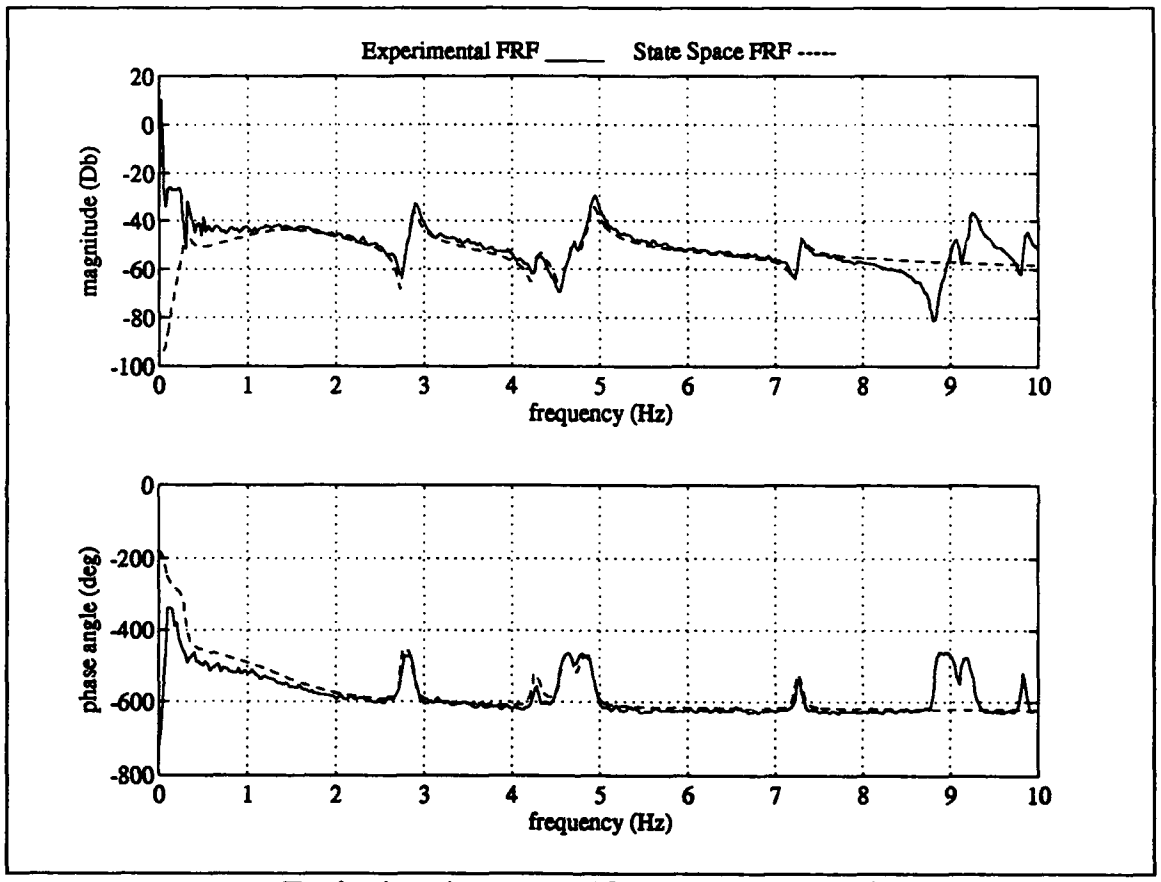

Excitation Actuator #10 Measurement #10

Vita

Chad T. Matheson was born on 16 November 1967 in Fresno, California. After graduating from Merced High School in Merced California in June 1986, he attended the United States Air Force Academy. He graduated in May 1990 with a Bachelor of Science Degree in Engineering Mechanics. His first assignment was to the Ballistic Missile Organization Detachment 1 at F.E. Warren AFB, WY where he served as a Mechanical Engineer working on the Rail Garrison Program. In May 1991, he entered the School of Engineering, Air Force Institute of Technology, Wright-Patterson AFB, Ohio to pursue a Master of Science degree in Aeronautical Engineering.

REPORT DOCUMENTATION PAGE

Form Approved
OMB No. 0704-0188

1. AGENCY USE ONLY (Leave blank)	2. REPORT DATE	3. REPORT TYPE AND DATES COVERED
	Dec 1992	Master's Thesis

4. TITLE AND SUBTITLE
VIBRATION SUPPRESSION IN LARGE FLEXIBLE SPACE STRUCTURES USING ACTIVE CONTROL TECHNIQUES

5. FUNDING NUMBERS

6. AUTHOR(S)
CHAD T. MATHESON
LT, USAF

7. PERFORMING ORGANIZATION NAME(S) AND ADDRESS(ES)
Air Force Institute of Technology
WPAFB OH 45433-6583

8. PERFORMING ORGANIZATION REPORT NUMBER
AFIT/GAE/ENY/92D-13

9. SPONSORING / MONITORING AGENCY NAME(S) AND ADDRESS(ES)
Kevin Slimak
OL-AC PL/VTS
9 Antares Rd. Edwards AFB, CA 93524-7620

10. SPONSORING / MONITORING AGENCY REPORT NUMBER

11. SUPPLEMENTARY NOTES

12a. DISTRIBUTION / AVAILABILITY STATEMENT
Approved for public release; distribution unlimited

12b. DISTRIBUTION CODE

13. ABSTRACT *(Maximum 200 words)*

This report investigates the use of active vibration control techniques applied to the PACOSS Dynamic Test Article as an experimental structure. In the course of the research, a mathematical model of the lightly damped experimental structure was created based on experimental data. This model was used in the design of two classes of controllers. The first class is pure rate feedback of the structure's measured states such that global stability is insured. The second type of controller investigated was an optimal controller (LQG) that was created using the truncated mathematical model. The rate feedback controller showed significant improvements in the damping of the structures flexible modes. The optimal controller proved to be stable only for negligible gains and did not improve structural damping significantly.

14. SUBJECT TERMS	15. NUMBER OF PAGES
Large Space Structures, Dynamic Control, Vibration Damping Structural Vibration, Active Control, Flexible Spacecraft	193
	16. PRICE CODE

17. SECURITY CLASSIFICATION OF REPORT	18. SECURITY CLASSIFICATION OF THIS PAGE	19. SECURITY CLASSIFICATION OF ABSTRACT	20. LIMITATION OF ABSTRACT
Unclassified	Unclassified	Unclassified	UL